Integrated geophysical studies at Masaya volcano, Nicaragua

Thesis

Integrated Geophysical Studies at Masaya Volcano, Nicaragua

A thesis presented for the degree of
Doctor of Philosophy

By

Glyn Williams-Jones
B.Sc. (Hons), M.Sc.
Université de Montréal, Canada

Department of Earth Sciences
The Open University

May 2001

Integrated Geophysical Studies at Masaya Volcano, Nicaragua

A thesis presented for the degree of
Doctor of Philosophy

By

Glyn Williams-Jones
B.Sc. (Hons), M.Sc.
Université de Montréal, Canada

Department of Earth Sciences
The Open University

May 2001

Frontispiece

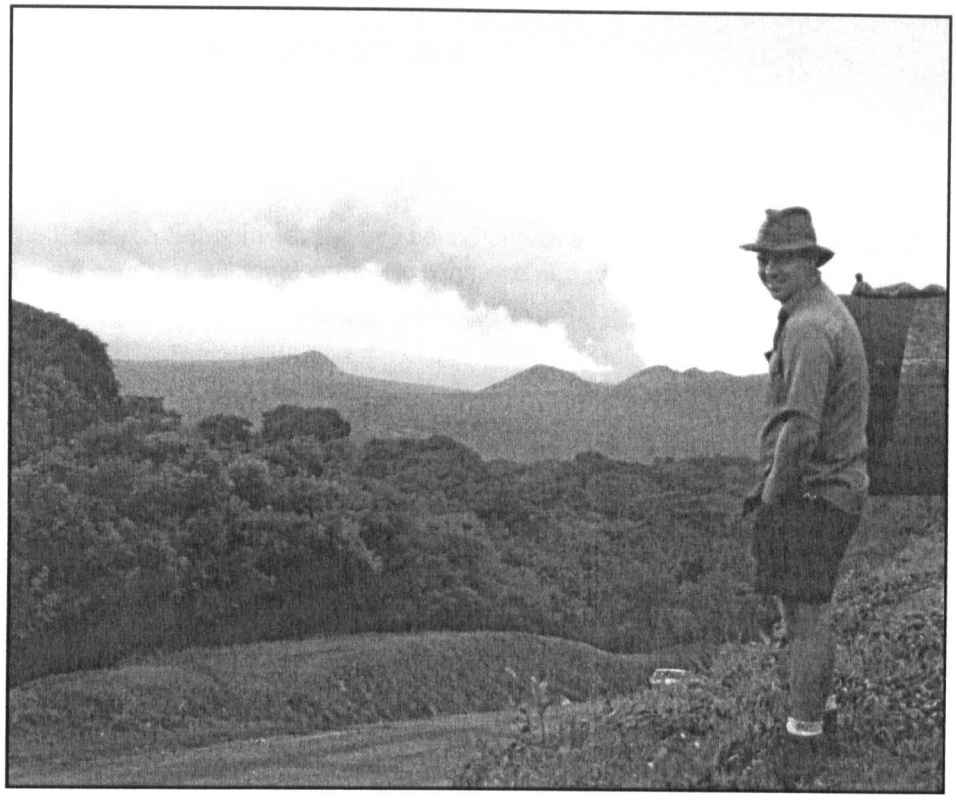

The smell of sulphur is strong, but not unpleasant for a sinner
- Mark Twain (1866)

Abstract

Research into the mechanisms responsible for the lasting, cyclic activity at Masaya volcano can lead to a better understanding of persistently degassing volcanoes. This study is greatly enhanced by the integration of dynamic micro-gravity, deformation and gas flux measurements. The acquisition of extended temporal and spatial geophysical data will also allow for the development of robust models for the dynamics of magmatic systems. Masaya volcano, Nicaragua, is one of the most active systems in Central America, making it an excellent natural laboratory for this study. It is noted for repeated episodes of lava lake formation, strong degassing and subsequent quiescence.

Ground-based geophysical measurements show two episodes of similar magnitude gravity decreases in 1993-1994 and 1997-1999, separated by a period of minor gravity increase. A major increase in SO_2 gas flux from 1997-1999 correlates well with the most recent episode of gravity decrease. The gravity changes are not accompanied by deformation in the summit areas and are interpreted in terms of sub-surface density changes. The persistent degassing at Masaya suggests that up to ~15 km^3 of magma may have degassed over the last 150 years, only a minute fraction of which has been erupted. Furthermore, thermal flux calculations suggest that 0.5 km^3 of magma (the estimated volume of the shallow reservoir) would cool from liquidus to just above solidus temperatures in only 5 years. The high rates of degassing and cooling at open-system volcanoes such as Masaya raise questions as to the ultimate fate of this degassed and cooled magma. A number of models have been proposed to explain this, but the most likely mechanism to explain persistent activity at Masaya and other similar volcanoes is convective removal of cooled and degassed magma and subsequent recharge by volatile-rich magma from depth.

Another fundamental question in modern volcanology concerns the manner in which a volcanic eruption is triggered; the intrusion of fresh magma into a reservoir is thought to be a key component. The amount by which previously ponded reservoir magma interacts with a newly intruded magma will determine the nature and rate of eruption as well as the chemistry of erupted lavas and shallow dykes. The physics of this interaction can be investigated through a conventional monitoring procedure that incorporates the Mogi model relating ground deformation (Δh) to changes in volume of a magma reservoir. Gravity changes (Δg) combined with ground deformation provides information on magma reservoir mass changes. Models developed here predict how, during inflation, the observed $\Delta g/\Delta h$ gradient will evolve as a volcano develops from a state of dormancy through unrest into a state of explosive activity.

Acknowledgements

I would first like to thank my supervisors, Hazel Rymer and Dave Rothery, for their support and advice and just putting up with a loud colonial! Thanks also to my examiners, Steve Self (internal) and Harry Pinkerton (external), for their helpful comments and for making a stressful Viva into a pleasant experience!

Being an acknowledgement, I can't get away without thanking Helen "Nano Spice" Williams, Pete Evans, Rob Hughes, Siobhan McGarry, Jo Rhodes and Bruce Schaefer for being willing partners in crime and aiding and abetting in the coffee/beer abuse! A huge thanks as well to everyone in the Dept. of Earth Sciences at the OU.

This thesis was very heavy on the field side of things and so could not have been done (well, not nearly as easily!) without the tonnes of help from Jean-Marc Séquin, Guillaume Matton, Katie-St-Amand, Alex Beaulieu, especially Isabelle Lépine and Bryn Williams-Jones (who finally got an idea of what I'd been up to all this time!). I am also indebted to all the staff of the Parque Nacional de Masaya and especially everyone at INETER-Geofisica (notably Martha Navarro, Wilfried Strauch and Julio Alvarez).

Like most scientific endeavours, a lot of the ideas for this work were bounced around in the field (and back in the office)over a glass or three of Flor de Caña...so a big round of applause to Pierre Delmelle, John Stix, Pierre Gauthier and Andy Harris for great discussions.

Thanks finally to Isabelle and all my family who put up with the long distance, but were always there for me, just when I needed them most.

Table of Contents

List of Figures

List of Tables

Chapter 1.

General Introduction

1.1. Introduction

Persistent volcanic activity is often characterised by the continual presence of features such as fumaroles, acid crater lakes, and active strombolian vents or lava lakes emitting high thermal and gas flux. At some volcanoes, active lava lakes and strombolian vents have persisted for periods of years to millennia, liberating significant amounts of volatiles and thermal energy. The occurrence of persistent activity in an open volcanic system that undergoes near continuous degassing and heat loss raises important questions about the mechanisms of gas supply and magma recharge from depth. As a consequence of this activity, significant volumes (several km^3) of magma must degas and cool, of which only a small fraction is generally erupted. Furthermore, geophysical and geochemical studies show little evidence of large shallow magma reservoirs beneath these volcanoes (cf. Capaldi et al., 1978; Pietruszka and Garcia, 1999; Chiarabba et al., 2000), suggesting rather that the persistent volcanism is necessarily supplied with magma, gas and/or heat by large deep reservoirs (>5 km). This raises the question of how continuously active volcanoes are supplied and the mechanisms responsible for the removal of the non-erupted, cooled and degassed magma.

Explosive volcanic eruptions are often initiated by magma intrusion into a pre-existing magma reservoir. The degree of interaction between the intruding magma and the pre-existing reservoir will determine the nature and rate of eruption as well as the

chemistry of erupted lavas and shallow dykes (Rymer and Williams-Jones, 2000). To understand the process therefore requires information on the physical and chemical processes occurring at depth within the magma reservoir.

The study of active volcanism and specifically, persistently degassing volcanoes, can be greatly enhanced through the integration of geophysical and geochemical data sets acquired by multiple techniques through space and time. The composition and concentration of volcanic gases are important indicators used to better understand and forecast volcanic activity. However, direct sampling of these gases is often dangerous or impossible due to the high level of activity and the common inaccessibility of the crater areas of many volcanoes. Indirect methods such as the use of remote sensing techniques are thus required. Remote sensing of gases such as sulphur dioxide has proved to be invaluable in the geochemical characterisation of both passively and actively degassing volcanoes (cf. Casadevall et al., 1981; Stoiber et al., 1986; Gerlach and McGee, 1994; Zapata et al., 1997).

Micro-gravity monitoring is now also recognised (cf. Rymer, 1996; Rymer et al., 1998a) as an important means of studying these volcanoes, especially when used in conjunction with measurements of deformation and gas flux. With the development of an extended "baseline" of data, it becomes possible to characterise eruption precursors. It is also possible to calculate the subsurface mass and/or density changes associated with volcanic activity and thus investigate the physical dynamics of volcanoes and their magma reservoirs. By integrating dynamic micro-gravity, deformation and SO_2 gas flux data, it is possible to investigate some of the fundamental mechanisms controlling persistently active volcanoes.

1.2. Location and Geological Setting

Masaya volcano is a basaltic shield volcano forming a large volcanic complex

located at 11.984°N 86.161°W in southwestern Nicaragua, 20 km south of the capital, Managua (Figure 1.1). The volcano, which lies within the Las Sierras Caldera (~15 km x 15 km), is composed of a series of nested calderas and pit craters, the largest being the Masaya caldera (~6 x 11.5 km). The currently active pit crater, Santiago, has been nearly continuously active since its formation in 1853, and is characterised by episodes of degassing and lava lake formation. This persistent activity, as well as the excellent road access to the active crater and surrounding region, makes Masaya an ideal natural laboratory for this study.

1.2.1. Regional Geology of western Nicaragua

Masaya is one of 18 distinct volcanic centres that make up the Nicaraguan portion of the Central American Volcanic Front (CAVF). Formed as a result of the subduction of the Cocos Plate beneath the Caribbean Plate, along the Mesoamerican trench, the CAVF runs from Tacaná volcano in Guatemala to Irazú volcano in Costa Rica (Stoiber and Carr, 1973). In western Nicaragua, the CAVF bisects the Nicaraguan Depression from Cosigüina volcano in the northwest to Maderas volcano in Lago Nicaragua. The Interior highlands in the northeast of the country make up the majority of Nicaragua. Western Nicaragua consists of three principal geological provinces paralleling the Mesoamerican trench: 1) Cretaceous-Tertiary basins; 2) Tertiary volcanics; and the 3) Active Quaternary volcanic range (Figure 1.2; Table 1.1).

Northwestern Nicaragua is believed to be underlain by Palaeozoic continental crust of the Chortsis block, while to the southwest, a Pre-Cretaceous to Cretaceous ophiolitic suite in the Nicoya Complex makes up the basement. The Cretaceous-Tertiary basin is made up of five formations of mainly marine origin (Figure 1.2; Table 1.1). The Rivas and

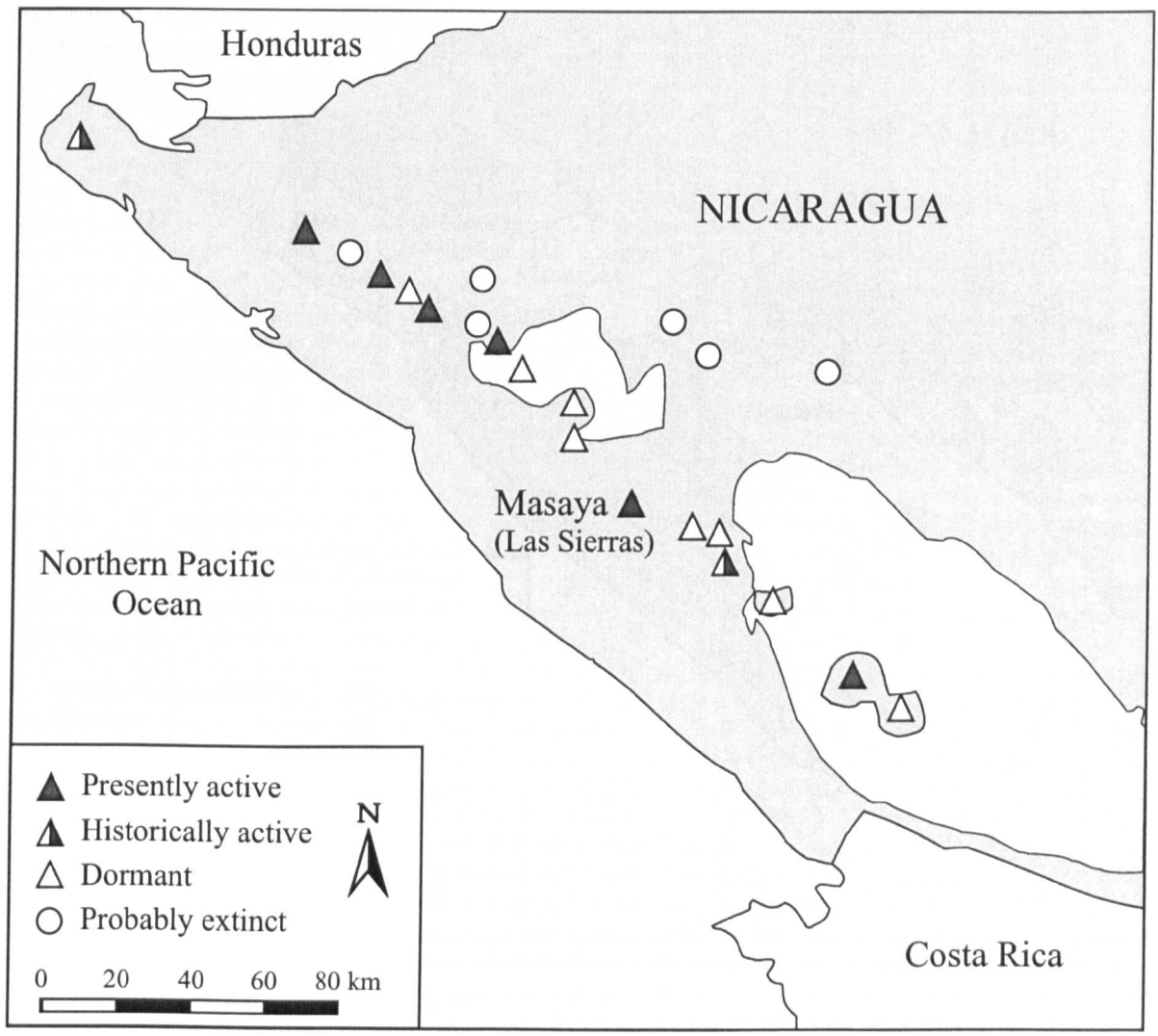

Figure 1.1: Geographic map of Nicaragua showing the location of the Masaya caldera complex and the volcanoes of the Central American Volcanic front. *Modified after van Wyk de Vries (1993).*

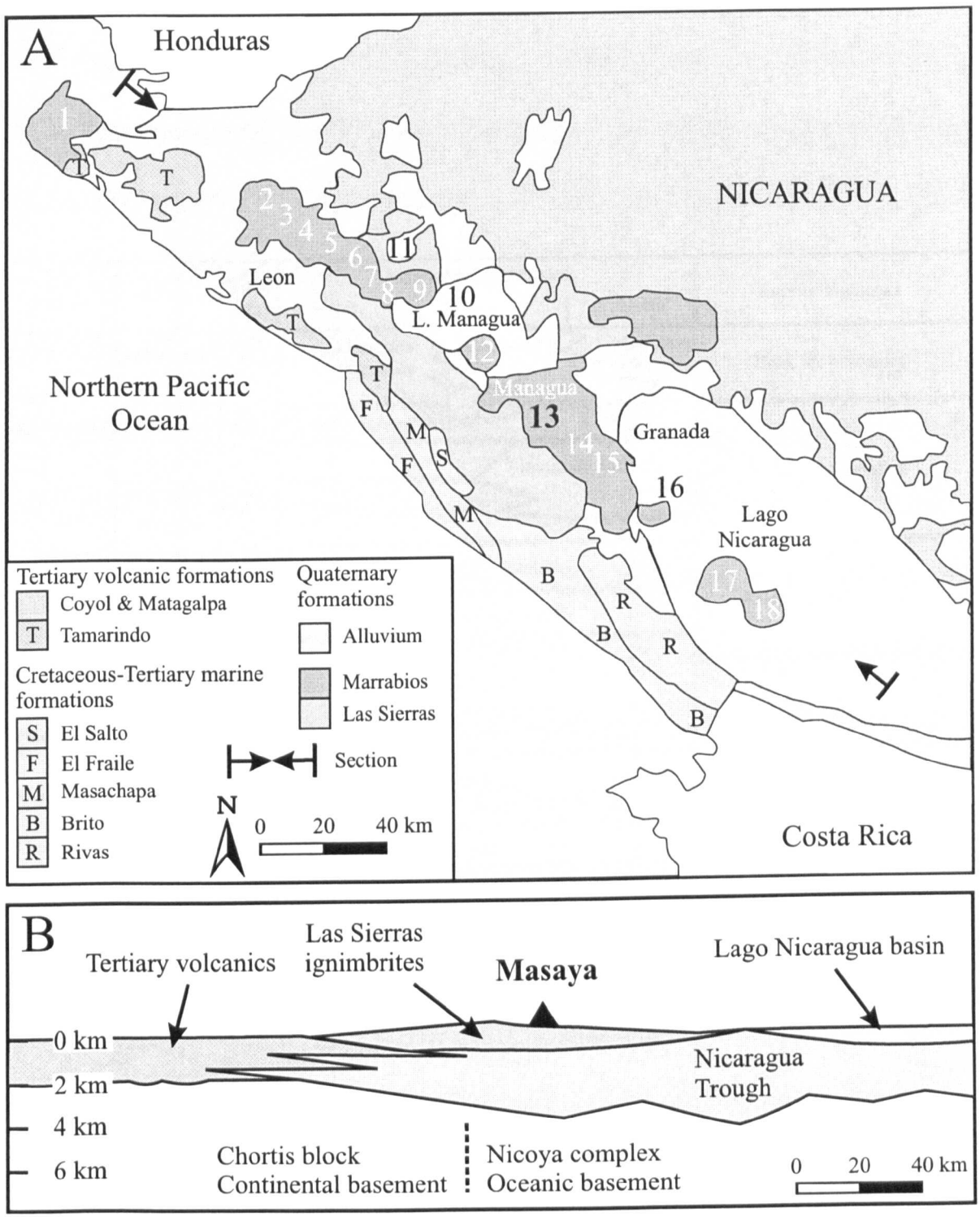

Figure 1.2: A) Geological map of western Nicaragua. Volcanoes: 1) Cosigüina; 2) San Cristobal; 3) Casita; 4) La Pelona; 5) Telica; 6) Rota; 7) El Hoyo; 8) Monte Galan; 9) Momotombo; 10) Momotombito; 11) Malpaisillo caldera; 12) Chiltepe; 13) Masaya-Las Sierras; 14) Apoyo; 15) Mombacho; 16) Zapatera; 17) Concepcion; 18) Maderas. B) Section through the crust along the volcanic arc.
Modified after "Mapa Geológico Preliminar 1:1,000,000", Managua (1973); van Wyk de Vries (1993) and van Wyk de Vries & Borgia (1996).

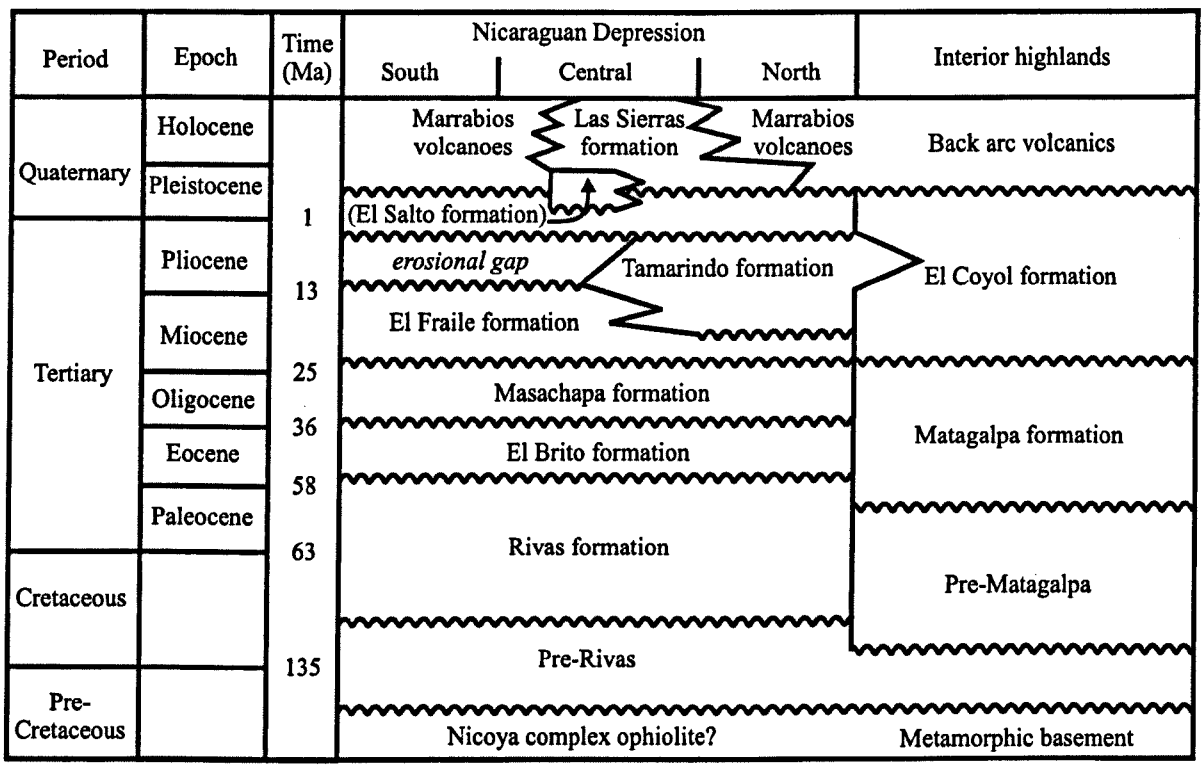

Table 1.1: Stratigraphic correlation of southwest Nicaragua.
Modified after "Mapa Geológico de Nicaragua Occidental 1:250,000", Managua (1972), Weyl (1980), and van Wyk de Vries (1993).

Brito formations are uplifted to the southeast and are overlain in the northwest by a slightly tilted marine near-shore sequence, the El Fraile formation. This in turn passes north into the undeformed Tamarindo formation, a sequence of shallow marine, lacustrine and terrestrial sediments interspersed with ignimbrites. The Nicaraguan Depression is a broad low-lying area located between the Central Highlands and the Pacific Ocean, previously interpreted as a large graben-like structure (McBirney, 1956; Weyl, 1980). Later geological investigation re-interprets it as a low-lying area formed by isostatic readjustment of the surrounding regions after the emplacement of the Tertiary volcanics (van Wyk de Vries, 1993). Northeast of the Depression, the Coyol and Matagalpa formations run from Honduras to Costa Rica and still show evidence of some volcanic centres, distinguishable as constructional landforms (Ehrenborg, 1987).

Quaternary volcanic rocks are found mainly in the Nicaraguan Depression and form two major groups: the Marrabios and Las Sierras formations. The Marrabios Cordillera starts in the northwest with Cosigüina volcano and continues to the southeast with San Cristobal, Casita, La Pelona, Telica and Rota volcanoes (Figure 1.2). Also in the Marrabios Cordillera, the El Hoyo, Monte Galan, Momotombo and Momotombito volcanoes are built upon ignimbrite deposits from the nearby Malpaisillo caldera. Southeast of Lago Managua lie Chiltepe, the Nejapa alignment, Masaya, Apoyo and Mombacho. These overlie the Las Sierras ignimbrites, which were erupted from the Las Sierras Caldera surrounding Masaya volcano. Further south in Lago Nicaragua, Zapatera, Concepcion and Maderas volcanoes mark the end of Nicaraguan section of the CAVF (Figure 1.2; van Wyk de Vries, 1993).

1.2.2. Local Geology

The Masaya caldera is thought to have formed between ~2250 and 6500 BP by a series of large ignimbrite eruptions, which ejected 8 km^3 of material (Williams, 1983a,b;

van Wyk de Vries, 1993). A new basaltic complex has developed within this caldera from eruptions on an arcuate series of vents with the main activity leading to the formation of the Masaya and Nindiri cones. Multiple episodes of pit crater formation have led to the development of the Masaya, Santiago, Nindiri and San Pedro pit craters; the currently active Santiago crater is believed to have formed in 1853 (Figure 1.3; McBirney, 1956; Rymer et al., 1998a). Seismic studies of the degassing-induced tremor suggest the presence of a very shallow magma body, approximately 400 m beneath the rim of Santiago crater, while volcano-tectonic earthquake hypocentres suggest that there may be a shallow reservoir ~1 km below sea level (Métaxian et al., 1997).

1.3. Volcanic Activity

1.3.1. Pre-caldera activity

The basaltic Plio-Pleistocene age Las Sierras ignimbrite shield was the site of a catastrophic collapse episode that formed the Las Sierras Caldera on the eastern flank of the shield (Walker et al., 1993). Continued eruption of basaltic lava and tephra resulted in the formation of a small shield volcano, called the proto-Masaya volcano by Maciejewski (1998), and evidenced by the gradual upwards-slope of the ground towards the walls of Masaya Caldera. Numerous tephra layers and lava flows, which outcrop in the caldera walls, suggest periods of both explosive and effusive eruptive activity at proto-Masaya. The more recent basaltic plinian eruptions centred on proto-Masaya have been interpreted in terms of small caldera-forming eruptions between 35 and 7 ka BP (Bice, 1980; Walker et al., 1993). The most recent deposit, the Masaya Tuff ignimbrite and proximal pyroclastic surge, was deposited between 6.5 and 2.25 ka as part of the eruption that resulted in the present Masaya caldera (Williams, 1983b; Bice, 1985)

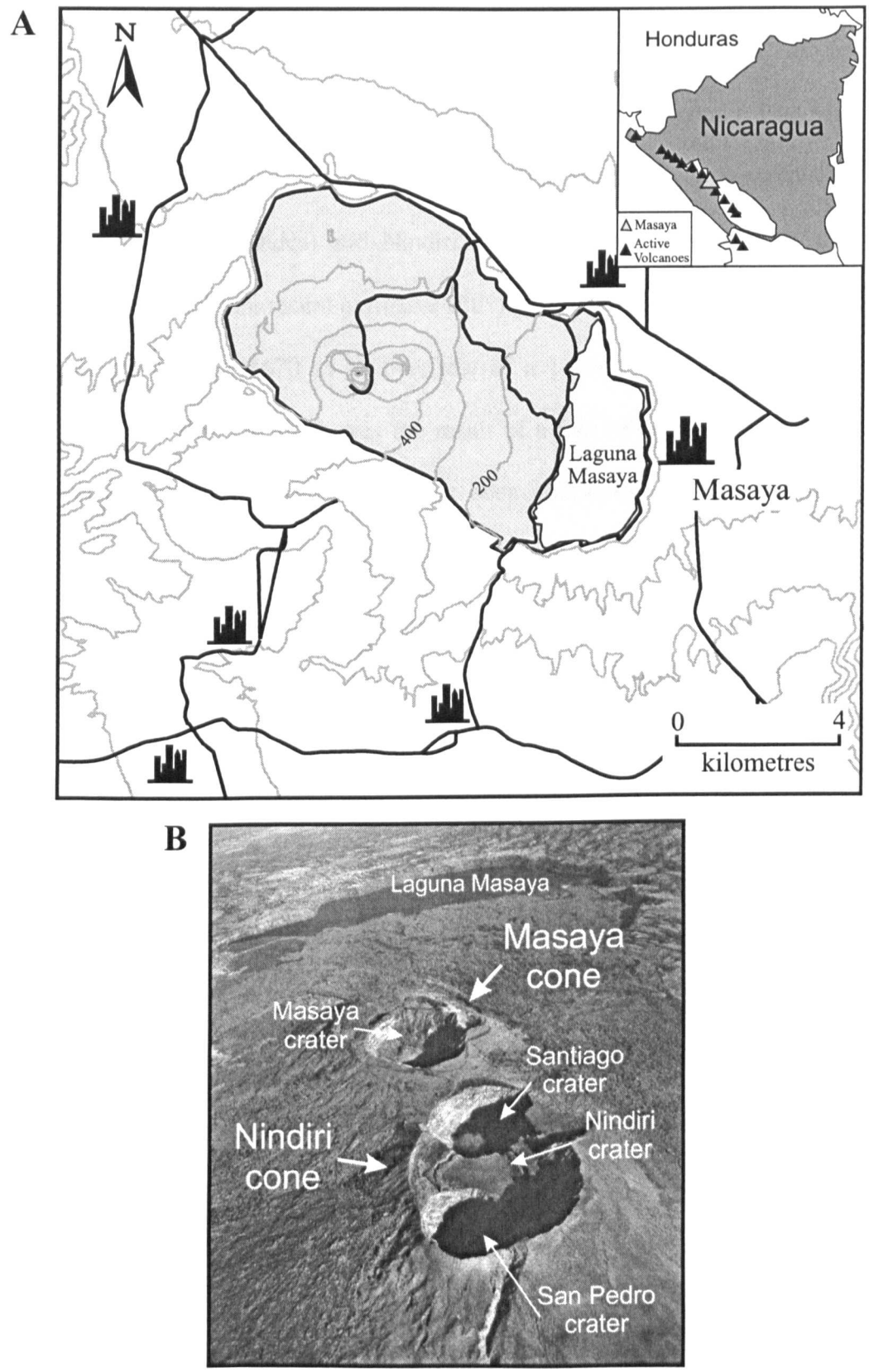

Figure 1.3: a) Masaya caldera (shaded area). Contours are 100 m. Inset map indicates Masaya (grey triangle) and the active volcanoes (black triangles) of the Central American Volcanic Front. b) Aerial view (looking SE) of Masaya and Nindiri cones. *Aerial photo courtesy of INETER (early 1990's?).*

1.3.2. Post-caldera activity

After the formation of Masaya caldera, a basaltic complex of cones and overlapping pit craters developed along an arcuate series of vents. The Masaya and Nindiri cones had developed by 1529 (the first recorded observations were by Conquistador Oviedo y Valdes) and Nindiri and Masaya pit craters were also present (Maciejewski, 1998). More recent extrusive activity at Masaya formed two lava flows, the first of which erupted in 1670 as an overflow of a 1-km-wide lava lake in the Nindiri crater. The second flow, in 1772, was the result of a fissure eruption on the flank of the Masaya cone. Subsequent surface lava has been confined within the presently active Santiago pit crater (Figure 1.3; Rymer et al., 1998a) which hosted lava lakes in 1948, 1965 (still visible as a solidified surface bordering the inner crater) and 1974-1978. Short-lived lava ponds were noted in February 1980 and February-March 1989 when 40-m-high fountaining was observed (Bulletin of the Global Volcanism Network, 1970-2000). More recently, ponding has periodically been observed in small, restricted vents (5-20 m diameter) in 1993 and 1994. Variations in the incandescence of the active vent (from visible during the day to presently only at night) suggests that although the magma column level has oscillated frequently, it nevertheless remains at very shallow levels (Bulletin of the Global Volcanism Network, 1970-2000; Rymer et al., 1998a).

Explosive activity at Santiago has typically been restricted to small strombolian explosions and ash emission with sporadic ejection of blocks and bombs, vesiculated scoria and juvenile ash. As mentioned above, fire fountaining has also been noted in conjunction with the formation of lava lakes. These may have also been responsible for formation of Pele's hair during the 1989 lava lake episode. However, Pele's hair was also noted in December 1996 and February 2000 and is more likely the result of intense gas bursts (Bulletin of the Global Volcanism Network, 1970-2000).

One of the most characteristic phenomena at Masaya are cycles of prolonged passive degassing. There have been at least five such cycles of activity at Masaya since the formation of Santiago crater in 1853 (Stoiber et al., 1986; Rymer et al., 1998a). The most recent cycle began in May 1993 and continues to date (Rymer et al., 1998a). Of these, only the last two (1979-1989 and 1993-present) have been studied in any detail. Work by Stoiber et al. (1986) clearly shows the onset of the 1979-1989 degassing crisis, although data are lacking for the later part of the episode. However, qualitative observations suggest that there was strong degassing until early 1989 (Bulletin of the Global Volcanism Network, 1970-2000). Weak fumarolic activity was reported throughout the early 1990s and is reported to have increased in May 1993 with a "diffuse white sulphur-rich plume" observed several kilometres from crater (Bulletin of the Global Volcanism Network, 1970-2000; Rymer et al., 1998a).

1.4. Previous studies at Masaya

The Masaya volcanic complex and surrounding caldera have long been a site of interest. The first recorded observations were made by the Conquistador Oviedo y Valdes in 1529 (McBirney, 1956 and references therein). Detailed observations of volcanic activity and pit crater shapes were reported by Sapper between 1897 and 1927 (McBirney, 1956). McBirney (1956) investigated the formation of Masaya caldera and described the historical evolution of the volcanic complex through a review of the historical activity. Detailed study of the pyroclastic deposits around Managua by Bice (1980, 1985) determined that the Masaya Tuff, Masaya Triple Layer, and Masaya Lapilli Bed originated from Masaya caldera. Crenshaw et al. (1982) used Rn and Hg soil degassing in order to delineate subsurface structures and investigate the hypothesis of coalescing calderas within the main caldera. While a number of subsurface circular features were suggested, data were insufficient to sufficiently define any coalescing structures. Further investigations of

the formation of Masaya caldera by Williams (1983a,b) concluded that the caldera was formed by a series of basaltic Plinian eruptions. In contrast, Kieffer and Creusot-Eon (1992) re-investigated the formation of the caldera and proposed a phreatomagmatic origin as a series of large coalescing maars. This seems unlikely, however, due to the lack of evidence in the ignimbrite deposits for interactions with meteoric water or the presence of a pre-caldera lake (Gregg and Williams, 1996). The chemistry of the basaltic lavas at Masaya caldera was modelled by Walker et al. (1993) who suggested that fractional crystallisation and magma mixing were dominant processes. Gregg and Williams (1996) compared the explosive formation of Masaya caldera to large mafic volcanoes on Mars. They discussed the origin and rise rate of the source magma for Masaya, suggesting that Masaya is a system open to rapid replenishment from depth.

Geophysical studies of Masaya were initiated by Stoiber et al. (1986) who were the first to measure SO_2 flux during the 1972-1989 degassing episode at Santiago crater. Connor and Williams (1990) re-interpreted a regional Bouguer gravity survey by Williams (1972) and reported the presence of a large positive anomaly, possibly due to the shallow emplacement of either a sill or laccolith immediately to the north of the caldera. A more extensive Bouguer gravity survey (as well as magnetotelluric and seismic studies) was performed across Masaya caldera in order to constrain the size and volume of the shallow magmatic system (Métaxian, 1994). The positive gravity anomaly detected by Connor and Williams (1990) was confirmed, but there was no gravity anomaly associated with the active crater. Métaxian et al. (1997) investigated the seismicity in detail, and they found that the persistent degassing-related tremor developed within a body 400 m below Santiago crater, while volcano-tectonic earthquake hypocentres suggested the presence of a reservoir ~1 km b.s.l.

Bonvalot et al. (1992) were the first to perform a dynamic micro-gravity survey on Masaya, although the data were never published. Rymer et al. (1998a) were the first to

correlate micro-gravity changes with SO_2 gas flux at Masaya (1993-1997) and proposed that variations in both were due to the emplacement of a low-density foam layer beneath Santiago crater. They suggested that the current degassing episode was the result of convective overturn of a single magma batch within the system. Maciejewski (1998) used published SO_2 flux data to propose a model for the possible 25-year cycles observed at Masaya. St-Amand (1999) looked at more recent SO_2 flux data as well as petrological estimates and CO_2 soil degassing to investigate passive degassing at Masaya, while Beaulieu (1999) studied short-term micro-gravity variations in the immediate proximity of Santiago crater, interpreting them in terms of fluctuations in the level of magma in the conduit. Horrocks et al. (1999) used Fourier Transform Infrared spectroscopy (FTIR) to measure gas species ratios in the passively emitted gas column and suggested that the lack in variation of S/Cl ratios implied that the magmatic system was open to constant recharge from depth. Delmelle et al. (1999) summarised the multidisciplinary geophysical and geochemical studies taking place at Masaya, and presented some of the preliminary results from this thesis.

1.5. Outline of present work

This thesis expands upon the research of Rymer et al. (1998a) to further investigate the processes involved in persistently active volcanism. The main objective of this study is to study the mechanisms responsible for the persistent and cyclic nature of volcanism at Masaya volcano through the application of micro-gravity, deformation and gas flux measurements. Specific questions to be investigated are:

1. What processes are responsible for the variations in gas flux and micro-gravity, and are these indicative of changes within the volcanic plumbing system of Masaya?
2. What processes are responsible for the large discrepancies between the rates of magma extrusion, magma cooling and magma degassing at Masaya and other persistently

active volcanoes?

3. By using extended micro-gravity and deformation measurements, is it possible to identify the precursory processes within a magma reservoir that may be related to the triggering mechanisms of a volcanic eruption at Masaya volcano.

Apart from the concluding chapter, each of the principal chapters is written in article form; Chapter 4 is currently in press. As such, some repetition is inevitable. However this format has the benefit that each chapter may be read as an individual piece and essentially without reference to other chapters. More detailed methodologies for Chapter 2 and 3 are presented in Appendix B and C, respectively.

Chapter 2 investigates the extensive degassing that has occurred at Masaya since 1972 and looks at that the rate at which this degassed magma will cool. In Chapter 3, the correlation between gas flux and micro-gravity change is investigated and a model for shallow degassing is proposed. Chapter 4 assesses the use of micro-gravity and deformation measurements at calderas in a state of unrest as a means of determining eruption precursors; two end-member models are suggested. Finally, in Chapter 5, the mechanisms responsible for persistent activity at open-system volcanoes are investigated and a model is proposed.

Much of the field work and discussion for this thesis was undertaken in collaboration with a number colleagues from the Instituto Nicaragüense de Estudios Territoriales (INETER, Nicaragua), Université de Montréal and McGill University (Canada), Université Catholique de Louvain (Belgium), University of Cambridge and the Open University. As the COSPEC data were collected collaboratively between 1996 and 2000, where parts of the data set are already published, references are cited. All of the data are nevertheless presented for completeness. Microgravity data from 1998 to 2000 were collected entirely by myself with the aid of my supervisors, Drs Hazel Rymer and Dave Rothery. As stated above, the work by Rymer et al. (1998a) is the starting point for much

of this study, with Chapter 2 and 3 expanding greatly upon it. Chapter 4 follows through on the work of Rymer and Williams-Jones (2000; Appendix G), published during this study. Chapter 5 is a wholly new work incorporating many of the ideas raised in the previous chapters. Bearing all this in mind, >80% of this thesis is my own work.

Chapter 2.

Magma degassing at an active basaltic volcano, Masaya, Nicaragua: Insights from gas flux measurements obtained between 1996-2000.

To be submitted to the Journal of Geophysical Research

2.1. Abstract

The Masaya volcano complex in western Nicaragua is one of the most active systems in Central America and is characterised by cycles of prolonged passive degassing. The most recent degassing episode (mid-1993 to present) has released at least 2.4 x 10^9 kg of SO_2 contributing ~4.6% and ~1.5% of the annual global subaerial volcanic SO_2 and CO_2 emissions, respectively. At least 21 Tg of SO_2 has been emitted from Masaya over the last ~150 years, resulting in a significant long-term impact on the local environment. Depending on the initial melt S concentration assumed, up to ~15 km^3 of magma may have been degassed since the formation of the active crater, Santiago, in 1853, but only a minute fraction of this has actually been erupted. The rate at which a magma reservoir cools may be estimated using thermal flux equations and measured gas flux and vent temperatures. A 0.5 km^3 reservoir degassing at rates similar to those of Masaya during 1998-2000 would cool from liquidus to just above solidus temperatures in ~5 years. A 1 km^3 reservoir would take ~9 years cool from liquidus to just above solidus temperatures, on the order of the "life span" of the current degassing episode. The persistent degassing may be influenced by the development of foam layers at shallow levels and at the roof of the magma

reservoir. However, a mechanism for downward removal of the degassed magma and replenishment of the system is required. Buoyancy-driven magma circulation aided by thermal and gas-driven convection is a plausible mechanism for supplying low-density gas-rich magma to the surface and removing cool, dense, degassed magma.

2.2. Introduction

The occurrence of persistent activity in an open volcanic system that undergoes near continuous degassing and heat loss raises significant questions about the mechanisms of gas supply and recharge of magma from depth. By applying thermal flux equations to measured gas flux and vent wall temperature data, it is possible to obtain estimates of cooling rates of magma reservoirs and thus a better understanding of subsurface processes. An excellent natural laboratory for this study is Masaya volcano, which is noted for repeated episodes of lava lake formation, strong degassing and subsequent quiescence. Although the direct measurement of volcanic gases from Masaya is not practical due to the inaccessibility of the active crater, remote sensing techniques make it possible to safely accumulate long-term data on degassing rates. Deviations from background gas levels are useful indicators of significant change in volcanic activity.

Ultraviolet correlation spectrometry (COSPEC) has been used to study volcanoes since the early 1970s and is a useful tool for the measurement of SO_2 flux (in metric tonnes; t d^{-1}) at active volcanoes such as Masaya (Stoiber et al., 1986; Rymer et al., 1998a). These measurements are now being supplemented and complemented through the use of Fourier Transform Infrared spectroscopy (FTIR) which allows for measurement of the ratio of selected gas species (cf. Francis et al., 1998; Horrocks et al., 1999). The two methods used together provide a measure of the total gas flux of the volcano. Here I present results from six recent field campaigns on Masaya, in which over 470 SO_2 flux measurements were made, representing one of the largest data sets for an active volcano.

All published COSPEC measurements made at Masaya since 1972 are also presented (see Appendix E).

2.3. Geological Background

Masaya is a low basaltic shield volcano located in western Nicaragua, 20 km south of Managua, and forms part of the Central American Volcanic Front (Figure 2.1). Masaya caldera is thought to have formed between ~2250 and 6500 BP by a series of large ignimbrite eruptions, which ejected ~8 km^3 of material (Williams, 1983a,b; van Wyk de Vries, 1993).

A basaltic complex has developed within the caldera from eruptions on an arcuate set of vents, with the main activity leading to the formation of the Masaya and Nindiri cones. Multiple episodes of pit crater formation have led to the development of the Masaya, Santiago, Nindiri and San Pedro pit craters; the currently active Santiago crater is believed to have formed in 1853 (McBirney, 1956; Rymer et al., 1998a). Seismic studies of the degassing-induced volcanic tremor suggest the presence of a very shallow resident magma body ~400 m beneath the rim of Santiago crater (Métaxian et al., 1997). This is most likely a feeder system linked to an underlying shallow reservoir (~1 km b.s.l.) suggested by geochemical analyses (Stoiber et al., 1986; Walker et al., 1993) and by the presence of volcano-tectonic earthquake hypocentres (Figure 2.2; Métaxian et al., 1997).

2.4. Methodology

For this study, the COSPEC was mounted in a vehicle and driven at constant velocity beneath the volcanic plume allowing for vertical scans of the plume. Detailed descriptions of the technique can be found in e.g., Millán (1980), Stoiber et al. (1983), Casadevall et al. (1987) and Appendix B. The largest source of uncertainty in COSPEC

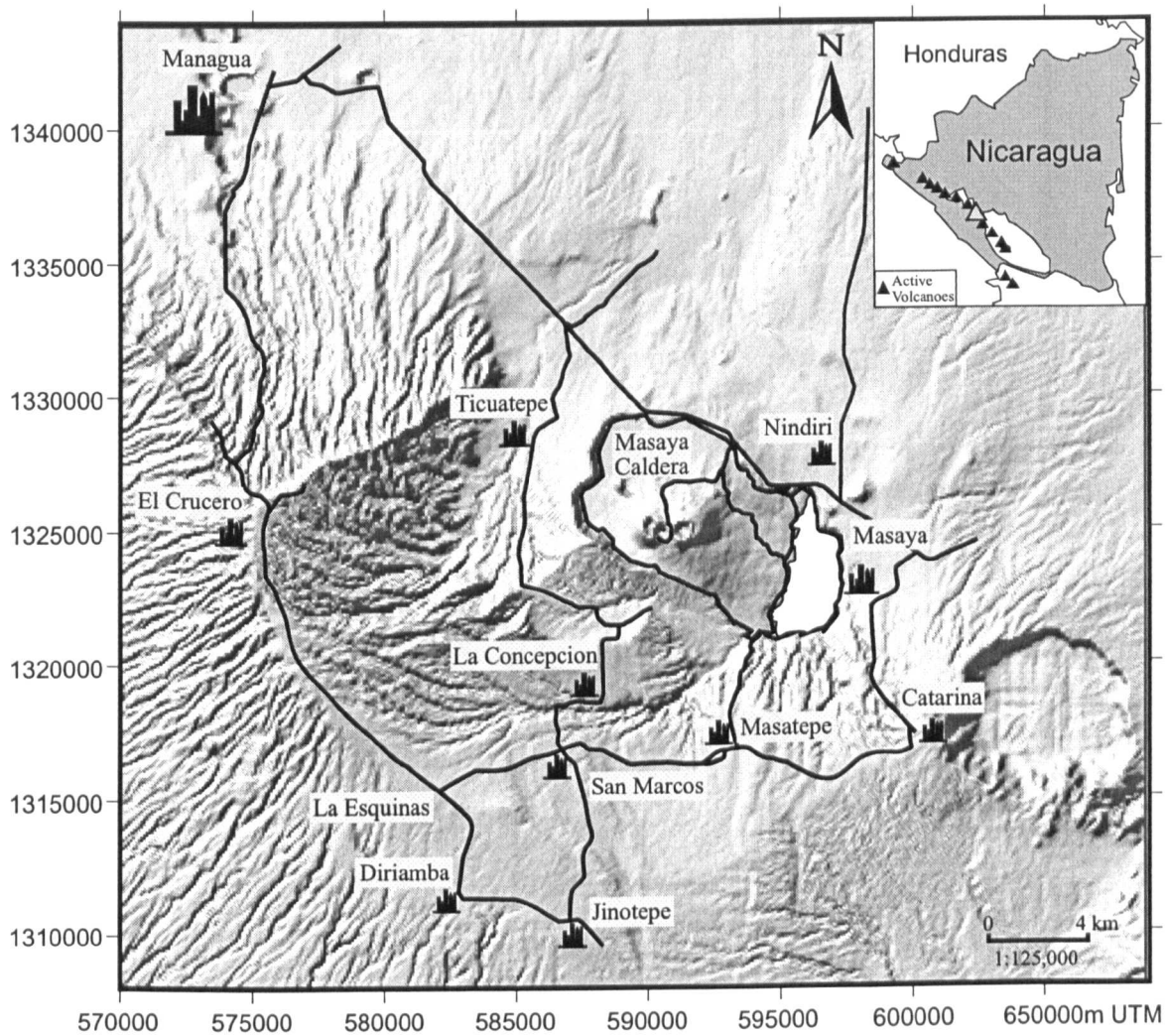

Figure 2.1: Masaya caldera and the network of roads upon which COSPEC measurements are made. Inset map shows the location of Masaya (grey triangle) within the Nicaraguan section of the Central American Volcanic Front.

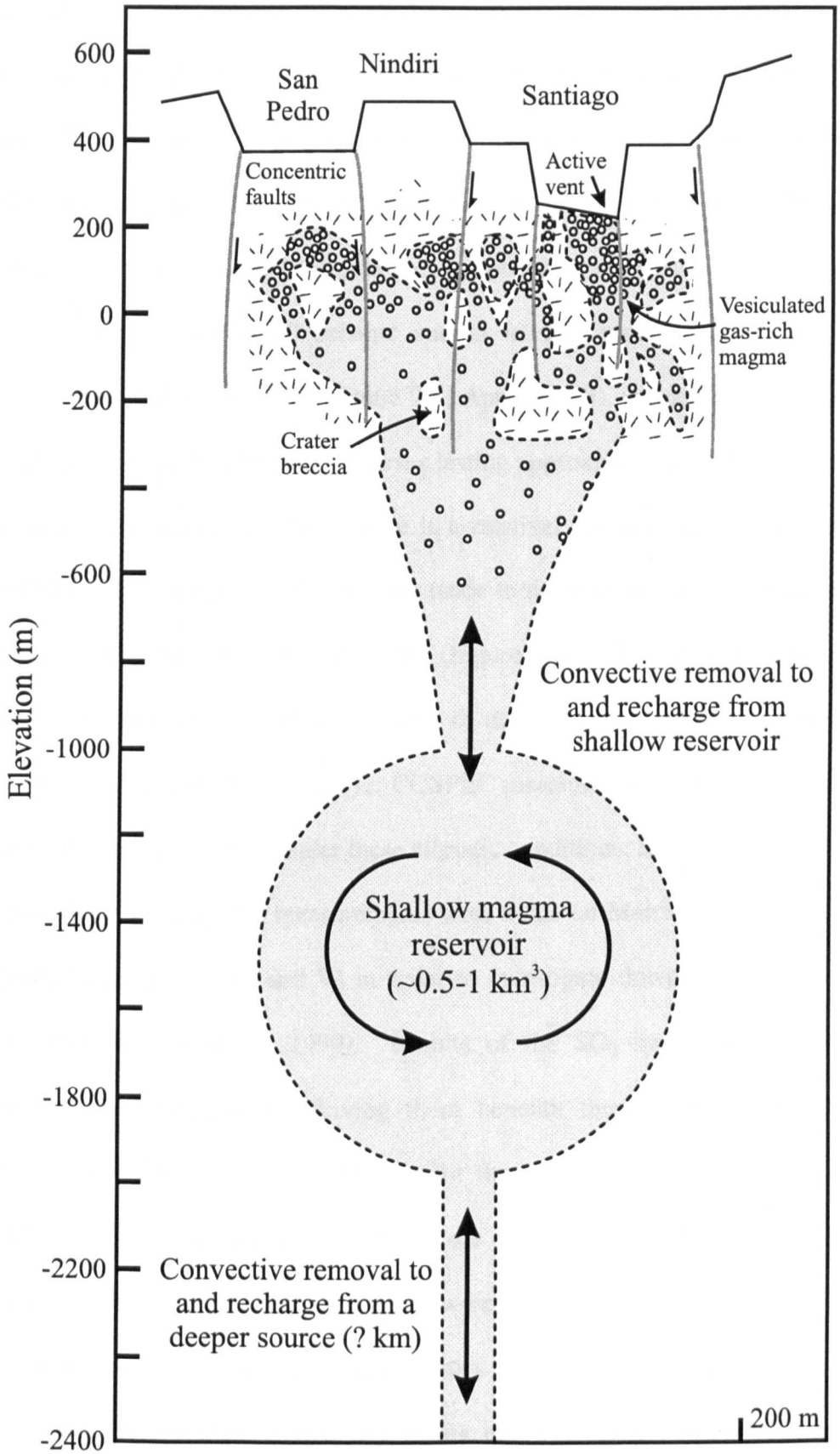

Figure 2.2: Schematic diagram of the possible plumbing system of Masaya volcano. Profile is NW-SE across the pit craters. The presence of a shallow reservoir at ~1-2 km b.s.l. is based on volcano-tectonic hypocentres (Métaxian et al., 1997). Same vertical and horizontal scale.
Modified after Rymer et al. (1998a).

measurements is caused by the difficulties in accurately measuring the windspeed, which is used as a proxy for the speed of the gas column (see detailed discussion of errors in Appendix B). However, at Masaya this uncertainty is greatly reduced as windspeed measurements are made virtually at the column height, from the rim of Masaya crater (~630 m a.s.l.) using a handheld digital anemometer and at an Instituto Nicaragüense de Estudio Territoriales (INETER) seismic station in El Crucero (930 m a.s.l.) with a continuous-recording anemometer (Figure 2.1; Appendix B). Generally, 5 to 10 traverses were made per day, with individual traverses lasting approximately 20-40 minutes. During the dry season (December to April), there is a relatively steady easterly trade wind, and thus COSPEC measurements typically were made to the west of the volcano, at a distance of between 4 and 20 km from the crater (Figure 2.1). In the wet season (May to November), winds tend to be more variable in direction and speed but generally blow towards the east over the city of Masaya; COSPEC measurements were therefore generally made to the east of the volcano under these climatic conditions. SO2

Simultaneous SO_2 flux measurements were made on March 17 and 18, 1998 using two COSPECs (a version IV and V) in order to investigate downwind plume dispersion and SO_2 removal (St-Amand, 1999). Results of the SO_2 measurements by the two instruments were compared by driving them beneath the plume and measuring the difference in SO_2 flux; a conversion factor for these two instruments of COSPEC V = COSPEC IV * 1.3 was determined (also see Appendix B.4.2 for details of error calculations). The COSPECs subsequently were used simultaneously on different but parallel roads west of Santiago crater, at distances of 5.5 km and 15 km (March 17, 1998) and 15 km and 30 km (March 18). By taking into account the windspeed (at time of measurement), the travel distance of the "portion" of plume between the two instruments, and measurement time, it is possible to compare the simultaneous COSPEC measurements (St-Amand, 1999).

2.5. Factors affecting SO_2 fluxes

Variations in measured SO_2 fluxes may be due, in part to measurement uncertainties including instrument calibration (± 2%), digital/analogue chart reading error (± 2%), varying vehicle speed (± 5%), and windspeed and direction (± 0-60%; Casadevall et al., 1981; Stoiber et al., 1983). Fluctuations in humidity, changes in cloud cover, and change in sun angle, can also result in variable amounts of solar ultraviolet radiation reaching the instrument. The opacity of an eruptive plume will also vary due to changes in ash content and result in an increase in absorption of ultraviolet radiation (Andres et al., 1989). Fortunately, the plume at Masaya is relatively free of ash. During the dry season (December to April), the arid environment at Masaya greatly reduces the effect of humidity on COSPEC measurements. By contrast, in the wet season (May to November), there is a significant amount of rain and cloud, greatly increasing the impact of humidity and is likely to be responsible for the low emission rates measured in September 1998 (see below; Appendix B).

2.5.1. SO_2 removal from plume – wet and dry deposition.

Sulphur dioxide may be removed from the plume by wet (rain, humidity) and dry deposition. Scavenging of SO_2 by rain is important at Masaya only during the wet season and may be partially responsible for the significantly lower emission rates determined in September 1998. The almost complete lack of rain during the dry seasons makes its effects negligible at that time. The average dispersion and dry deposition of the SO_2-bearing plume was monitored in February-March 1999 using a network of diffusion tubes and sulfation plates (Delmelle et al., 2000). This survey revealed that the gas plume affects a downwind region of ~1250 km^2 with a daily mean of 1.5 x 10^5 kg SO_2 deposited within 44 km of the source. This represents <10% of the daily average SO_2 flux from Masaya and is

very similar to dry deposition amounts measured for industrial plumes (Freedman and Hutchinson, 1980). Compared to the uncertainties from windspeed, this data suggests that dry deposition of sulphur has only a small impact on the total SO_2 flux estimates (Delmelle et al., 2000). This is further supported by the simultaneous COSPEC measurements made on March 17, 1998 on two roads 5 km and 15 km from the vent (Figure 2.1). Average fluxes were measured at 2530 ± 520 t d^{-1} along Llano Pacaya (5 km) and 2620 ± 1080 t d^{-1} at Ticuantepe (15 km) which suggests only negligible SO_2 loss during the 10 km transport (St-Amand, 1999; Appendix B).

2.5.2. Blowback – exaggeration of actual SO_2 flux

At coastal volcanoes, the effect of the sea breeze or positive ocean pressure fronts can be important. On a number of occasions at Masaya, abnormally wide gas columns were measured along the Pan American highway (Figure 2.1, 2.3). These results, which were significantly higher than normally measured (~5000 vs. ~1700 t d^{-1}) at similar windspeeds, were initially interpreted as the result of larger than normal pulses of gas (e.g., Mar. 1, 1998 and Feb. 18, 1999, Appendix E). However, further investigation of the chart records and simultaneous COSPEC measurements on March 18, 1998 along the Ticuantepe (15 km) and Pacific coast (30 km) roads, indicate important SO_2 excesses near the coast (St-Amand, 1999). Visually, the chart records showed a very dispersed signal in contrast to the normal, very restricted signal (Figure 2.3). It appears that the presence of either a strong positive pressure system coming inland from the ocean or a strong sea breeze (Arya, 1999) forced the gas plume back upon itself. This effectively resulted in a "reconcentration" of the plume, with sections being measured more than once as the column was forced slowly back upon itself. Where this was recognised as being the case, these measurements have been removed from our analysed data set, as they are clearly not representative of the actual SO_2 flux from the volcano.

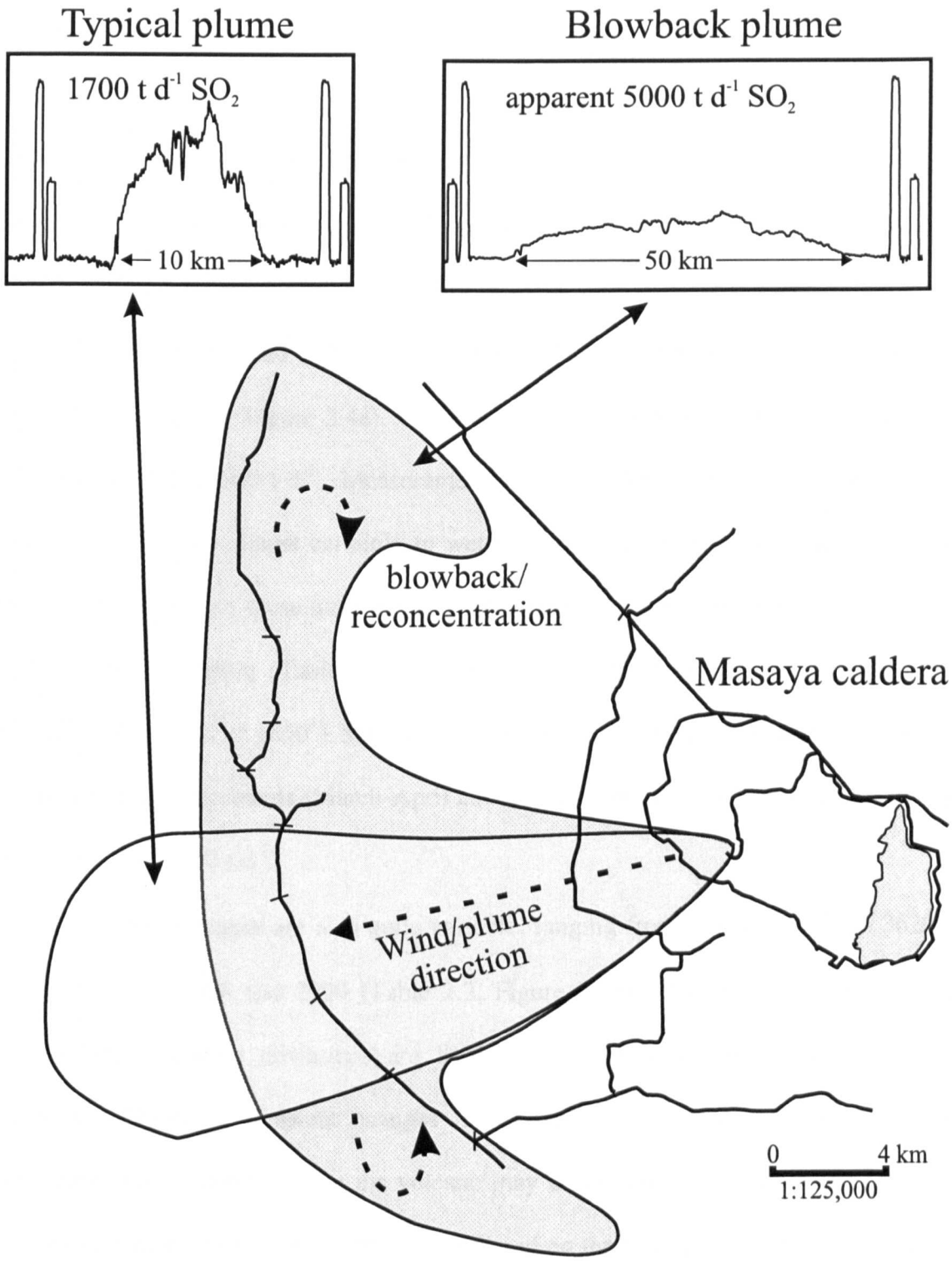

Figure 2.3: An example of the typical and blowback plumes which reconcentrate and result in apparently increased SO_2 flux. Blowback plumes generally result in significantly wider UV absorption spectra for similar windspeed conditions.

2.6. Results

2.6.1. SO_2 Fluxes

After a hiatus of almost nine years, COSPEC measurements were resumed briefly in April 1992 by Williams et al. with an estimated SO_2 flux of <10 t d^{-1} (Bulletin of the Global Volcanism Network, 2000). Starting in 1996, comprehensive monitoring showed elevated emissions with 600 ± 290 t d^{-1} in March 1996 and 390 ± 200 t d^{-1} in February-March 1997 (Table 2.1, Figure 2.4a). Emission rates increased significantly in February-April 1998 to 1850 ± 960 t d^{-1}. Measurements in September 1998 were notably reduced (670 ± 520 t d^{-1}), due almost certainly to wet weather and low-wind velocity conditions during the rainy season; these have not been included in yearly flux averages as they are clearly not representative (Table 2.1, Figure 2.4a; see detailed discussion of errors in Appendix B.5). Rates of 1650 ± 560 t d^{-1} were measured in February-March 1999, while the most recent measurements (March-April 2000) show a possible decrease in the average SO_2 flux to 1310 ± 430 t d^{-1}.

Daily flux averages are also quite variable, ranging from 160 ± 75 t d^{-1} to 3620 ± 260 t d^{-1} between 1996 and 2000 (Table 2.2, Figure 2.4b). As discussed above, these relatively large standard deviations are likely to be the result of plume-atmosphere interactions. However, transient changes (i.e., changes in rate of convection, bubble accumulation and collapse, etc.) at the volcano may also contribute to the variations such as the SO_2 emission rates above 3000 t d^{-1} measured on three days in February-April 1998 (Table 2.2).

Table 2.1: Monthly average SO_2 flux at Masaya, 1972-2000.

Date	Avg. SO_2 flux (t d^{-1})	1 Standard deviation (t d^{-1})	n
Oct-72	180		
Nov-76	660	220	3
Oct-77	400	50	4
May-78	320	90	16
Jan-80	1400	290	6
Jul-80	870	170	5
Feb-81	1070	490	12
Mar-81	730	160	4
Aug-81	1170	710	66
Nov-81	770	240	19
Dec-81	1490	440	7
Jan-82	640	200	7
Feb-82	700	480	9
Mar-82	2390		9
Dec-82	1000	70	4
Apr-92	<10		
Mar-96	600	290	8
Feb-97	350	260	15
Mar-97	410	170	39
Feb-98	1770	840	37
Mar-98	1770	1050	103
Apr-98	2170	790	46
Sep-98	670	520	35
Feb-99	1790	620	49
Mar-99	1570	520	74
Mar-00	1430	400	74
Apr-00	1200	430	74

t d^{-1} = metric tonnes per day; n = number of measurements
1972-1982: *Stoiber et al. (1986).*
1992: *Williams et al., Bulletin of the Global Volcanism Network (1992).*
1996-1997: *Rymer et al. (1998).*

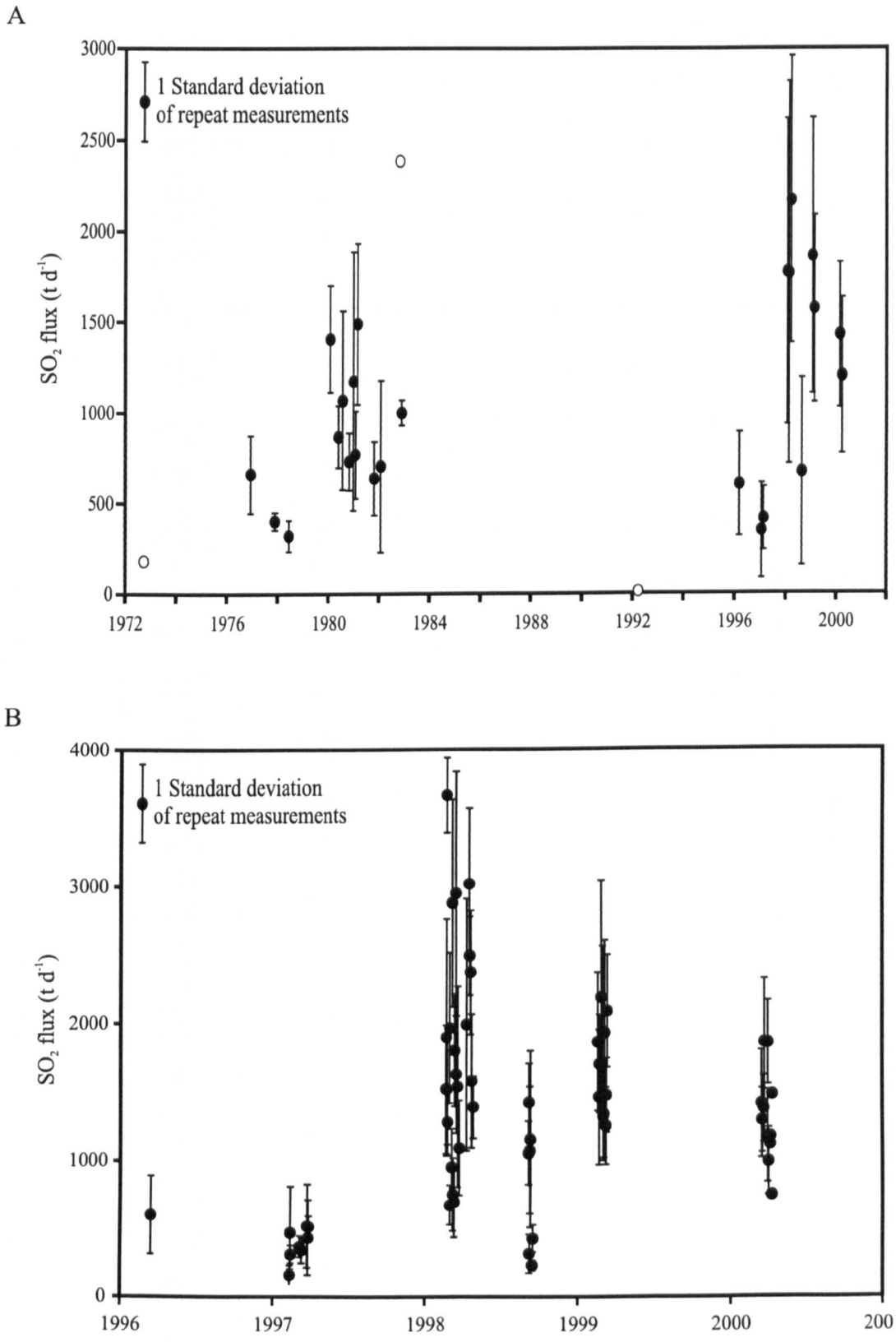

Figure 2.4: a) Average monthly SO_2 flux (t d^{-1}) at Masaya between 1972 and 2000 and b) average daily SO_2 flux between 1996 and 2000. Black circles denote repeat measurements, white circles denote single measurements. Error bars are 1 standard deviation of repeat measurements. See Table 2.1 and 2.2, respectively.

Table 2.2: Daily average SO_2 flux at Masaya, 1996-2000.

Date	Avg. SO_2 flux ($t\ d^{-1}$)	1 Standard Deviation ($t\ d^{-1}$)	Avg. Windspeed ($m\ s^{-1}$)	n
16/03/96	600	290	3.9	8
12/02/97	160	75	3.5	4
13/02/97	470	340	2.4	7
14/02/97	310	65	3.9	4
07/03/97	370	80	9.6	8
12/03/97	340	95	8.0	14
25/03/97	520	305	6.1	5
27/03/97	440	280	4.9	6
28/03/97	520	80	7.0	6
21/02/98	1520	465	8.8	6
22/02/98	1870	725	6.3	8
23/02/98	3620	255	9.1	4
24/02/98	1520	400	9.2	9
25/02/98	1100	225	7.9	10
02/03/98	1960	545	8.0	4
03/03/98	680	145	4.7	3
07/03/98	950	275	5.8	8
08/03/98	2880	755	5.8	3
10/03/98	750	265	6.4	4
13/03/98	700	260	10.5	12
14/03/98	1670	405	16.2	6
17/03/98	2950	890	10.6	28
18/03/98	1630	425	8.1	10
21/03/98	1540	730	4.6	11
25/03/98	1090	345	8.8	10
11/04/98	1990	915	10.8	11
17/04/98	3020	550	11.2	9
18/04/98	2490	285	11.0	7
20/04/98	2370	450	12.3	6
23/04/98	1580	485	12.8	6
27/04/98	1390	225	12.8	7
07/09/98	1050	230	2.4	2
08/09/98	1420	285	3.4	4
09/09/98	320	140	1.2	6
10/09/98	1070	460	3.4	4
11/09/98	1160	645	2.1	4
16/09/98	230	35	0.5	8
17/09/98	430	100	1.0	7
19/02/99	1760	460	3.1	10
22/02/99	1460	490	9.9	11
23/02/99	1700	355	9.2	10
27/02/99	2080	810	10.2	10
02/03/99	1940	620	5.7	10
04/03/99	1300	315	11.2	10
05/03/99	1340	315	10.9	16
07/03/99	1930	670	10.9	10
10/03/99	1250	280	10.9	11
11/03/99	1470	270	10.9	10
13/03/99	2080	405	10.9	7
17/03/00	1400	390	8.6	8
18/03/00	1280	230	8.6	8
22/03/00	1370	245	9.6	8
24/03/00	1850	455	10.0	8
31/03/00	1170	335	8.3	6
01/04/00	1850	305	12.5	6
02/04/00	990	240	10.2	8
04/04/00	1150	370	6.7	7
06/04/00	1110	235	11.4	10
07/04/00	1170	545	10.4	6
10/04/00	740	205	10.8	2
11/04/00	1470		8.7	1

n = number of measurements.
1996 data from *Rymer et al. (1998)*.

The average daily flux of ~1700 ± 510 t d^{-1} between 1998 and 2000 contributed approximately 4.6% of the annual global subaerial volcanic SO_2 emissions (13.4 Tg yr^{-1}; Andres and Kasgnoc, 1998). An estimated total SO_2 flux can be calculated by multiplying the yearly average flux (in tonnes per day) by the number of days in the year. Thus, assuming that 1993-1995 flux values were similar to those measured in 1996, we estimate that Masaya has released at least 2.43 Tg of SO_2 since onset of the degassing episode in 1993 (Table 2.3b). This is in addition to the estimated total of 18.5 Tg of SO_2 emitted during the degassing episodes of 1902, 1919, 1947, and 1979 and any interim background emissions; these estimates assume degassing rates comparable to 1979-1985 levels (Stoiber et al., 1986). This results in ~21 Tg SO_2 emitted from Santiago crater since 1853. In contrast, the Total Ozone Mapping Spectrometer on the Nimbus-7 satellite measured at between 17 and 24 Tg SO_2 during the paroxysmal eruption of Mount Pinatubo (Philippines) on June 15-16, 1991 (Bluth et al., 1992; Daag et al., 1996; Gerlach et al., 1996).

The total gas flux (H_2O + CO_2 + SO_2+ HCl + HF) for the current Masaya degassing event can be estimated using the ratios of gas species measured by open-path Fourier Transform Infrared spectroscopy (OP-FTIR) in February-March 1998, March 1999 and April, 2000 (Delmelle et al., 1999; Horrocks et al., 1999; Bulletin of the Global Volcanism Network, 2000; Burton et al., 2000). As there was no significant change in ratios between 1998 and 2000 (Table 2.3a), the average of these ratios and the average yearly SO_2 flux can be used to estimate the total gas flux at Masaya. Between 1993 and the present, Masaya has emitted at least 46 Tg H_2O, 4.0 Tg CO_2, 2.4 Tg SO_2, 0.85 Tg HCl, and 0.10 Tg HF, and a total gas flux of 54 Tg (Table 2.3b). Based on these ratios and the average daily flux (1998-2000, ~1700 t d^{-1} SO_2), Masaya is responsible for 1.5% of annual volcanic CO_2 emissions, equivalent to only

Table 2.3a: Mass ratios of gas species measured by OP-FTIR at Masaya, 1998-2000.

Species	1998	1999	2000*	1 Std. Dev.
$HCl:SO_2$	0.36	0.35	0.33	0.01
$CO_2:SO_2$	1.51	1.58	n.a.	0.05
$H_2O:SO_2$	20.24	18.53	n.a.	1.21
$HF:SO_2$	0.04	0.04	n.a.	0.00

1998-1999 data: Burton et al., 2000; Horrocks, 2001
2000 data: BGVN, 2000.

Table 2.3b: Estimated gas flux at Masaya, 1993-2000.

Year	days	Avg. SO_2 flux ($t\ d^{-1}$)	Annual output				
			SO_2 (Tg)	H_2O (Tg)	CO_2 (Tg)	HCl (Tg)	HF (Tg)
1993	270	600	0.16	3.09	0.27	0.06	0.01
1994	365	600	0.22	4.17	0.36	0.08	0.01
1995	365	600	0.22	4.17	0.36	0.08	0.01
1996	365	600	0.22	4.17	0.36	0.08	0.01
1997	365	395	0.14	2.72	0.23	0.05	0.01
1998	365	1870*	0.68	12.9	1.11	0.24	0.03
1999	365	1680	0.61	11.6	1.00	0.21	0.03
2000	121	1410	0.17	3.23	0.28	0.06	0.01
Total	**2581**		**2.43**	**46.1**	**3.96**	**0.85**	**0.10**

*excludes rainy season (September) measurements
1 Tg = 10^{12} g = 1 Mt

0.005% of the estimated 23882 Tg yr^{-1} of anthropogenic CO_2 (Williams et al., 1992; Marland et al., 1999).

2.6.2. Petrological data

Petrological estimates of volcanic sulphur content are commonly made using melt inclusion data (e.g., Gerlach and McGee, 1994). Samples from two juvenile bombs ejected from Santiago crater by a small strombolian explosion on November 12, 1997 are tholeiitic basalts of similar composition to lava and pyroclastic material previously erupted by Masaya (e.g., Walker et al., 1993) and likely represent the shallowest portion of the magma beneath the crater. Electron microprobe (JEOL 8900) analyses of matrix glasses and melt inclusions in plagioclase phenocrysts were made by St-Amand (1999), with a melt volume fraction of approximately 0.65. Melt inclusions in phenocrysts contain an average of 100 ± 50 ppm S and 440 ± 60 ppm Cl as compared with 30 ± 20 ppm and 370 ± 40 ppm, respectively, in the matrix glass (St-Amand, 1999). For an arc basaltic system, such S contents are low and are unlikely to reflect the deeper magma conditions, but rather suggest partial degassing of magma before melt entrapment in phenocrysts. In addition, the generally lower S and Cl contents in the matrix glasses suggest that degassing also continued after melt entrapment. The S/Cl ratio varies from 0.04 to 0.57 in the melt inclusions and from <0.01 to 0.30 in the matrix glasses (St-Amand, 1999). While some of this variability arises from the low S contents (at or near the detection limit), the generally lower S/Cl value in the matrix glasses is consistent with preferential fractionation of S with respect to Cl in the vapour phase during gas exsolution from the magma (Carroll and Webster, 1994).

2.6.3. Vent Temperatures

The temperature of gas emitted from the active vent at the bottom of Santiago crater has been measured periodically since 1993 with a number of types of infrared thermometers (e.g., IR pyrometer and Minolta Compac 3). The assumption is made that the gas temperature is in equilibrium with the conduit walls. Vent temperatures have varied significantly over time, ranging from a low of ~50°C in May 1993, prior to the onset of the current degassing crisis, to a high of 1085°C prior to a small strombolian eruption on December 5, 1996 (Bulletin of the Global Volcanism Network, 1970-2000). The most recent gas temperatures were found to range from 170 to 330°C (Table 2.4). As many of these temperatures are taken from field reports, they are only used in a semi-quantitative fashion.

2.7. Discussion

2.7.1. Variability of SO_2 flux measurements at Masaya

The variability of COSPEC measurements, excluding instrumental and environmental effects, may be related in part to sporadic gas output, Earth tide oscillations, and episodes of long-period seismicity. Chartier et al. (1988) stated that "puffing" might be responsible for the observed 7-45 min periodicity in flux measurements from Pu'u 'O'o. Large variations in non-eruptive SO_2 flux at Mt. Etna (November 1993-May 1994), with weekly and biweekly periodicities, are believed to be due to intermittent pulses of gas (Bruno et al., 1999). Connor et al. (1988) noted a correlation between fluctuations in the SO_2 flux from Halemaumau crater, Kilauea volcano (Hawaii), and daily Earth tides affecting the vesiculation and thus degassing rate of the magma. At Galeras volcano, Colombia, simultaneous SO_2 flux and long-period seismic events are clearly related to sealing and pressurisation of the volcanic system leading to explosive eruptions (Fischer et al., 1994).

Table 2.4: Infrared thermometer measurements from the southern rim of Santiago crater.

Date	Temperatures °C	1 Standard deviation	Instrument	Source
May-93	50		IR pyrometer	BGVN19:09
Jul-93	250		IR pyrometer	BGVN19:09
May-94	400		IR pyrometer	BGVN19:09
Jul-94	600		IR pyrometer	BGVN19:09
Dec-96	360-1085		Compac 3	BGVN22:03
Feb-98	330	70	Compac 3	This study
Sep-98	170	30	Compac 3	This study
Feb-99	260	60	Compac 3	This study
Mar-99	280	30	Compac 3	This study
Jun-99	190	30	Compac 3	This study
Mar-00	330	100	Compac 3	This study

Temperatures from 1998-2000 are averages of 5-20 measurements.
BGVN: *Bulletin of the Global Volcanism Network (1970-2000)*

At Masaya, field observations show visible puffing on the scale of seconds to minutes, too short a time scale to be detected downwind by COSPEC traverses which last for 20 minutes or more. There also appears to be little correlation with Earth tides or seismicity; the latter is characterised by constant tremor related to shallow degassing (Métaxian et al., 1997). As stated above, environmental effects such as dry and wet deposition represent only minor (<10%) reductions in daily flux (Delmelle et al., 2000). The important variations in gas flux seen over the course of days and months must therefore be attributed to other factors.

2.7.2. Source of sulphur and volatiles

Compared with other basaltic systems in the region (e.g., Cerro Negro; Roggensack et al., 1997), sulphur concentrations measured in melt inclusions in Pele's hair and bombs from Masaya (St-Amand, 1999) are significantly lower and are not thought to reflect the deep magma conditions. Instead, the samples are considered to represent a degassed froth located just beneath the crater floor (Delmelle et al., 1999). If so, the common assumption that melt inclusions found in erupted material represent undegassed magma (e.g., Gerlach and McGee, 1994) is not appropriate in the case of Masaya. Recent evidence from experimental and melt inclusion studies of subduction-related basaltic magmas (e.g., Sisson and Grove, 1993; Gaetani et al., 1993; Sisson and Layne, 1993; Roggensack et al., 1997; Métrich et al., 1999) suggest that they may have high volatile contents. Nevertheless, even assuming higher initial sulphur contents in the melt, most volcanoes show significant discrepancies between SO_2 flux estimates from COSPEC and petrological methods and necessitate a source for this excess sulphur (cf. Andres et al., 1991; Gerlach and McGee, 1994).

Various mechanisms have been proposed to explain sources of excess sulphur. At El Chichón and Nevado del Ruiz, for example, excess sulphur may have been derived from

magmatic anhydrite and/or a S-rich vapour phase (Luhr et al., 1984; Sigurdsson et al., 1990; Fournelle, 1990). Redox reactions following the injection of reduced sulphide-saturated basaltic magma into oxidised sulphate-saturated dacitic melt are thought to have been responsible for the excess SO_2 and eruption at Mount Pinatubo (Kress, 1997). SO_2 also may be absorbed directly by a hydrothermal system (SO_2 in the presence of H_2O may yield H^+, HSO_4^- and H_2S). The clays and acidic brine formed by the hydrothermal system can also act to seal a volcano, allowing for the accumulation of an independent vapour phase (Williams et al., 1990) and subsequent release of a large sulphur-rich gas bubble (Westrich and Gerlach, 1992; Gerlach et al., 1996). Exsolution and upward migration of a less soluble CO_2 phase has also been suggested as a mechanism for the transport of more soluble SO_2 phases (Andres et al., 1991). Excess sulphur also may derive from the syn-eruptive degassing of sulphur from non-erupted convecting magma (cf. Andres et al., 1991; Kazahaya et al., 1994; Stevenson and Blake, 1998).

Stoiber et al. (1986) estimated that at least 1.2 km^3 of basaltic magma must have been completely degassed between 1979 and 1985 and at least 10 km^3 of magma since the formation of Santiago crater in 1853 (assuming a 270 ppm initial sulphur content in the magma). This may, however, be a significant overestimate (due to sulphur degassing prior to melt entrapment) and the presence of such a large magma volume near the surface (~ 1 km b.s.l.) is also inconsistent with geophysical data (Figure 2.2; Rymer et al., 1998a; Delmelle et al., 1999). A larger reservoir, however, may exist at depths greater than can be detected by geophysical techniques. Although we lack sulphur contents for recent parental material, we can assume a reasonable initial sulphur content of between 800 and 1500 ppm and make a revised estimate of the mass of degassed magma (Roggensack et al., 1997; Métrich et al., 1999). Since Masaya has emitted at least 2.4×10^9 kg of SO_2 from the onset of the most recent degassing episode in 1993 (Table 2.3), the resulting amount of degassed

magma is between 1.2 x 10^{12} and 0.8 x 10^{12} kg or 0.6 and 0.3 km^3, respectively. As stated previously, a negligible amount of this magma has actually been erupted.

Of the possible scenarios for excess sulphur degassing, the purely basaltic nature of Masaya, the ophiolitic basement and lack of subducted sediment, the lack of any significant observable hydrothermal system, and the negligible volume of erupted magma suggest that buoyancy-driven magma circulation is a reasonable mechanism for transporting low density, gas-rich magma to the surface.

2.7.3. Open vs. Closed system behaviour at Masaya

A common question for volcanoes that are characterised by persistent activity is whether they are open systems continuously supplied from depth, or whether they are closed, slowly degassing and cooling systems. At Masaya, the persistent degassing over the last ~150 years and negligible variation in S/Cl ratios (Horrocks et al., 1999; Bulletin of the Global Volcanism Network, 2000) suggest that the system can be considered to be essentially open. It also has been suggested that individual gas episodes result from degassing of batches of magma emplaced in a small shallow surface reservoir (Figure 2.2; Stoiber et al., 1986) and raises the question as to the ultimate fate of this degassed magma. These batches may originate from a larger, deeper (mid-crust), vigorously convecting reservoir that is open to periodic influx of more primitive magma (Walker et al., 1993).

Masaya's history of periodic lava lake formation and persistently glowing vents with occasional strombolian activity suggest that there is magma no more than a few tens of metres below the surface (Rymer et al., 1998a). Active lava lakes are characterised by very stable volumes; since no lava is erupted, circulation and convection are required for mass balance (Francis et al., 1993). Recent remote sensing insights allow us to estimate the heat and mass flux and thus cooling rate of the active lava lake or glowing vent at Masaya (Harris et al., 1999 and references therein).

For either an active lava lake or glowing vent scenario, the total thermal flux, Q_{tot}, is equal to $Q_{rad} + Q_{conv} + Q_{cond} + Q_{gas} + Q_{ejecta}$, which are the heat fluxes of radiation, convection, conduction, degassing and ejecta, respectively (Equations 1-5, Appendix C). As only insignificant amounts of material have been erupted from Masaya since the formation of Santiago crater, Q_{ejecta} is considered to be negligible. The majority of the parameters required to determine Q_{tot} are known constants or reasonable estimates taken from the literature (Appendix C, Table C.1). However, the crucial variables for Masaya are the total gas flux and vent area and temperature. The total gas flux and water flux for Masaya are estimated from COSPEC and FTIR measurements (Table 2.3), while vent temperatures have been measured between 1993 and 2000 (Table 2.4).

For a vent area of 100 m^2, vent gas temperature of 300°C, magma depth of <100 m, and average SO_2 flux of 1700 t d^{-1}, the total thermal flux (Q_{tot}) is calculated to be ~1600 MW, of which 99% is produced directly from gas heat flux (Q_{gas}). Variations in the vent temperature have minor effects on the total thermal flux, ranging from 1586 to 1602 MW for temperatures between 100 and 1000°C. During periods of lava lake activity the significant increase in exposed surface area (e.g., 0.13 km^2 for the pre-1965 lake in Santiago) greatly increases the thermal flux (Q_{tot} = ~7100 MW). In this case, radiation and convection become the controlling factors, responsible for over 80% of the thermal flux.

Using the total thermal flux (Q_{tot}), one can obtain a first-order estimate of the rate at which magma will cool (h_c/°C yr^{-1}; Appendix C, Eqn. 6). As the magma in active lakes and glowing vents is by definition not solid, cooling is from its liquidus to near its solidus temperature ($\Delta T_{l\text{-}s}$ ~150°C; Archambault and Tanguy, 1976; Harris et al., 1999). Thus, the time required to cool a volume of magma by ~150°C is estimated by $h_c/\Delta T$. For the small, glowing vent degassing scenario (~1700 t d^{-1} SO_2 flux) and small magma volume (0.5 km^3) of the order of that degassed since 1993, a cooling time of ~5 years is required to cool the magma from liquidus to just above the solidus (Figure 2.5). If a magma volume

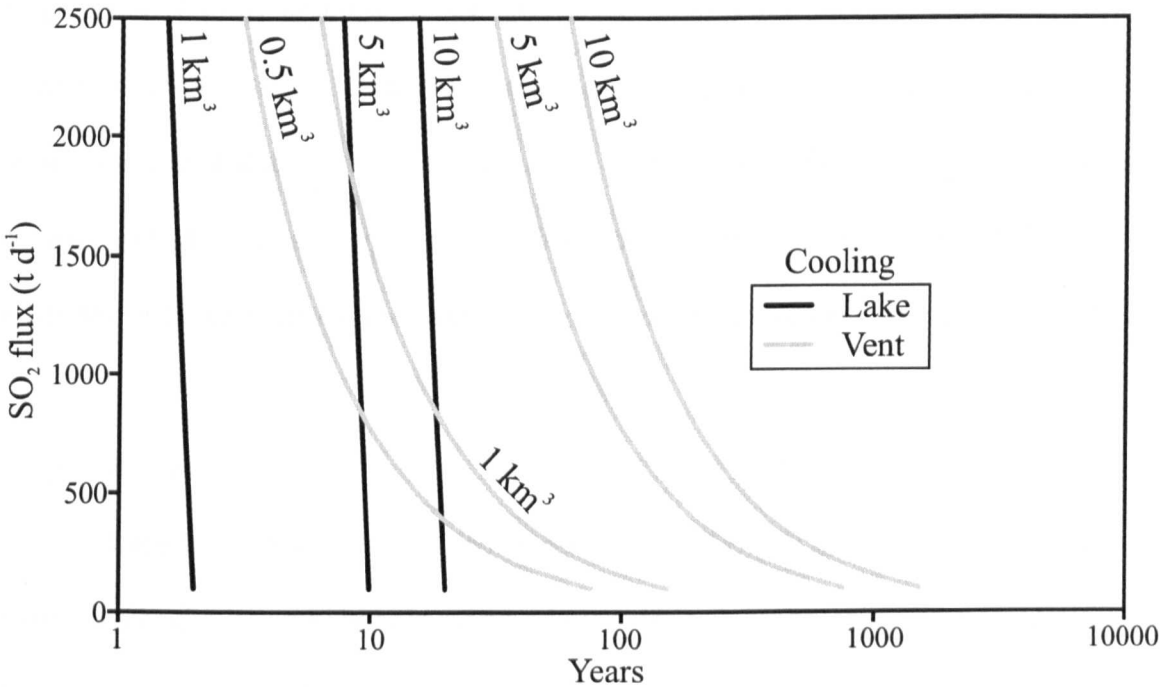

Figure 2.5: Cooling (from liquidus to near solidus) for magma volumes of between 0.5 and 10 km^3, depending on emission rate of SO_2. Black lines represent cooling during a lava lake scenario, grey lines denote cooling during a small open-vent degassing scenario. Cooling in a conduit is modelled as a cylinder. See Appendix C for relevant parameters and equations.

of 1 km^3 is used, as suggested by Stoiber et al. (1986), cooling times are ~9 years. The lava lake, with its significantly larger cooling surface, requires 1.6 years to cool (Figure 2.5). At lower degassing rates (e.g., 1000 t d^{-1} SO_2 flux), cooling times of ~15 and 1.8 years are required for the vent degassing and lava lake scenarios, respectively. As Masaya has gone through periods of lava lake activity (rapid cooling) and open vent degassing (slower cooling), the cooling rate during the last ~150 years is probably somewhere between the two. In the unlikely case that there is a shallow 10 km^3 reservoir present (as suggested by Walker et al., 1993), it would take ~90 and ~16 years to cool from liquidus to just above the solidus for the degassing and lava lake scenarios, respectively. If Masaya were a completely closed system, a 10 km^3 reservoir should have cooled to within its solidus since the formation of Santiago crater. Even if one accepts that Masaya is an open system, it is apparent that any reservoir (shallow or deep) must be episodically recharged, while the cooler degassed magma is removed (Figure 2.2).

2.7.4. Foam collapse

A mechanism that may influence persistent activity at Masaya is the formation of a foam layer due to gas bubble accumulation in a low-viscosity system (Jaupart and Vergniolle, 1989). There may in fact be a series of foam layers which develop immediately beneath the crater floor (as suggested by Rymer et al., 1998a) and deeper, at the roof of the shallow reservoir (Figure 2.2). The stability of a foam layer is essentially controlled by the flux of bubbles from depths (thickening) and flow of bubbles toward a conduit (thinning) and thus is critically affected by the mass flux of gas (Vergniolle and Jaupart, 1990). The generally consistent SO_2 flux rates measured at Masaya during a given degassing episode may be indicative of a steady foam flow regime (Jaupart and Vergniolle, 1989). In this regime, steady degassing causes bubbles to accumulate into a "permanent" foam layer which flows along the roof of the reservoir and escapes into the

conduit. In some cases, however, this foam layer may collapse, due perhaps to changes in the degassing rate, and lead to large gas jets or fire fountaining (Vergniolle and Jaupart, 1986). High velocity eruptions of low viscosity magma by gas jetting or fire fountaining are believed to be in part responsible for the formation of Pele's hair (Duffield et al., 1977; Shimozuru, 1994) such as that found around the Nindiri cone at Masaya. At a much smaller spatial and temporal scale, bubble accumulation and collapse in the voids immediately beneath Santiago crater may be somewhat responsible for the puffing observed on time scales of seconds to minutes. While foam development may be a factor influencing persistent degassing at Masaya, the mechanism responsible for changes in the degassing rate must be explained. A small amount of material has been ejected to date and textural analyses of these samples could shed light on the potential existence of this foam layer.

2.7.5. Convection

As stated above, episodes of strong magma degassing occur repeatedly at Masaya. However the mechanism that controls this process is poorly understood. Since the formation of Santiago crater in 1853, elevated degassing has been accompanied by the eruption of negligible amounts ($<10^3$ kg) of this degassed magma and during this same period, significant volumes of magma would have cooled to near-solidus temperatures with a consequent increase in density. As the intrusion of magma into the volcanic edifice is not supported by geophysical data (i.e., gravity or deformation measurements can show changes from metres to tens of km depth; Rymer et al., 1998a; Delmelle et al., 1999; Chapter 3), convective removal of this degassed, cooled and dense material is therefore necessary.

Degassing-driven convection of magma within a conduit has been shown to be a plausible mechanism for degassing from a magma reservoir at up to several kilometres

depth (Kazahaya et al., 1994; Stevenson and Blake, 1998). For an average gas flux similar to that of 1998-2000 (1700 ± 510 t d^{-1}), a mass rate of magma degassing of 0.7-1.2 x 10^4 kg s^{-1} is calculated assuming initial S contents of 1500 and 800 ppm, respectively, and can be assumed to represent the ascent rate of non-degassed magma. In a simple model of Poiseuille flow in a double-walled pipe, Kazahaya et al. (1994) showed that only a small density contrast (caused by degassing) was required to maintain convection with an inferred ascent rate of 1 x 10^4 kg s^{-1} in ~10 m diameter conduit. It may therefore be a plausible mechanism in a low viscosity system such as Masaya. Furthermore, it will complement thermal convection which, due to the large heat flux and subsequent thermal gradient within the plumbing system, must be occurring at Masaya.

2.8. Conclusions

The magmatic plumbing system at Masaya may be viewed as a near-surface magma body linked to, and periodically replenished by, a long-lived crustal magma reservoir (Figure 2.2). Once buoyant gas-rich magma from deep levels is emplaced near the surface, it will convect, degas vigorously, cool, crystallise and increase in density. Approximately 1.2 x 10^9 kg of sulphur was emitted at Masaya from mid-1993 through April 2000 suggesting that up to 0.6 km^3 of magma had been degassed at shallow levels since reactivation. Gas-rich material continually arrives at the shallow vesiculated layer where it degasses, cools and then sinks to be replaced by gas-rich magma rising from depth. This degassed and denser material is not being intruded into that edifice and must therefore be removed from the system; thermal and degassing-driven convection is the most reasonable mechanism to achieve this.

While orders of magnitude more SO_2 can be erupted explosively by volcanoes such as Mount Pinatubo, the persistent activity of Masaya makes it a significant source of degassing, with up to 21 Tg SO_2 emitted since the formation of Santiago crater. In the

most recent degassing episode, Masaya alone was responsible for 4.6% and ~1.5% of the annual global subaerial volcanic SO_2 and CO_2 emissions, respectively. Thus, although Masaya is not in continuous activity, its prolonged history of intense periodic degassing has likely resulted in serious localised environmental impact over time.

Continued measurement of combined geochemical, gas emission and composition through integrated COSPEC and FTIR studies will allow us to better constrain the evolution of this and other magmatic systems. Furthermore, recent studies of short-lived radioisotopes in erupted gasses (Gauthier et al., 2000) may prove useful in determining the residence time and supply rate of magma in the upper reservoir and plumbing system. The installation of a permanent seismic network would also better constrain the actual sizes and depths of reservoirs and the plumbing system and facilitate further investigation of persistent degassing at Masaya.

Chapter 3.

Gravity changes and passive degassing at the Masaya caldera complex, Nicaragua

---

To be submitted to the Journal of Volcanology and Geothermal Research

3.1. Abstract

A better understanding of the mechanisms responsible for persistent volcanism can be acquired through the integration of multiple geophysical and geochemical data sets. By interpreting micro-gravity, deformation and SO_2 flux data collected at Masaya volcano since 1993, it is now apparent that the characteristic cyclical nature of activity is not due to the intrusion of fresh magma. Rather, it is due in large part to the convective overturn of pre-existing magma immediately beneath the active crater and at greater depth. Buoyant gas-rich magma rises from depth and is emplaced near the surface, resulting in the formation and fluctuation of a low-density gas-rich layer centred beneath Nindiri and Santiago craters. As this magma vigorously degasses, it will cool, increase in density and convect downwards. Four stages of activity have been identified, with the most recent data suggesting that the system may be entering another period of reduced degassing.

3.2. Introduction

Located in western Nicaragua, Masaya is a persistently active basaltic shield volcano and caldera complex (Figure 3.1). Thought to have formed between ~2250 and

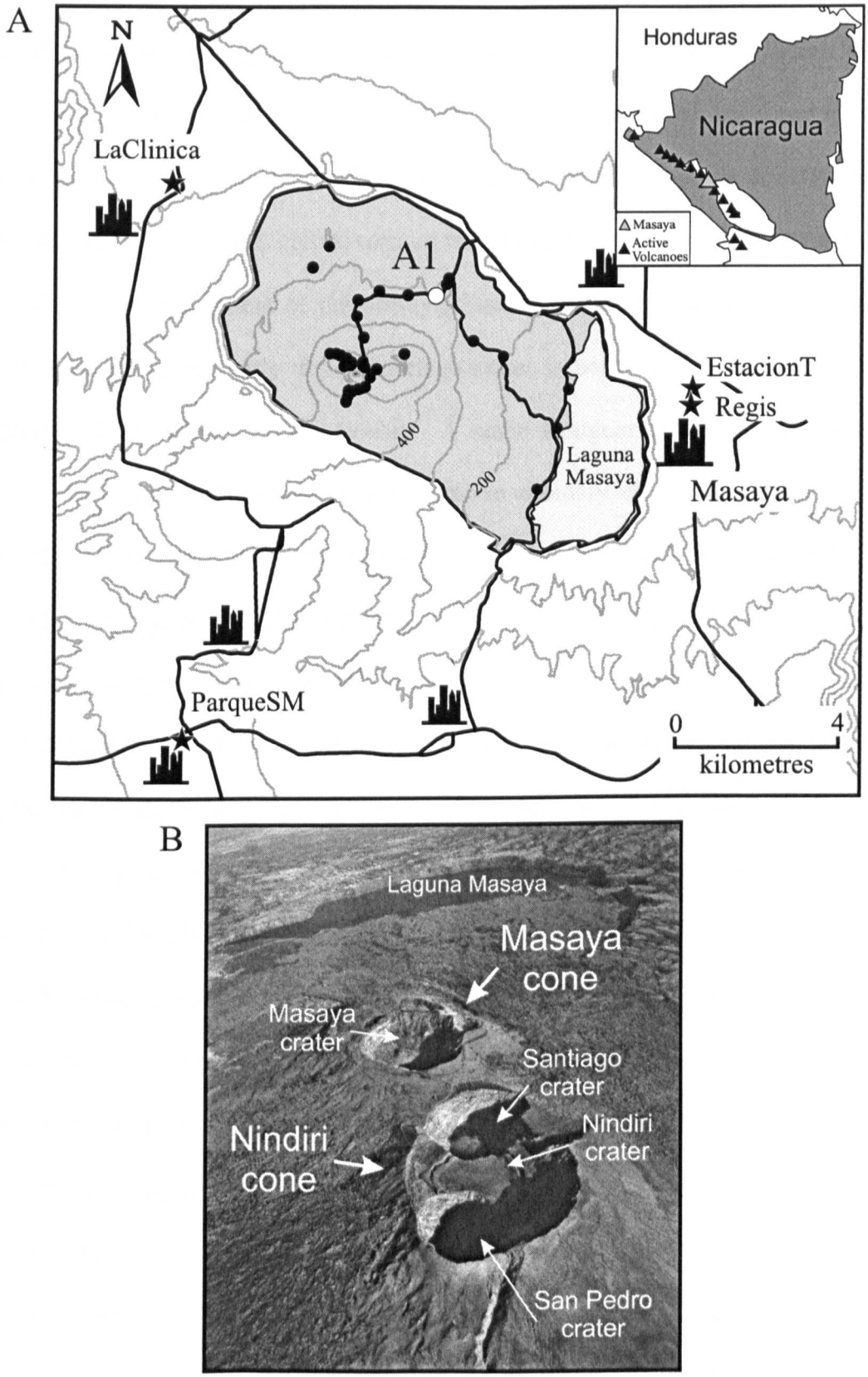

Figure 3.1: a) Masaya caldera (shaded area) with the inter-caldera gravity/GPS stations (black dots) and extra-caldera reference stations (black stars). All gravity measurements are quoted relative to station A1 (white dot). Contours are 100 m. Inset map indicates Masaya (grey triangle) and the active volcanoes (black triangles) of the Central American Volcanic Front. b) Aerial view of Masaya and Nindiri cones from the northwest

6500 BP by a series of large basaltic ignimbrite eruptions (8 km^3), Masaya caldera is believed to be underlain by a 10 km^3 open-system magma reservoir (Williams, 1983a,b; Walker et al., 1993; van Wyk de Vries, 1993). A basaltic complex has developed within the caldera from eruptions along an arcuate series of vents. The main activity has led to the formation of the Masaya and Nindiri cones. Multiple episodes of pit crater formation have led to the development of the Masaya, Santiago, Nindiri and San Pedro pit craters (Figure 3.1b). The currently active Santiago crater is believed to have formed in 1853 (McBirney, 1956; Rymer et al., 1998a). A static Bouguer gravity survey carried out between 1991 and 1992 revealed a large positive anomaly off centre with respect to the main axis of the caldera and thought to be due to a dense relatively shallow body (2-3 km b.s.l.) emplaced prior to caldera formation (Métaxian, 1994). There is, however no significant Bouguer gravity anomaly associated with the present magma system and current activity at Santiago crater. Seismic and magnetotelluric studies however do indicate the presence of a very shallow magma body resident immediately beneath the floor of Santiago crater, while volcano-tectonic earthquake hypocentres were found to be at depths of ~1.5 km b.s.l. (Métaxian, 1994; Métaxian et al., 1997).

Prolonged episodes of passive degassing and oscillations in the level of the magma column, the top of which is occasionally visible within the vent or as a lava lake, are characteristic of activity at Santiago crater. There may have been at least five cycles of degassing and frequent changes in the magma column height since the formation of Santiago crater in 1853 (Stoiber et al., 1986; Rymer et al., 1998a). The most recent cycle of activity began in May 1993 and continues to the present (Bulletin of the Global Volcanism Network, 1970-2000; Rymer et al., 1998a). An excellent means of studying this activity is through the integration of dynamic micro-gravity surveys with SO_2 flux measurements by ultraviolet correlation spectrometry (COSPEC).

3.3. Methodology

3.3.1. Dynamic micro-gravity and deformation

Subsurface mass and density changes within a volcano can be quantified and located using a combination of high-resolution ground deformation and micro-gravity monitoring techniques. I have increased the monitoring network, initially installed at Masaya by S. Bonvalot (ORSTROM), Métaxian (1994) and Rymer et al. (1998a), to 38 stations across the caldera (Figure 3.1, 3.2; see Appendix A for full descriptions of station locations). For this study, micro-gravity measurements were made during 5 field campaigns between January 1998 and March 2000 using the LaCoste and Romberg gravity meter G513; the same instrument used by Rymer et al. (1998a) for measurements between 1993 and 1997. Gravity values are quoted relative to the base station A1 which has previously been assumed to be outside the area of gravity variation (Figure 3.1, 3.2; Rymer et al., 1998a). In order to confirm that gravity at this base station remains stable, a series of 4 secondary reference stations were installed in 1998 (Regis) and 1999 (LaClinica, ParqueSM, EstacionT) outside the caldera, at distances of up to 15 km from the active craters (Figure 3.1). Results are detailed in section 3.4.1. All raw gravity measurements have been corrected for the effects of solid Earth tides using software developed by Broucke et al. (1972). More detailed descriptions of the technique can be found in Appendix D.

It is frequently possible to achieve high precision micro-gravity measurements (~10 μGal) at volcanoes when following strict survey procedures (Rymer, 1989). However, in the case of Masaya, the continuous degassing-induced volcanic tremor (Métaxian et al., 1997) and potential for temporary "tares" from this seismic noise (Davies et al., 2000) makes precise measurements difficult. Therefore, the uncertainty in a single measurement is estimated at 20 μGal. In fact, this is a conservative estimate, as each value is actually the difference between measurements at two stations (e.g., A7 – A1).

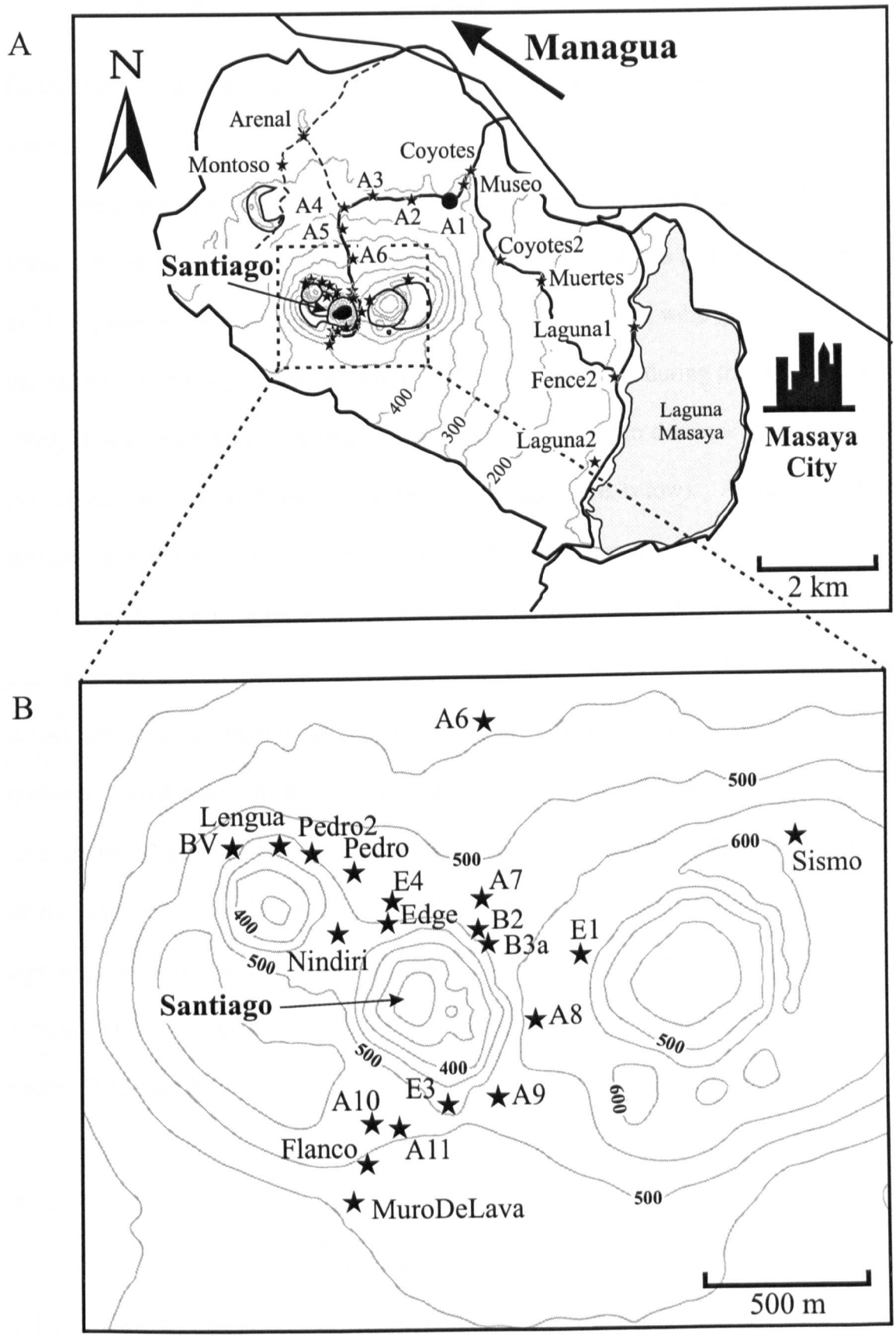

Figure 3.2: Map of a) the distal (>2 km from Santiago crater) and b) proximal inter-caldera gravity/GPS stations (black stars). Black dot is the reference base station A1. Contour interval is 50 m.

Thus, the uncertainty on these $\frac{20\mu Gal}{\sqrt{2}} \approx 14\mu Gal$ (3.1)

Furthermore, each value has actually been measured between 1 and 5 times during each survey.

Seasonal effects can produce significant apparent gravity changes. However, at Masaya the effects are generally quite limited as the water table is at a depth of at least 300 m. For consistency and ease of measurement, field campaigns were generally carried out during the dry season (January to April). One field campaign during the wet season (June 1999) showed no obvious seasonal effect (gravity continued to decrease at a similar rate to that of the previous and subsequent field campaigns; see below). A seasonal effect is therefore not thought to be a significant factor in the discussion below.

Ground deformation over the entire network was measured at least once every field campaign using a Leica GPS 200 dual-frequency differential receiver, following strict survey procedures (Murray et al., 1995; Rymer, 1996). Due to technical problems however, height measurements are unavailable for the June 1999 campaign. Nevertheless, measurements made during the 4 other field campaigns, and for that matter, since the start of measurements in 1993, suggest that elevation changes have been below the level of significance in affecting gravity measurements (<2-4 cm; Appendix D, F; Rymer et al., 1998a). The typical effect of such a height change on gravity measurements is discussed in section 3.3.2 and 3.5.

3.3.2. Free Air Gradient measurements

Gravity varies with elevation along the free air gradient (FAG) which has a theoretical value of –308.6 μGal m^{-1}. However, terrain effects and Bouguer anomalies can cause this value to differ by up to 40% from the theoretical value (Rymer, 1994 and references therein). Therefore, when possible, the actual FAG should always be measured at each

station during a micro-gravity/deformation survey (Berrino et al., 1984; Yokoyama, 1989; Rymer, 1994). This was easily accomplished at Masaya by making micro-gravity measurements first at the surface and then some distance off the ground (e.g., ~1 m using a levelling tripod). The difference in gravity (Δg) is then divided by the difference in elevation (Δh) to obtain the FAG.

3.3.3. SO_2 gas flux

A valuable means of studying the current degassing episode at Masaya is through the use of a COSPEC that allows for the measurement of SO_2 flux (metric tonnes per day; t d^{-1}). For this study, the COSPEC was mounted in a vehicle and repeatedly driven along routes crossed by the volcanic plume, allowing for vertical scans of the plume. Detailed descriptions of the results and technique can be found in Chapter 2 and Appendix B, respectively.

3.4. Results

3.4.1. Dynamic micro-gravity and deformation

As mentioned above, dynamic or "relative" micro-gravity entails relating measurements at a given station to a base station (A1 for Masaya). However, this assumes that gravity at this base station is invariant. In order to confirm this supposition, four reference stations were installed outside the caldera in 1998 and 1999, with measurements made at least once (for the more distal stations of LaClinica, ParqueSM and EstacionT) during a given field campaign (Figure 3.3). The first reference station, Regis, proved to be quite unstable with respect to A1, likely due to the poor placement of the station. Located in the Hotel Regis, the station was quite "noisy" because of vibrations from the movement of the many hotel guests and major renovations. The more distal stations were therefore

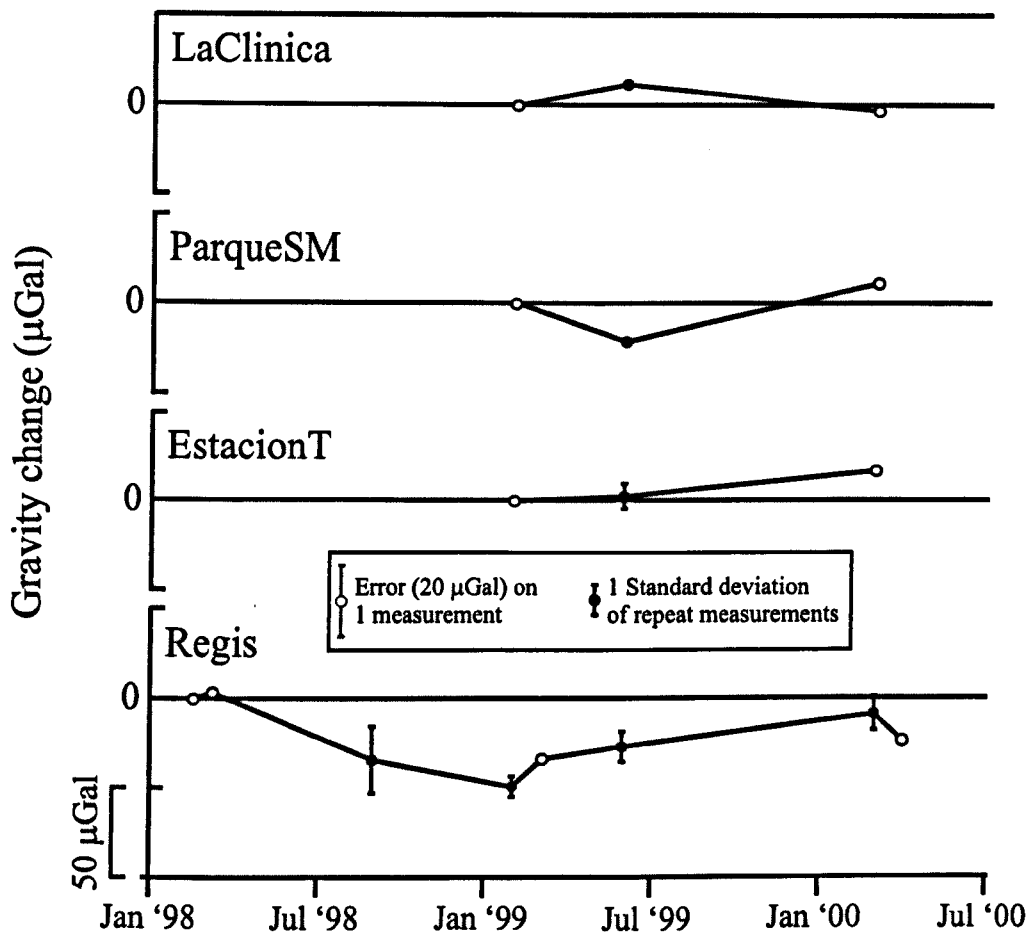

Figure 3.3: Gravity changes at 4 reference stations outside the caldera (relative to A1). Black circles denote repeat measurements; white circles denote a single measurement. See Figure 3.1 for station locations.

installed and generally show variations of less than 20 μGal at a 95% confidence level relative to station A1. This confirms that A1 is stable with respect to the outer caldera region. This is further supported by data from the inter-caldera stations located at least 2 km from Santiago crater. A majority of these distal stations fall within 20 μGal of zero at a 95% confidence level. A few show irregular variations >20 μGal, but these variations are likely to be the consequence of secondary effects such as instabilities in the station location. For example, Muertes and Coyotes2 are located on an asphalt road and Laguna1 and 2 are very close to the edge of Laguna Masaya and may be affected by variations in water level (Figure 3.2, Appendix F). Furthermore, the lack of any consistent trends in gravity values of distal stations suggests that the variations are not related to changes in volcanic activity (Figure 3.4). These stations are therefore not considered further.

Between February 1993 and April 1994, summit stations underwent a gravity decrease of ~70 μGal, followed by a gradual increase of up to 56 μGal (station A10) between April 1994 and March 1997 relative to station A1 (Figure 3.5, Rymer et al., 1998a). This was followed by a second relatively consistent gravity decrease of ~50 μGal yr^{-1} between March 1997 and June 1999; of the same order as that observed between 1993 and 1994 (Figure 3.5). A more detailed investigation of the post-1997 data confirms the gravity decrease between March 1997 and June 1999 and also reveals an apparent "levelling off" of the gravity variations between June 1999 and April 2000 (Figure 3.6).

The spatial extent of gravity change between 1993 and 1994 indicates a crater-centred negative anomaly of at least -90 μGal (Figure 3.7b; Rymer et al., 1998a). Compared to other summit stations, E3 appeared to behave anomalously between 1993 and 1994 (Figure 3.5). This was thought to be due perhaps to an unreliable initial reading in 1993, dilation of fissures on the crater edge, or the station's close proximity to the crater rim indicating larger gravity changes within the crater (Rymer et al., 1998a). However, the

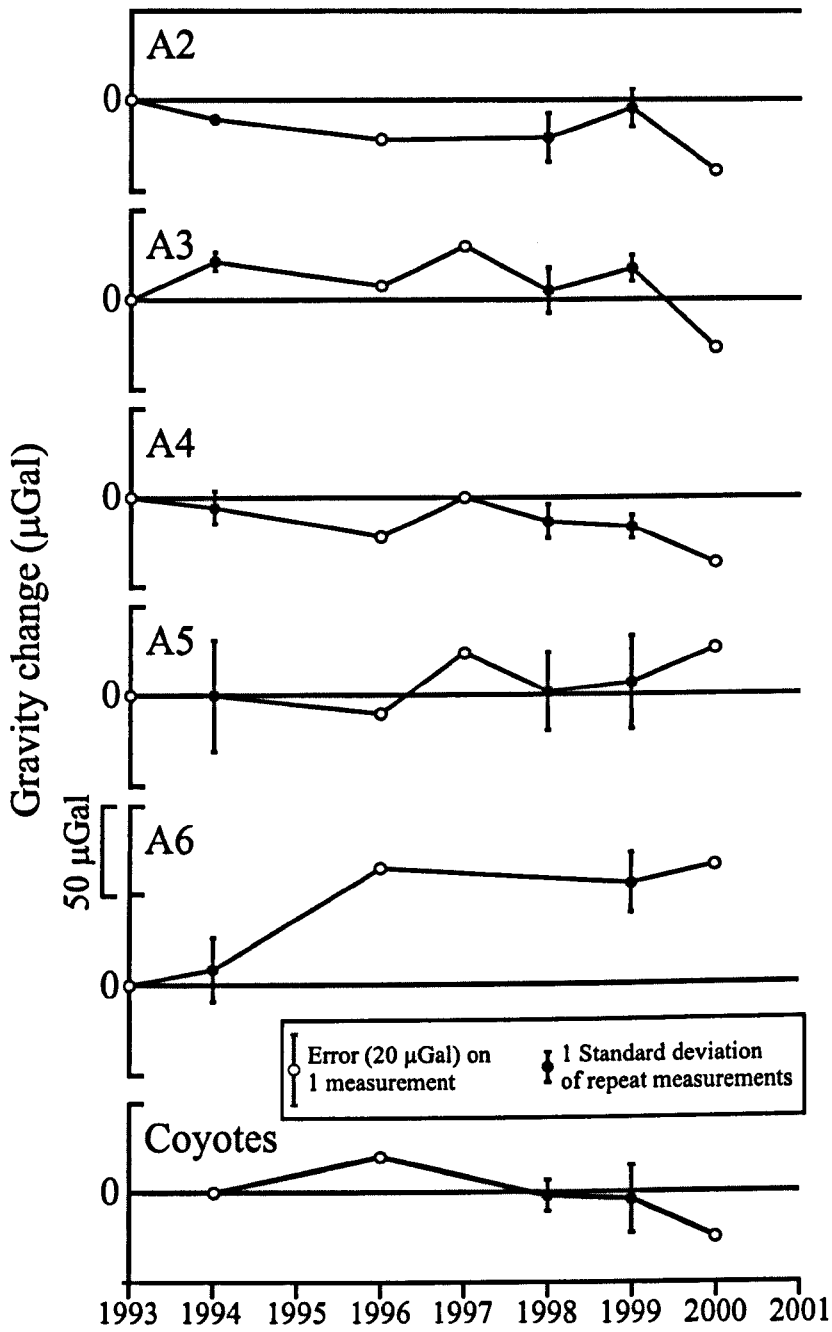

Figure 3.4: Gravity changes at representative distal stations (>2 km from summit) quoted relative to A1. Black circles denote repeat measurements; white circles denote a single measurement. The apparently large gravity change at station A6 between 1994 and 1996 is likely due to a poor initial measurement. See Figure 3.1 for station locations.

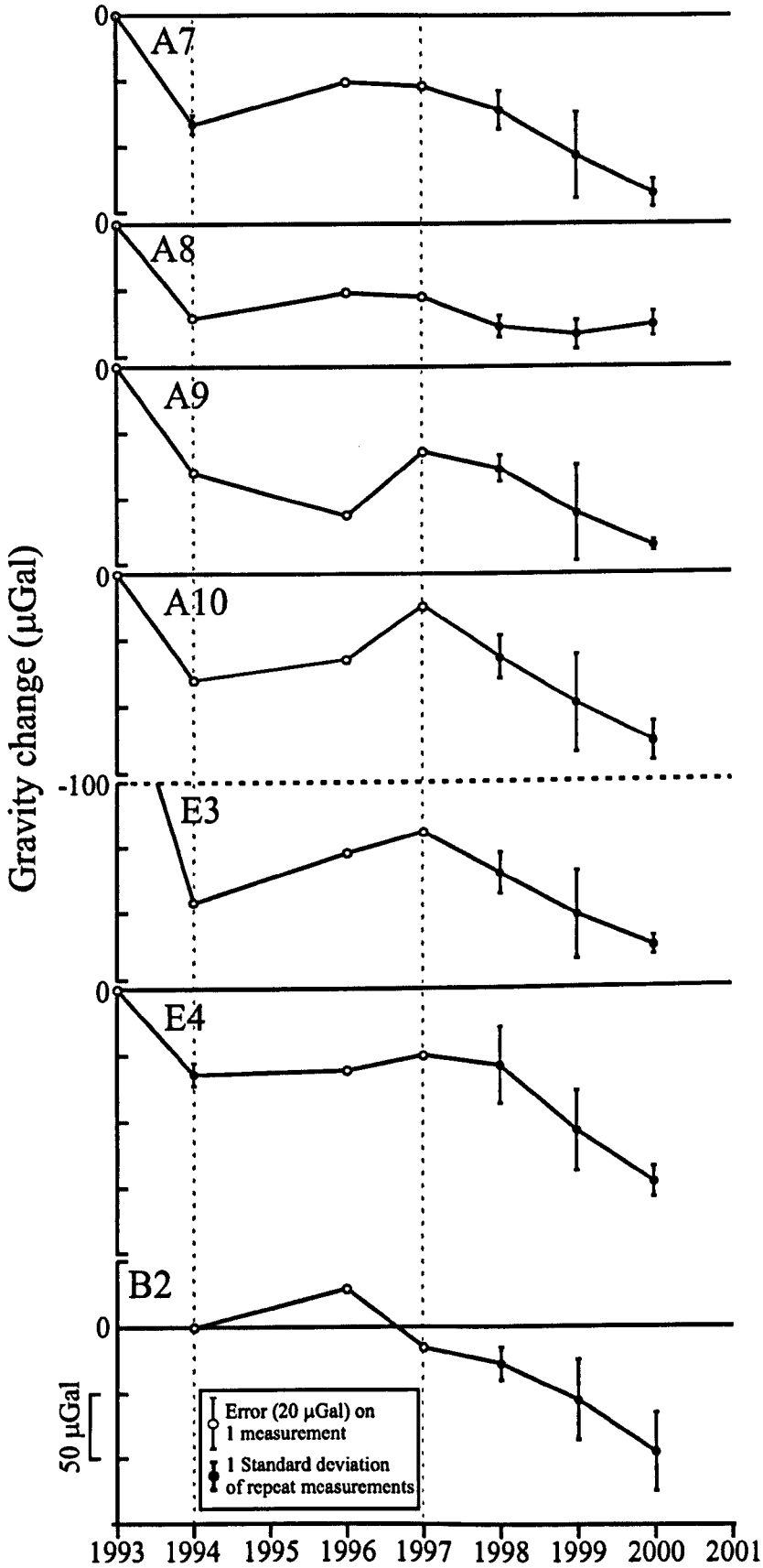

Figure 3.5: Average yearly gravity changes at summit stations (relative to A1) within Masaya caldera. Black circles denote repeat measurements (i.e., average of all measurements that year); white circles denote single measurements. Dashed lines highlight the end and beginning of the 1993-1994 and 1997-1999 periods of gravity decrease, respectively. Note that E3 starts at -100 μGal.

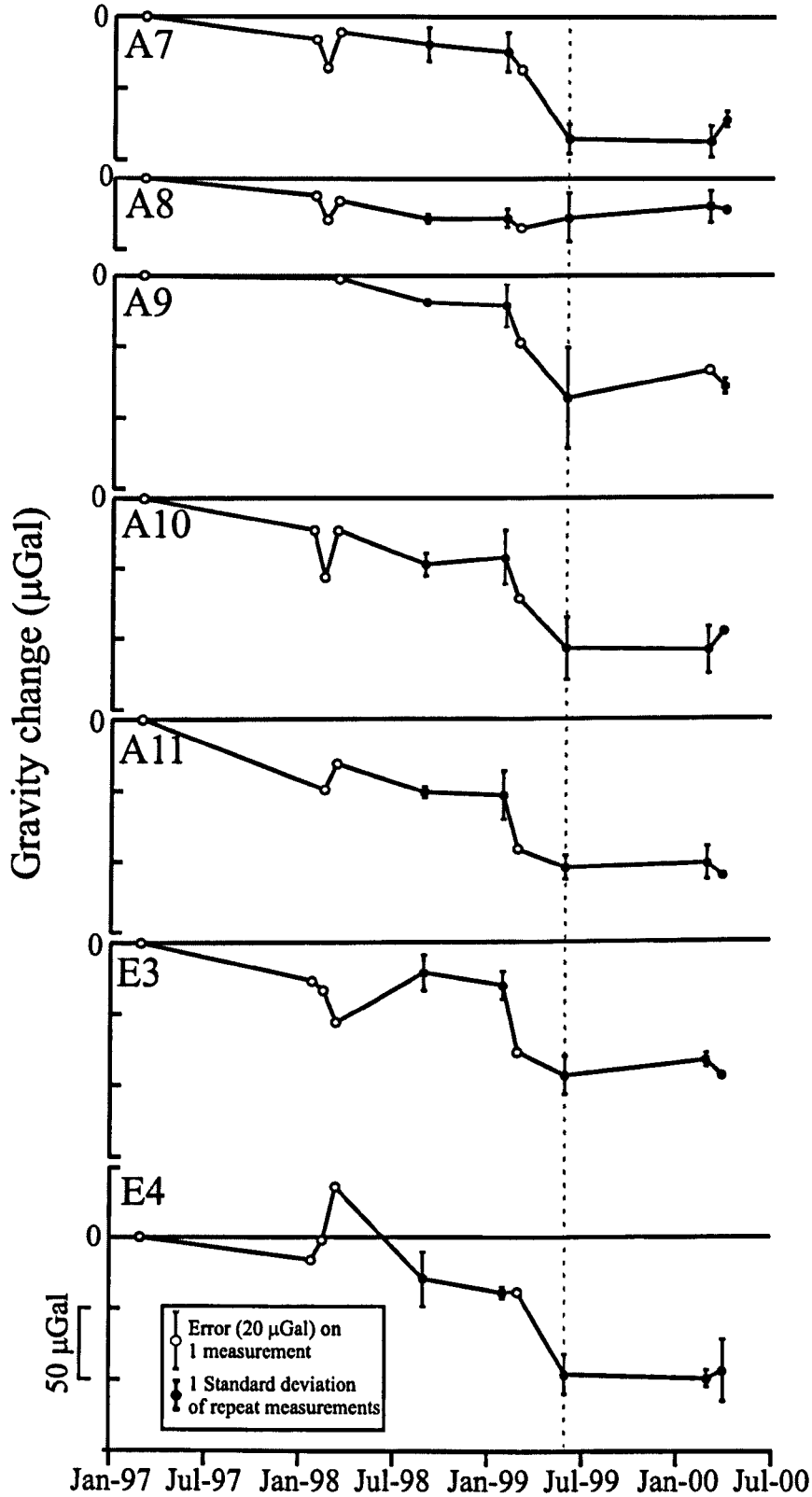

Figure 3.6: Monthly average gravity changes at summit stations between 1997 and 2000 (quoted relative to station A1). Black circles denote repeat measurements; white circles denote single measurements. Dashed line highlights the end of the 1997-1999 period of gravity decrease.

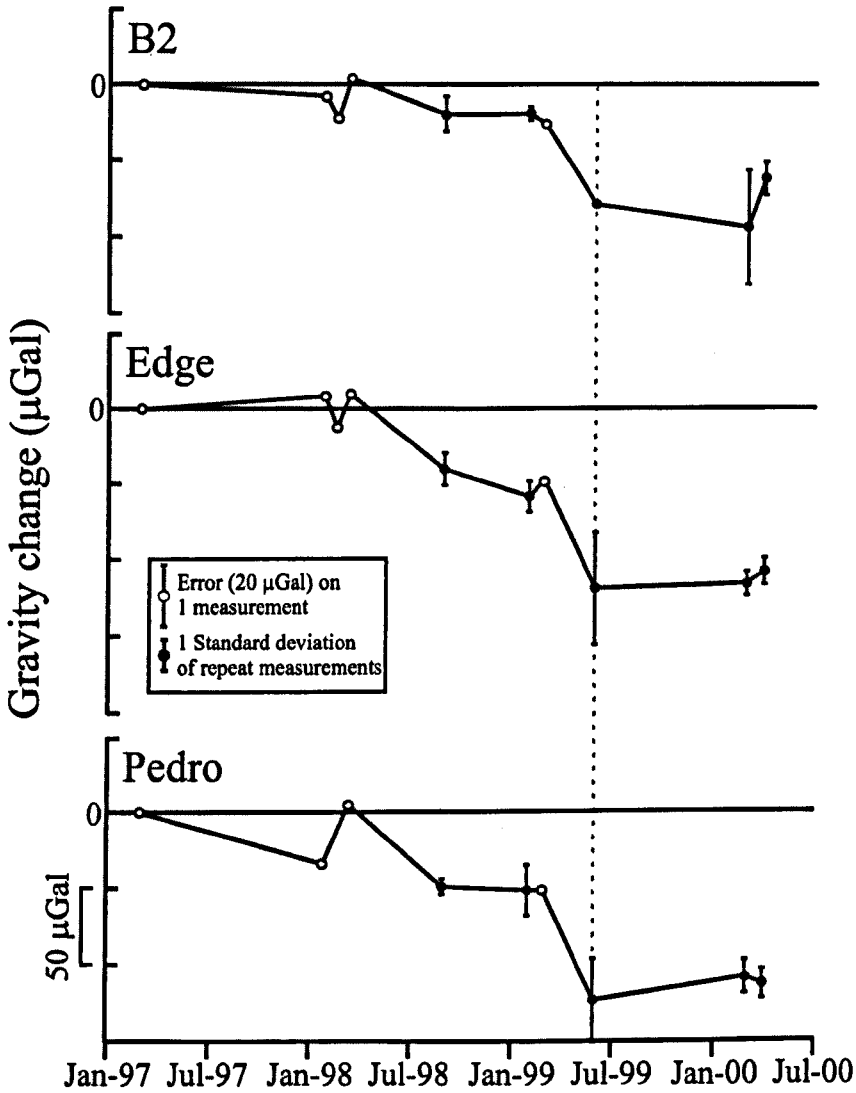

Figure 3.6: Continued.

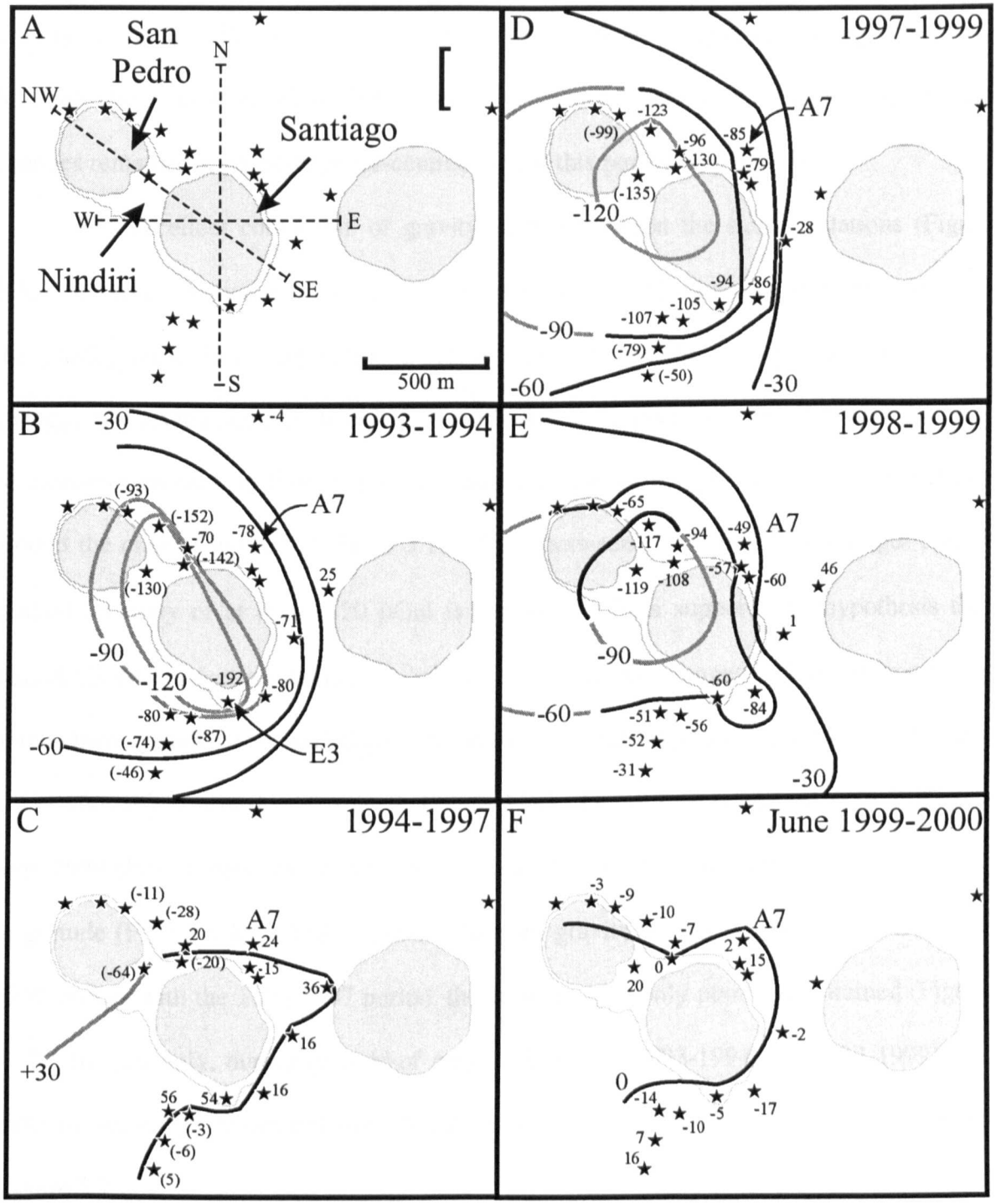

Figure 3.7: Schematic contour maps of approximate gravity change through time for b) 1993-1994, c) 1994-1997, d) 1997-1999, e) 1998-June 1999, and g) June 1999-2000. Numbers at stations indicate gravity changes for each station quoted relative to A1. Numbers in parentheses are estimated values. Grey contours are based on estimated values. Contour interval is 30 μGal. a) Dashed lines represent NS, WE and NW-SE profiles for Figure 3.10. Note station A7 for reference.

paucity of summit stations during this period makes it difficult to fully constrain the gravity anomaly. The installation of additional crater rim stations during this study between 1997 and 1999 allows for a better-constrained anomaly and suggests that gravity changes remained essentially crater-centred during this period (Figure 3.7d).

The excellent correlation of gravity change between the summit stations (Figure 3.5, 3.6, Table 3.1), irrespective of absolute amounts, can also be used to better constrain the gravity anomalies. By taking a linear regression of the average monthly gravity changes of selected summit stations (1998-2000) with respect to station A7, new data can be extrapolated back in time to provide semi-quantitative insights into gravity variations around the crater (Figure 3.7, Table 3.1). Thus, between 1993 and 1994, a larger crater-centred anomaly of at least -120 μGal is suggested. This supports the hypothesis that station E3 was in fact representative of even larger gravity changes within the crater. As noted above, gravity increased slightly between 1994 and 1997, although the lateral extent of the anomaly is poorly constrained (Figure 3.7c). Gravity decreases between 1997 and June 1999 show a very similar anomaly to that of 1993-1994, in both spatial extent and magnitude (Figure 3.7d). There was no observed gravity change between June 1999 and 2000, and as with the 1994-1997 period, the anomaly was only poorly constrained (Figure 3.7f). Interestingly, during periods of gravity decrease (1993-1994 and 1997-1999), the anomaly seems to be centred over Nindiri crater rather than the active Santiago crater (Figure 3.7).

3.4.2. Free Air Gradient

In June 1999, free air gradient measurements were made at 19 of the 38 network stations across the caldera. As would be expected, the FAG at Masaya is essentially controlled by topography, ranging from –250 μGal m^{-1} at distal stations (> 2 km from Santiago) up to –390 μGal m^{-1} at summit stations; the average FAG for summit stations is

Table 3.1: Correlations (R^2) of monthly average gravity changes from selected summit stations with respect to station A7.

Station	1993-2000	1998-2000
A8*	0.5459	0.3197
A9	0.8247	0.9511
A10	0.9185	0.9486
A11		0.8253
E1*	0.4499	0.4690
E3	0.7437	0.8099
E4	0.8489	0.9386
B2	0.9180	0.7963
Edge		0.9355
Pedro		0.9564
Pedro2		0.7992
MuroDeLava		0.9021
Flanco		0.9254
Nindiri		0.9253

*Poor correlations are likely due to topographic effects.

-340 μGal m^{-1}. As there has been insignificant change in elevation (in terms of micro-gravity) at Masaya, the FAG measurements provide little information. However, continued of measurements of the FAG may prove useful in monitoring changes in activity in the future.

3.4.3. SO_2 Flux

The most recent degassing episode at Masaya was preceded by weak fumarolic activity (throughout the early 1990s) leading to increased degassing in May 1993 with a "diffuse white sulphur-rich plume" observed several kilometres from Santiago crater (Bulletin of the Global Volcanism Network, 1970-2000; Rymer et al., 1998a). In contrast to an April 1992 COSPEC measurement of <10 t d^{-1} (Bulletin of the Global Volcanism Network, 2000), comprehensive COSPEC monitoring started in 1996 showed moderately elevated emissions of 600 ± 290 t d^{-1} and 390 ± 200 t d^{-1} in March 1996 and February-March 1997, respectively (Figure 3.8; Rymer et al., 1998a; Delmelle et al., 1999). These rates increased significantly in 1998 and 1999 to 1850 ± 960 t d^{-1} and 1650 ± 560 t d^{-1}, respectively. The most recent measurements (March-April 2000) show a possible decrease in the average SO_2 flux to 1310 ± 430 t d^{-1}.

The rate at which magma degassed during these same periods can be estimated from the measured gas flux. Using the degassing data presented in Chapter 2, it is estimated that between 2.0 x 10^8 and 6.5 x 10^8 kg yr^{-1} of SO_2 were emitted between 1993 and 2000 (Table 3.2). Based on Fourier Transform Infrared (FTIR) spectroscopic measurements of the major gas species in the plume, the emission rate of total gas during these periods ranges from 4.3 x 10^9 to 1.4 x 10^{10} kg yr^{-1} (Chapter 2, Table 3.2). Assuming initial sulphur contents (in the melt) of between 270 and 1500 ppm, the minimum rate of magma degassing for these intervals varied between 7.3 x 10^{10} and 1.2 x 10^{12} kg yr^{-1} (Table 3.2).

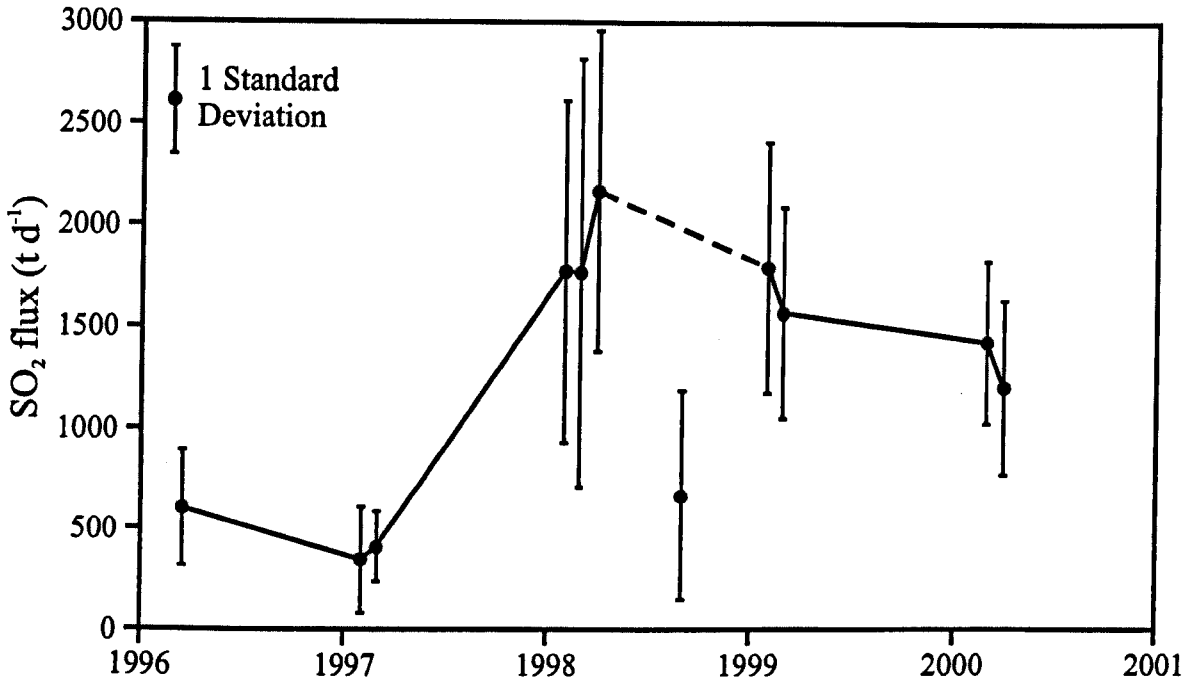

Figure 3.8: Average monthly SO_2 flux measured downwind from Santiago crater. Black circles represent an average of 43 measurements (ranging from 8 to 99 measurements) for a given month, where a measurement is one complete transect beneath the plume. Note that the measurements in September 1998, the only wet season data on this plot, are probably anomalous due to environmental effects (rain and low wind speeds) and are not considered representative (see Chapter 2 for more detail).

Table 3.2: SO_2 and Total gas flux and estimated magma degassing rate from Masaya, 1993-2000.

Degassing period	SO_2 flux (kg yr_{-1})	Total gas flux (kg yr_{-1})	Magma degassing rate (kg yr^{-1}) assuming initial melt S concentrations		
			270 ppm	800 ppm	1500 ppm
1993-1994	2.2×10^{8}	4.7×10^{9}	4.1×10^{11}	1.4×10^{11}	7.3×10^{10}
1994-1997	2.0×10^{8}	4.3×10^{9}	3.7×10^{11}	1.3×10^{11}	6.7×10^{10}
1997-1999	4.8×10^{8}	1.0×10^{10}	8.9×10^{11}	3.0×10^{11}	1.6×10^{11}
1998-1999	6.5×10^{8}	1.4×10^{10}	1.2×10^{12}	4.0×10^{11}	2.2×10^{11}
1999-2000	5.6×10^{8}	1.2×10^{10}	1.0×10^{12}	3.5×10^{11}	1.9×10^{11}

Degassing period is arbitrarily chosen to match the periods of gravity change, Figure 3.7.
Total gas flux is $H_2O + CO_2 + SO_2 + HCl + HF$; see Chapter 2 for ratios.

3.5. Micro-gravity analysis

Micro-gravity variations may be due to changes in elevation, changes in edifice volume, and/or subsurface density/mass changes. The maximum size of any height correction required would be only ~16 μGal (for 4 cm elevation change at a maximum measured FAG of -390 μGal m^{-1}), while a calculated Bouguer-corrected free air gradient of -317 μGal m^{-1} would result in a maximum correction of only ~12 μGal. Thus, for the conservative uncertainty on the gravity data of 20 μGal, the maximum uncertainty including height corrections would be 36 μGal. Given the lack of any recent significant extrusive events or elevation changes and the periods of large gravity variation (~70 μGal yr^{-1}), the micro-gravity data has not been height-corrected. Gravity changes are therefore interpreted here in terms of subsurface mass/density variations.

Subsurface mass/density changes at Masaya may be caused by (a) water-table fluctuations, (b) magma drainage or input and (c) magma vesiculation or devesiculation. The first case is unlikely here because as mentioned above, the water table is quite deep in this area (>300 m) and as can be seen from Figure 3.7, gravity changes are essentially restricted to the active crater area.

It has also been suggested that daily micro-gravity variations at the summit stations may be due to short-term changes in the level of magma in the conduit beneath Santiago (Beaulieu, 1999). On three separate occasions in 1998, Beaulieu (1999) made micro-gravity measurements at station A7, every 15 minutes for periods of between 12 and 15 hours. When this tide-corrected data are plotted against the change in theoretical Earth tide for the same period, there is an apparent fluctuation of up to 40 μGal (Figure 3.9a). This raises the possibility that single gravity measurements (e.g., between 1993 and 1997) may not in fact be representative. However, although this preliminary data suggests the

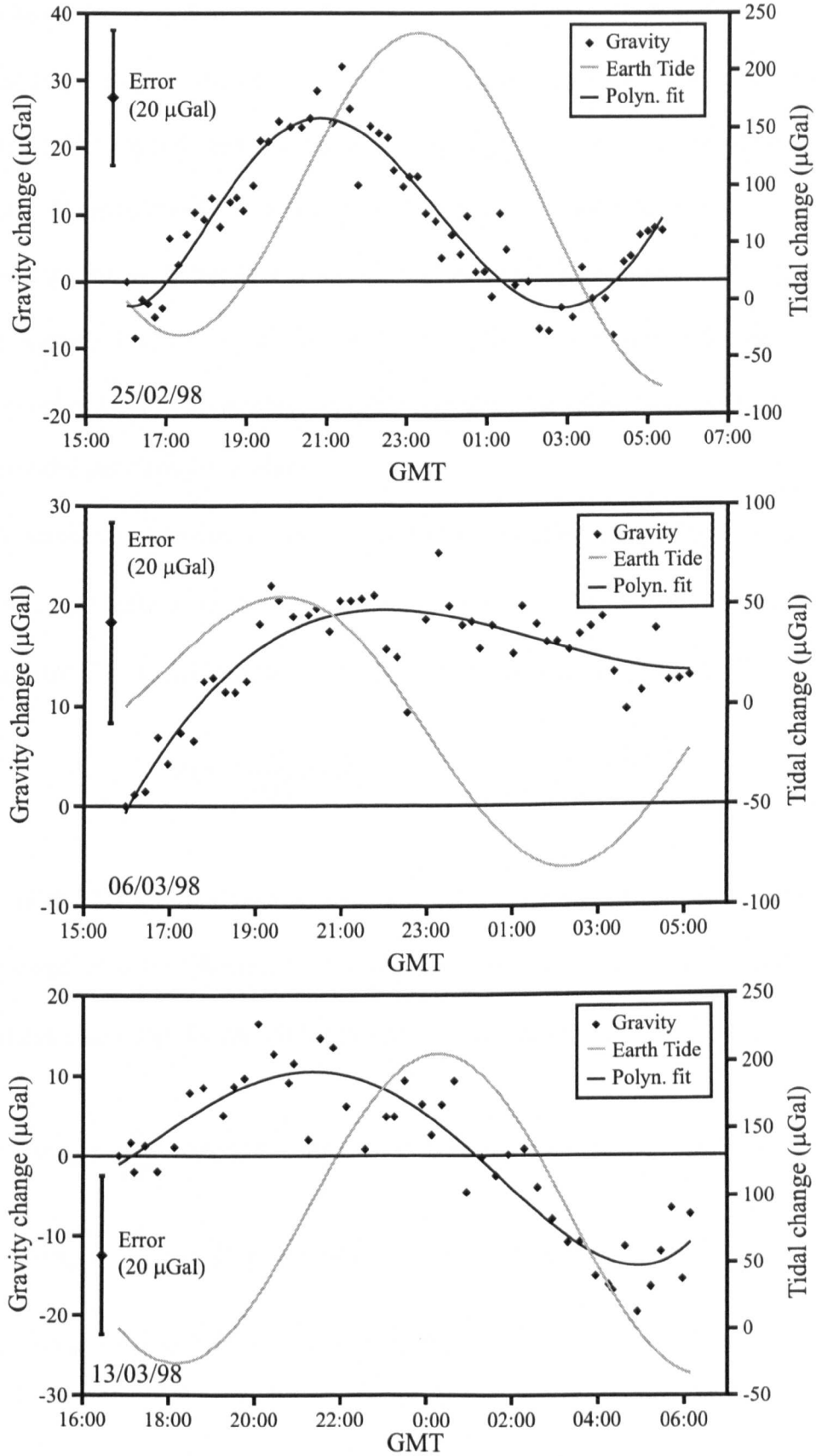

Figure 3.9: Measured (black diamond) and tidal gravity change (grey line) at station A7 for a) 25/02/98, b) 06/03/98 and c) 13/03/98. Black lines are best-fit polynomials. Note the different scales. Error on a single gravity measurement is ~20 μGal. Tidal gravity is calculated using software developed by Broucke et al. (1972). *Modified after Beaulieu (1999).*

potential for tidal influence on volcanic activity, the limited data (only one station) and large measurement errors (~20 μGal) make it inconclusive. The remarkably consistent behaviour of the summit stations through time suggests that one would expect to see these variations in the repeat measurements during a given day and throughout the field campaign. A more extensive and prolonged study with continuously recording gravity meters is required to clarify this potential relationship. Furthermore, even if there were daily fluctuations in the level of subsurface magma, the increasing gas flux (1997-2000) and continually visible incandescent vent suggests that there has been no significant magma withdrawal during this study.

A minimum estimate of the mass change (Δm/kg) responsible for the observed gravity changes (Δg/m s^{-2}) can be calculated by integrating the area of the residual gravity change (ΔS/m^2; Figure 3.7) using Gauss' theorem (Telford et al., 1990, p. 43):

$$\Delta m = \frac{1}{2\pi G}\Delta S \Delta g \qquad (3.2)$$

where G is the Universal Gravitational constant (6.67×10^{-11} N m^2 kg^{-2}). Thus, for the gravity change between 1998 and 1999, the total mass change (Δm_{tot}) is equal to the sum of mass changes calculated for the –90 μGal (Δm_{90}) and –60 μGal (Δm_{60}) anomalies, where:

$$\Delta m_{90} = \frac{1}{2\pi G} \cdot 230844 \cdot -90 \times 10^{-8} = -4.96 \times 10^{8}\,\text{kg} \qquad (3.3)$$

$$\Delta m_{60} = \frac{1}{2\pi G} \cdot 634821 \cdot -60 \times 10^{-8} = -9.09 \times 10^{8}\,\text{kg} \qquad (3.4)$$

$$\Delta m_{tot} = \Delta m_{90} + \Delta m_{60} = -1.40 \times 10^{9}\,\text{kg} \qquad (3.5)$$

Note that the actual area affected by the –60 μGal anomaly (634821 m^2) is equal to the total area within the –60 μGal anomaly (855432 m^2) minus the area affected by the –90 μGal anomaly (230844 m^2; Figure 3.7e).

Ideally, one would attempt to "close" the zero μGal anomaly contour, but as this is not feasible only a minimum estimate of mass change is possible. In the case of gravity changes between 1997 and 1999 (Figure 3.7d), the -120 and -90 μGal contours are used giving a total mass change (Δm_{tot}) of at least -2.1 x 10^9 kg. Similarly, the 1993-1994 gravity changes (using -60, -90 and -120 μGal contours; Figure 3.7b) are likely the result of a total mass change of at least -2.2 x 10^9 kg.

The subsurface structure of the magma system may also be partially deduced from the gravity anomalies. Density changes within a feeder pipe of reasonable dimensions (e.g., tens of metres in diameter) would result in a gravity anomaly of shorter wavelength than observed. On the other hand, changes within a deep magma reservoir would produce an anomaly with a wavelength larger than the ~2 km signature observed at Masaya (Rymer et al., 1998a).

It is sensible to use the structural evidence, such as the diameter of Santiago and Nindiri craters and their inferred boundary faults (Rymer et al., 1998a), to constrain the depth and lateral extent of the body responsible for the anomaly. However, the craters grow through erosion and collapse of the walls, therefore these estimates are maxima. In this study, the implications of the observed periods of gravity decrease (1993-1994 and 1997-1999) have been investigated using the interactive 2.5-dimension forward modelling programme GRAVMAG (Pedley, 1991). The gravitational effect of subsurface geology measurable at the topographic surface (taken from a Digital Elevation Model) is calculated along a given profile. Geology is represented by a series of user-defined polygons, each assigned a density and half strike. The models are 2.5D rather than 3D, as each polygon

must be symmetrical across (but not along) the profile. By modifying the physical parameters of each polygon (e.g., size, density, half strike), the calculated gravity profile can be "fitted" to the observed gravity profile. Unfortunately, the software does not allow for rapid iterative modelling of the data. A time-consuming process of "manual" modelling is thus necessary. Thus, while there may be more complex models that better "fit" the data, those presented below are the simplest models.

In an attempt to constrain the causative bodies responsible for the observed gravity anomalies, north-south and west-east profiles were initially made across the active crater, Santiago (Figure 3.7a). A north-south profile of the 1993-1994 gravity decrease, can be modelled in terms of a stratified body approximately 490 m wide, with a 200 m half strike and 180 m thick stratified body; a 30 m upper layer of high density change (-600 kg m^{-3}) above a body of lower relative density change (-100 kg m^{-3}; Figure 3.10a). A west-east profile for the same period suggests a body of similar dimensions (450 m wide, 200 m half strike, 30 m thick at -600 kg m^{-3} and 150 m thick at -100 kg m^{-3}; Figure 3.10b). The 1997-1999 gravity anomaly can also be modelled in terms of a stratified body, though with different density changes. The north-south profile indicates a body approximately 560 m wide, with a 200 m half strike, and 190 m thick with an upper layer of high density change (20 m at –300 kg m^{-3}), a middle layer with marginally lower density change (80 m at -250 kg m^{-3}) and a bottom layer of low density change (90 m at -100 kg m^{-3}; Figure 3.10c). The west-east profile again is modelled as a body with similar dimensions (465 m wide, 200-m half strike, 20 m at -300 kg m^{-3}, 80 m at -250 kg m^{-3} and 90 m at -100 kg m^{-3}; Figure 3.10d). Modelling of the 1998-1999 gravity anomaly, which is based on a larger number of measurements, supports the 1997-1999 model (Figure 3.10e, f).

The west-east profiles for 1993-1994 and 1997-1999 may also be modelled in terms of two causative bodies (though with different density changes) and suggest that some of observed density changes within the system are centred beneath Nindiri crater (Figure

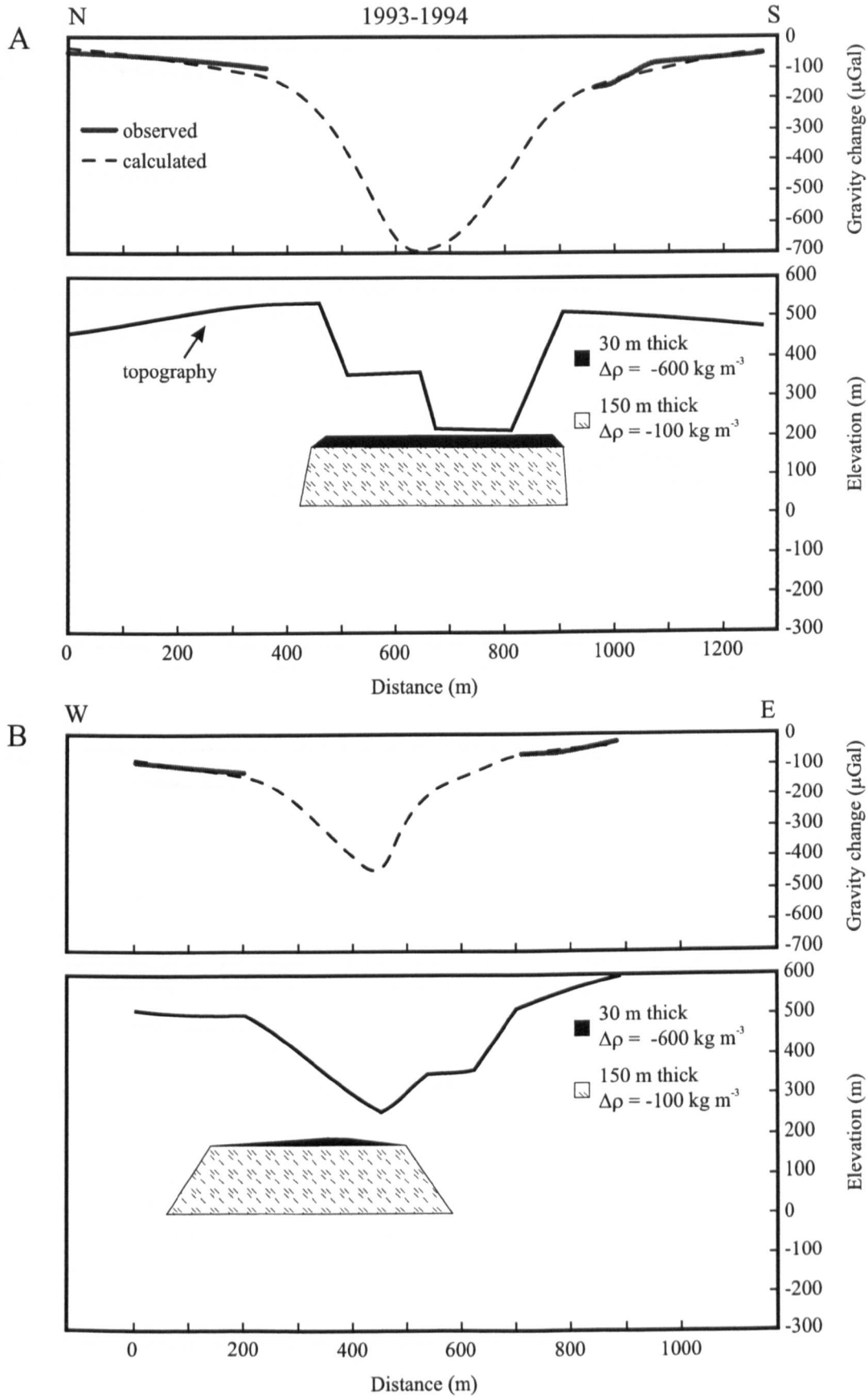

Figure 3.10: Observed and calculated gravity changes and modelled causative body for the a) north-south and b) west-east profile of the 1993-1994 gravity decrease. Modelled bodies have thicknesses of 30 and 150 m with density changes of -600 and -100 kg m^{-3}, respectively. All bodies have a constant half strike of 200 m. Profiles from Figure 3.7a.

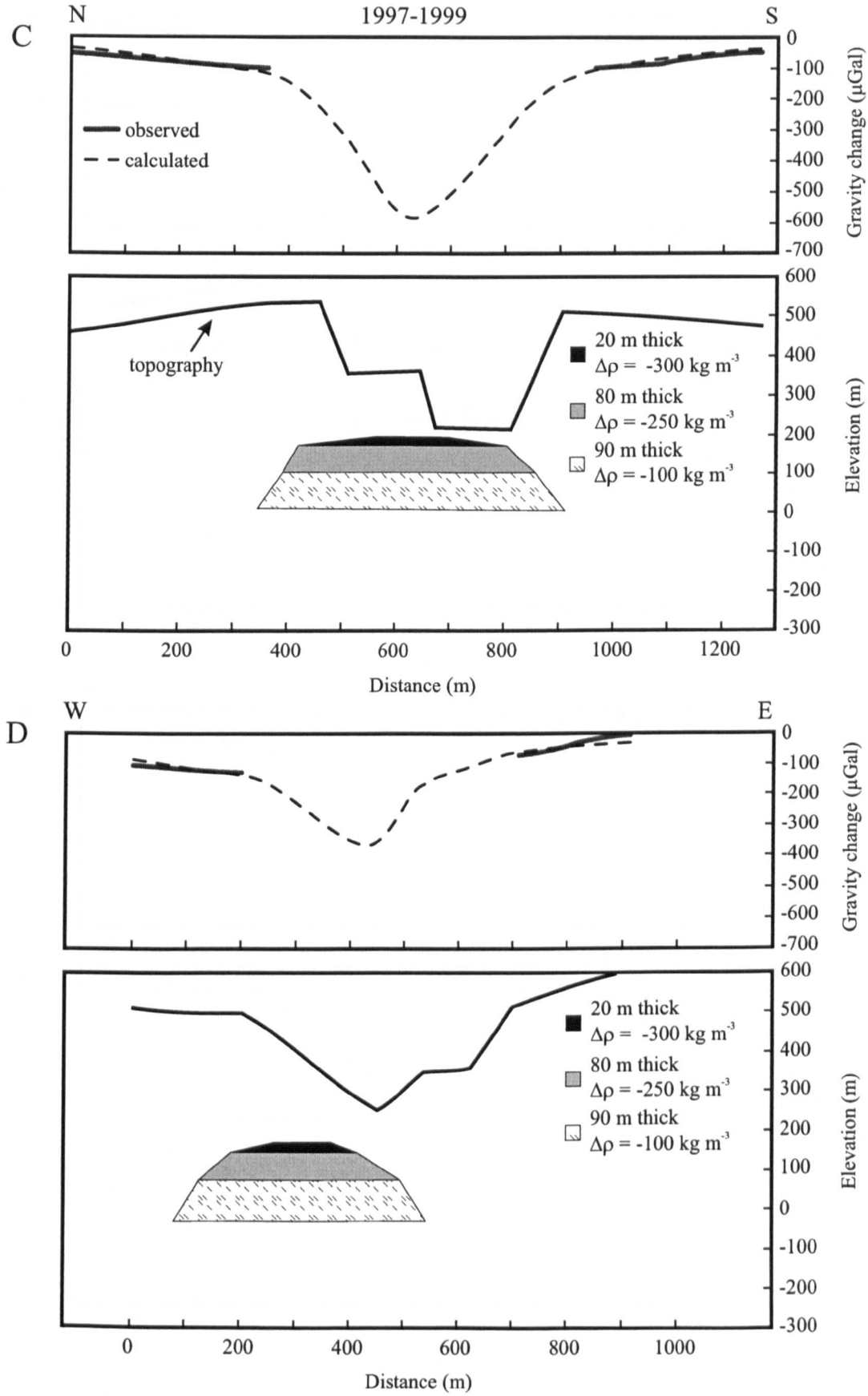

Figure 3.10 - Continued: Observed and calculated gravity changes and modelled causative body for the c) north-south and d) west-east profile of the 1997-1999 gravity decrease. Modelled bodies have thicknesses of 20, 70 and 90 m with density changes of -300, -250 and -100 kg m^{-3}, respectively. All bodies have a constant half strike of 200 m. Profiles from Figure 3.7a.

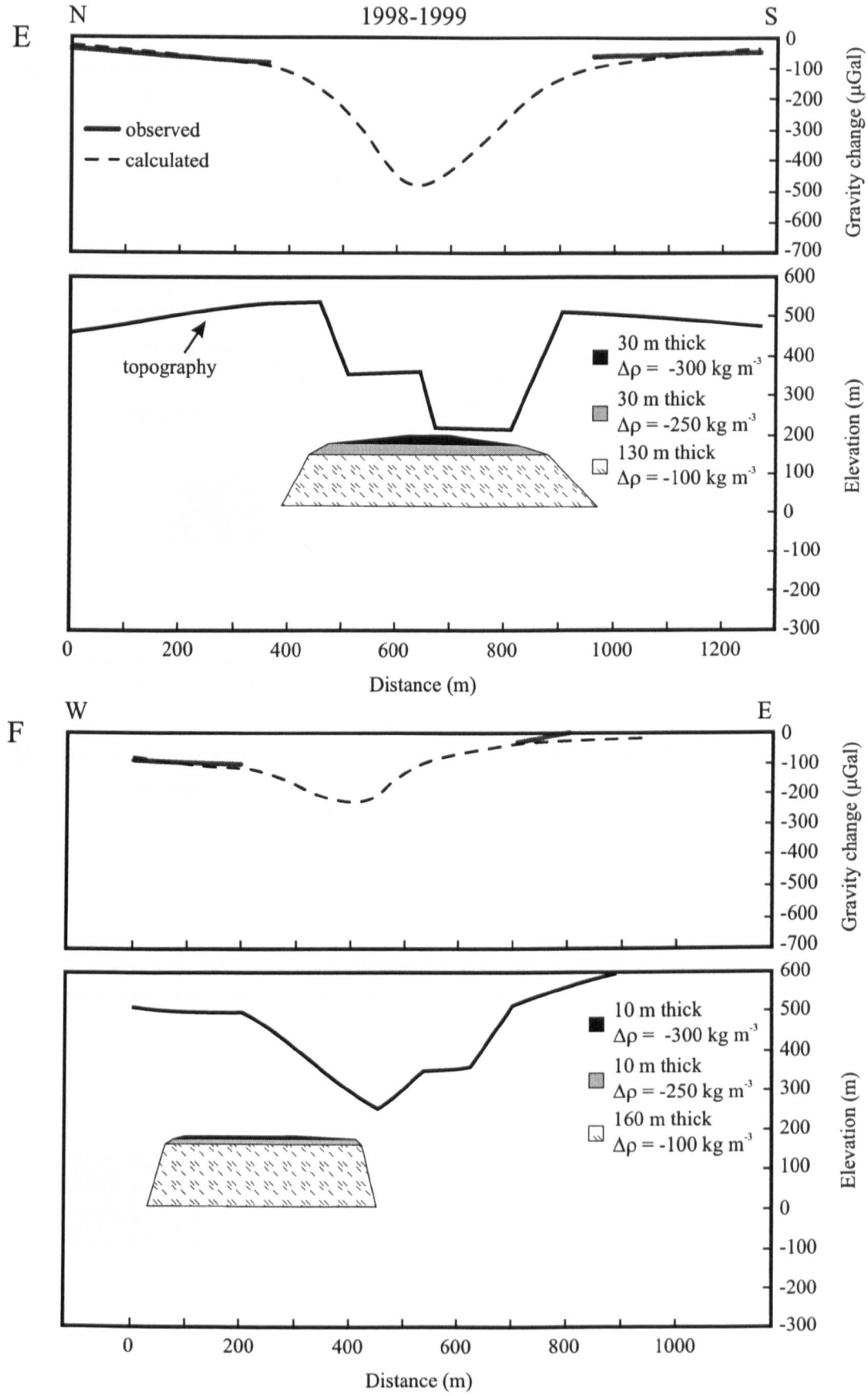

Figure 3.10 - Continued: Observed and calculated gravity changes and modelled causative body for the e) north-south and f) west-east profile of the 1998-1999 gravity decrease. All bodies have a constant half strike of 200 m. Profiles from Figure 3.7a.

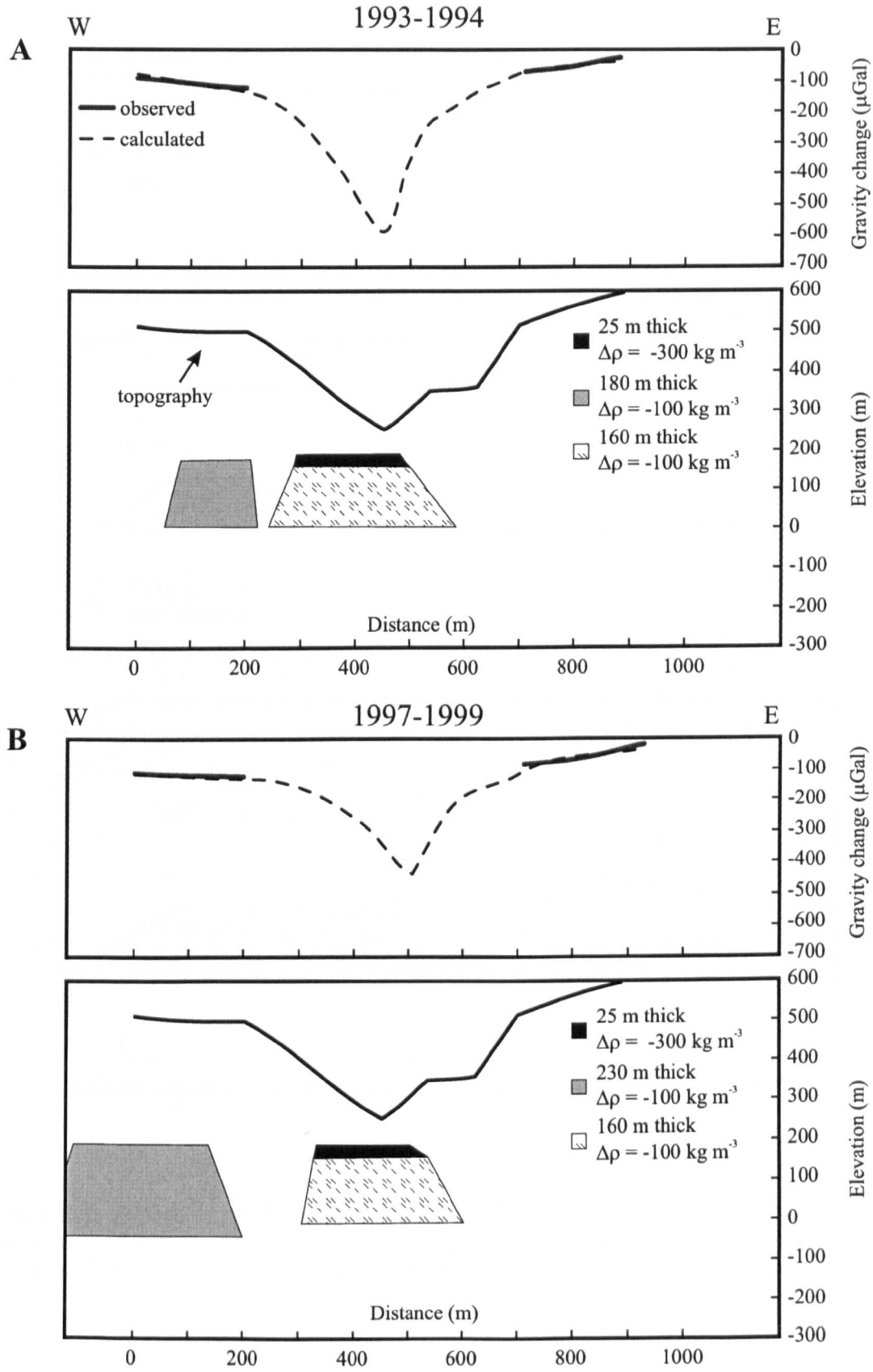

Figure 3.10 - Continued: Observed and calculated gravity changes and modelled causative bodies for the west-east profile of the a) 1993-1994 and b) 1997-1999 gravity decreases. Note that the grey and hatched bodies are the same density change. All bodies have a constant half strike of 200 m. Profiles from Figure 3.7a.

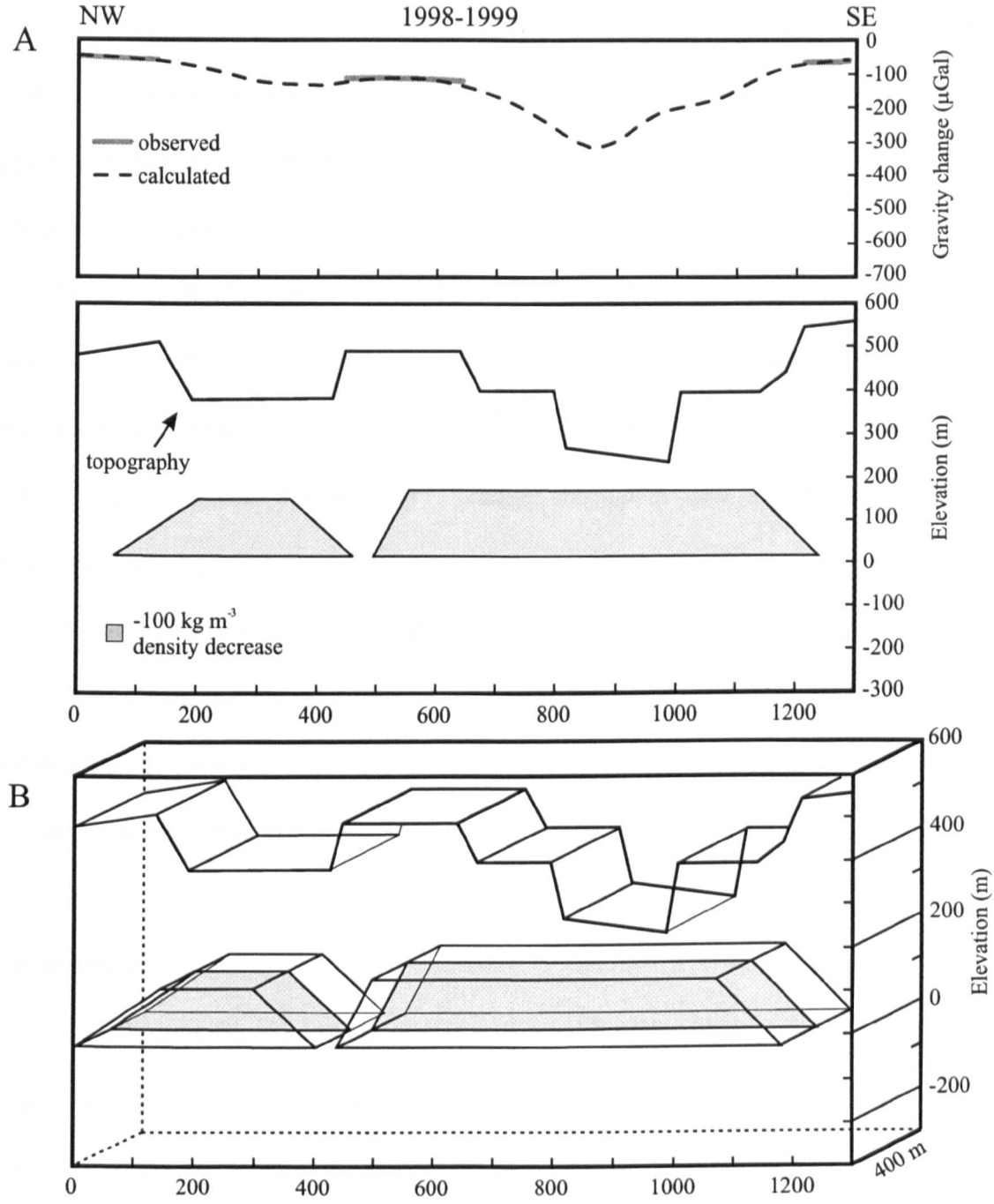

Figure 3.11: a) Observed and calculated gravity changes and modelled causative body for the northwest-southeast profile of the 1998-1999 gravity decrease. b) Perspective view shows the 2.5D modelled bodies with a symmetrical 200-m half strike. Profiles from Figure 3.7a.

3.10g, h). In order to investigate this further, an oblique profile running NW-SE across the craters was made for the 1998-1999 period (Figure 3.7a, 3.11). Modelling of these data, although limited by the lack of data for the floors of San Pedro and Santiago pit craters, suggests that there may be areas of density change (-100 kg m^{-3} for 1998-1999) beneath the entire pit crater complex.

These modelled density changes can most easily be explained by increased vesiculation, the 1993-1994 model being the result of ~20% vesiculated upper layer above a less vesiculated layer (~5%; Figure 3.12). Similarly, the 1997-1999 model may be the result of ~12% vesiculated upper layer, grading through a 10% middle layer to a ~5% vesiculated lower layer.

It is important to note that the significant lack of measurements on the crater floors (i.e., the areas with the greatest likely gravity anomalies) reduces the level to which the modelled gravity profile can be "fitted" to the observed data (Figure 3.10). This greatly limits the extent to which these causative bodies can be confidently modelled.

3.6. Interpretation

Modelling of the gravity anomalies is limited by the rather poor spatial resolution and geographic coverage of the data. However, the most likely cause of the observed gravity variations is the change in density of a region of stratified vesiculated bodies located immediately beneath Santiago, Nindiri and San Pedro craters (Figure 3.10, 3.11, and 3.12). A four-stage model can be used to explain the observed fluctuations in micro-gravity and gas flux, with Stage 1 being arbitrarily set at the beginning of significant degassing in May 1993 (Figure 3.13). The initial state of the vesiculated region, Stage 0, is unknown but the low SO_2 flux in April 1992 from COSPEC measurements (<10 t d^{-1}; Bulletin of the Global Volcanism Network, 1970-2000) suggest that it was probably of only limited thickness. During Stage 1 (May 1993-1994), the significant gravity decrease

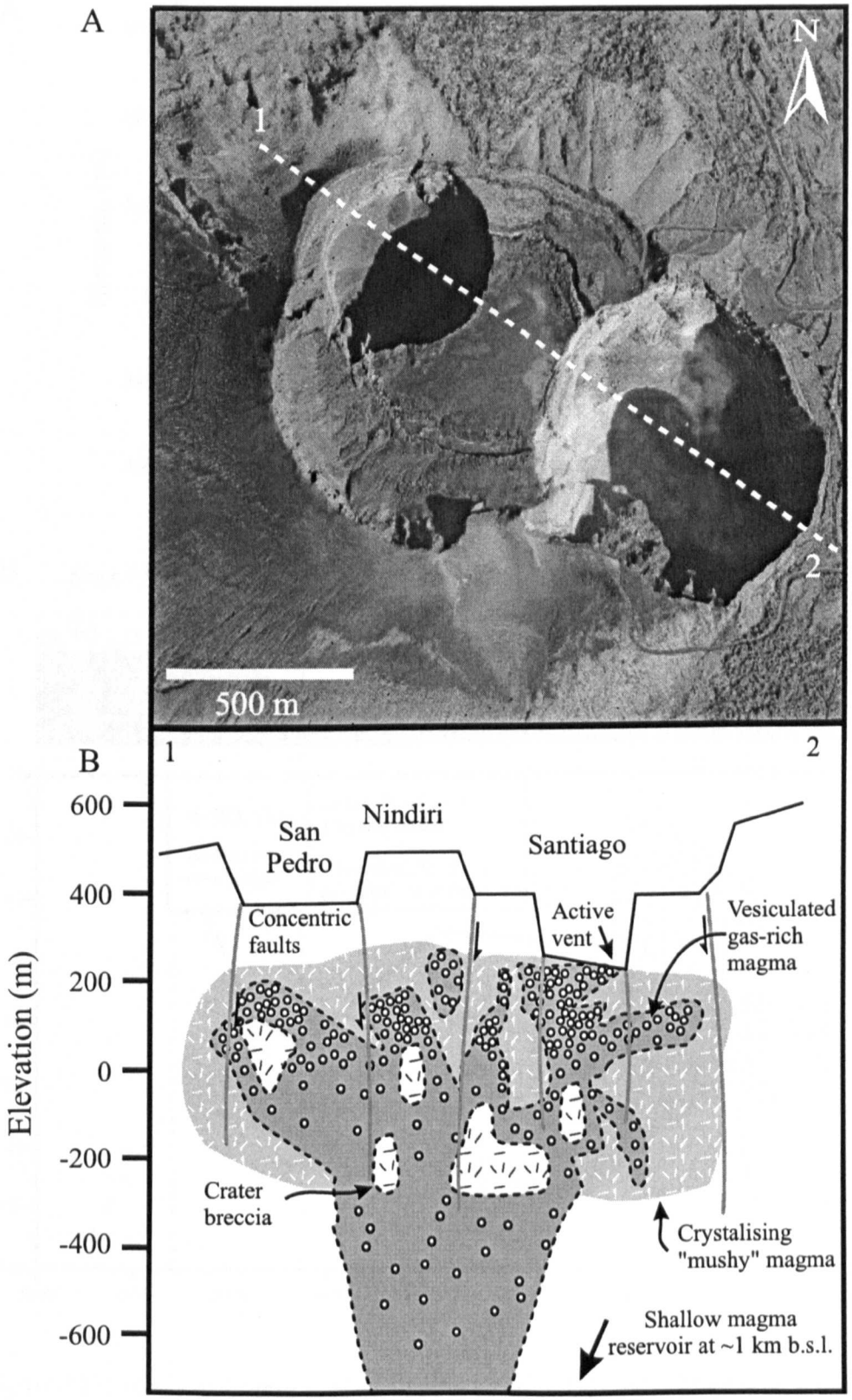

Figure 3.12: a) Aerial photo and b) schematic cross-section (profile 1-2, from left to right) of San Pedro, Nindiri and Santiago pit craters. The location of the proposed zone of vesiculated gas-rich magma is based on the gravity models. The crystallising "mushy" magma is purely conceptual. Concentric faults are inferred from observed structure and collapse history. *Modified after Rymer et al., 1998a.*

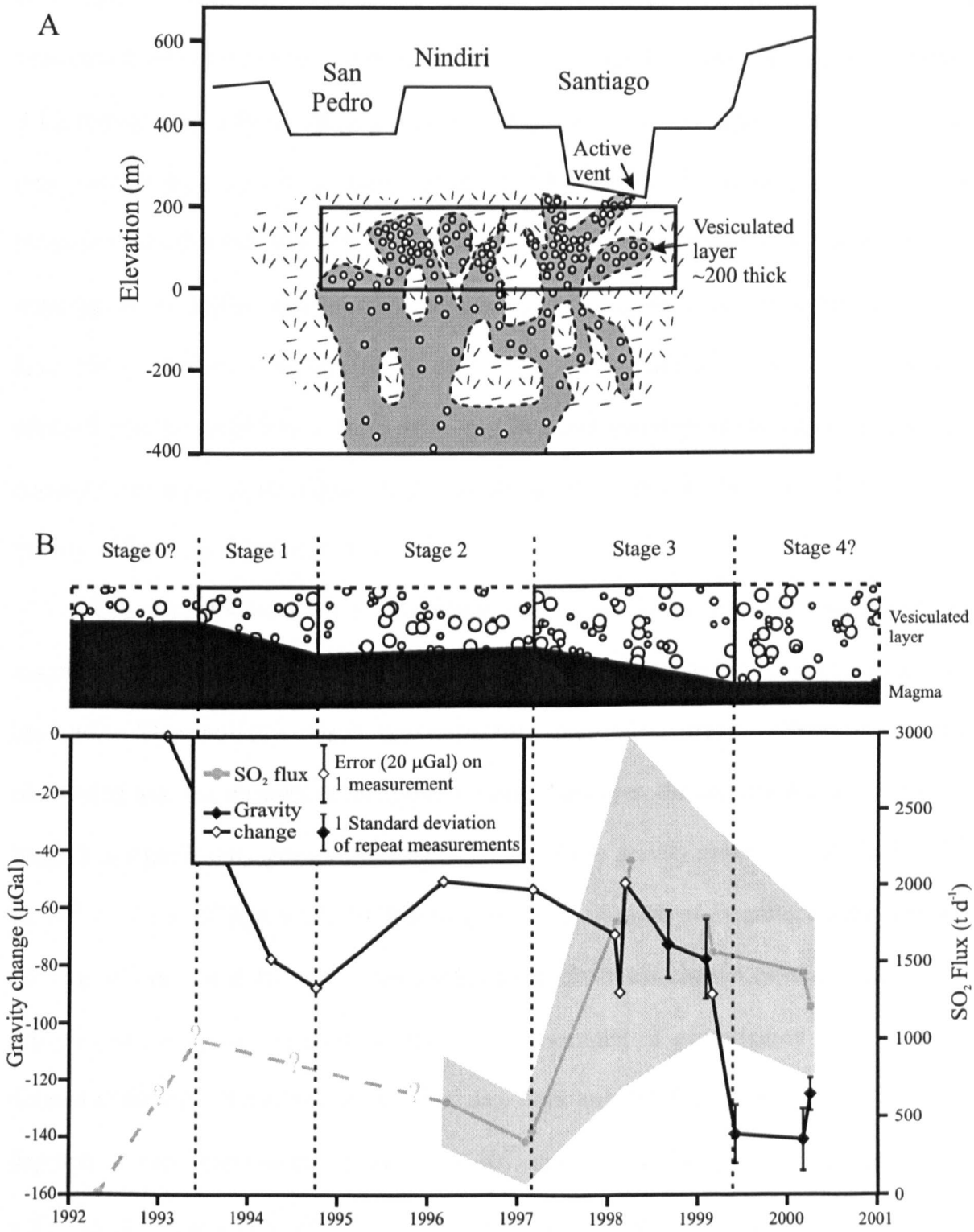

Figure 3.13: a) Schematic profile of the shallow plumbing system at Masaya. b) Average monthly gravity change (diamonds) at a representative crater rim station (A7) compared with average monthly SO_2 flux (circles) at Masaya. Black diamonds denote repeat gravity measurements; white diamonds denote single measurements. Grey circles represent average COSPEC measurements while shaded region represents one standard deviation of flux values (~30%). Dashed lines denote the 5 stages of activity between 1992 and 2000. The schematic cross-section illustrates the possible stages of thinning and thickening of the vesiculated gas-rich layer due to changes in gas flux. Boxes represent the ~200 m thick layer (gravity modelled for Stage 1 and 3). Dashed boxes are unmodelled.

is thought to have been caused by the formation of an ~200-m thick low-density vesiculated layer (above higher-density magma) as a result of elevated gas flux (Figure 3.13; Rymer et al., 1998a). With a reduction in gas flux, this vesiculated layer stabilised or may have thinned somewhat during Stage 2 (1994-1997). Subsequently, a significant increase in gas flux between 1997 and 1998 coincided with a thickening of this low-density zone (again to ~200 m thick), causing the gravity decrease observed during Stage 3 (1997-June 1999). Finally, levelling off of the gravity change during Stage 4 (June 1999 to present) may be related to a decrease in gas flux and therefore stabilisation of the low-density layer once again (Figure 3.13). However, this can only be clarified by ongoing gravity and gas flux measurements.

The estimated total gas flux in Stage 1 (4.7×10^9 kg yr^{-1}) is of the same order of magnitude as the estimated mass decrease (2.2×10^9 kg) responsible for observed gravity changes. This initially raised the possibility that micro-gravity observations were identifying gas flux changes in the upper system. However, the estimated total gas flux in Stage 3 is significantly greater than that estimated from gravity measurements (1.0×10^{10} kg yr^{-1} vs. 2.1×10^9 kg), while 1998-1999 gas flux is an order of magnitude greater (1.4×10^{10} kg yr^{-1} vs. 1.4×10^9 kg). This suggests that the mass change estimated by micro-gravity can not in fact be directly related to the amount of gas released or amounts of magma degassed. Nevertheless, gas flux data does suggest that during Stage 1, magma degassed at minimum rate of between 7.3×10^{10} and 4.1×10^{11} kg yr^{-1} and increased to 1.2×10^{12} kg yr^{-1} in Stage 3 (Table 3.2). Assuming a magma density of 2600 kg m^{-3}, these are equivalent to degassed magma volumes of between 0.03 and 0.5 km^3 yr^{-1}.

Initially, this gas-rich magma would rise buoyantly towards the surface where it would degas, cool, crystallise and become denser, before descending the conduit. Convection in the crater feeder conduit has been proposed as a mechanism for removing the degassed magma (Kazahaya et al., 1994; Stevenson and Blake, 1998; Rymer et al.,

1998a). The fate of this degassed magma however, remains uncertain. Two end-member models have been suggested: 1) intrusion into the edifice or cryptically beneath the volcano and 2) recycling back into the underlying magma reservoir (Harris et al., 1999 and references therein). In the case of Masaya, edifice and/or cryptic intrusion of the degassed magma are unlikely as this would result in inflation and gravity increase, neither of which has been observed. The magma must therefore be recycled back into the underlying magma reservoir.

The rate at which this magma is recycled may be inferred to some degree from the micro-gravity and gas flux data. After the initial rise of gas-rich magma and formation of the vesiculated layer beneath Santiago and Nindiri in Stage 1 (~1.5 years), the rate of degassing decreased progressively over a period of approximately 2.5 years (Stage 2) resulting in a stabilisation or slight increase in gravity. The slight increase in gravity may be a response to the density increase of degassed magma or the replacement of vesiculated magma by less vesicle-rich magma. This period was followed by the renewal of elevated degassing and progressive gravity decrease over a period of ~2.5 years (Stage 3). Preliminary data suggest that the system may have entered another period of decreased degassing and stabilisation of gravity change (Stage 4). It is clearly presumptuous to predict the duration of Stage 4, but it may be of the same order as Stage 2.

Thus, in summary, gas-rich magma may have risen to the surface in early 1993 and degassed over a period of ~1.5 years, releasing sufficient gas to form the low-density vesicular area. The apparent stabilisation of the low-density area and decreasing gas flux in Stage 2 suggest that the degassed, dense magma may have sunk downwards. This would have been followed by convective overturn at depth of new or recharged gas-rich magma that then rose buoyantly to the surface during Stage 3, releasing gas and thickening the shallow low-density area. Preliminary observations of slightly decreased gas flux and stabilised gravity change in July 1999 suggest that this magma may have degassed,

increased in density and begun to descend. This convective overturn should not be thought of as a series of individual events but rather as a continuous process with the rise, degassing and sinking of magma, at least during a given degassing episode (e.g., since 1993). Similar activity may also have been responsible for the variations in SO_2 flux observed during the 1979-1989 degassing episode (Stoiber et al., 1986; Figure 2.2).

This raises the important question of whether the periods between degassing episodes are indicative of the rates of convection within the deeper source region. In many cases the magma eruption rate at a volcano is used as a proxy for the magma supply rate (cf. Denlinger, 1997). However, as only negligible amounts of magma have been erupted at Masaya, the magma-degassing rate may also be used as a proxy (Francis et al., 1993). With a time-averaged SO_2 flux (1972-2000) of $4.4 \pm 2.7 \times 10^8$ kg yr^{-1} (Chapter 2), magma could be supplied from depth, to the shallow (~1 km b.s.l.) magma reservoir at a rate on the order or 2-7 x 10^{11} kg yr^{-1}. Unfortunately, the near-complete lack of erupted material makes it difficult to determine (through decay-series disequilibria methods; cf. Pyle, 1992) the residence time of magma in the shallow reservoir and deeper source. However, recent work at Stromboli using short-lived disequilibria of ^{210}Pb-^{210}Bi-^{210}Po in volcanic gases has enabled an estimate of magma residence time in the upper reservoir (Gauthier et al., 2000). This, in conjunction with continued long-term geophysical monitoring, has the potential to better constrain the rate of convection at the different levels of the magmatic system beneath Masaya.

3.7. The magmatic system of Masaya

While the exact shape of both the shallow and deep magmatic systems of Masaya is unknown, several suppositions can be made. Pit craters such as Santiago and San Pedro vary in size due the wall collapse and floor subsidence (Rymer et al, 1998), suggesting that the immediate area beneath the crater floor is likely a chaotic region of gas/magma-filled

voids interspersed with sunken crater wall/floor material (Fig. 3.12). This is supported by the visual observations of unroofing of small "caverns" (5-30 m diameter) located beneath the crater floor of Santiago (Rymer et al, 1998). These voids may also allow for the accumulation of gas and result in the "puffing" (on the order of tens of seconds), characteristic of degassing at Santiago. Furthermore, the spatially restricted (i.e., small wavelength) micro-gravity anomalies of 1993-1994 and 1997-1999 (Fig. 3.7), suggest that significant density changes are occurring at shallow levels (<200 m below the crater floor), centred on and in the immediate vicinity of Nindiri crater. Below this, earthquake hypocentre data suggest the presence of a small shallow reservoir at ~1.5-2 km b.s.l. (Fig. 2.2; Métaxian et al., 1997). The significant degassing and cooling rates, as well as geochemical evidence (Walker et al., 1993), suggest that this upper reservoir must, at least periodically, be recharged from a deeper source.

3.8. Conclusions

The integration of micro-gravity and COSPEC measurements over an extended period of time allows for a better understanding of persistent volcanism. Recent activity at Masaya (1993-present) is characterised by repeated fluctuations in micro-gravity and gas flux and is thought to be due to at least two convective pulses which lead to the formation and oscillation of a gas-rich vesiculated zone immediately beneath the Nindiri and Santiago craters. Four stages of activity within the most current degassing episode have been identified, with the most resent data suggesting that the system may be entering another period of reduced degassing. The cyclical nature of the observed variations in micro-gravity and gas flux and lack of any significant gravity increase or deformation discount intrusion of new magma into the shallow magmatic system. Rather, it necessitates the convective overturn of shallow, pre-existing, degassed, cooled, dense magma that is replaced periodically by lower density, hot, gas-rich magma from depth. It

is clear that this is a continuous process that occurs at shallow levels immediately beneath the craters as well as at depth in the magma reservoir.

Chapter 4.

Detecting volcanic eruption precursors: A new method using gravity and deformation measurements

---

G. Williams-Jones and H. Rymer
Paper published in the *Journal of Volcanology and Geothermal Research*, 2000, In press.

4.1. Abstract

One of the fundamental questions in modern volcanology is the manner in which a volcanic eruption is triggered; the intrusion of fresh magma into a reservoir is thought to be a key component. The amount by which previously ponded reservoir magma interacts with a newly intruded magma will determine the nature and rate of eruption as well as the chemistry of erupted lavas and shallow dykes. The physics of this interaction can be investigated through a conventional monitoring procedure that incorporates the simple and much used Mogi model relating ground deformation (most simply represented by Δh) to changes in volume of a magma reservoir. Gravity changes (Δg) combined with ground deformation provides information on magma reservoir mass changes. Our models predict how, during inflation, the observed $\Delta g/\Delta h$ gradient will evolve as a volcano develops from a state of dormancy through unrest into a state of explosive activity. Calderas in a state of unrest and large composite volcanoes are the targets for the methods proposed here and are exemplified by Campi Flegrei, Rabaul, Krafla and Long Valley. We show here how the simultaneous measurement of deformation and gravity at only a few key stations can

identify important precursory processes within a magma reservoir prior to the onset of more conventional eruption precursors.

4.2. Introduction

Explosive volcanic eruptions are often initiated by magma intrusion into a pre-existing magma reservoir (cf. Sparks et al., 1977; Pallister et al., 1992) The degree of interaction between the intruding magma and the pre-existing reservoir will determine the nature and rate of eruption as well as the chemistry of erupted lavas and shallow dykes. To understand the process therefore requires information on the physical and chemical processes occurring at depth within the magma reservoir. The majority of geophysical techniques, however, focus on shallow processes within the volcanic edifice. Micro-gravity monitoring, for example, has been used at numerous active volcanoes in order to identify the relatively shallow processes occurring within the feeder conduit (cf. Eggers and Chavez, 1979; Johnson and Sigurdsson, 1980; Yokoyama, 1989; Rymer and Brown, 1989; Berrino et al., 1992; Rymer et al., 1998a,b). The conventional micro-gravity survey involves repeated measurements of gravity change (Δg) and deformation (Δh) at a network of stations in and around the active crater or caldera (Rymer, 1994; Rymer et al., 1998b). The recent deaths of some well-known volcanologists (cf. Baxter and Gresham, 1997; Fujii and Nakada, 1999) emphasise the need to monitor volcanoes at a safe distance from the active centre. This, however, can often lead to reduced data quality. Here we discuss a new approach, first proposed by Rymer and Williams-Jones (2000; see Appendix G), which actually benefits from gravity and deformation measurements made up to 6 km from the centre of activity. Physical processes deep within the magma reservoir, which can occur months to years before conventional precursors, can now be interpreted from $\Delta g/\Delta h$ gradients measured at a safe distance from the central volcanic edifice. This is exemplified

by important examples from the calderas of Campi Flegrei, Rabaul, Krafla, and Long Valley, examined below.

4.3. Gravity and height correlations

Conventional gravity and deformation data are usually modelled in terms of either a sphere or a Bouguer slab. Both are mathematically simple to model. To a first approximation, a magma reservoir can usually be most realistically modelled as a spherical body. If the depth of the magma reservoir is large compared to its radius, the gravitational effect of the reservoir can be considered to be that of a point source (Rymer, 1994). The Mogi model (Mogi, 1958) quantifies the deformation at the surface caused by dilation of a point source in a homogeneous elastic half space. The deformation will depend on the amount of dilation and the elastic properties of the medium (Figure 4.1). Using ground deformation measurement techniques such as the Global Positioning System (GPS), Synthetic Aperture Radar differential interferometry (DInSAR), altimetry or levelling (cf. Smith et al., 1989; Murray et al., 1995; Dixon et al., 1997; Avallone et al., 1999), the change in edifice volume (ΔV_e) of the volcano can be estimated by integrating the observed height changes over the area of deformation. Measured or estimated values for the elastic properties of the country rock along with the amount of ground deformation can then be used to estimate the change in volume of subsurface magma reservoir (ΔV_r; McKee et al., 1989; Vasco et al., 1990; Dvorak and Mastrolorenzo, 1991; Wicks et al., 1998). However, the change in volume alone provides little information on the actual processes taking place within the magma reservoir. If in addition, small variations in the acceleration due to gravity are monitored, the changes in subsurface magma mass (ΔM_m) can be quantified

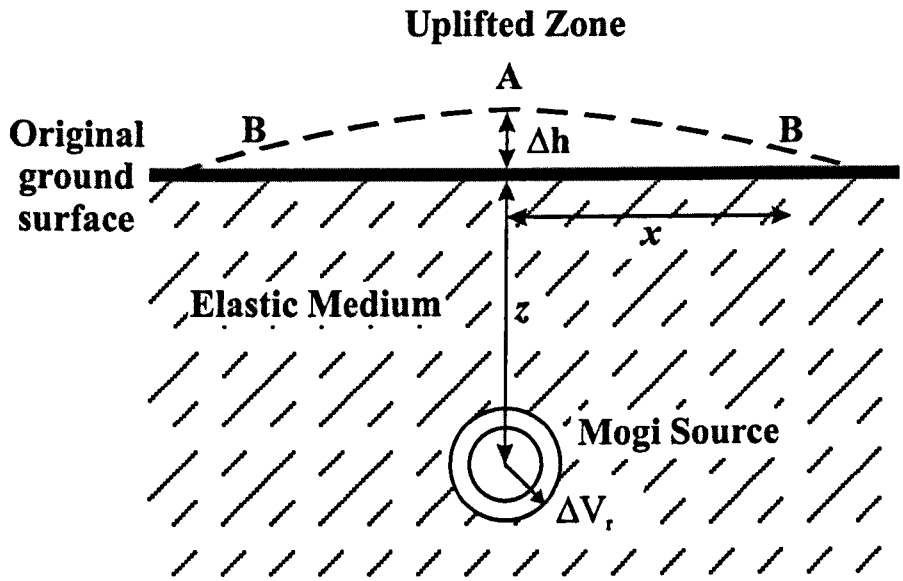

Figure 4.1: A Mogi-type magma reservoir modelled in an elastic half space. The largest ground deformation changes (Δh) are observed in zone A. Measurable effects are also seen at some distance (x) from the centre of activity, such as at B. Using the measured or estimated values of the elastic properties of the country rock and the amount of ground deformation allows for the estimation of the change in volume of the sub-surface magma reservoir (ΔV_r). Small changes in gravity (Δg) may also be observed at these points (A & B) and when combined with ground deformation data, one can quantify the change in sub-surface magma mass (Δm_m). *Modified after Rymer and Williams-Jones (2000).*

(Berrino et al., 1992). Simultaneous gravity and deformation measurements can therefore provide an estimate of ΔM_m and ΔV_r in order that changes in the average density of the magma reservoir may be deduced.

Changes in gravity and elevation are normally inversely correlated. The amount by which gravity varies with elevation is given by the free air gradient (FAG). If there is no change in the density (ρ) of the magma reservoir, the amount by which gravity varies with elevation can be described by the Bouguer-corrected free air gradient (BCFAG) of a spherical body. The $BCFAG_{spherical}$ can be calculated using the following relationship in which the result is in units of $\mu Gal\ m^{-1}$:

$$BCFAG_{spherical} = FAG + \frac{4\pi G \times 10^8}{3}\rho \qquad (4.1)$$

where G is the Universal Gravitational constant (6.67×10^{-11} N m^2 kg^{-2}) and ρ is in kg m^{-3}. The theoretical value for the FAG is –308.6 $\mu Gal\ m^{-1}$. Terrain effects and Bouguer anomalies can cause this value to differ by up to 40% from its theoretical value (Rymer, 1994 and references therein). The actual gradient of the BCFAG, which will vary depending on the density assumed for the surrounding rock, ranges from –253 to -230 $\mu Gal\ m^{-1}$ for magma densities of 2000 to 2800 kg m^{-3}, respectively, assuming the theoretical FAG.

If at all possible, the actual FAG should always be measured at each station during a micro-gravity/deformation survey. This can easily be accomplished in the field by making measurements first at the surface and then some distance off the ground (e.g., ~1 m using a levelling tripod), and then dividing the difference of the two sets of measurements (Δg) by the difference in elevation (Δh) (Berrino et al., 1984; Yokoyama, 1989; Rymer, 1994).

Gravity/elevation gradients are most easily visualised using a $\Delta g/\Delta h$ diagram (Figure 4.2). $\Delta g/\Delta h$ gradients that deviate from the FAG are interpreted in terms of

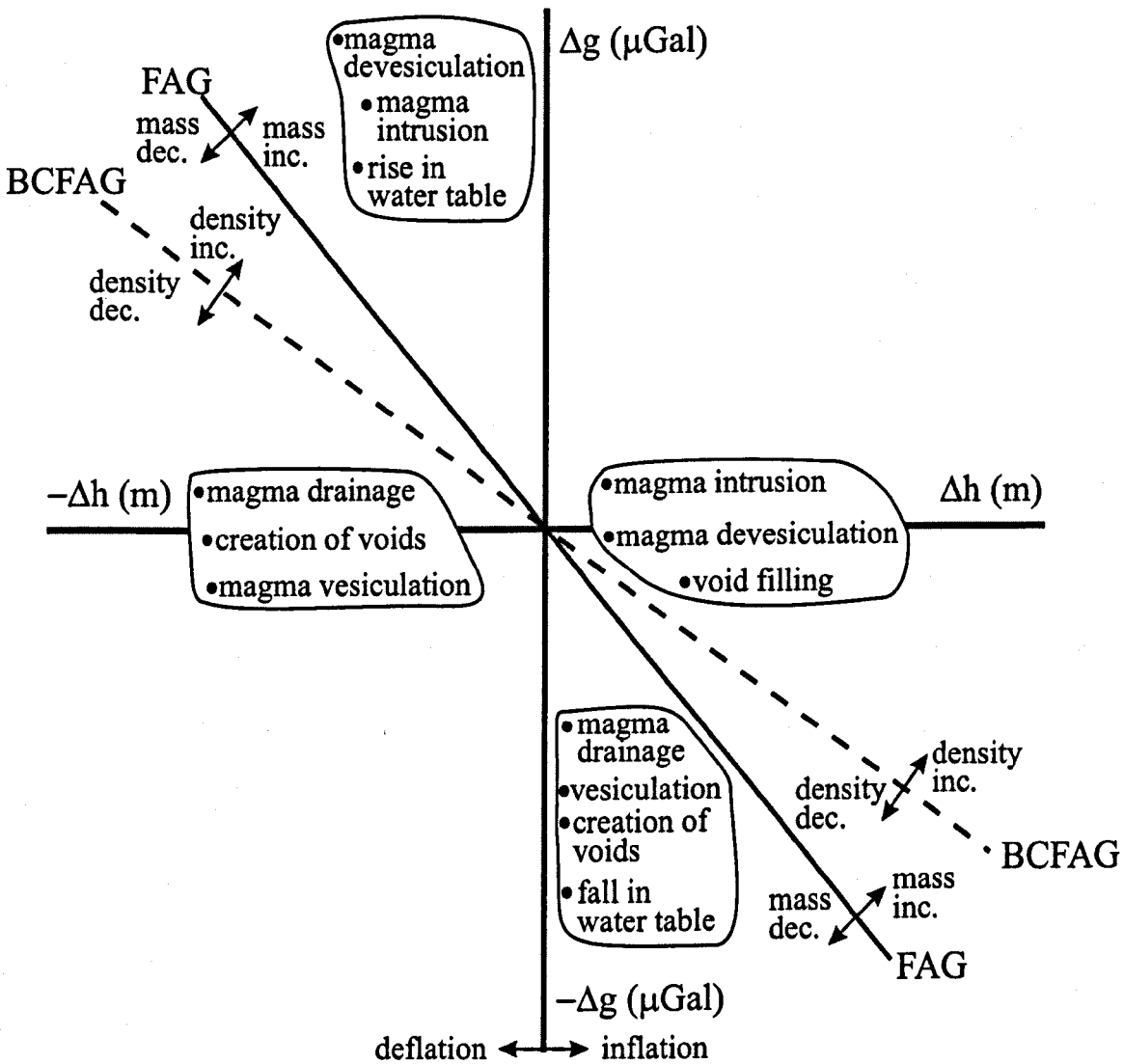

Figure 4.2: Changes in gravity (Δg) and elevation (Δh) can be plotted in terms of Δg/Δh gradients. When the gradient differs from the free air gradient (FAG), the variations are interpreted in terms of mass changes. Changes in density are shown by deviations from the Bouguer-corrected free air gradient (BCFAG) and FAG (-FAG + BCFAG). The theoretical FAG is commonly taken as -308.6 μGal m^{-1} but may vary by ~40% depending on the local terrain and Bouguer anomaly. Assuming a Mogi point-source model and a theoretical FAG, the BCFAG may vary between -253 and -230 μGal m^{-1} for densities between 2000 and 2800 kg m^{-1}. *Modified after Brown and Rymer (1991).*

subsurface mass changes. Data plotting above the FAG reflect mass increases while data plotting below it reflect mass decreases. Similarly, deviations from the BCFAG are interpreted as subsurface density changes (Brown et al., 1991; Berrino et al., 1992; Rymer et al., 1995). During periods of inflation, data plotting above the BCFAG reflect density increases whereas data plotting below the BCFAG reflect density decreases. There is an important and intriguing region between the FAG and the BCFAG, in the lower right quadrant of Figure 4.2, where during inflation there are mass increases and yet density decreases. Recognition of this is fundamental to understanding the physics of magma reservoir processes and the detection of eruption precursors (Figure 4.3).

In order to investigate relatively shallow subsurface processes, micro-gravity and ground deformation surveys are commonly carried out in the region of maximum uplift, central to the volcanically active region (zone A, Figure 4.1). However, sensitive instrumentation and techniques (e.g., LaCoste and Romberg or Scintrex gravity meters coupled with precise levelling or differential GPS) can detect small off axis variations (Δg >20 μGals, Δh >1 cm) at significant lateral distances (several km) from the active region (zone B, Figure 4.1). Shallow volcanic events within the edifice (such as vesiculation and fracturing; Rymer et al., 1998a), may be responsible for elevated "noise" in the gravity data in region A. However, by making measurements away from the active centre, the signal to noise ratio of the data is significantly increased. Another potential source of uncertainty, the variation in groundwater levels, can be minimised in several ways; the seasonal variation may be reduced by making measurements at approximately the same time every year (Arnet et al., 1997) while the effects of water table fluctuations can be reduced by measuring at stations located on crystalline bedrock (Jachens and Roberts, 1985). The depth and distance at which it is possible to detect subtle changes within a Mogi-type magma reservoir can be calculated by solving for the total observed gravity

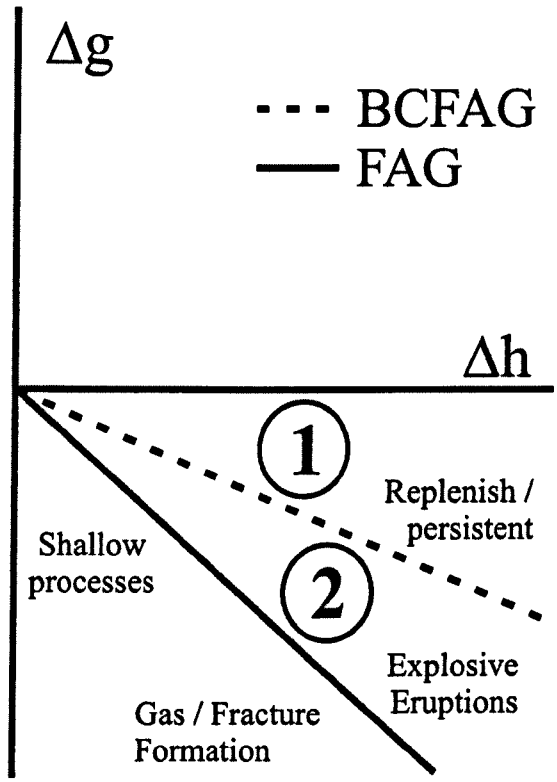

Figure 4.3: During periods of inflation, increasing elevation (Δh) is accompanied by decreasing gravity (negative Δg), defined by the BCFAG. Region 1 represents anomalously large gravity increases and may be interpreted in terms of magma intrusion into a magma reservoir resulting in an increase in the average density of the reservoir. Region 2 reflects an overall density decrease and mass increase that may be interpreted in terms of gas build up within the magma reservoir, an important trigger mechanism for explosive eruptions. Data falling below the FAG and close to the Δg line may reflect shallow processes such as magma and gas fluctuations within the feeder conduit. *Modified after Rymer and Williams-Jones (2000).*

change, Δg (μGal), in the following relationship (Dzurisin et al., 1980; Johnson, 1987; Eggers, 1987):

$$\Delta g = \left(\frac{\Delta M_m \cdot G \cdot z}{\left(x^2 + z^2\right)^{3/2}} \right) \cdot 10^7 \qquad (4.2)$$

where ΔM_m is the change in subsurface magma mass, G is the Universal Gravitational constant (6.672 x 10^{11} N m^2 kg^{-2}), x is the surface distance (m) out from the centre of the Mogi source, and z is the depth (m) to the Mogi point source (Figure 4.1). Thus, for subsurface magma mass changes of 10^{11} kg (e.g., Rabaul, Campi Flegrei; McKee et al., 1989; Berrino et al., 1992) at a depth between 2 and 6 km, gravity variations (> 20 μGal) can be measured at a horizontal distance of up to ~4 km. For a mass change of the order of 10^{12} kg in a reservoir between 2 and 7 km deep, gravity changes are detectable at up to ~10 km distance (Figure 4.4).

4.4. Modelling a Magma Reservoir

Although the Mogi model represents a very simple magma reservoir, many published geophysical data are consistent with this type of source (Berrino et al., 1992; Arnet et al., 1997; Avallone et al., 1999). Here we present two end member models that illustrate how, by observing density changes within the magma reservoir, the hazard potential of a volcanic system can be determined.

An intruding magma with a relatively low Reynolds number (i.e., laminar flow; Sparks et al., 1980) will have little or no interaction with the surrounding magma reservoir (model 1, Figure 4.5a). There will, however, be an overall mass increase in the system, measurable at the surface as a gravity increase along with limited ground deformation. This will result in a Δg/Δh gradient that will plot between the BCFAG and the Δh axis (region 1) or along the BCFAG (Figure 4.3) implying an overall density increase (region 1)

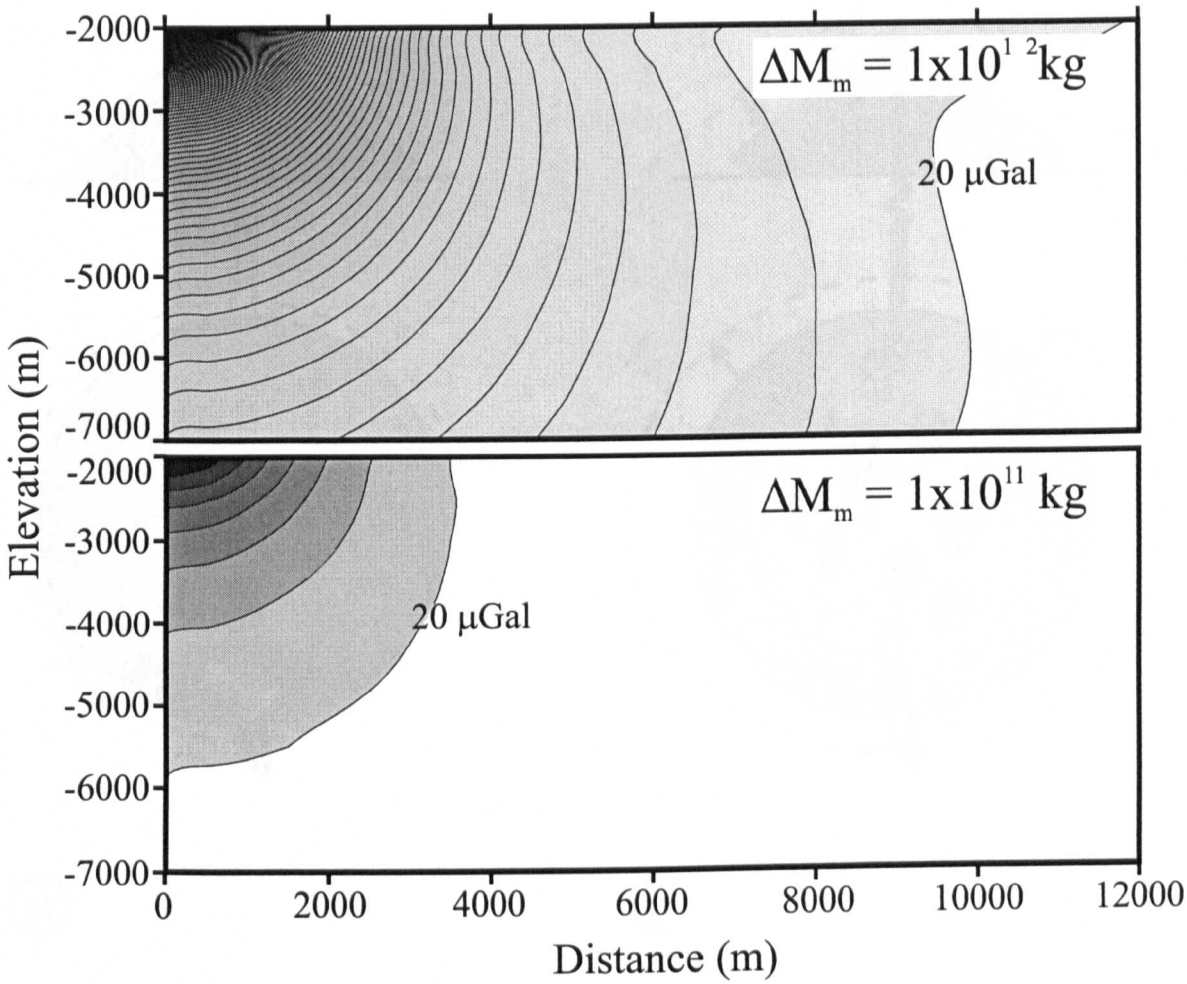

Figure 4.4: The depth and distance at which it is possible to measure gravity changes (Δg) within a Mogi source can be determined for given changes in sub-surface magma mass (Equation 4.2). For mass changes on the order of 10^{11} kg (similar to those of Campi Flegrei and Rabaul calderas), small gravity changes (>20 μGal) can be measured at horizontal distances of up to ~4 km. For larger changes, e.g., 10^{12}kg, variations in gravity could be measured at up to 10 km from the centre of activity. Contours are 20 μGal. Depth (z) and distance (x) from the Mogi source are in metres (see Figure 4.1).

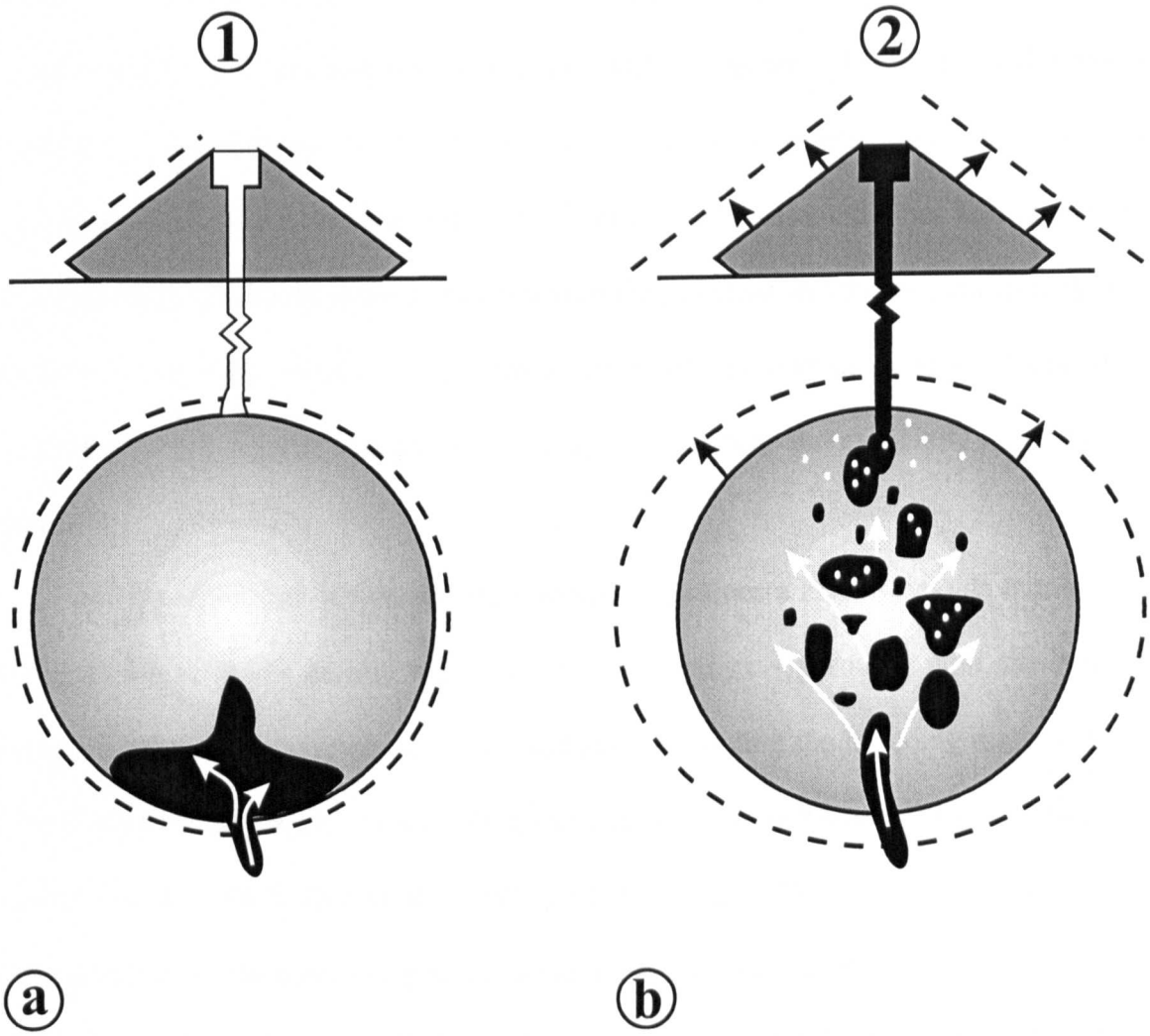

Figure 4.5: (a). Model 1 depicts the intrusion of a low Reynolds number magma (i.e., laminar flow) into a magma reservoir. Importantly, there is little or no interaction with the surrounding magma. The observed $\Delta g/\Delta h$ gradient will fall into region 1 of Figure 4.3. (b). Model 2 represents the other end member. Assuming an identical magma mass influx as model 1 but higher Reynolds number (i.e., turbulent flow), the intruding magma will interact vigorously with the surrounding magma, resulting in heating, convection, vesiculation and expansion of the reservoir. The observed gradient will fall into region 2 of Figure 4.3. *Modified after Rymer and Williams-Jones (2000).*

or no density change (BCFAG) within the reservoir. Increasing density within a magma reservoir is often interpreted in terms of magma devesiculation and/or void filling (cf. Brown et al., 1991; Rymer, 1994). The dense intruded magma may be unable to rise and, in a closed system, the reservoir would eventually stagnate. However, if the magma pressure exceeds the local lithostatic pressure, dykes may be injected into the country rock and can in some cases eventually feed lava eruptions. The essential point here is that there is very limited interaction between the new intruding magma and the magma already in the reservoir. The mass increase is associated either with an overall density increase in the reservoir or in no density change. Either way, an eruption, and especially a large one, is unlikely.

At the other end of the spectrum, model 2 assumes a high Reynolds number (i.e., turbulent flow; Sparks et al., 1980) which will interact vigorously with the reservoir magma, heating it, causing convection, and therefore cooling the intruding magma (Figure 4.5b; Eichelberger, 1980). This cooling can then lead to oversaturation and vesiculation (Huppert et al., 1982; Tait et al., 1989; Pallister et al., 1992), while superheating and decompression of the convecting reservoir magma may also cause volatile supersaturation and exsolution (Sparks et al., 1977). Consequent gravity and deformation variations would plot as a $\Delta g/\Delta h$ gradient between the FAG and BCFAG (region 2, Figure 4.3) due to a net subsurface mass increase and density decrease. Significantly, the interaction between the intruding magma and the older ponded magma is much more pervasive than in model 1. Magma mixing and mingling will cause significant bubble formation and the resulting increase in gas pressure within the reservoir is an essential pre-requisite to explosive eruptive activity (Eichelberger, 1980; Woods and Koyaguchi, 1994).

These models suggest that the observed $\Delta g/\Delta h$ gradient will evolve as a volcano develops from a state of dormancy through unrest into explosive eruptive activity. The application of these models to hazard warning is as follows. As the gradient migrates from

region 1 towards the BCFAG, the density of the magma reservoir decreases (Figure 4.3) as a result of reduced crystallisation, increased buoyant melt and vesicle content. On the BCFAG, the magma reservoir volume increases but its density remains constant. In either scenario, eruption hazard is minimal. Once the measured $\Delta g/\Delta h$ gradient crosses the BCFAG, the density of the magma reservoir has decreased below the previous average value of the reservoir and the system becomes unstable. It is at this stage that the magma will be able to rise and presents an increased eruption hazard. If there is only limited heating, magma convection within the reservoir will follow; this has recently been linked with pulses of activity at the surface (Kazahaya et al., 1994; Stevenson and Blake, 1998). However, with excess heating, as gas pressure increases, the likelihood of an explosive eruption will increase (Woods and Koyaguchi, 1994).

4.5. Application of the Models

Calderas in a state of unrest and large composite volcanoes are the most appropriate targets for the models proposed here. In an open volcanic system (i.e., one that displays persistent surface manifestations such as a stable lava lake, frequent explosive eruptions, etc.) gravity and deformation measurements made in region A (Figure 4.1) will typically be dominated by shallow processes. Thus, in order to study processes within such a Mogi-type source, measurements must be made in region B, off the central axis of activity. A closed volcanic system on the other hand, generally has little or no surface activity allowing for $\Delta g/\Delta h$ gradient measurements to be made safely in both regions A and B. Some examples of these systems are presented below.

4.5.1. Campi Flegrei, Italy

The Campi Flegrei caldera (Naples, Italy) is a prime example of a persistently active closed system and a caldera in a state of unrest. Formed ~35 000 years ago with the

explosion of the Campanian Ignimbrite, the 12-km-diameter caldera last erupted in 1538. More recently however, in the 1970s and early 1980s, the caldera was characterised by a bradyseismic crisis (an extended period of very slow vertical instability of the crust; Jackson, 1997) and a maximum uplift and gravity change of 1.616 m and -331 μGal, respectively. The measured FAG was -290 ± 5 μGal m^{-1} and assuming a point source density of 2500 km m^{-3}, the BCFAG was calculated to be -220 μGal m^{-1} (Berrino et al., 1992). The $\Delta g/\Delta h$ gradient during inflation was -213 ± 6 μGal m^{-1} and fell into region 1 (Figure 4.6a) and as our model predicts, there was no eruption. In fact, between February 1981 and March 1983, the gradient actually evolved from the BCFAG towards the horizontal axis, well into region 1 (Figure 4.3; Berrino, 1994). This episode was interpreted in terms of intrusion into a magma reservoir with a resulting overall subsurface mass increase of ~2 x 10^{11} kg (Berrino et al., 1984). Mobilisation of the hydrothermal system has also been proposed as a possible cause of the observed uplift (Bonafede and Mazzanti, 1998).

Our model predicts that during inflation, once the $\Delta g/\Delta h$ gradient steepens beyond the BCFAG (-220 μGal m^{-1} in this case) into region 2, an explosive eruption is likely to follow. A modern explosive eruption of the same magnitude as the 1538 Pozzuoli eruption would affect an estimated 80 000, while 200 000 people would be at risk if the eruption was of similar magnitude to the larger 4400 BP Agnano-Monte Spina eruption (Barberi and Carapezza, 1996). Due to the extensive history of caldera unrest at Campi Flegrei and the increasing population of the Naples region, the need to distinguish between magma chamber processes (models 1 and 2, Figure 4.5) is of critical importance to hazard mitigation.

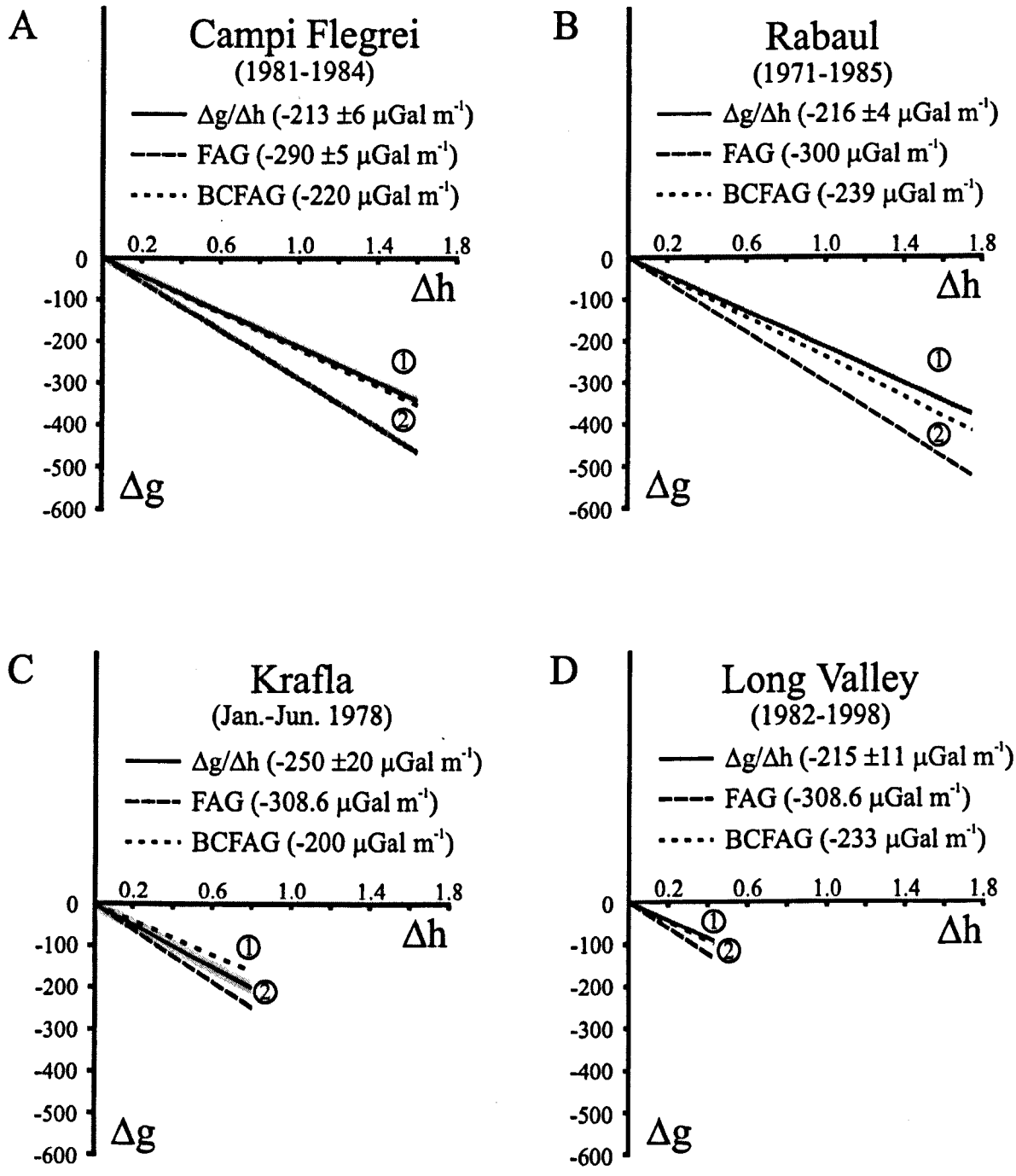

Figure 4.6: The Δg/Δh gradients observed during periods of inflation at the calderas of a) Campi Flegrei, b) Rabaul, c) Krafla, and d) Long Valley. The FAG and BCFAG gradients are measured or estimated/calculated values. Δh is in m and Δg in μGal. Grey shading represents estimated error for the measured gradients. *Modified after Berrino et al. (1992).*

4.5.2. Rabaul, Papua New Guinea

Another excellent example of a closed system is the Rabaul caldera (New Britain Island, Papua New Guinea) which has been in a state of unrest since at least the late 1800s. The caldera (14 x 9 km) lies within a shallow ignimbrite volcano and was modified by an earlier explosive episode 1400 years ago (Walker et al., 1981). In a more recent crisis (1973-1985), there was an overall uplift of ~100 mm yr^{-1} with a maximum inflation of 1.8 m and gravity change of up to -410 μGal (McKee et al., 1989). Although no FAG was measured, given the amplitude and wavelength of a static Bouguer anomaly, the FAG has been estimated at -300 μGal (Berrino et al., 1992). Assuming a point source density of 2500 kg m^{-3}, the BCFAG was then calculated to be -239 μGal m^{-1} (Berrino et al., 1992). This episode was believed to have been caused by an intrusion of basic magma into a pre-existing reservoir that resulted in an overall subsurface mass increase of 10^8 kg (McKee et al., 1989; Rymer, 1994). As at Campi Flegrei, the $\Delta g/\Delta h$ gradient (-216 ± 4 μGal m^{-1}) measured at Rabaul fell into region 1 (Figure 4.6b); there was no eruption observed during this period. If the gradient were to have progressed below the BCFAG of -239 μGal m^{-1} (into region 2), our model predicts that an explosive eruption would have followed.

The most recent period of activity (1992-1999) which has been characterised by inflation and seismic swarms, in fact developed into an extensive series of explosive and effusive eruptions. Petrological analyses of material erupted between 1997 and 1998 suggest that, as with the 1973-1985 crisis, current activity was initiated by the intrusion of new basaltic magma into the shallow dacitic reservoir (Bulletin of the Global Volcanism Network, 1992-1999). Unfortunately, no gravity data are available for this period and thus it is not known whether the $\Delta g/\Delta h$ gradient had actually progressed into region 2 prior to the onset of eruptive activity (Figure 4.6b). Although the town of Rabaul is not as densely populated as Naples, the activity at this centre poses a threat to the livelihood of tens of

thousands of people. The population is well informed about volcanic activity and more than 50 000 were successfully and safely evacuated prior to the eruption in 1994 (Bulletin of the Global Volcanism Network, 1992-1999).

4.5.3. Krafla, Iceland

The Krafla caldera (northeast Iceland) is part of the large Krafla central volcano that straddles a 100 km-long N-S trending fissure swarm. The 8 by 10-km caldera is believed to have formed ~0.1 Ma ago during the last inter-glacial period with the explosive eruption of rhyolitic and dacitic rocks (Saemundsson, 1978). Krafla was last active during the 1975-1984 rifting episode that was characterised by lava extrusion, dyke emplacement and steady inflation interrupted by rapid subsidence within the caldera. The inflationary periods are interpreted in terms of pressure increase within a shallow magma reservoir followed by rupture of the reservoir walls with rifting and dyke formation leading to rapid subsidence (Tryggvason, 1984). The January-June 1978 inflationary period was characterised by gravity and height variations which followed a gradient of -250 ± 20 μGal m^{-1} (Johnson and Sigurdsson, 1980). A FAG and BCFAG for the caldera were calculated at –308.6 and –200 μGal m^{-1}, respectively (Rymer et al., 1998b). This is the only published example, where during inflation, the observed $\Delta g/\Delta h$ gradient fell into region 2 (Figure 6c). Our model suggests that magma reservoir mass increase but density decrease is likely to lead to an eruption. In this basaltic extensional tectonic regime, fire fountaining occurred, feeding lava flows and there was also considerable dyke injection. Post-eruptive activity has been characterised by continued deflation (30 mm yr^{-1}; Sigmundsson et al., 1997) and a net gravity decrease caused mainly by the drainage of 4×10^{10} kg of magma (Rymer et al., 1998b). The hazard to the population is extremely small at this site. However Lake Myvatn, just a few km away, is a very popular tourist centre and Krafla

supports an industrial geothermal power plant so that eruptive activity affects thousands of people directly.

4.5.4. Long Valley, USA

Long Valley caldera (California, USA) which is located on the eastern edge of the Sierra Nevada tectonic block, formed 730 ka ago during the Bishop Tuff eruption. This was followed shortly by the formation of a resurgent rhyolite dome (Bailey et al., 1976). A negative Bouguer anomaly, with a steep gradient > 20 mGal in some places, is concentric with the caldera and reflects the lateral transition from low-density caldera material to the high-density crystalline rocks of the Sierra Nevadas (Kane et al., 1976; Jachens and Roberts, 1985). During the 1982-1998 inflationary period, centred on the resurgent dome, a gravity decrease of up to 107 ± 6 μGal and maximum residual inflation of 0.42 ± 0.05 m occurred, giving an average $\Delta g/\Delta h$ gradient of -215 ± 11 μGal m^{-1} (Dzurisin et al., 1990; Battaglia et al., 1999). This episode has most recently been interpreted in terms of a mass increase (3.8 x 10^{11} to 17.8 x 10^{11} kg) due to the intrusion of basaltic magma into a rhyolitic reservoir beneath the resurgent dome (Battaglia et al., 1999). Assuming the theoretical FAG and a density of 2700 kg m^{-3}, the calculated BCFAG is -233 μGal m^{-1} and as for some of the previous examples, the measured $\Delta g/\Delta h$ gradient falls above the BCFAG into region 1. Our model predicts that the net density of the reservoir will increase thus making an eruption unlikely (Figure 4.6d).

4.6. Conclusions

Large composite volcanoes and calderas in a state of unrest are appropriate targets at which to consider the models presented here where they are characterised by a spherical Mogi-type source. Conventional micro-gravity surveys involve the measurement of a large network of stations, often in proximity to centres of volcanic activity, and inevitably focus

on relatively shallow processes. Here, we require simultaneous measurements of deformation and gravity at only a few key stations off axis of the centre of activity. Clearly the number of stations required would depend on the individual circumstances and available instrumentation, but at 1-5, will be considerably less than required for conventional micro-gravity surveys. The advent of continuous gravity and deformation monitoring (cf. Berrino et al., 1997; Dixon et al., 1997) will allow for a dramatically increased temporal resolution by this method. The spatial resolution is not compromised badly, since the sources of interest in the proposed method are deeper than for conventional micro-gravity surveys. Very small changes in mass or density of a magma reservoir at depths of 2-7 km can be made at a safe distance (up to 10 km) from the active centre, greatly reducing the risk to scientists. By quantifying the magnitude and rate of these changes, eruption precursors within the reservoir may be detected well before the magma begins to rise towards the surface, offering significantly more time for hazard mitigation and evacuation. Determining the nature of these processes is also critical for evaluating the potential magnitude of the hazard. About 140 calderas have shown a degree of unrest in historical times, however of the 94 well-documented cases, only 45 resulted in eruption (Newhall and Dzurisin, 1988). At silicic calderas only 15% of the cases of unrest resulted in eruption, but increasing population and vulnerability to explosive eruptions means that a better understanding of caldera unrest is an essential goal for the new millennium.

4.7. Acknowledgements

This research was supported by the Royal Society, The Open University Research Development Fund and NERC. We thank J. B. Murray, C.A. Locke, J. Cassidy and D. Rothery for many useful discussions about this work. This work was greatly improved by the comments of an anonymous reviewer.

Chapter 5.

Processes controlling persistent volcanism

To be submitted to the Bulletin of Volcanology

5.1. Abstract

An ongoing question in volcanology is the cause for the large discrepancy between measured degassing rates and extrusion rates, which indicate great differences between the rate at which magma is degassed (fast) and the rate at which it is crystallised (slow). A number of models have been proposed to explain this discrepancy, including endogenous and cryptic intrusion, convection, and cumulate emplacement at depth. Investigation of the published physical characteristics (e.g., gas flux, extrusion rates, magma residence times, etc.) of four well-studied volcanoes suggests that while endogenous and cumulate emplacement may account for some of the unerupted material, convection is a viable mechanism to explain much of the large difference in volumes of erupted and degassed magma. The high rates of degassing and cooling at these open-system volcanoes necessitates convection for the removal of the cooled and degassed magma and suggests that it may in fact be a fundamental processes controlling persistent volcanism.

5.2. Introduction

Persistent volcanism has commonly been defined by the continuous presence of fumaroles, acid crater lakes, active strombolian vents and lava lakes with prolonged high

thermal and gas flux (Francis et al., 1993; Stevenson and Blake, 1998). However, for the purpose of this study, persistent volcanism refers to volcanoes with continuous degassing, eruptive activity, and the presence of surface magma in the form of active lava lakes or glowing vents. At some volcanoes, active lava lakes and strombolian vents have persisted for periods of years to millennia, liberating copious amounts of volatiles and thermal energy. As a consequence of this persistent activity, significant volumes (several km^3) of magma must have degassed and cooled, only a small fraction of which has been erupted. Furthermore, geophysical and geochemical studies have shown little evidence of large shallow magma reservoirs beneath these volcanoes (cf. Capaldi et al., 1978; Pietruszka and Garcia, 1999; Chiarabba et al., 2000) suggesting rather that the persistent volcanism is necessarily supplied with magma, gas and/or heat by large deep reservoirs (>5 km). This raises the question of how continuously active volcanoes are supplied and the mechanisms responsible for the removal of the non-erupted, cooled and degassed magma. In order to investigate these processes, four of the best-studied persistently active volcanoes (Mt. Etna, Stromboli, Kilauea and Masaya) are discussed here.

5.3. Geological Setting

Mt. Etna (3315 m a.s.l.) is a large composite basaltic stratovolcano located in Sicily, near the city of Catania (37.73°N, 15.00°E) that has been active for over 500 000 years (Gillot et al., 1994; Figure 5.1). Current activity is characterised by nearly continuous degassing and periods of explosive and effusive activity (c.f. Calvari et al., 1994; Allard, 1997; Harris et al, 2000). Stromboli (924 m a.s.l.) is also a basaltic stratovolcano, located in the Aeolian islands north of Sicily (38.79 N, 15.21 E) which has been continuously active for between 2000 and 5000 years (cf. Mercalli, 1881; Allard et al., 1994; Rosi et al., 2000; Figure 5.1). Its current activity is characterised by persistent

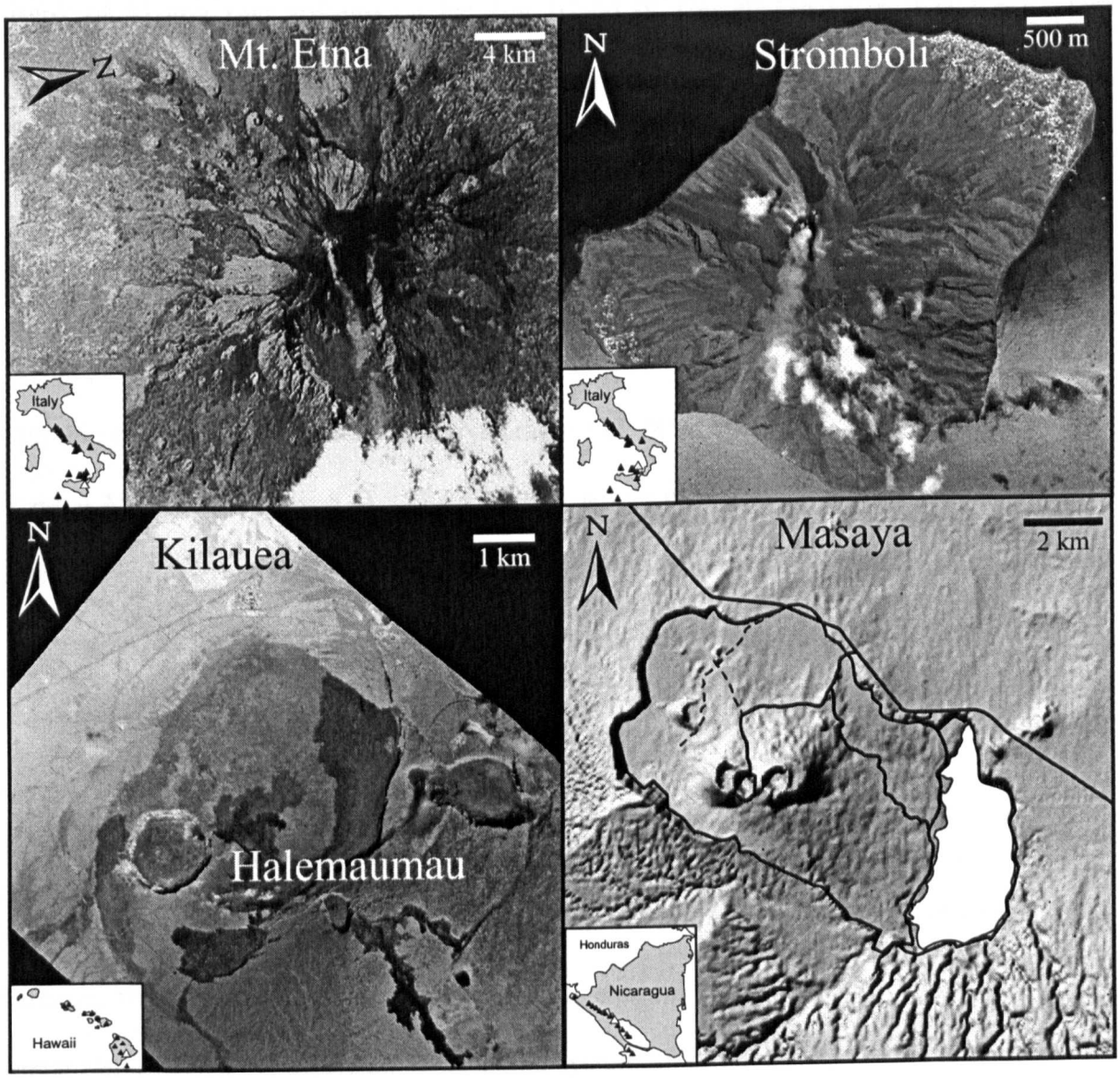

Figure 5.1: Location maps of Mt. Etna, Stromboli, Kilauea and Masaya. Open triangles on the insets indicate the locations of the volcanoes. Note the different orientation of the Mt. Etna photo. *Modified after M. Scheele, DLR (1996), NASA Skylab SL3-87-355 and P. Mouginis-Mark (1996).*

degassing and small strombolian explosions from three summit craters (c.f. Chouet et al., 1974; Allard et al., 1994).

Kilauea (1222 m a.s.l.) is a large basaltic shield volcano located on the southeastern flank of Mauna Loa volcano on the Big Island of Hawaii (19.53°N, 155.3°W). The volcano hosts the Kilauea caldera and Halemaumau pit crater, with eruptions originating primarily from the summit caldera and/or along E or SW rift zones (Figure 5.1). Activity has been characterised by fire fountaining, lava lake formation and extensive effusive eruptions. The most recent eruption began in January 1983 along the East Rift Zone with activity eventually shifting to the Pu`u `O`o crater. Masaya (635 m a.s.l.) is also a large basaltic caldera complex, situated in Nicaragua (11.98 N, 86.16 W), 20 km southeast of the capital Managua (Figure 5.1). The currently active pit crater, Santiago, has been nearly continuously active since its formation in 1853, and is characterised by episodes of degassing and lava lake formation. The most recent degassing episode started in 1993 and continues to present (Rymer et al., 1998a; Chapter 2).

5.4. Supplying persistently active volcanoes – Source regions

While the source regions and tectonic environments of these volcanoes differ greatly, they all lack evidence of substantial summit reservoirs with which to support persistent activity. The magmatic plumbing system of Kilauea is one of the most intensely studied in the world. It essentially consists of a vertical conduit (or conduits) that supplies a shallow (2-3 km b.s.l.) summit reservoir by tapping mantle-generated melt from 60-170 km (Figure 5.2; cf. Eaton and Murata, 1960; Ryan, 1988; Tilling and Dvorak, 1993; Pietruszka and Garcia, 1999). Estimates of the volume of the upper reservoir have ranged from 0.08 to 40 km^3 but it is now believed to be approximately 2-3 km^3 (Pietruszka and Garcia, 1999). Once the reservoir is filled (at a rate of 2-6 x 10^{11} kg yr^{-1}) to approximately

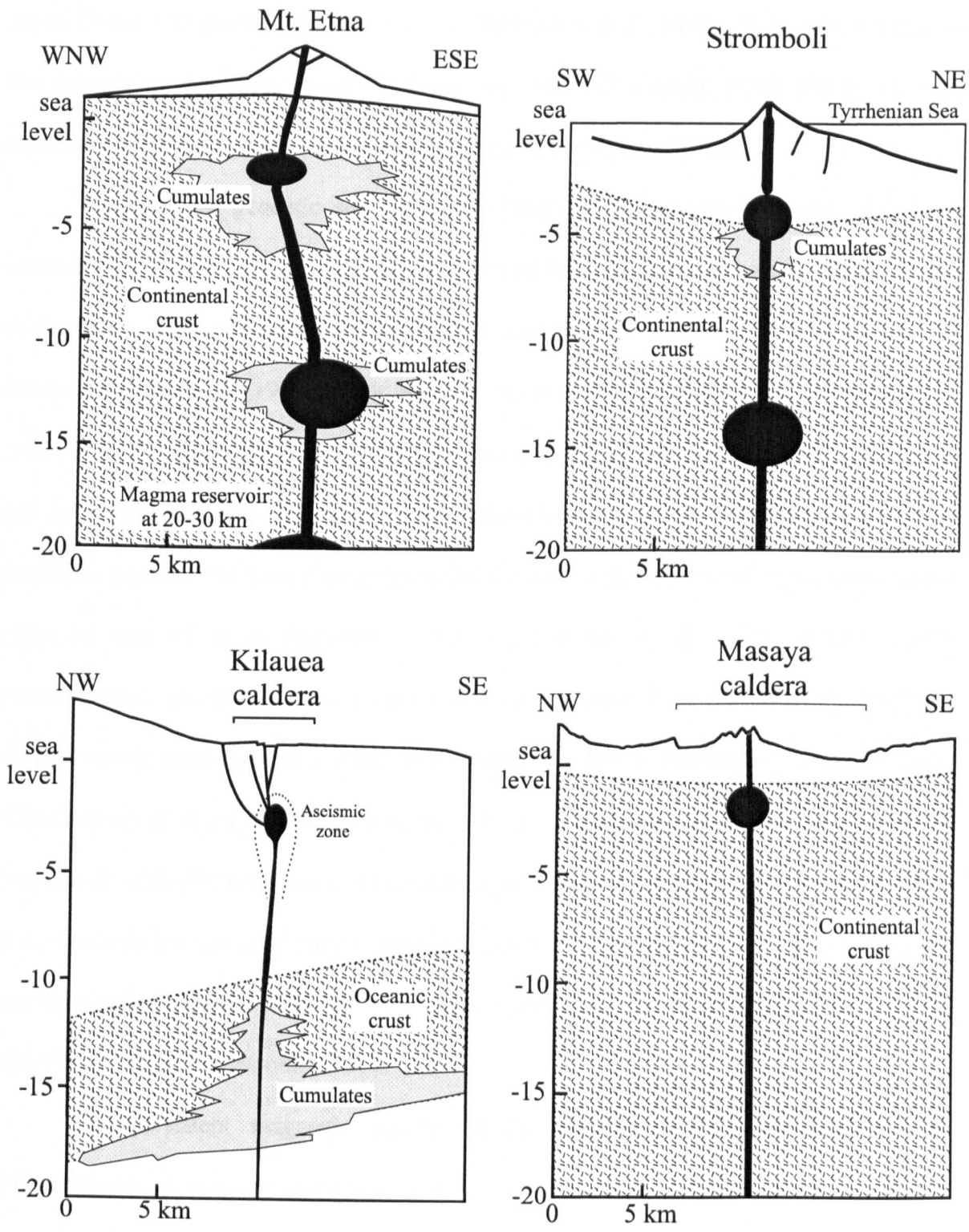

Figure 5.2: Comparative schematic diagrams of the plumbing systems of Mt. Etna, Stromboli, Kilauea, and Masaya volcanoes. Masaya topography has a vertical exaggeration of 3 times. *Mt. Etna: modified after Tanguy et al. (1997) & Murru et al. (1999); Stromboli: modified after Allard et al. (1994) & Francis et al. (1993); Kilauea: modified after Francis et al. (1993) & Pietruszka and Garcia (1999).*

lithostatic pressure, the magma is emplaced upwards as dikes or laterally into the rift zones (Table 5.1; Decker, 1987; Denlinger, 1997; Elias et al., 1998). The residence time of the magma in the upper reservoir during the late 20th century (1961-1982) has been estimated at approximately 30-40 years (Pietruszka and Garcia, 1999).

Seismic and geodetic studies at Mt. Etna also show little evidence of a large reservoir (i.e., a low velocity zone) in the upper 18 km b.s.l. (Chiarabba et al., 2000; Harris et al., 2000). Moreover there is some seismic evidence for smaller reservoirs at 2 and 11 km b.s.l. (Murru et al., 1999) which is further supported by studies of melt inclusions (0.3 ± 0.03 wt% S) suggesting that sulphur begins to exsolve at ~140-100 MPa or 2-0 km below sea level (Métrich and Clocchiatti, 1989; Métrich et al., 1993). The upper plumbing system is estimated to have a capacity of 0.4-0.6 km^3 with magma residence times on the order of tens of years (Albarède, 1993; Condomines et al., 1995; Allard, 1997). Petrochemical, geochemical and geophysical evidence suggest the presence of a 20-30 km deep reservoir composed of crystal mush which may be the remnant of a mantle diapir (Condomines et al., 1995; Tanguy et al., 1997). While magma in this deep reservoir (volume of ~150-200 km^3) has an estimated upper limit of 1500 years residence time, there is no evidence for rise and shallow emplacement of a large magma body prior to eruption but rather pressurisation of the entire volcanic system and rise from depth of the majority of erupting magma (Condomines et al., 1995).

The persistent magmatic activity at the surface of Stromboli and lack of differentiation in isotopic species in gases from the three summit craters suggests a relatively simple plumbing system (Gauthier et al., 2000). Shallow and weak seismicity (Capaldi et al., 1978; Ntepe and Dorel, 1990) does not support direct supply from depth but rather, in conjunction with geochemical data, suggests that a small, very shallow source (200-300 m beneath the crater floor; Harris and Stevenson, 1997; Gauthier et al., 2000) may be connected to a larger mid-level reservoir (3-4 km b.s.l; Allard et al., 1994). This

Table 5.1: Characteristics of Kilauea, Mt. Etna, Stromboli and Masaya volcanoes

	Etna[1] (1975-1995)	Stromboli[2] (1980-2000)	Kilauea[3] (1979-1997)	Masaya[4] (1972-2000)	References
Shallow reservoir (km b.s.l.)	0-2	S: 0.2-0.3^{depth} M: ~3-4?	2-4	~1	1) Allard (1997) 2) Allard et al. (1994); Harris & Stevenson (1997); Gauthier et al. (2000) 3) Pietruszka & Garcia (1999) 4) Stoiber et al. (1986); Métaxian & Lesage (1997)
Deep reservoir (km)	20-30	10-15	?	?	1) Allard (1997); Tanguy et al. (1997) 2) Francalanci et al. (1989)
S content in melt (wt%)	0.3	0.05-0.29	0.05	0.03-0.15	1) Métrich & Clocchiatti (1989) 2) Allard et al. (1994) 3) Francis et al. (1993) 4) This study
Time-averaged SO_2 flux (kg yr^{-1})	15±3.0 x 10^8	1.1±0.3 x 10^8	~6 x 10^8	4.4±2.7 x 10^8	1) Allard (1997) 2) Allard et al. (1994, 2000) 3) Elias et al. (1998) 4) This study
Total gas flux (kg yr^{-1})	>1.5 x 10^{10}	~2-4 x 10^9	~6 x 10^9	~1.0 x 10^{10}	1) Allard et al. (1991); Allard (1997); Francis et al. (1998) 2) Allard et al. (1994, 2000) 3) Gerlach & Graeber (1985); Elias et al. (1998) 4) This study
Total thermal flux (MW)	?	420±230^{vent}	460-680^{lake}	1600^{vent} 7100^{lake}	1) 2) Harris & Stevenson (1997) 3) Francis et al. (1993) 4) This study
Magma supply rate (kg yr^{-1})	~6x $10^{11\ Eff}$ ~3 x $10^{11\ SO2}$	~2-14x10^{10SO2} ~0.6-4x$10^{10\ Th}$	~2 x $10^{11\ Eff}$ ~6 x $10^{11\ SO2}$	~2-7 x $10^{11\ SO2}$	1) Allard (1997); Harris et al. (2000) 2) Allard et al. (1994); Giberti et al. (1992); Harris & Stevenson (1997) 3) Denlinger (1997); Elias et al. (1998); This study 4) Stoiber et al. (1986); This study
Magma eruption rate (kg yr^{-1})	~7-9 x 10^{10}	~1 x 10^7	1.9-2.2 x 10^{11}	~10^2?	1) Allard (1997); Harris et al. (2000) 2) Francis et al. (1993) 3) Denlinger (1997) 4) This study
Magma degassing rate (kg yr^{-1})	~8 x 10^{11}	~2-14 x 10^{10}	~6 x 10^{11}	~2-7 x 10^{11}	1) Allard (1997) 2) Allard et al. (1994) 3) This study; Francis et al. (1993) 4) Stoiber et al. (1986); This study
Erupted/Degassed magma	1.1 x 10^{-1}	0.7-7 x 10^{-4}	~3-7 x 10^{-1}	5 x 10^{-10}?	1) Allard (1997) 2) Allard et al. (1994) 3) This study 4) This study
Residence time in shallow reservoir (years)	A few tens	S: 0.03-0.5 M: 19±12	~30-40	?	1) Albarède (1993); Condomines et al. (1995) 2) Francalanci et al. (1999); Gauthier et al. (2000) 3) Pietruszka & Garcia (1999)
Estimated volume of shallow reservoir (m^3)	3.5-6 x 10^8	S: 7±2 x 10^5 M: 4-30 x 10^7	~2-3 x 10^9	~0.5-1 x 10^9?	1) Condomines et al. (1995); Allard (1997) 2) Francalanci et al. (1999); Gauthier et al. (2000) 3) Pietruszka & Garcia (1999) 4) Stoiber et al. (1986); This study
Time to cool ~ reservoir volume to solidus (years)	?	S: ~0.02 M: ~1-10	~40-100	~1-10	This study

S and M symbols for Stromboli denote possible summit and mid-level reservoirs. Depth of summit reservoir is 200-300 m below the surface. SO_2, Th and Eff superscripts in "Magma supply rate" refer to estimates based on SO_2 and thermal flux, and measured effusion rates, respectively. Vent and Lake superscripts in "Total thermal flux" refer to thermal flux from small open vents and larger area lava lakes. See text.

would then tap an even larger, deeper reservoir at ~10-15 km below sea level (Figure 5.1; Capaldi et al., 1978; Francalanci et al., 1989; Allard et al., 1994). Magma in the small summit reservoir ($7 \pm 2 \times 10^5$ m^3) has an estimated residence time of only 10-200 days (Gauthier et al., 2000). However, Sr isotope evidence suggests a magma residence of ~19 years in a $3\text{-}40 \times 10^7$ m^3 reservoir (Francalancia et al., 1999). Considering the discrepancy in estimated shallow reservoir volumes and residence times, the latter may refer to the mid-level reservoir suggested by (Allard et al., 1994). The upper magma system is nevertheless estimated to be supplied at a steady rate of $0.6\text{-}14 \times 10^{10}$ kg yr^{-1} (Giberti et al., 1992; Allard et al., 1994; Harris and Stevenson, 1997).

Static and dynamic micro-gravity measurements at Masaya also show no evidence of a large shallow reservoir (Métaxian, 1994; Rymer et al., 1998a; Chapter 3). Rather, data from seismic hypocentres and degassing suggest the presence of a small shallow reservoir at approximately 1 km b.s.l (Stoiber et al., 1986; Métaxian et al., 1997; Chapter 2). Micro-gravity measurements and visible observations of persistent incandescence also suggest that magma is present tens of metres beneath the floor of Santiago crater (Rymer et al., 1998a; Chapter 3). The lack of a coherent seismic network at Masaya makes it difficult to determine the location of a possible deeper reservoir. It has been suggested, in order to explain the large plinian eruption which formed Masaya caldera (Williams, 1983a,b), that there must have been extremely rapid ascent (>1 m s^{-1}) of magma from depth (~80-125 km) without any period storage in a large shallow reservoir (Carr and Stoiber, 1973; Gregg and Williams, 1996).

5.5. The degassing problem

A fundamental problem in volcanology has been the discrepancy between measured gas flux and extruded material. Although there are inconsistencies due to the limitations of melt inclusion analysis and remote gas flux measurements (cf. Gerlach and

McGee, 1994; Chapter 2), the rate of magma degassing can nevertheless be estimated using gas flux measurements and melt inclusion analyses of initial sulphur contents. Even with large estimates of the initial sulphur content, it is clearly apparent that in some cases, orders of magnitude more magma is degassed than erupted.

At Mt. Etna, extensive COSPEC measurements between 1975-1995 show that SO_2 flux ranges from <1000 t d^{-1} during passive degassing to 10 000-12 000 t d^{-1} during explosive strombolian activity with some events of lava fountaining (1990-1991) exceeding 20 000 t d^{-1} (Allard, 1997). Together, these give a time-averaged SO_2 flux of $1.5 \pm 0.3 \times 10^9$ kg yr^{-1} or a minimum total gas flux ($H_2O + CO_2 + SO_2 + HCl + HF$) of at least 1.5×10^{10} kg yr^{-1} (Table 5.1; Allard et al., 1991; Allard, 1997; Francis et al., 1998). Assuming that there was an initial concentration of 0.3 wt% S in the melt (Métrich and Clocchiatti, 1989), this suggests that between 4 and 6 km^3 of basalt degassed during this period at a rate of $5.6 \pm 3.3 \times 10^{11}$ kg yr^{-1}. However, only 13% (~9×10^{10} kg yr^{-1}) of this was extruded (Table 5.1; Allard, 1997; Harris et al., 2000).

Similarly, a large set of degassing data exists for Kilauea and shows that between 1979 and 1997, ~2500 t d^{-1} of SO_2 was normally emitted from the summit and East Rift Zone with a time-averaged SO_2 emission rate of ~6×10^8 kg yr^{-1} (Elias et al., 1998). Measurements of the ratios of other gas species imply a minimum total gas flux of ~6×10^9 kg yr^{-1} (Gerlach and Graeber, 1985; Greenland et al., 1985; Elias et al., 1998). Assuming an initial melt content of 0.05 wt% S (Francis et al., 1993), ~6×10^{11} kg yr^{-1} of magma was degassed, 30-70% of which can be accounted for by the high eruption rate (~2×10^{11} kg yr^{-1}; Table 5.1).

Although the degassing data for Stromboli are more sporadic than either Mt. Etna or Kilauea, COSPEC measurements suggest that it typically emits 300-1200 t d^{-1} of SO_2 with a time-averaged flux of $1.1 \pm 0.3 \times 10^8$ kg yr^{-1} over the last 20 years (Table 5.1; Allard et al., 1994). Assuming initial concentrations of 0.06-0.3 wt% S in the melt, Stromboli

degassed the magma at a rate of 2.5-5 x 10^{10} kg yr^{-1}, orders of magnitude more than that which is estimated to have erupted (~1 x 10^7 kg yr^{-1}; Francis et al., 1993; Allard et al., 2000). Based on recent degassing rates and the extremely persistent nature of activity at Stromboli, it may have degassed 50-100 km^3 (assuming a density of 2700 kg m^{-3}) in the last 5000 years of activity (Allard et al., 1994).

As with Stromboli, gas flux data for Masaya are sporadic. However, measurements from the active crater, Santiago, over the last 28 years suggest a time-averaged SO_2 flux rate of 4.4 ± 2.7 x 10^8 kg yr^{-1} (Table 5.1; Stoiber et al., 1986; Rymer et al., 1998a; Chapter 2). This is equivalent to a total gas flux rate of ~1 x 10^{10} kg yr^{-1}. If one assumes reasonable initial melt concentrations of 0.03 to 0.15 wt% S (cf. Stoiber et al., 1986; Roggensack et al., 1997; Métrich et al., 1999), magma must degas at a rate of ~2-7 x 10^{11} kg yr^{-1} to explain this gas flux (Table 5.1). During this period, however, negligible amounts of material have been ejected such that the magma-degassing rate is many orders of magnitude greater than the eruption rate (<10^2 kg yr^{-1}). During the most recent degassing episode at Masaya (1993-present), up to 0.6 km^3 may have been degassed, with up to ~15 km^3 of magma being degassed since the formation of Santiago in 1853 (Chapter 2).

Thus, even though there are differences in the degassing/eruption ratios of these volcanoes, the data nevertheless suggests that the majority of SO_2 comes from endogenous degassing of non-erupted magma. Another notable observation is that the magma degassing rates at these four very different volcanoes are, to within an order of magnitude, the same.

5.6. The cooling problem

The estimated degassing rate may also be used as a proxy for the magma supply rate (Gerlach and Graeber, 1985) which can then be compared with estimates of thermal

flux (Harris et al., 1999). Significant work has been done to investigate the activity of volcanoes that host persistent lava lakes. Specifically, thermal budgets have been estimated for a number of these in order to determine mass flux rates (e.g., Erta Ale: Oppenheimer and Francis, 1998; Erebus: Kyle et al., 1994; Niragongo: Tazieff, 1984). Importantly, the prodigious amounts of heat released by these active lava lakes suggest that large volumes of magma are cooled, as these are the source of heat. While Kilauea (Macdonald et al., 1970) and Masaya (Stoiber et al., 1986; Rymer et al., 1998a) have clearly had periods of lava lake activity, neither Stromboli nor Mt. Etna have been known to support lava lakes. However, there is generally evidence of magma present near the surface. Defined as "a lake of molten lava, usually basaltic, in a volcanic crater or depression" (Jackson, 1997), the only differences between an active lava lake and a glowing vent are the exposed surface area and height of the magma column. They are both essentially the same feature, and importantly, evidence for an open volcanic system.

In terms of cooling, the only important difference between active lake and open vent is surface area open to radiative and convective heat lost. By using the first-order cooling equations presented in Appendix C, a rough idea of the cooling rate for Kilauea (during periods of lava lake activity) can be calculated from surface heat flux estimates of Halemaumau (1880; Francis et al., 1993 and references therein) and Pu'u 'O'o (July 1991; Harris et al., 1999). Assuming that there was no extrusion and an active lava lake was present (with an area of ~4000 m^2; Harris et al., 1999), Kilauea would have a heat flux on the order of 460-680 MW mainly by convection and radiation. At this rate, it would take between 40 and 100 years to cool the ~2-3 km^3 of magma (from liquidus to just above solidus temperatures) estimated to be in the shallow surface reservoir (Table 5.1).

Although the magma level at Masaya has not been sufficiently high to sustain a lava lake since 1993, micro-gravity and seismic data suggest that it is no more than a few tens of metres below the surface of the currently active Santiago crater (Métaxian et al.,

1997; Rymer et al., 1998a; Chapter 3). During periods of lava lake activity such as in 1965, the thermal flux is estimated at ~7100 MW (for an active surface area of ~126 000 m^2) with radiation and convection being responsible for the majority of heat loss (Chapter 2). At this rate, 1 km^3 of magma (possible volume of the shallow reservoir for Masaya; Stoiber et al., 1986) would cool from liquidus temperatures to just above the solidus in ~2 years (Table 5.1). Heat loss from the small, currently active open-vent (~100 m^2) is controlled mainly by degassing and may be on the order of 1600 MW assuming a gas flux ~1700 t d^{-1} SO_2. At this rate, ~0.5 km^3 of magma (similar to that estimated to have degassed since 1993) would cool from liquidus to just above the solidus in ~5 years (Chapter 2).

Although there is currently no evidence of Stromboli having hosted an active lava lake, the persistent strombolian activity and visible incandescent vent suggests the presence of a shallow magma body (200-300 m below the crater floor; Gauthier et al., 2000). The estimated heat loss of 420 ± 230 MW, the majority of which is by degassing (Harris and Stevenson, 1997), would cool 7 ± 2 x 10^5 m^3 of magma (estimated volume of upper plumbing system; Gauthier et al., 2000) from liquidus to near solidus in only ~10 days. The potentially larger mid-level reservoir (3-40 x 10^7 m^3; Francalancia et al., 1999) located at ~3-4 km below sea level (Allard et al., 1994), would cool from liquidus to near solidus in 1-10 years.

While there is no evidence for a summit lava lake at Mt. Etna, the periods of extensive effusive activity (e.g., the 1991-1993 eruption; Stevens et al., 1997) suggest that significant amounts of magma are often, at least temporarily, present at very shallow levels. Based on heat flux estimates from Masaya, the important amounts of gas released during non-effusive, passive-degassing activity could cool significant amounts of magma. Thus, although the heat flux estimates and cooling rates may be oversimplifications, it is nevertheless clear that significant volumes of magma may cool without being erupted.

5.7. Where does the cooled and degassed magma go?

Clearly the mass of degassed and cooled magma far exceeds the volume of erupted magma which poses the question as to the ultimate fate of this cooled and degassed magma. Two end-member models have been proposed to explain the discrepancy. In the first, the cool dense magma may be emplaced endogenously into the edifice or cryptically beneath it; the second model would have it removed convectively and recharged at depth, and/or emplaced as cumulates in the underlying magma reservoir (Harris et al., 1999 and references therein).

5.7.1. Endogenous emplacement

Endogenous growth has been proposed in order to explain the discrepancy in volumes of degassed and erupted magma (Francis et al., 1993). Dyke intrusion and rift zone widening is clearly responsible for storage of much of the non-erupted magma at Kilauea (Dzurisin et al., 1984; Francis et al., 1993). There is also evidence at Mt. Etna that some of the degassed, unerupted magma is emplaced endogenously, either as dykes into the edifice or through crustal-scale extension (Laigle and Hirn, 1999). In some cases the intruded magma can be injected back into the feeding system and contribute to an eruption (e.g., 1989 eruptions; Budetta and Carbone, 1998; Harris et al., 2000).

While there is also evidence that some of the unerupted magma at Stromboli may be emplaced as dykes in the edifice (Rittman, 1962; Bonaccorso et al., 1998), the relatively stable subaerial morphology of the volcano (Rosi, 1980) and lack of evidence for sub-aqueous eruptions (Allard et al., 1994) implies that the majority of unerupted magma cannot be accounted for by endogenous growth. Although there have been instances of large flank collapse at Stromboli, specifically the Sciara del Fuoco collapse >5000 years ago (Francalanci et al., 1989), this can not account for the more recently degassed, and essentially unerupted magma.

In the case of Masaya, intrusion is also unlikely, as emplacement of the degassed magma into the edifice would result in inflation and gravity increase, neither of which has been observed (Chapter 3). Although cryptic emplacement beneath the edifice could occur without visible deformation, it would nevertheless cause a gravity increase with an anomaly significantly larger than observed. The degassed and cooled magma must have therefore been removed below the region of detection by these geophysical techniques. Thus, although the extensional regimes and evidence of dyke emplacement at Kilauea and Mt. Etna can account for much of the unerupted and degassed magma, Stromboli and Masaya, which have the greatest differences in erupted/degassed magma of the four, cannot be supported purely by endogenous growth.

5.7.2. Convection

It has long been recognised that crystallisation, melting and dissolution at the floors of basaltic magma reservoirs can cause buoyant basalt to rise into the overlying magma resulting in thermal and compositional convection (cf. Campbell, 1978; Campbell, 1986; Huppert and Sparks, 1988; Kerr, 1994). Recent modelling of degassing-driven convection in the upper plumbing system of volcanic systems also suggests that only small density differences are required for magma to be able to rise buoyantly to the surface where it degasses and cools (Kazahaya et al., 1994; Stevenson and Blake, 1998). It would then sink again in order to complete the convection cycle.

Active lava lakes such as those mentioned above are characterised by very stable volumes and thus as virtually no lava is erupted, circulation and convection are required in order for mass balance (Francis et al., 1993; Harris et al., 1999). The significant heat flux and rapid cooling will lead to the development of a temperature gradient in the magma column and promote thermal convection. The short residence times of magma in the upper plumbing systems of these volcanoes further supports convective removal. Once buoyant,

gas-rich magma from deep levels is emplaced near the surface in the shallow reservoirs of these volcanoes, it will convect, degas vigorously and cool. This degassed and denser material must be removed from the system and convection (thermal and/or gas-driven) is the most reasonable mechanism for this. In some instances (e.g., Kilauea, Stromboli and perhaps Masaya), foam collapse within a deep reservoir may periodically cause large slugs of gas to rise to the surface and drive explosive activity such as fire fountaining (Jaupart and Vergniolle, 1988; Harris and Stevenson, 1997; Chapter 2). Furthermore, the extremely low erupted vs. degassed magma ratios of Stromboli and Masaya may be the result of efficient convective circulation. This will allow extensive degassing from persistently active vents and result in density increases that will inhibit eruption of lavas and promote cumulate formation at depth (Francis et al., 1993).

5.7.3. Cumulates

As the dense, cool and degassed magma sinks back towards the reservoir, some will be recharged by mingling with fresh gas-rich magma and thus again rise buoyantly towards the surface. However, some of the dense and cooling magma will crystallise and may lead to the emplacement of cumulates at the floor of the reservoir. There is geochemical evidence that suggests the presence of cumulates beneath Stromboli (Francalanci et al., 1989; Francis et al., 1993), while seismic data also support the existence of dense cumulate material seen as areas of high-velocity (Hill and Zucca, 1987) beneath Kilauea and Mt. Etna (Laigle and Hirn, 1999; Chiarabba et al., 2000). These regions are interpreted as dense, congealed cumulates of unerupted degassed magma (Chiarabba et al., 2000) and not as endogenous growth as they are located beneath the edifice where space for magma may also be formed by crustal-scale extension.

The presence of cumulates at depth has interesting potential implications for the detection of volcanic eruption precursors using gravity and deformation measurements

(Chapter 4). Cumulate emplacement may lead to an overall density increase, measurable at the surface as a gravity increase, and hinder vigorous interaction between freshly injected magma and the surrounding reservoir. This may therefore reduce the possibility of a large eruption (Model 1, Chapter 4).

5.8. Conclusion

While the four basaltic systems presented here have very different regional and tectonic environments, convective overturn and recharge plays an important role in maintaining the persistent activity evidenced at these volcanoes. This suggests, by extrapolation, that convection, especially in low viscosity basaltic systems, may in fact be the controlling mechanism of persistent activity. The presence of long-lived lava lakes and incandescent vents (manifestations of essentially the same feature) are evidence for efficient convection in a relatively open-system. Even when a lava lake is not present, as is currently the case at Masaya, Stromboli and Mt. Etna, the extremely shallow level of the magma in the conduit implies that significant cooling will occur resulting in density increases and necessitating downward removal by convection. This material may then be recharged at depth or emplaced as cumulates, which may limit the conditions leading to large explosive eruptions.

Chapter 6.

Conclusions and Future Work

6.1. General Conclusions

This study of micro-gravity, deformation and gas flux changes at Masaya volcano has provided a better understanding of the mechanisms responsible for persistent volcanism at open-system volcanoes. Some important conclusions from this work are the following:

1. The magmatic plumbing system at Masaya may be viewed as a near-surface magma body linked to, and periodically replenished by, a long-lived deep magma reservoir.
2. Masaya is a significant source of degassing, with 21 Tg SO_2 emitted since the formation of Santiago crater in 1853. In the most recent degassing episode (1993-2000), Masaya alone was responsible for 4.6% and ~1.5% of the annual global subaerial volcanic SO_2 and CO_2 emissions, respectively. Thus, although Masaya is not in continuous activity, its prolonged history of intense periodic degassing has likely resulted in serious environmental impact over time. Between mid-1993 and 2000, up to 0.6 km^3 of magma was degassed at shallow levels. The elevated degassing rate during this period would cool (mainly by advection) this volume of magma from liquidus to near solidus temperatures in only ~5 years. Furthermore, the maintenance of open pathways (e.g., during prolonged degassing) over periods of years requires a renewal of heat. This suggests that convective overturn of cooled and degassed magma

must have occurred during this period, followed by renewal of hot gas-rich magma from depth.

3. Recent activity at Masaya (1993-present) is characterised by repeated fluctuations in micro-gravity and gas flux due to at least two convective pulses which lead to the formation and oscillation of a gas-rich vesiculated zone immediately beneath the Nindiri and Santiago craters. The lack of any significant gravity increase or deformation to accompany the observed variations in micro-gravity and gas flux would seem to disprove the intrusion of new magma into the shallow magmatic system and instead indicate the convective overturn of a deep seated magma reservoir.
4. Simultaneous measurements of deformation and gravity at a few key stations off axis of the centre of activity can be used to investigate very small changes in mass or density in a magma reservoir at depths of 2-7 km. By quantifying the magnitude and rate of these changes, eruption precursors within the reservoir may be detected well before the magma begins to rise towards the surface, offering significantly more time for hazard mitigation and evacuation.
5. Whether or not an active lava lake is present, the extremely shallow level of the magma and high degassing rates of many persistently active volcanoes implies that significant cooling will occur. This will result in density increases and necessitate downward removal by convection; this material may then be recharged at depth or emplaced as cumulates, which may limit the conditions leading to large explosive eruptions.
6. Convective overturn and recharge clearly plays a significant role in maintaining the persistent activity evidenced at Stromboli and Masaya and to a less extent at Kilauea and Mt. Etna. Convection, especially in low viscosity basaltic systems, may in fact be the controlling mechanism of persistent activity.

6.2. Recommendations for Future Work at Masaya

1) Investigate the possibility of using satellite remote sensing data (e.g., ATSR) in order to develop a relationship between the optical depth of the gas plume and the ground-based measurements of SO_2 flux. This could greatly facilitate the remote measurement of degassing at otherwise inaccessible volcanoes. As there is ATSR coverage of Masaya back to early 1993, i.e., before the start of the current degassing episode, it may be possible constrain the gas flux for the first three years of the current episode. This could also be applied to other persistently active volcanoes (e.g., Mt. Etna, Kilauea) where large ground-based SO_2 flux data sets exist.
2) Expanding the network of gravity and GPS stations around to the south and west of Nindiri and San Pedro craters would better constrain the observed gravity anomalies and potentially increase the accuracy of 2.5D modelling of changes within the shallow magma plumbing system. This could also be facilitated through the installation of a permanent seismic network.
3) Study short-lived radioisotopes in the erupted gasses in order to determine the residence time of magma in the upper reservoir and plumbing system.
4) Expand the FTIR and COSPEC data sets in order to shed light upon any changes in activity as well as to further constrain evolution of the magmatic system, including sizes and depths of reservoirs involved and degassing processes. Investigate in detail the potential cyclicity in SO_2 flux data. Study the potential link between variations in gas chemistry with changes in gas flux and micro-gravity.
5) Build upon the initial work of Delmelle et al. (2000) in order to study the environmental impact of persistently active volcanoes. Comparison of older Landsat TM images with more recent images may prove beneficial in investigating the environmental effects of periods of continuous degassing versus episodic degassing as well as the differences in low flux levels versus high flux.

6) Deployment of continuously recording gravimeters or gradiometers (currently being developed at The Open University) may allow for better spatial and temporal resolution with which to investigate gravity changes at different temporal and spatial levels. In conjunction with continuous deformation monitoring, there is the potential of further investigating eruption precursors at large caldera complexes. In lieu of a gradiometer, the expanded use of FAG measurements may prove useful for continued monitoring.

References

Albarède, R., 1993. Residence time analysis of geochemical fluctuations in volcanic series. Geochim. Cosmochim. Acta, 57, 615-621.

Allard, P., Carbonnelle, J., Dajlevic, D., Le Bronec, J., Morel, P., Robe, M. C., Maurenas, J. M., Faivre-Pierret, R. and Martin, D., 1991. Eruptive and diffuse emissions of CO_2 from Mount Etna. Nature, 351, 387-391.

Allard, P., Carbonnelle, J., Métrich, N., Loyer, H. and Zettwoof, P., 1994. Sulphur output and magma degassing budget of Stromboli volcano. Nature, 368, 326-330.

Allard, P., 1997. Endogenous magma degassing and storage at Mount Etna. Geophys. Res. Lett., 24, 2219-2222.

Allard, P., Aiuppa, A., Loyer, H., Carrot, F., Gaudry, A., Pinte, G., Michel, A. and Dongarrà, G., 2000. Acid gas and metal emission rates during long-lived basalt degassing at Stromboli volcano. Geophys. Res. Lett., 27, 1207-1210.

Andres, R. J., Kyle, P. R., Stokes, J. B. and Rose, W. I., 1989. SO_2 from episode 48A eruption, Hawaii; sulfur dioxide emissions from the episode 48A East Rift Zone eruption of Kilauea Volcano, Hawaii. Bull. Volcanol., 52, 113-117.

Andres, R. J., Rose, W. I., Kyle, P. R., DeSilva, S., Francis, P., Gardeweg, M. and Moreno Roa, H., 1991. Excessive sulfur dioxide emissions from Chilean volcanoes. J. Volcanol. Geotherm. Res., 46, 323-329.

Andres, R. J. and Kasgnoc, A. D., 1998. A time-averaged inventory of subaerial volcanic sulfur emissions. J. Geophys. Res., 103, 25251-25261.

Archambault, C. and Tanguy, J. C., 1976. Comparative temperature measurements on Mount Etna lavas: problems and techniques. J. Volcanol. Geotherm. Res., 1, 113-125.

Arnet, F., Kahle, H.-G., Klingelé, E., Smith, R. B., Meertens, C. M. and Dzurisin, D., 1997. Temporal gravity and height changes of the Yellowstone caldera, 1977 - 1994. Geophys. Res. Lett., 24, 2741-2744.

Arya, S. P. 1999. Air Pollution Meteorology and Dispersion. Oxford University Press, Oxford, 310 pp.

Avallone, A., Zollo, A., Briole, P., Delacourt, C. and Beauducel, F., 1999. Subsidence of Campi Flegrei (Italy) detected by SAR interferometry. Geophys. Res. Lett., 26, 2303-2306.

Bailey, R. A., Dalrymple, G. B. and Lanphere, M. A., 1976. Volcanism, structure and geochronology of Long Valley Caldera, Mono County, California. J. Geophys. Res., 81, 725-744.

Barberi, F. and Carapezza, M. L., 1996. The problem of volcanic unrest: The Campi Flegrei case history. In: R. Scarpa and R. I. Tilling (Editors), Monitoring and Mitigation of Volcano Hazards, Springer-Verlag, Berlin, pp. 771-786.

Battaglia, M., Roberts, C. and Segall, P., 1999. Magma intrusion beneath Long Valley Caldera confirmed by temporal changes in gravity. Science, 285, 2119-2122.

Baxter, P. J. and Gresham, A., 1997. Deaths and injuries in the eruption of Galeras Volcano, Colombia, 14 January 1993. J. Volcanol. Geotherm. Res., 77, 325-338.

Beaulieu, A., 1999. The Nature and Origin of Spatial and Temporal Variations in the Gravity Fields of Telica and Masaya Volcanoes, Nicaragua, M.Sc. Thesis, Université de Montréal, Canada.

Berrino, G., Corrado, G., Luongo, G. and Toro, B., 1984. Ground deformation and gravity changes accompanying the 1982 Pozzuoli uplift. Bull. Volcanol., 47, 187-200.

Berrino, G., Rymer, H., Brown, G. C. and Corrado, G., 1992. Gravity-height correlations for unrest at calderas. J. Volcanol. Geotherm. Res., 53, 11-26.

Berrino, G., 1994. Gravity changes induced by height-mass variations at the Campi Flegrei caldera. J. Volcanol. Geotherm. Res., 61, 293-309.

Berrino, G., Corrado, G., Magliulo, R. and Umberto, R., 1997. Continuous record of the gravity changes at Mt. Vesuvius. Annali di Geofisica, 40, 1019-1028.

Bice, D. C., 1980. Tephra stratigraphy and physical aspects of recent volcanism near Managua, Nicaragua, Ph.D. Thesis, University of California Berkeley, U.S.A.

Bice, D. C., 1985. Quaternary stratigraphy of Managua, Nicaragua: Correlation and source assignment for multiple overlapping plinian deposits. Geol. Soc. Am. Bull., 96, 533-566.

Bluth, G. J. S., Doiron, S. D., Schnetzler, C. C., Krueger, A. J. and Walter, L. S., 1992. Global tracking of the SO_2 clouds from the June 1991 Mount Pinatubo eruptions. Geophys. Res. Lett., 19, 151-154.

Bonaccorso, A., Falzone, G., Gambino, S., Mattia, M., Rossi, M., and Villari, L., 1998. Monitoraggio delle deformazioni lente del suolo a Stromboli (Abstract). Stromboli Workshop, Gr. Naz. Vulcanol., 5.

Bonafede, M. and Mazzanti, M., 1998. Modelling gravity variations consistent with ground deformation in the Campi Flegrei caldera (Italy). J. Volcanol. Geotherm. Res., 81, 137-157.

Bonvalot, S., Albouy, Y., Remy, D., Métaxian, J. P., Lesage, P., and Perez, O., 1992. Geophysical survey of the Masaya Caldera (Nicaragua) (Abstract). EOS Trans. Am. Geophys. Union, 73, 348.

Broucke, R. A., Zürn, W. E. and Slichter, L. B., 1972. Lunar tidal acceleration on a rigid earth. Flow and Fracture of Rocks, American Geophysical Union, Geophysical Monograph, 16, pp. 319-324.

Brown, G. C., Rymer, H. and Stevenson, D., 1991. Volcano monitoring by microgravity and energy budget analysis. J. Geol. Soc. London, 148, 585-593.

Bruno, N., Caltabiano, T. and Romano, R., 1999. SO_2 emissions at Mt. Etna with particular reference to the period 1993-1995. Bull. Volcanol., 60, 405-411.

Budetta, G., Carbone, D., 1998. Temporal variations in gravity at Mt. Etna (Italy) associated with the 1989 and 1991 eruptions. Bull. Volcanol., 59, 311-326.

Bulletin of the Global Volcanism Network, 1970-2000. Masaya. Smithsonian Institution, 38:70-25:09, (http://www.volcano.si.edu/gvp/volcano/region14/nicarag/masaya/var.htm).

Bulletin of the Global Volcanism Network, 1992-1999. Rabaul. Smithsonian Institution, 17:05-24:10, (http://www.volcano.si.edu/gvp/volcano/region05/newbrit/rabaul/var.htm).

Bulletin of the Global Volcanism Network, 2000. Masaya. Smithsonian Institution, 15:09, (http://www.volcano.si.edu/gvp/volcano/region14/nicarag/masaya/var.htm).

Burton, M. R., Oppenheimer, C., Horrocks, L. A. and Francis, P. W., 2000. Field measurement of CO_2 and H_2O emissions from Masaya volcano, Nicaragua, by Fourier Transform spectroscopy. Geology, 28, 915-918.

Calvari, S., Cortelli, M., Neri, M., Pompilio, M. and Scribano, V., 1994. The 1991-1993 Etna eruption: chronology and lava flow-field evolution. Acta Volcanol., 4, 1-14.

Campbell, I. H., 1978. Some problems with the cumulus theory. Lithos, 11, 311-323.

Campbell, I. H., 1986. A fluid dynamic model for potholes of the Merensky Reef. Econ. Geol., 81, 1118-1125.

Capaldi, G., Guerra, I., Lo Bascio, A., Luongo, G., Pece, R., Rapolla, A., Scarpa, R., Del Pezzo, E., Martini, M., Ghiara, M. R., Lirer, L., Munno, R. and La Volpe, L., 1978. Stromboli and its 1975 eruption. Bull. Volcanol., 41, 259-285.

Carr, M. J. and Stoiber, R. E., 1973. Intermediate depth earthquakes and volcanic eruptions in Central America, 1961-1972. Bull. Volcanol., 37, 327-337.

Carroll, M. R. and Webster, J. D., 1994. Solubilities of sulfur, noble gases, nitrogen, chlorine, and fluorine in magmas. In: Carroll, M. R. and Holloway, J. R. (Editors), Volatiles in Magma, Min. Soc. Amer., 30, pp. 231-279.

Casadevall, T. J., Johnson, D. A., Harris, D. M., Rose, W. I., Malinconico, L. L., Stoiber, R. E., Bornhorst, T. J., Williams, S. N., Woodruff, L., and Thompson, J. M. 1981. SO_2 emission rates at Mount St. Helens from March 29 through December, 1980. In: Lipman, P. W. and Mullineaux, D. R. (Editors), The 1980 Eruptions of Mount St.

Helens. 1250: 193-200

Casadevall, T. J., Stokes, J. B., Greenland, L. P., Malinconico, L. L., Casadevall, J. R. and Furukawa, B. T., 1987. SO_2 and CO_2 emission rates at Kilauea Volcano, 1979-1984. In: R. W. Decker, T. L. Wright and P. H. Stauffer (Editors), Volcanism in Hawaii, U.S.G.S. Prof. Pap., pp. 771-780.

Chartier, T. A., Rose, W. I. and Stokes, J. B., 1988. Detailed record of SO_2 emissions from Pu'u 'O'o between episodes 33 and 34 of the 1983-86 ERZ eruption, Kilauea, Hawaii. Bull. Volcanol., 50, 215-228.

Chiarabba, C., Amato, A. and Boschi, E., 2000. Recent seismicity and tomographic modeling of the Mount Etna plumbing system. J. Geophys. Res., 105, 10923-10938.

Chouet, B., Hamisevicz, N. and McGetchin, T. R., 1974. Photoballistics of volcanic jet activity at Stromboli, Italy. J. Geophys. Res., 79, 4961-4976.

Condomines, M., Tanguay, J.-C. and Michaud, V., 1995. Magma dynamics at Mt. Etna: Constraints from U-Th-Ra-Pb radioactive disequilibria and Sr isotopes in historical lavas. Earth Planet. Sci. Lett., 132, 25-41.

Connor, C. B., Stoiber and R. E., Malinconico, L. L., 1988. Variation in sulfur dioxide emissions related to Earth tides, Halemaumau crater, Kilauea volcano, Hawaii. J. Geophys. Res., 93, 14867-14871.

Connor, C. B. and Williams, S. N., 1990. Interpretation of gravity anomalies, Masaya caldera complex, Nicaragua. In: Larue, D. K. and Draper, G. Transactions of the 12th Caribbean Geological Conference, United States Virgin Islands.

Crenshaw, W. B., Williams, S. N. and Stoiber, R. E., 1982. Fault location by radon and mercury detection at an active volcano in Nicaragua. Nature, 300, 345-346.

Daag, A. S., Tubianosa, B. S., Newhall, C. G., Tuñgol, N. M., Javier, D., Dolan, M. T., Delos Reyes, P. J., Arboleda, R. A., Martinez, M. M. L. and Regalado, M. T. M., 1996. Monitoring sulfur dioxide emission at Mount Pinatubo. In: Newhall, C. G. and

Punongbayan, R. S. (Eds), Fire and Mud: Eruptions and Lahars of Mount Pinatubo, Philippines, University of Washington Press, London, pp. 409-414.

Davies, M. A., Harrop, N. D. and Rymer, H., 2000. Experimental investigation of temporary tares induced by ground vibration in LaCoste and Romberg gravity meters. Geophys. Prospect., In press.

Decker, R. W., 1987. Dynamics of Hawaiian volcanoes: A review. Volcanism in Hawaii. Decker, R. W., Wright, T. L., and Stauffer, P. H. (Editors), U.S.G.S. Prof. Pap., 1350, 997-1018.

Delmelle, P., Baxter, P., Beaulieu, A., Burton, A., Francis, P., Garcia-Alvarez, J., Horrocks, L., Navarro, M., Oppenheimer, C., Rothery, D., Rymer, H., St. Amand, K., Stix, J., Strauch, W. and Williams-Jones, G., 1999. Integrated geochemical, geophysical, and petrological studies illuminate magmatic processes at Masaya volcano, Nicaragua. EOS Trans. Am. Geophys. Union, 80, 575-581.

Delmelle, P., Stix, J., Bourque, C. P. A., Baxter, P. J., Garcia-Alvarez, G. and Barquero, J., 2000. Dry deposition and heavy acid loading in the vicinity of Masaya volcano, a major sulfur and chlorine source in Nicaragua. Env. Sci. Tech., Submitted.

Denlinger, R. P., 1997. A dynamic balance between magma supply and eruption rate at Kilauea volcano, Hawaii. J. Geophys. Res., 102, 18091-18100.

Dixon, T. H., Mao, A., Bursik, M., Heflin, M., Langbein, J., Stein, R. and Webb, F., 1997. Continuous monitoring of surface deformation at Long Valley Caldera, California, with GPS. J. Geophys. Res., 102, 12017-12034.

Duffield, W. A., Gibson, E. K. and Heiken, G. H., 1977. Some characteristics of Pele's hair. J. Res. U. S. Geol. Surv., 5, 93-101.

Dvorak, J. and Mastrolorenzo, G., 1991. The mechanisms of recent vertical crustal movements in Campi Flegrei caldera. Spec. Pap. Geol. Soc. Am., 263, 47.

Dzurisin, D., Anderson, L. A., Eaton, G. P., Koyanagi, R. Y., Lipman, P. W., Lockwood, J.

P., Okamura, R. T., Puniwai, G. S., Sako, M. K. and Yamashita, K. M., 1980. Geophysical observations of Kilauea volcano, Hawaii, 2. Constraints on the magma supply during November 1975-September 1977. J. Volcanol. Geotherm. Res., 7, 241-269.

Dzurisin, D., Koynagi, R. T. and English, T. T., 1984. Magma supply and storage at Kilauea Volcano, Hawaii, 1956-1983. J. Volcanol. Geotherm. Res., 21, 177-206.

Dzurisin, D., Savage, J. C. and Fournier, R. O., 1990. Recent crustal subsidence at Yellowstone caldera, Wyoming. Bull. Volcanol., 52, 247-270.

Eaton, J. P. and Murata, K. J., 1960. How volcanoes grow. Science, 132, 925-938.

Eggers, A. A. and Chavez, D., 1979. Temporal gravity variations at Pacaya volcano, Guatemala. J. Volcanol. Geotherm. Res., 6, 391-402.

Eggers, A. A., 1987. Residual gravity changes and eruption magnitudes. J. Volcanol. Geotherm. Res., 33, 201-216.

Ehrenborg, J., 1987. Semi-regional mapping of the Boaco-Tecolostote areas, Nicaragua. Swedish Geological, Uppsala, Sweden, 46 pp.

Eichelberger, J. C., 1980. Vesiculation of mafic magma during replenishment of silicic magma reservoirs. Nature, 288, 446-450.

Elias, T., Sutton, A.J., Stokes, J.B. and Casadevall, T.J., 1998.Sulfur dioxide emission rates of Kilauea Volcano, Hawaii, 1979-1997. U.S.G.S. Open-File Report 98-462, pp. 41.

Fischer, T. P., Morrissey, M. M., Calvache, M. L. V., Gomez, D. M., Torres, R. C., Stix, J. and Williams, S. N., 1994. Correlations between SO_2 flux and long-period seismicity at Galeras Volcano. Nature, 368, 135-137.

Fournelle, J., 1990. Anhydrite in Nevado del Ruiz November 1985 pumice: Relevance to the sulfur problem. J. Volcanol. Geotherm. Res., 42, 189-201.

Francalanci, L., Manetti, P. and Peccerillo, A., 1989. Volcanological and magmatological evolution of Stromboli volcano (Aeolian Islands): the roles of fractional crystallisation,

magma mixing, crustal contamination and source heterogeneity. Bull. Volcanol., 51, 355-378.

Francalancia, L., Tommasini, S., Conticelli, S. and Davies, G. R., 1999. Sr isotope evidence for short magma residence time for the 20th century activity at Stromboli volcano, Italy. Earth Planet. Sci. Lett., 167, 61-69.

Francis, P., Oppenheimer, C. and Stevenson, D., 1993. Endogenous growth of persistently active volcanoes. Nature, 366, 554-557.

Francis, P., Burton, M. R. and Oppenheimer, C., 1998. Remote measurements of volcanic gas compositions by solar occultation spectroscopy. Nature, 396, 567-570.

Freedman, B. and Hutchinson, T. C., 1980. Pollutant inputs from the atmosphere and accumulations in soils and vegetation near a nickel-copper smelter at Sudbury, Ontario, Canada. Can. J. Bot., 58, 108-132.

Fujii, T. and Nakada, S., 1999. The 15 September 1991 pyroclastic flows at Unzen Volcano (Japan): a flow model for associated ash-cloud surges. J. Volcanol. Geotherm. Res., 89, 159-172.

Gaetani, G. A., Grove, T. L. and Bryan, W. B., 1993. The influence of water on the petrogenesis of subduction-related igneous rocks. Nature, 365, 332-334.

Gauthier, P.-J., Le Cloarec, M.-F. and Condomines, M., 2000. Degassing processes at Stromboli volcano inferred from short-lived disequilibria (^{210}Pb-^{210}Bi-^{210}Po) in volcanic gases. J. Volcanol. Geotherm. Res., 102, 1-19.

Gerlach, T. M. and Graeber, E. J., 1985. Volatile budget of Kilauea Volcano. Nature, 313, 273-277.

Gerlach, T. M. and McGee, K. A., 1994. Total sulfur dioxide emissions and pre-eruption vapor-saturated magma at Mount St. Helens, 1980-88. Geophys. Res. Lett., 21, 2833-2836.

Gerlach, T. M., Westrich, H. R. and Symonds, R. B., 1996. Preeruption vapor in magma of

the climactic Mount Pinatubo eruption: Source of the giant stratospheric sulfur dioxide cloud. In: Newhall, C. G. and Punongbayan, R. S. (Editors), Fire and Mud: Eruptions and Lahars of Mount Pinatubo, Philippines, University of Washington Press, Seattle, pp. 415-433.

Giberti, G., Jaupart, C. and Satoris, G., 1992. Steady-state operation of Stromboli volcano, Italy: constraints on the feeding system. Bull. Volcanol., 54, 535-541.

Gillot, P. Y., Kieffer, G. and Romano, R., 1994. The evolution of Mt. Etna in light of potassium-argon dating. Acta Volcanol., 5, 81-87.

Greenland, L. P., Rose, W. I. and Stokes, J. B., 1985. An estimate of gas emissions and magmatic gas content from Kilauea volcano. Geochim. Cosmochim. Acta, 49, 125-129.

Gregg, T. K. P. and Williams, S. N., 1996. Explosive mafic volcanoes on Mars and Earth: Deep magma sources and rapid rise rate. Icarus, 122, 397-405.

Harris, A. J. L. and Stevenson, D. S., 1997. Magma budgets and steady-state activity of Vulcano and Stromboli. Geophys. Res. Lett., 24, 1043-1046.

Harris, A. J. L., Flynn, L. P., Rothery, D. A., Oppenheimer, C. and Sherman, S. B., 1999. Mass flux measurements at active lava lakes: Implications for magma recycling. J. Geophys. Res., 104, 7117-7136.

Harris, A. J. L., Murray, J. B., Aries, S. E., Davies, M. A., Flynn, L. P., Wooster, M. J., Wright, R. and Rothery, D. A., 2000. Effusion rate trends at Etna and Krafla and their implications for eruptive mechanisms. J. Volcanol. Geotherm. Res., 102, 237-270.

Hill, D. P. and Zucca, J. J., 1987. Geophysical constraints on the structure of Kilauea and Mauna Loa volcanoes and some implications for seismomagmatic processes. Volcanism in Hawaii. Decker, R. W., Wright, T. L., and Stauffer, P. H. (Editors), U.S.G.S. Prof. Pap., 1350, 903-918.

Horrocks, L., Burton, M., Francis, P. and Oppenheimer, C., 1999. Stable gas plume

composition measured by OP-FTIR spectroscopy at Masaya Volcano, Nicaragua, 1998-1999. Geophys. Res. Lett., 26, 3497-3500.

Horrocks, L., 2001. Volatile fluxes in active volcanoes, Ph.D. Thesis, The Open University, UK.

Huppert, H. E., Sparks, R. S. J. and Turner, J. S., 1982. Effects of volatiles on mixing in calc-alkaline magma systems. Nature, 297, 554-557.

Huppert, H. E. and Sparks, R. S. J., 1988. The fluid dynamics of crustal melting by injection of basaltic sills. Philos. Trans. R. Soc. Edinburgh, 79, 237-243.

Jachens, R. C. and Roberts, C. W., 1985. Temporal and areal gravity investigations at Long Valley Caldera, California. J. Geophys. Res., 90, 11210-11218.

Jackson, J. A. (Editor), 1997. Glossary of Geology. American Geological Institute, Alexandria, Virginia, 769 pp.

Jaupart, C. and Vergniolle, S., 1988. Laboratory models of Hawaiian and Strombolian eruptions. Nature, 331, 58-60.

Jaupart, C. and Vergniolle, S., 1989. The generation and collapse of a foam layer at the roof of a basaltic magma chamber. J. Fluid Mech., 203, 347-380.

Johnson, D. J., 1987. Elastic and inelastic magma storage at Kilauea Volcano. Volcanism in Hawaii. Decker, R. W., Wright, T. L., and Stauffer, P. H. (Editors), U.S.G.S. Prof. Pap., 1350, 1297-1306.

Johnson, G. V., Björnsson, A. and Sigurdsson, S., 1980. Gravity and elevation changes caused by magma movement beneath the Krafla caldera, Northeast Iceland. J. Geophys. Res., 47, 132-40.

Kane, M. F., Mabey, D. R. and Brace, R. L., 1976. A gravity and magnetic investigation of the Long Valley caldera, Mono County, California. J. Geophys. Res., 81, 754-762.

Kazahaya, K., Shinohara, H. and Saito, G., 1994. Excessive degassing of Izu-Oshima volcano: magma convection in a conduit. Bull. Volcanol., 56, 207-216.

Kerr, R. C., 1994. Dissolving driven by vigorous compositional convection. J. Fluid Mech., 280, 287-302.

Kieffer, G. and Creusot-Eon, A., 1992. La caldeira de Masaya (Nicaragua): une dépression polyphasée de type "maar". Comptes rendus de l'Academie des sciences, Paris, Série II, 315, 1403-1409.

Kress, V., 1997. Magma mixing as a source for Pinatubo sulphur. Nature, 389, 591-593.

Kyle, P. R., Sybeldon, L. M., McIntosh, W. C., Meeker, K. and Symonds, R., 1994. Sulfur dioxide emission rates from Mount Erebus, Antarctica. In: P. R. Kyle (Editor), Volcanological and environmental studies of Mount Erebus, Antarctica, Antarctic Research Series, pp. 69-82.

Laigle, M. and Hirn, A., 1999. Explosion-seismic tomography of a magmatic body beneath Etna: volatile discharge and tectonic control of volcanism. Geophys. Res. Lett., 26, 2665-2668.

Luhr, J. F., Carmichael, I. S. E., Varekamp, J. C., 1984. The 1982 eruptions of El Chichón Volcano, Chiapas, Mexico: Mineralogy and petrology of the anhydrite-bearing pumices. J. Volcanol. Geotherm. Res., 23, 69-108.

Macdonald, G. A., Abbott, A. T., and Peterson, F. L. 1970. Volcanoes in the Sea. Univ. of Hawaii Press, Honolulu, 517 pp.

Maciejewski, A. J. H., 1998. Remote measurements of volcanic gases: Applications of Open-path Fourier transform infra-red spectroscopy (OP-FTIR) and Correlation spectroscopy (COSPEC), Ph.D. Thesis, The Open University, UK.

Marland, G., Boden, T. A., Andres, R. J., Brenkert, A. L. and Johnston, C., 1999. Global, Regional, and National CO_2 Emissions. In: Carbon Dioxide Information Analysis Center Trends: A Compendium of Data on Global Change, Oak Ridge National Laboratory, U.S. Department of Energy, Oak Ridge, Tenn., U.S.A.

McBirney, A. R., 1956. The Nicaraguan volcano Masaya and its caldera. EOS Trans. Am.

Geophys. Union, 37, 83-96.

McKee, C., Mori, J. and Talai, B., 1989. Microgravity changes and ground deformation at Rabaul caldera, 1973-1985. In: Latter, J. H. (Editor), Volcanic Hazards: assessment and monitoring. IAVCEI Proceedings in Volcanology 1., Springer-Verlag, Berlin, Germany, pp. 399-428.

Mercalli, G., 1881. Natura dell'eruzione dello Stromboli ed in generale dell'attività sismo-vulcanica nelle isole Eolie. Atti. Soc. It. Sc. Nat., 24, 105-135.

Métaxian, J.-P., 1994. Étude Sismologique et Gravimétrique d'un Volcan Actif: Dynamisme Interne et Structure de la Caldera Masaya, Nicaragua, Ph.D. Thesis, Université de Savoie, France.

Métaxian, J.-P., Lesage, P. and Dorel, J., 1997. Permanent tremor of Masaya Volcano, Nicaragua: Wave field analysis and source location. J. Geophys. Res., 102, 22529-22545.

Métrich, N. and Clocchiatti, R., 1989. Melt inclusion investigation of the volatile behaviour in historic alkali basaltic magmas of Etna. Bull. Volcanol., 51, 185-198.

Métrich, N., Clocchiatti, R., Mosbah, M. and Chaussidon, M., 1993. The 1989-1990 activity of Etna magma mingling and ascent of H_2O-Cl-S-rich basaltic magma. Evidence from melt inclusions. J. Volcanol. Geotherm. Res., 59, 131-144.

Métrich, N., Schiano, P., Clocchiatti, R. and Maury, R. C., 1999. Transfer of sulfur in subduction settings: an example from Batan Island (Luzon volcanic arc, Philippines). Earth Planet. Sci. Lett., 167, 1-14.

Millán, M. M., 1980. Remote sensing of air pollutants. A study of some atmospheric scattering effects. Atmos. Environ., 14, 1241-1253.

Mogi, K., 1958. Relations between the eruptions of various volcanoes and the deformations of the ground surfaces around them. Bull. Earth. Res. Inst., 36.

Murray, J. B., Pullen, A. D. and Saunders, S., 1995. Ground deformation surveying of

active volcanoes. In: B. McGuire, C. R. J. Kilburn and J. Murray (Editors), Monitoring Active Volcanoes, UCL Press, London, pp. 113-150.

Murru, M., Montuori, C., Wyss, M. and Privitera, E., 1999. The locations of magma chambers at Mt. Etna, Italy, mapped by *b*-values. Geophys. Res. Lett., 26, 2553-2556.

Newhall, C. G. and Dzurisin, D., 1988. Historical unrest at large calderas of the world. U.S.G.S. Bull., 1855, 1108.

Ntepe, N. and Dorel, J., 1990. Observations of seismic volcanic signals at Stromboli volcano (Italy). J. Volcanol. Geotherm. Res., 43, 235-251.

Oppenheimer, C. and Francis, P., 1998. Implications of longeval lava lakes for geomorphological and plutonic processes at Erta 'Ale volcano, Afar. J. Volcanol. Geotherm. Res., 80, 101-111.

Pallister, J. S., Hoblitt, R. P. and Reyes, A. G., 1992. A basalt trigger for the 1991 eruptions of Pinatubo volcano. Nature, 356, 426-428.

Pedley, R. 1991. Gravmag user manual. Integrated Geophysical Services, BGS Keyworth, UK.

Pietruszka, A. J and Garcia, M. O., 1999. The size and shape of Kilauea Volcano's summit magma storage reservoir: a geochemical probe. Earth Planet. Sci. Lett., 167, 311-320.

Pyle, D. M., 1992. The volume and residence time of magma beneath active volcanoes determined by decay-series disequilibria methods. Earth Planet. Sci. Lett., 112, 61-73.

Rittman, A. 1962. Volcanoes and their activity. Wiley, New York, 305 pp.

Roggensack, K., Hervig, R. L., McKnight, S. B. and Williams, S. N., 1997. Explosive basaltic volcanism from Cerro Negro volcano: influence of volatiles on eruptive style. Science, 277, 1639-1642.

Rosi, M., 1980. The island of Stromboli. Rend. Soc. It. Mineral. Petrol., 36, 345-368.

Rosi, M., Bertagnini, A. and Landi, P., 2000. Onset of the persistent activity at Stromboli Volcano (Italy). Bull. Volcanol., 10.1007/s004450000098, 1-11.

Ryan, M. P., 1988. The mechanics and three-dimensional internal structure of active magmatic systems: Kilauea Volcano, Hawaii. J. Geophys. Res., 93, 4213-4248.

Rymer, H., 1989. A contribution to precision microgravity data analysis using LaCoste and Romberg gravity meters. Geophys. J., 97, 311-322.

Rymer, H. and Brown, G. C., 1989. Gravity changes as a precursor to volcanic eruptions at Poás volcano, Costa Rica. Nature, 342, 902-905.

Rymer, H., Murray, J. B., Brown, G. C., Ferrucci, F. and McGuire, W. J., 1993. Mechanisms of magma eruption and emplacement at Mt Etna between 1989 and 1992. Nature, 361, 439-441.

Rymer, H., 1994. Microgravity change as a precursor to volcanic activity. J. Volcanol. Geotherm. Res., 61, 311-328.

Rymer, H., Cassidy, J., Locke, C. A. and Murray, J. B., 1995. Magma movements in Etna volcano associated with the major 1991-1993 lava eruption: evidence from gravity and deformation. Bull. Volcanol., 57, 451-461.

Rymer, H., 1996. Microgravity monitoring. In: R. Scarpa and R. I. Tilling (Editors), Monitoring and Mitigation of Volcano Hazards, Springer-Verlag, Berlin, pp. 169-198.

Rymer, H., van Wyk de Vries, B., Stix, J. and Williams-Jones, G., 1998a. Pit crater structure and processes governing persistent activity at Masaya Volcano, Nicaragua. Bull. Volcanol., 59, 345-355.

Rymer, H., Cassidy, J., Locke, C. A. and Sigmundsson, F., 1998b. Post-eruptive gravity changes from 1990 to 1996 at Krafla volcano, Iceland. J. Volcanol. Geotherm. Res., 87, 141-149.

Rymer, H. and Williams-Jones, G., 2000. Volcanic eruption prediction: Magma chamber physics from gravity and deformation measurements. Geophys. Res. Lett., 27, 2389-2392.

Saemundsson, K., 1978. Fissure swarms and central volcanoes of the neo-volcanic zones

of Iceland. Geol. J. Spec. Issue 10, 415-432.

Shimozuru, D., 1994. Physical parameters governing the formation of Pele hair and tears. Bull. Volcanol., 56, 217-219.

Sigmundsson, F., Vadon, H. and Massonnet, D., 1997. Readjustment of the Krafla spreading segment to crustal rifting measured by satellite radar interferometry. Geophys. Res. Lett., 24, 1843-1846.

Sigurdsson, H., Carey, S. N., Palais, J. M. and Devine, J., 1990. Pre-eruption compositional gradients and mixing of andesite and dacite magma erupted from Nevado del Ruiz Volcano, Colombia in 1985. J. Volcanol. Geotherm. Res., 41, 127-151.

Sisson, T. W. and Layne, G. D., 1993. H_2O in basalt and basaltic andesite glass inclusions from four subduction-related volcanoes. Earth Planet. Sci. Lett., 117, 619-635.

Sisson, T. W. and Grove, T. L., 1993. Temperatures and H_2O content of low-MgO high-alumina basalt. Contrib. Mineral. Petrol., 113, 167-184.

Smith, R. B., Reilinger, R. E., Meertens, C. M., Hollis, J. R., Holdahl, S. R., Dzurisin, D., Gross, W. K. and Klingele, E. E., 1989. What's moving at Yellowstone? The 1987 crustal deformation survey from GPS, levelling, precision gravity, and trilateration. EOS Trans. Am. Geophys. Union, 70, 113-125.

Sparks, R. S. J., Meyer, P. and Sigurdsson, H., 1980. Density variation amongst Mid-Ocean Ridge basalts: Implications for magma mixing and the scarcity of primitive lavas. Earth Planet. Sci. Lett., 46, 419-430.

Sparks, S. R. J., Sigurdsson, H. and Wilson, L., 1977. Magma mixing: a mechanism for triggering acid explosive eruptions. Nature, 267, 315-318.

St-Amand, K., 1999. The Distribution and Origin of Radon, CO_2 and SO_2 Gases and Multifractal Behaviour of SO_2 at Masaya Volcano, Nicaragua, M.Sc. Thesis, Université de Montréal, Canada.

Stevens, N. F., Murray, J. B. and Wadge, G., 1997. The volume and shape of the 1991-1993 lava flow field at Mount Etna, Sicily. Bull. Volcanol., 58, 449-454.

Stevenson, D. S. and Blake, S., 1998. Modelling the dynamics and thermodynamics of volcanic degassing. Bull. Volcanol., 60, 307-317.

Stoiber, R. E. and Carr, M. J., 1973. Quaternary volcanic and tectonic segmentation of Central America. Bull. Volcanol., 37, 304-325.

Stoiber, R. E., Malinconico, L. L. and Williams, S. N., 1983. Use of the correlation spectrometer at volcanoes. In: H. Tazieff and J. C. Sabroux (Editors), Forecasting Volcanic Events, Elsevier, New York, pp. 424-444.

Stoiber, R. E., Williams, S. N. and Huebert, B. J., 1986. Sulfur and halogen gases at Masaya caldera complex, Nicaragua: Total flux and variations with time. J. Geophys. Res., 91, 12215-12231.

Tait, S., Jaupart, C. and Vergniolle, S., 1989. Pressure, gas content and eruption periodicity of a shallow, crystallising magma chamber. Earth Planet. Sci. Lett., 92, 107-123.

Tanguy, J.-C., Condomines, M. and Kieffer, G., 1997. Evolution of the Mount Etna magma: Constraints on the present feeding system and eruptive mechanism. J. Volcanol. Geotherm. Res., 75, 221-250.

Tazieff, H., 1984. Mt. Niragongo: Renewed activity of the lava lake. J. Volcanol. Geotherm. Res., 20, 267-280.

Telford, W. M., Geldart, L. P., and Sheriff, R. E. 1990. Applied Geophysics. Cambridge University Press, Cambridge, U.K., 770 pp.

Tilling, R. I. and Dvorak, J. J., 1993. Anatomy of a basaltic volcano. Nature, 363, 125-133.

Tryggvason, E., 1984. Widening of the Krafla fissure swarm during the 1975-1981 volcano-tectonic episodes. Bull. Volcanol., 47, 47-69.

van Wyk de Vries, B., 1993. Tectonics and magma evolution of Nicaraguan volcanic systems, Ph.D. Thesis, The Open University, U.K.

van Wyk de Vries, B. and Borgia, A., 1996. The role of basement in volcano deformation. In: McGuire, W. J., Jones, A. P., and Neuberg, J. (Editors), Volcano Instability on the Earth and Other Planets, Geol. Soc. Spec. Pub., 110, pp. 95-110.

Vasco, D. W., Smith, R. B. and Taylor, C. L., 1990. Inversion for sources of crustal deformation and gravity change at the Yellowstone caldera. J. Geophys. Res., 95, 19839-19856.

Vergniolle, S. and Jaupart, C., 1986. Separated two-phase flow and basaltic eruptions. J. Geophys. Res., 91, 12842-12860.

Vergniolle, S. and Jaupart, C., 1990. Dynamics of degassing at Kilauea Volcano, Hawaii. J. Geophys. Res., 95, 2793-2809.

Walker, G. P. L., Heming, R. F., Sprod, T. J. and Walker, H. R., 1981. Latest major eruptions of Rabaul volcano. In: Johnson, R. W. (Editor), Cooke-Ravian Volume of Volcanological Papers, Geol. Surv. Papua New Guinea, 10, pp. 81-193.

Walker, J. A., Williams, S. N., Kalamarides, R. I. and Feigenson, M. D., 1993. Shallow open-system evolution of basaltic magma beneath a subduction zone volcano: the Masaya Caldera Complex, Nicaragua. J. Volcanol. Geotherm. Res., 56, 379-400.

Westrich, H. R. and Gerlach, T. M., 1992. Magmatic gas source for the stratospheric SO_2 cloud from the June 15, 1991, eruption of Mount Pinatubo. Geology, 20, 867-870.

Weyl, R. 1980. Geology of Central America. Gebruder Borntraeger, Berlin, Germany, 371 pp.

Wicks, C., Thatcher, W. and Dzurisin, D., 1998. Migration of fluids beneath Yellowstone caldera inferred from satellite radar interferometry. Science, 282, 458-462.

Williams, R. L., 1972. The geology of western Nicaragua: Tax Improvement and Natural Resources Inventory Project, Final Technical Report. Managua, Nicaragua, 4.

Williams, S. N., 1983a. Geology and eruptive mechanisms of Masaya Caldera Complex, Nicaragua, Ph.D. Thesis, Dartmouth College, Hanover, New Hampshire.

Williams, S. N., 1983b. Plinian airfall deposits of basaltic composition. Geology, 11, 211-214.

Williams, S. N., Sturchio, N. C., Calvache V., M. L., Mendez F., R., Londono C., A. and Garcia P., N., 1990. Sulfur dioxide from Nevado del Ruiz Volcano, Colombia: Total flux and isotopic constraints on its origin. J. Volcanol. Geotherm. Res., 42, 53-68.

Williams, S. N., Schaefer, S. J., Calvache V., M. L. and Lopez, D., 1992. Global carbon dioxide emission to the atmosphere by volcanoes. Geochim. Cosmochim. Acta, 56, 1765-1770.

Woods, A. W. and Koyaguchi, T., 1994. Transitions between explosive and effusive eruptions of silicic magmas. Nature, 370, 641-644.

Yokoyama, I., 1989. Microgravity and height changes caused by volcanic activity: four Japanese examples. Bull. Volcanol., 51, 333-345.

Zapata, J. A., Calvache V., M. L., Cortés J., G. P., Fischer, T. P., Garzon V., G., Gómez M., D., Narváez M., L., Ordoñez V., M., Ortega E., A., Stix, J., Torres C., R. and Williams, S. N., 1997. SO_2 fluxes from Galeras Volcano, Colombia, 1989-1995: Progressive degassing and conduit obstruction of a Decade Volcano. J. Volcanol. Geotherm. Res., 77, 195-208.

Appendix A.

GPS and Gravity Station Locations

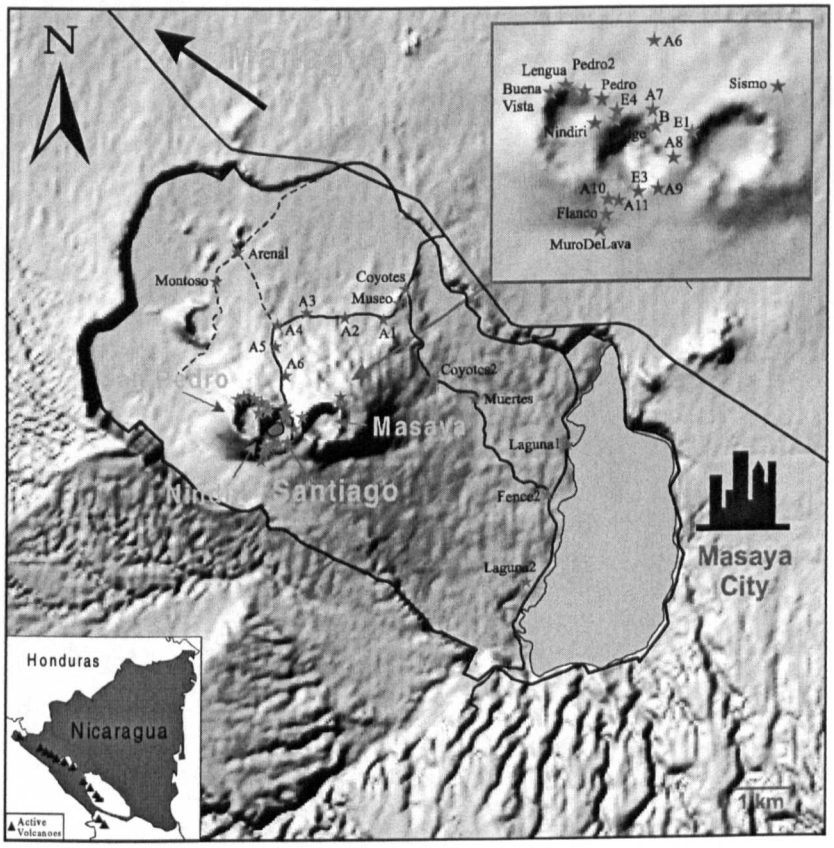

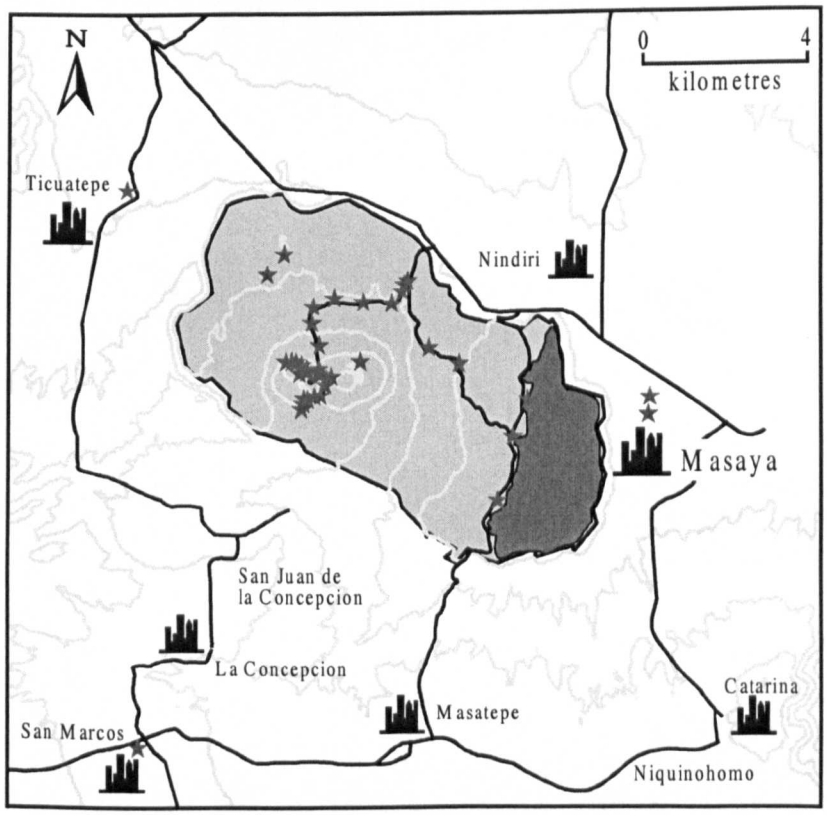

Station: *A1*

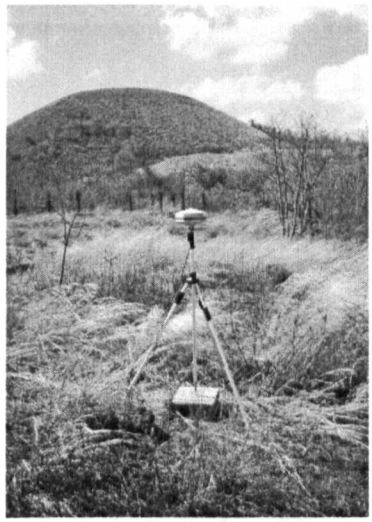

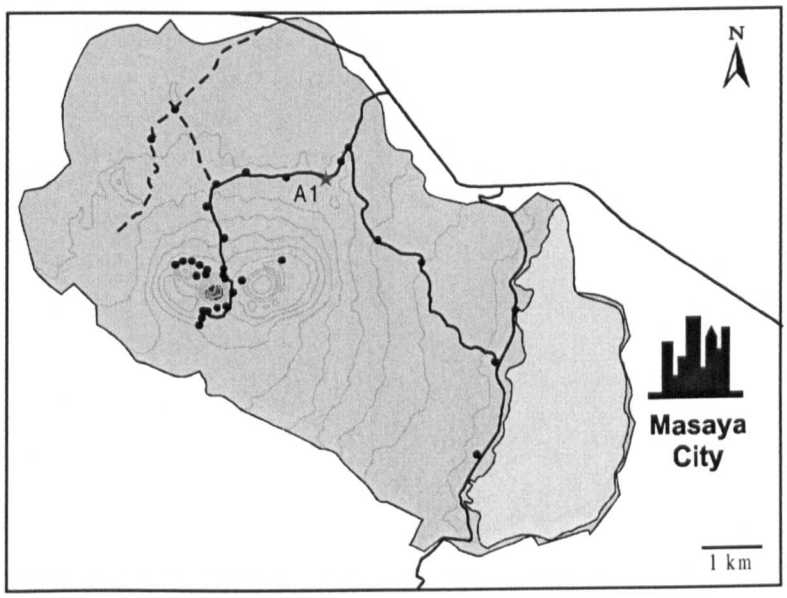

Location:

Elevation	Easting	Northing	Latitude	Longitude
302.11 m	592431.60 m	1326779.00 m	12°00'02.7"	86°09'03.4"

Description:

Station is in an open field on the left of the main road up towards the craters. Just up the road from the Museum/Visitor centre. The pin is in a concrete plinth (Benchmark) located in the centre of the field. Comalito cinder cone to the left (from the road).

Station: *A2*

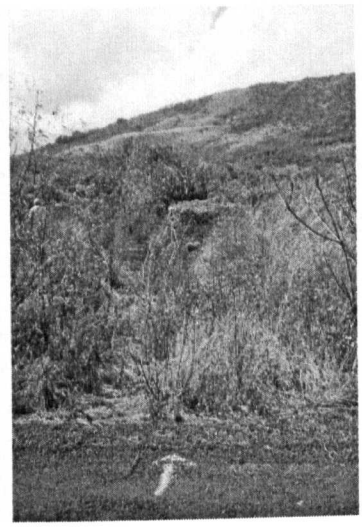

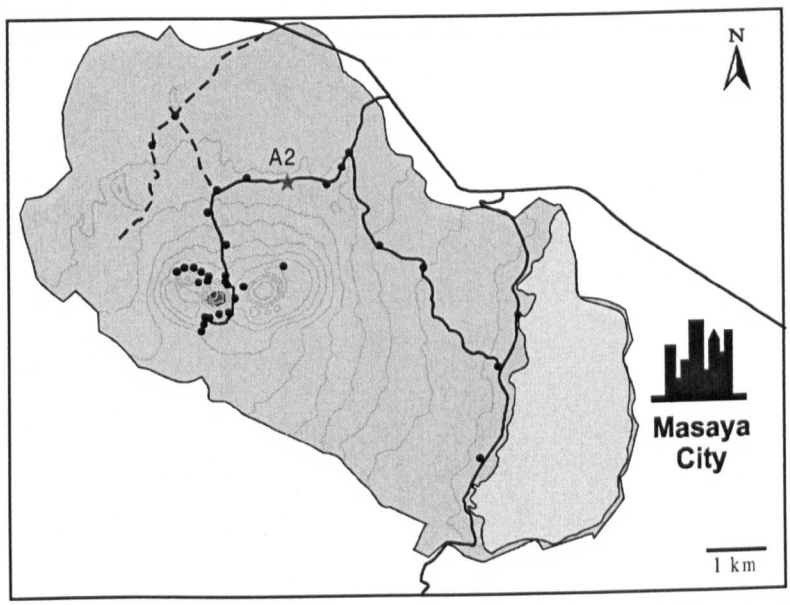

Location:

Elevation	Easting	Northing	Latitude	Longitude
295.55 m	591776.60 m	1326814.00 m	12º00'03.9"	86º09'25.0"

Description:

Approximately 700 m up the road from A1 towards the craters. On the left side of the road and off ~5 m. Marked on the road by a white line. The station is a concrete plinth (Benchmark).

Station: *A3*

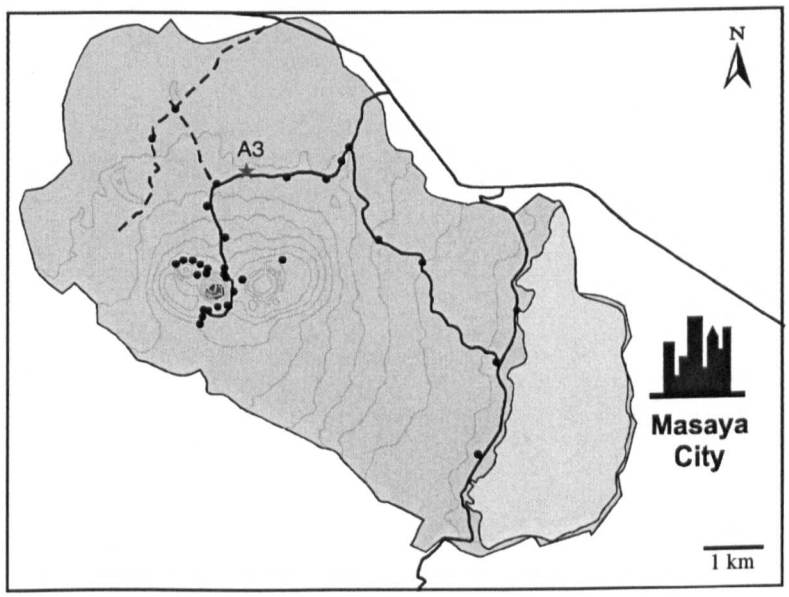

Location:

Elevation	Easting	Northing	Latitude	Longitude
297.78 m	591115.10 m	1326896.00 m	12°00'06.6"	86°09'46.9"

Description:

Approximately 1.4 km up the road from A1 towards the craters. On the right side of the road and at the intersection of a dirt road. Marked on the road by a white line. The station is a concrete plinth (Benchmark) sunk in the ground. Just down the road from a "No parking" sign (on the right).

Station: *A4*

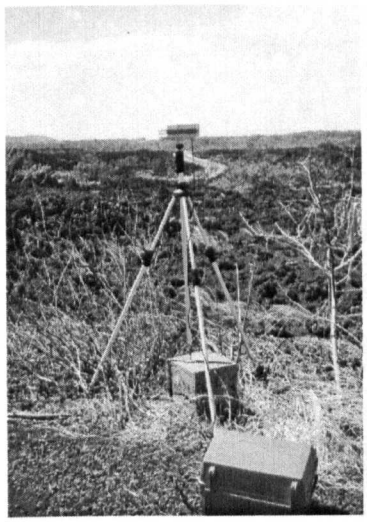

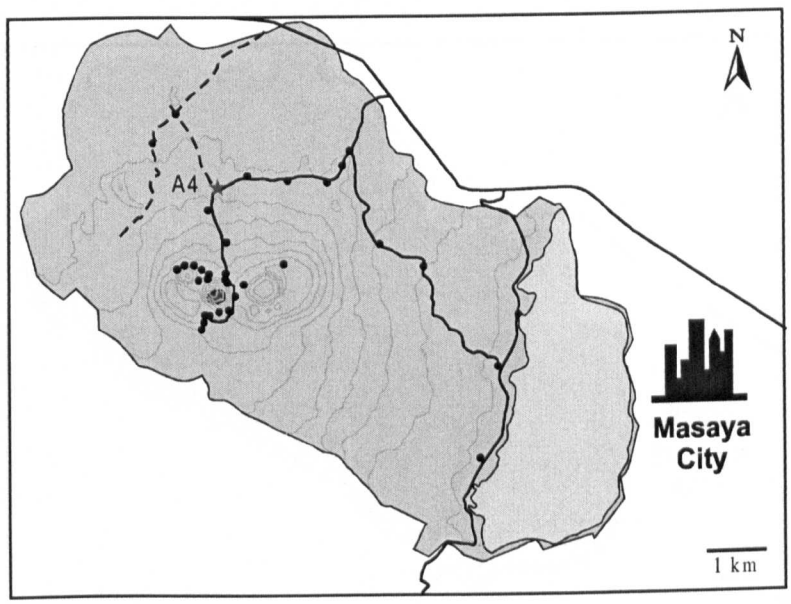

Location:

Elevation	Easting	Northing	Latitude	Longitude
319.66 m	590621.30 m	1326699.00 m	12°00'00.3"	86°10'03.2"

Description:

Approximately 1.9 km up the road from A1 towards the craters. On the right side of the road and at the intersection (Sendero de las Pencas) of a dirt road heading off to the right across an open lava field. Marked on the road by a white line. The station is a concrete plinth (Benchmark).

Station: *A5*

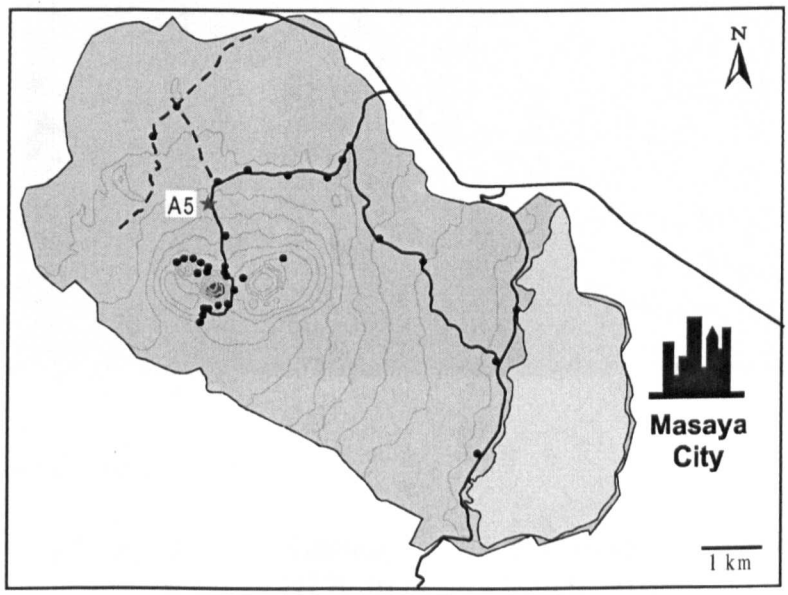

Location:

Elevation	Easting	Northing	Latitude	Longitude
353 m	590588 m	1326334 m	11°59'48.4"	86°10'04.4"

Description:

On the main road (right side) up to the craters. Marked by a white arrow. Just after the "Colada de lava" sign on the right before the curve. The station is a concrete plinth (Benchmark) sunk in the ground.

Station: *A6*

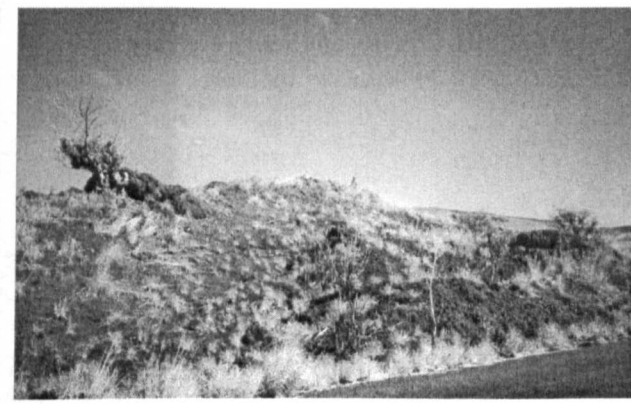

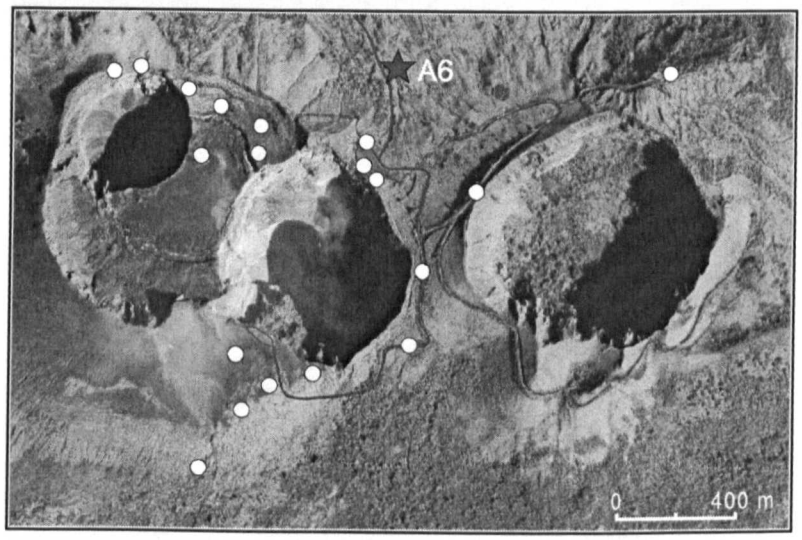

Location:

Elevation	Easting	Northing	Latitude	Longitude
439.17 m	590759.10 m	1325833.00 m	11°59'32.1"	86°09'58.8"

Description:

On a ridge to the left of the main road up to the craters and ~20 m from the road. Marked on the left of the road by a white arrow. The station is a concrete plinth (Benchmark).

Station: *A7*

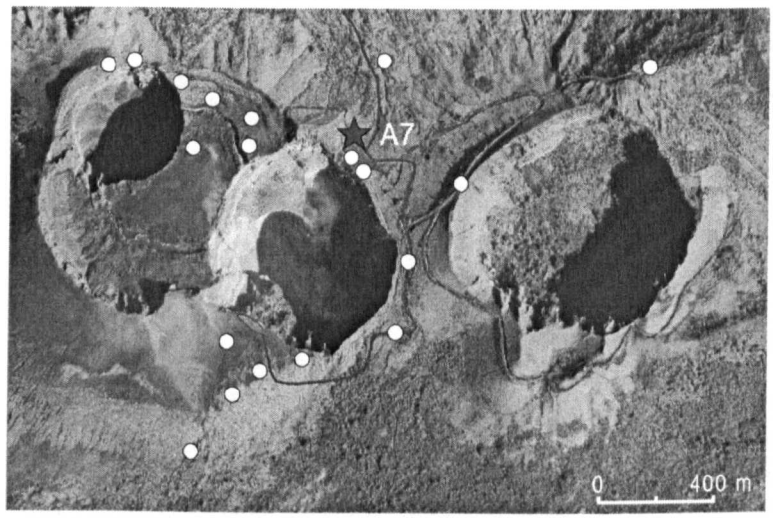

Location:

Elevation	Easting	Northing	Latitude	Longitude
520.74 m	590748.80 m	1325303.00 m	11°59'14.8"	86°09'59.1"

Description:

On an open lava flow immediately to the right of the road as one enters the main car park next to the craters. Near the remains of an old shed (walls). The station is a concrete plinth (Benchmark).

Station: *A8*

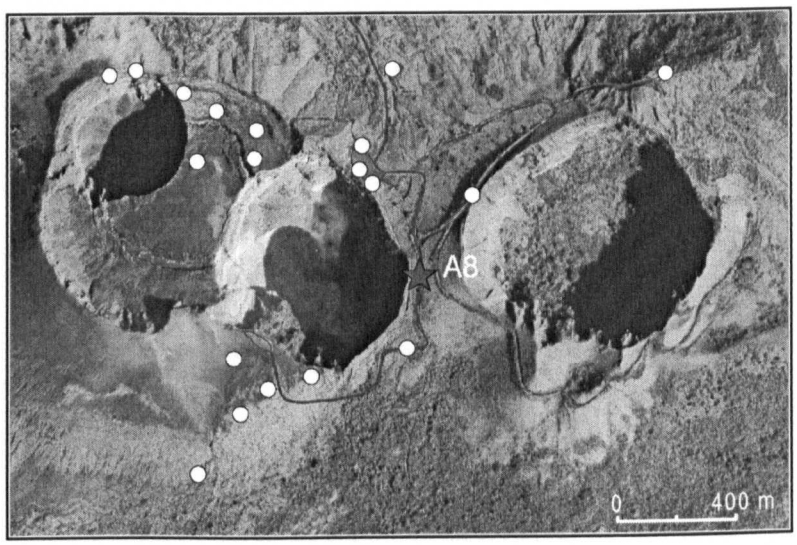

Location:

Elevation	Easting	Northing	Latitude	Longitude
565.94 m	590910.10 m	1324937.00 m	11°59'02.9"	86°09'53.9"

Description:

On the right of the road running around (to the left of) Santiago craters. On the crest of the ridge. Just up the road from a small lookout. Marked by a white arrow and "8" on the road. The station is a concrete plinth (Benchmark).

Station: *A9*

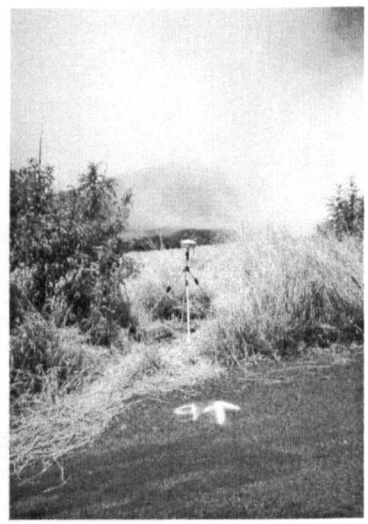

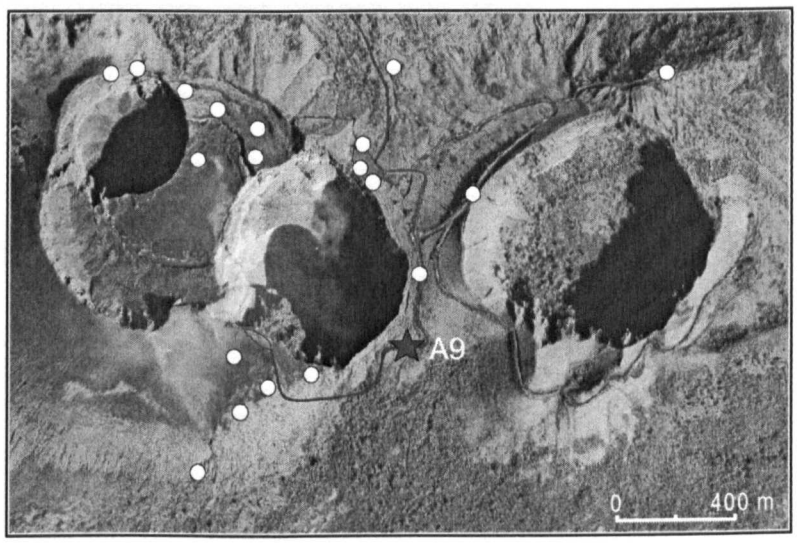

Location:

Elevation	Easting	Northing	Latitude	Longitude
511.97 m	590794.30 m	1324705.00 m	11°58'55.3"	86°09'57.7"

Description:

On the right of the road running around (to the left of) Santiago crater. Down hill from the crest of the ridge and station A8. Marked by a white arrow and "9" on the road. Approximately 1 m from the road edge. The station is a concrete plinth (Benchmark) sunk in the ground.

Station: *A10*

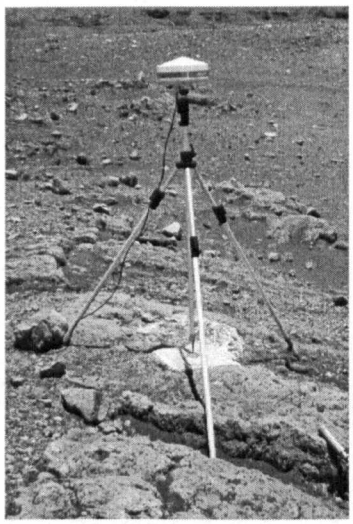

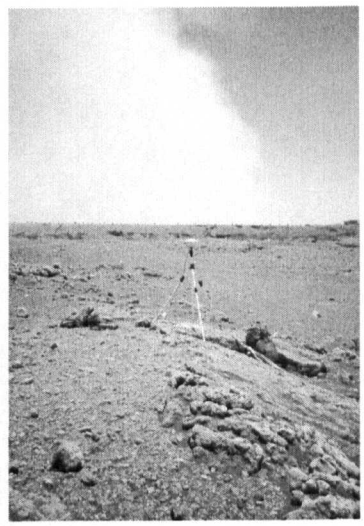

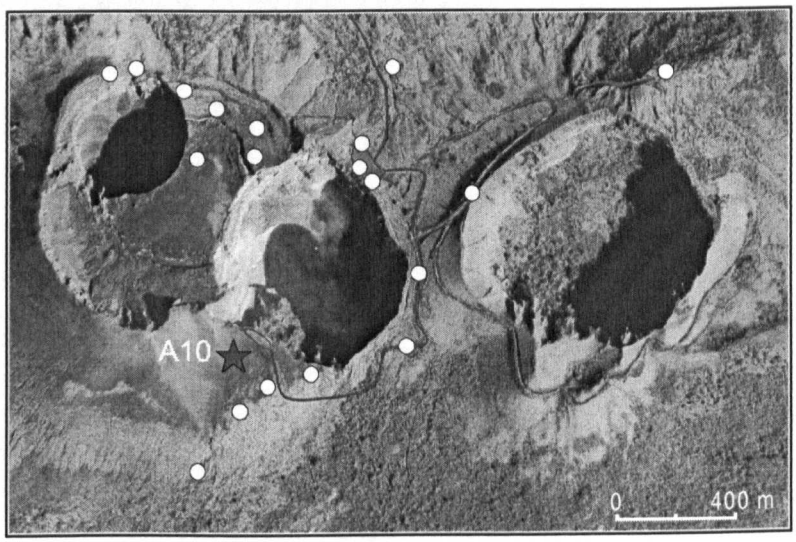

Location:

Elevation	Easting	Northing	Latitude	Longitude
509.12 m	590408.00 m	1324630.00 m	11°58'52.9"	86°10'10.5"

Description:

Down slope (~150 m) from the 2nd car park (across Santiago crater from the 1st car park). Site 30°N towards the car park and a wide separation in the fence posts. The station is a concrete plinth (Benchmark) sitting on pahoehoe lava.

Station: *A11*

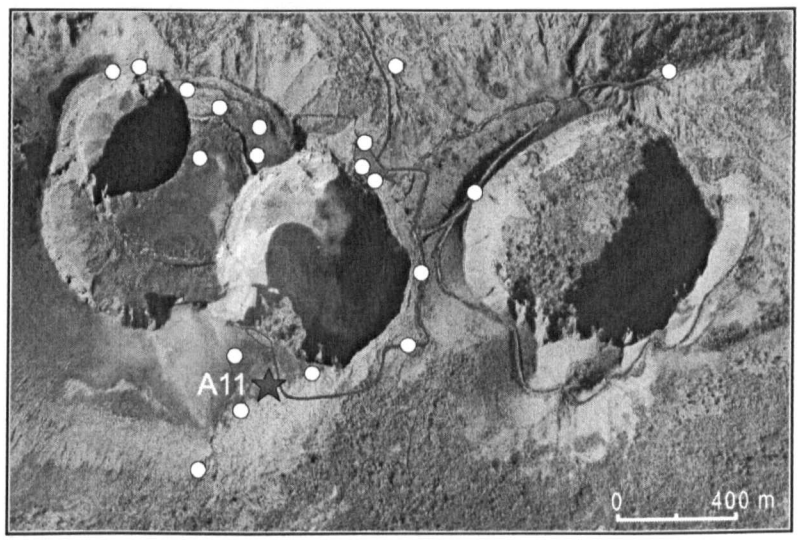

Location:

Elevation	Easting	Northing	Latitude	Longitude
503.19 m	590492.20 m	1324617.00 m	11°58'52.5"	86°10'07.7"

Description:

Down slope from the 2nd car park (across Santiago crater from the 1st car park) and to the left of the road leading to the car park. Approximately 25 paces from a fence post (on the left side of the road) marked with two white stars. The station is a steel pin planted in pahoehoe lava and circled in white.

Station: *Arenal*

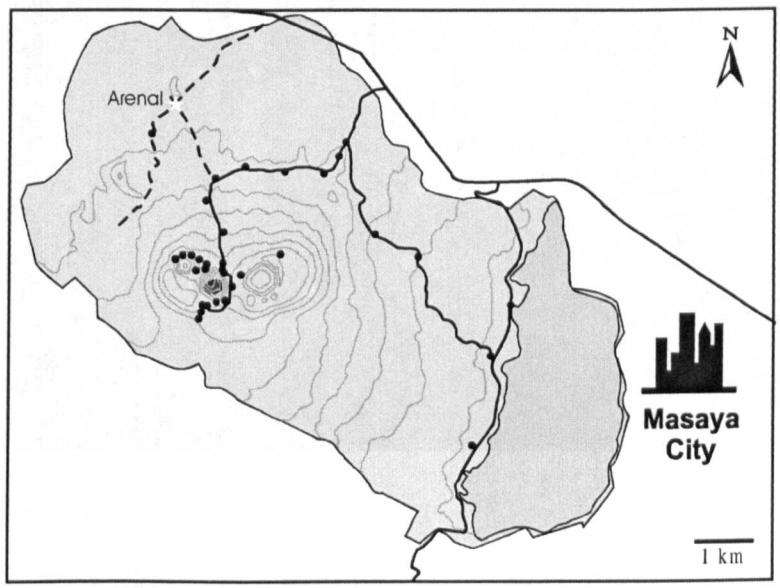

Location:

Elevation	Easting	Northing	Latitude	Longitude
281.98 m	589934.80 m	1327908.00 m	12°00'39.7"	86°10'25.8"

Description:

Located on a dirt road, approximately 1.4 km from the main road (to the craters) and station A4. At an intersection (right angles) with another dirt road, in an open area of old lava flows. To the right is the Arenal cinder cone. The station is a steel pin planted in wall made from lava blocks and circled in white.

Station: *B2*

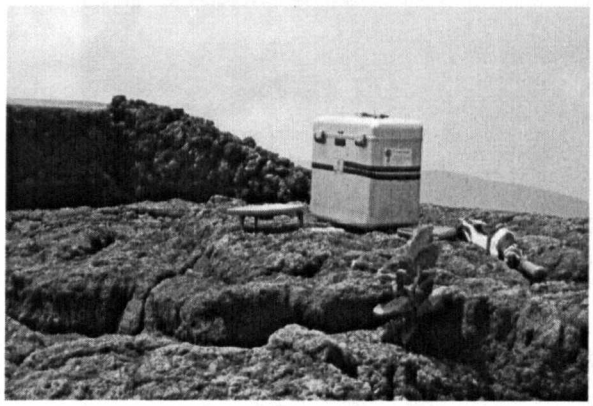

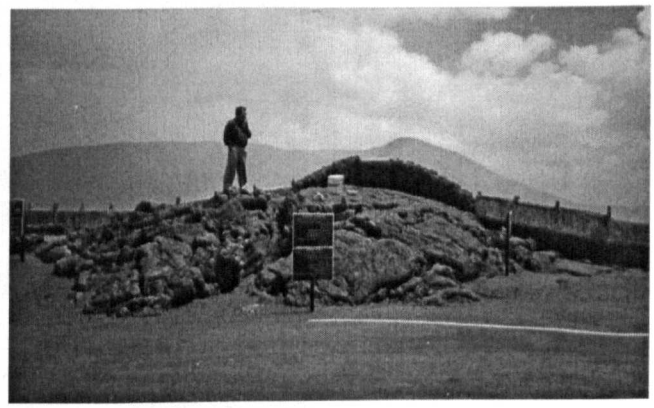

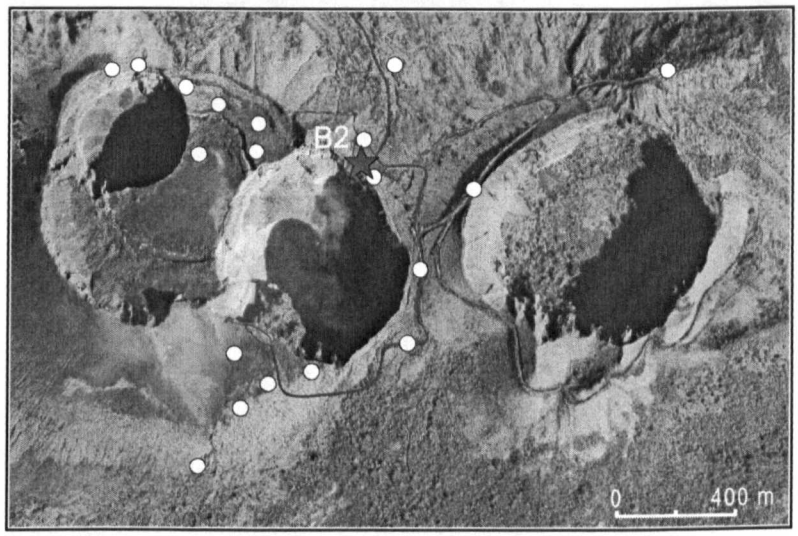

Location:

Elevation	Easting	Northing	Latitude	Longitude
524.77 m	590736.30 m	1325210.00 m	11°59'11.8"	86°09'59.6"

Description:

Near the edge of the car park on a mound of lava (lookout) looking directly over Santiago crater (in the "middle" of the wall). The station is a steel pin planted in concrete and wedged between a crack in the lava.

Station: *B3a*

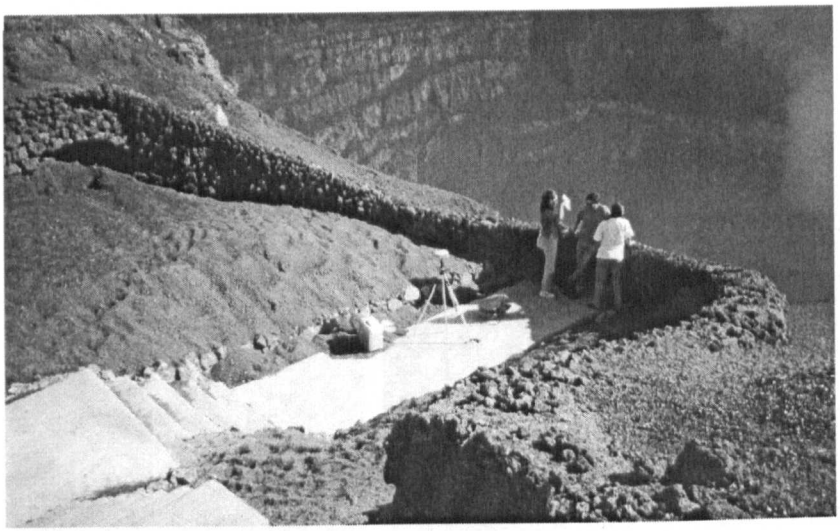

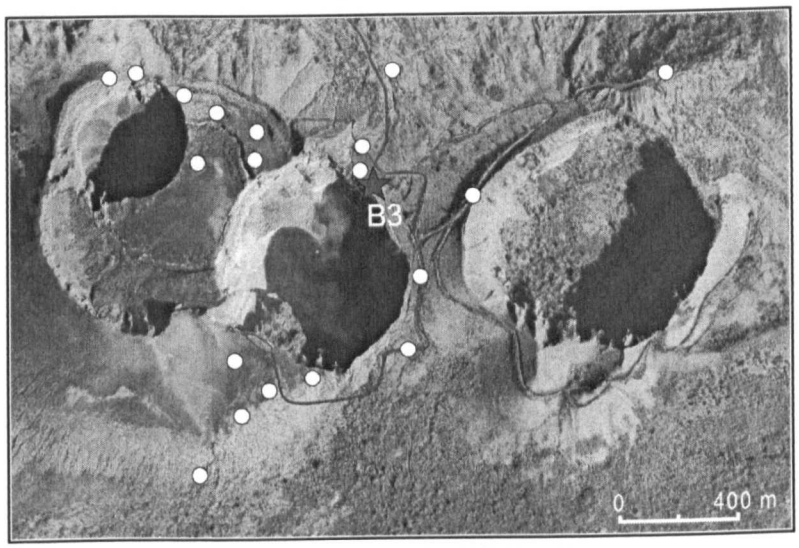

Location:

Elevation	Easting	Northing	Latitude	Longitude
521.40 m	590767.30 m	1325166.00 m	11°59'10.4"	86°09'58.6"

Description:

Near the edge of the 1st car park looking directly over Santiago crater and in a lookout down from the small hut. The lookout is at least 5 m below the car park. The station is a steel pin planted in the concrete floor. Often covered by sediment/pyroclastics that wash down from the walls of the lookout, i.e. dig for it!

Station: *Coyotes*

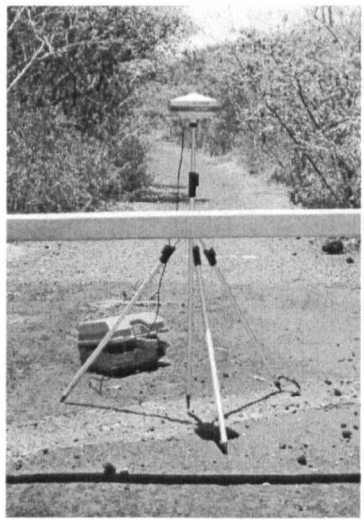

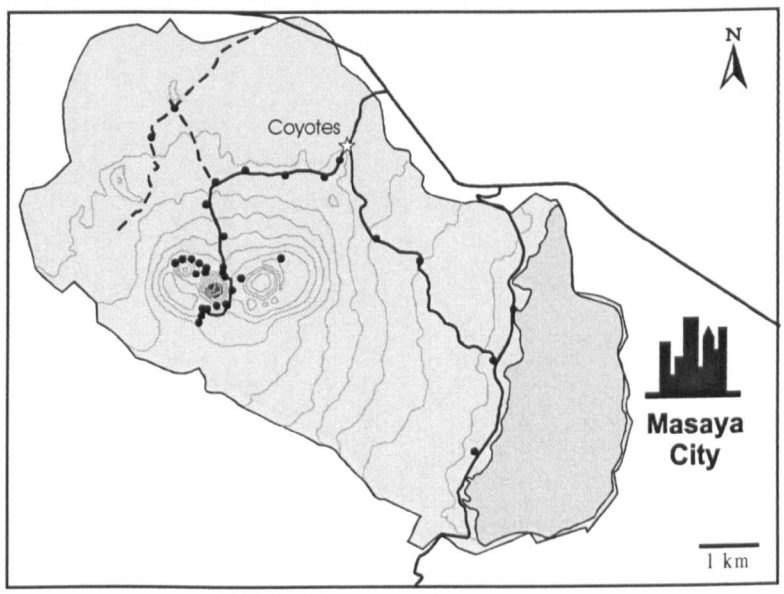

Location:

Elevation	Easting	Northing	Latitude	Longitude
284.65 m	592802.40 m	1327291.00 m	12º00'19.3"	86º08'51.0"

Description:

At the intersection of the main road (up to the craters) and the Los Coyotes road (on the left). Marked by a sign and large yellow barrier. The station is a steel pin planted in the concrete directly below the barrier and approximately in the middle.

Station: *Coyotes2*

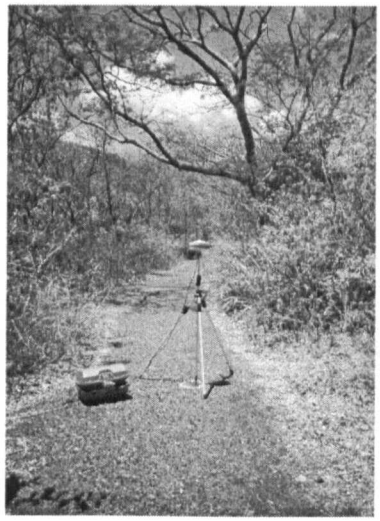

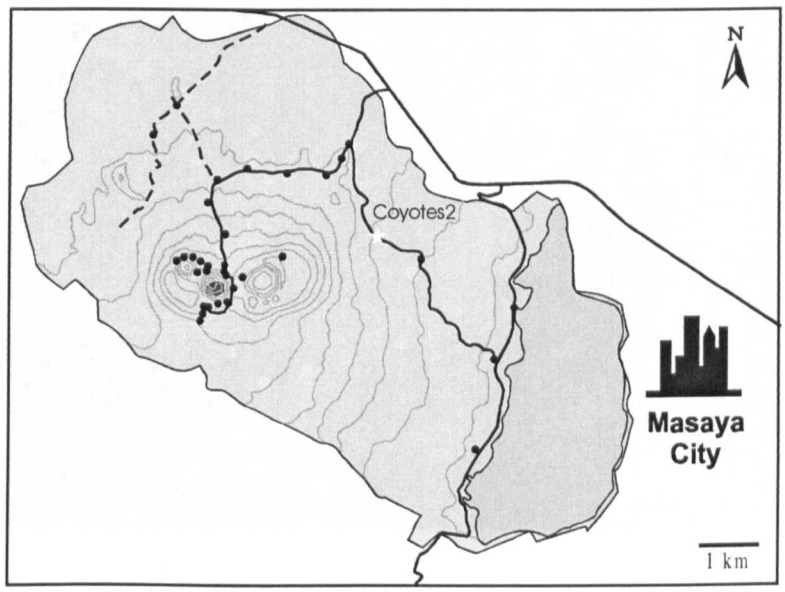

Location:

Elevation	Easting	Northing	Latitude	Longitude
236.69 m	593294.90 m	1325784.00 m	11°59'30.2"	86°08'34.9"

Description:

Approximately 1.7 km down the Los Coyotes road (intersecting the main road). The station was a steel pin (now stolen!) planted in middle of the road. The spot in marked by a white circle.

Station: *BuenaVista*

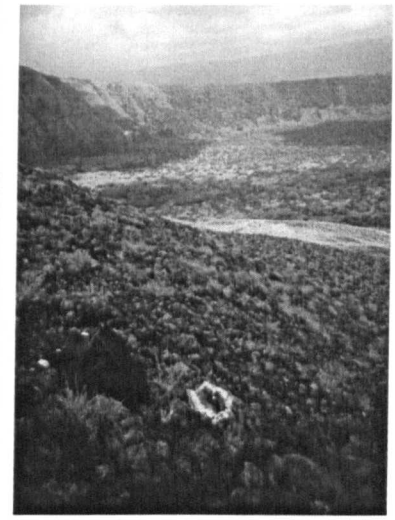

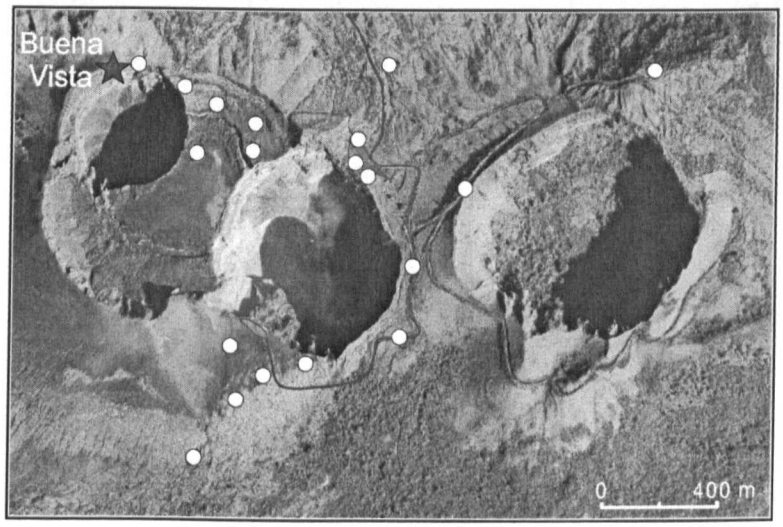

Location:

Elevation	Easting	Northing	Latitude	Longitude
570 m	589985 m	1325463 m	11°59'20.1"	86°10'24.4"

Description:

Located ~100 m along the trail from Lengua @ 102° around the rim of San Pedro crater. ~20 m below the crater rim. Across from the Cerro Montoso cinder cone. The pin is marked by a white circle and arrows.

Station: *E1*

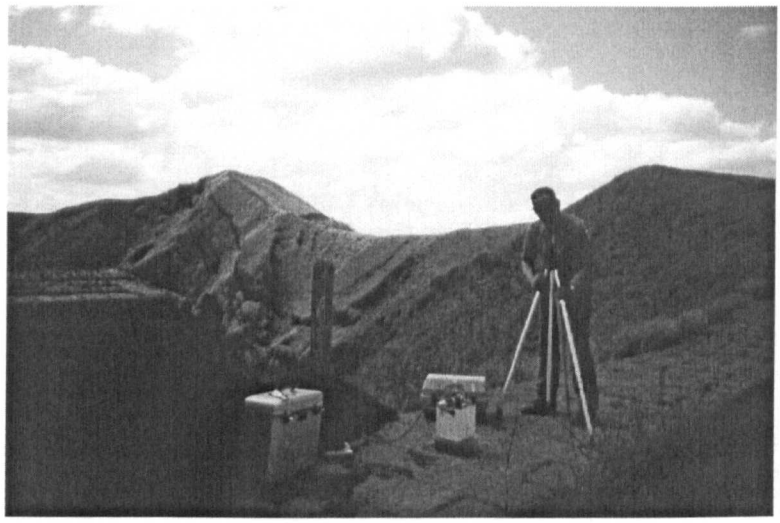

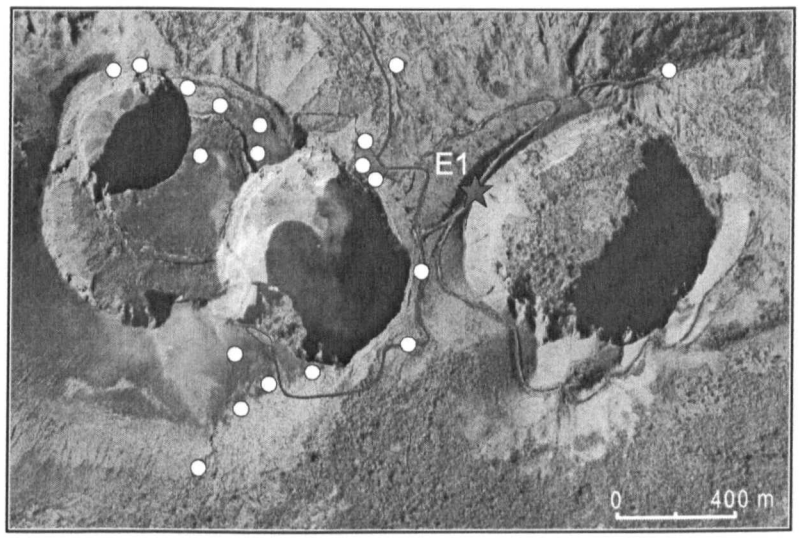

Location:

Elevation	Easting	Northing	Latitude	Longitude
587.70 m	591049.70 m	1325129.00 m	11°59'09.1"	86°09'49.2"

Description:

At the lookout over the San Fernando/Masaya crater. On a dirt road leading up from the main road circling Santiago crater. The station is a steel pin in concrete planted in middle of tiles.

Station: *E3*

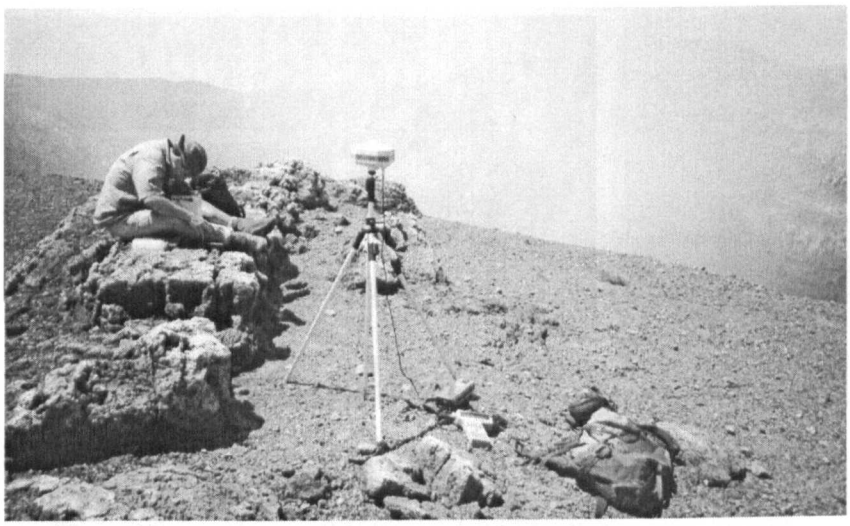

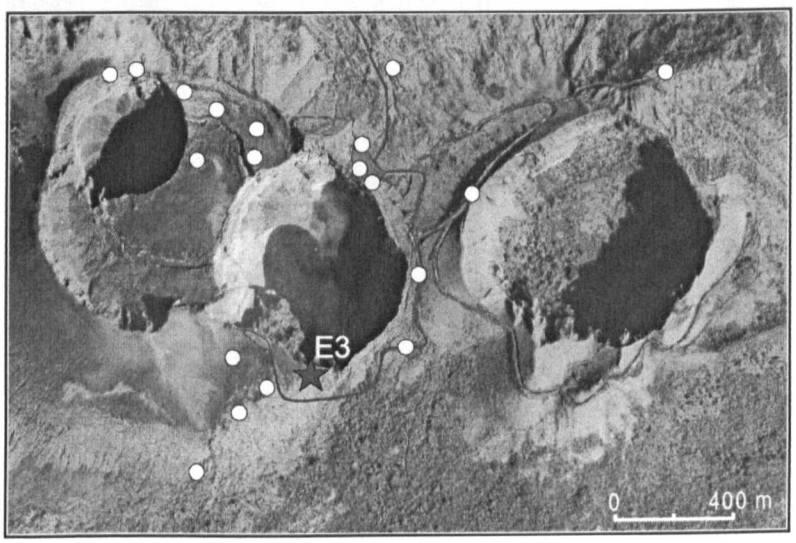

Location:

Elevation	Easting	Northing	Latitude	Longitude
509.54 m	590641.70 m	1324684.00 m	11°58'54.7"	86°10'02.8"

Description:

Located on a ridge of lava near the edge of Santiago crater. Across the crater from the 1st car park and to the right of the 2nd car park. Up from an old gate house on the circling road (to the S). The station was a steel pin (now stolen!) planted in concrete and on the lava.

Station: *E4*

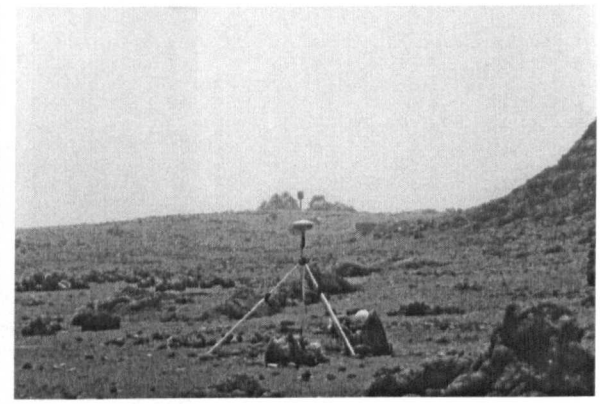

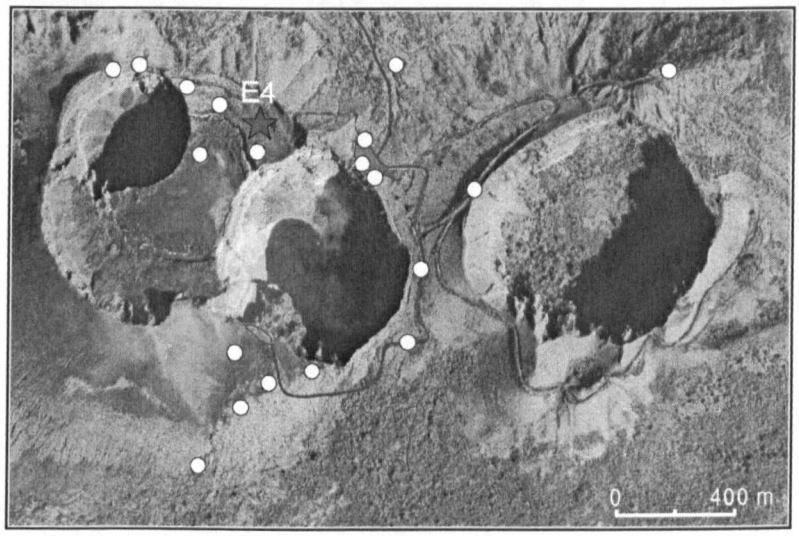

Location:

Elevation	Easting	Northing	Latitude	Longitude
517.35 m	590473.60 m	1325297.00 m	11°59'14.7"	86°10'08.2"

Description:

West, around behind the cross (on the ridge), from the 1st car park. On an old, subsided lava lake. Can look towards a large outcrop of lava and out across Nindiri (and Santiago to the SE). The station is a steel pin in concrete footing planted in the lava.

Station: *Edge*

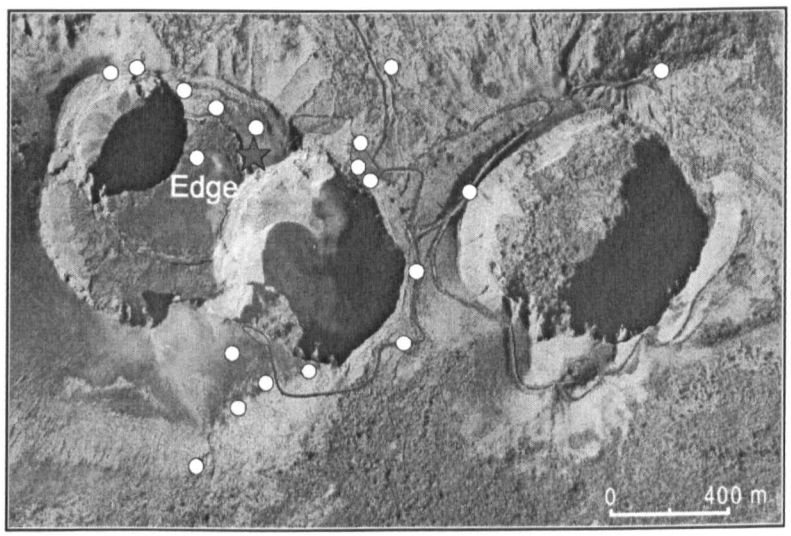

Location:

Elevation	Easting	Northing	Latitude	Longitude
519.73 m	590459.50 m	1325231.00 m	11°59'12.5"	86°10'08.7"

Description:

West, around behind the cross (on the ridge), from the 1st car park. On an old, subsided lava lake. Virtually on the edge of Nindiri crater. Approximately 70 m from station E4 and about 10 paces from a Japanese box overlooking Santiago crater. The station is a steel pin planted in pahoehoe lava. Marked by a white circle (now yellow due to the gas!).

Station: *EstacionT*

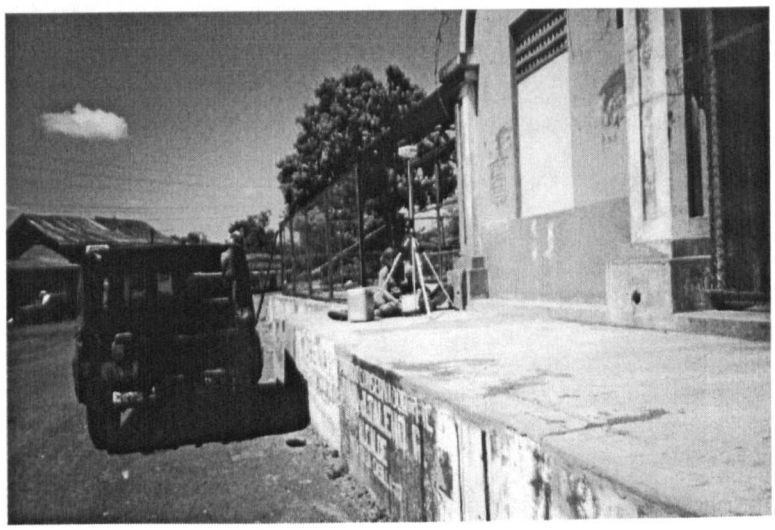

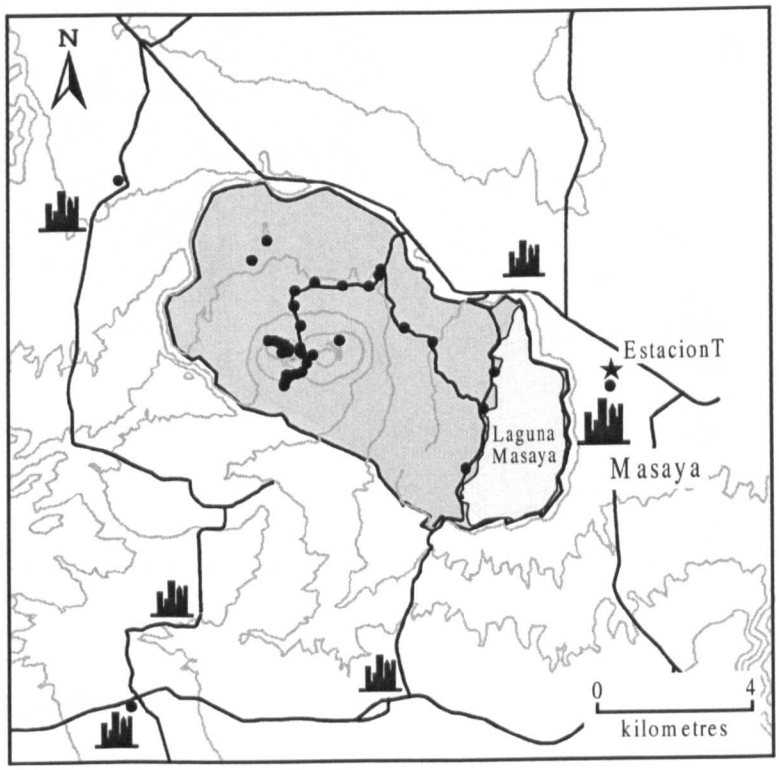

Location:

Elevation	Easting	Northing	Latitude	Longitude
229.16 m	598390.00 m	1324663.59 m	11°58'53.2"	86°05'46.6"

Description:

At the old train station (now a technical college) in Masaya City. The station is a steel pin planted in the concrete, towards the end of the platform.

Station: *Fence2*

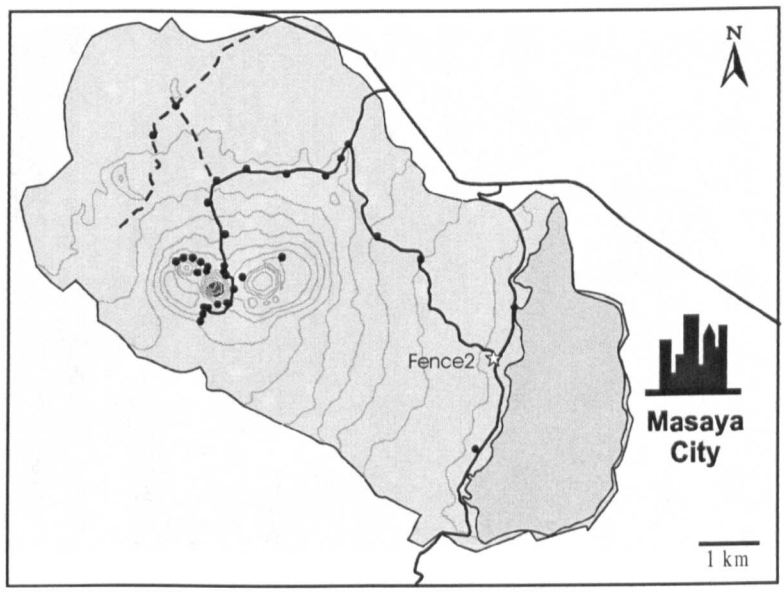

Location:

Elevation	Easting	Northing	Latitude	Longitude
123.87 m	595238.60 m	1323777.00 m	11°58'24.7"	86°07'30.9"

Description:

At the base of a lava-wall and bellow a yellow barrier at the intersection of the Los Coyotes (leading SE from the park) and the lake road. The station is a steel pin planted in the asphalt. Sometimes covered by debris in the rainy season. Best to access via the lake road.

Station: *Flanco*

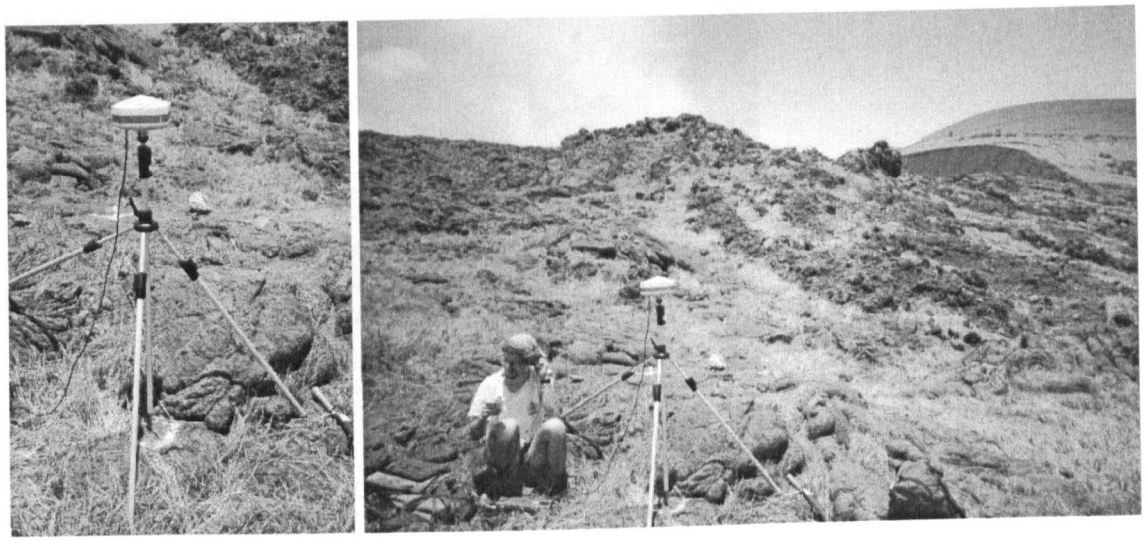

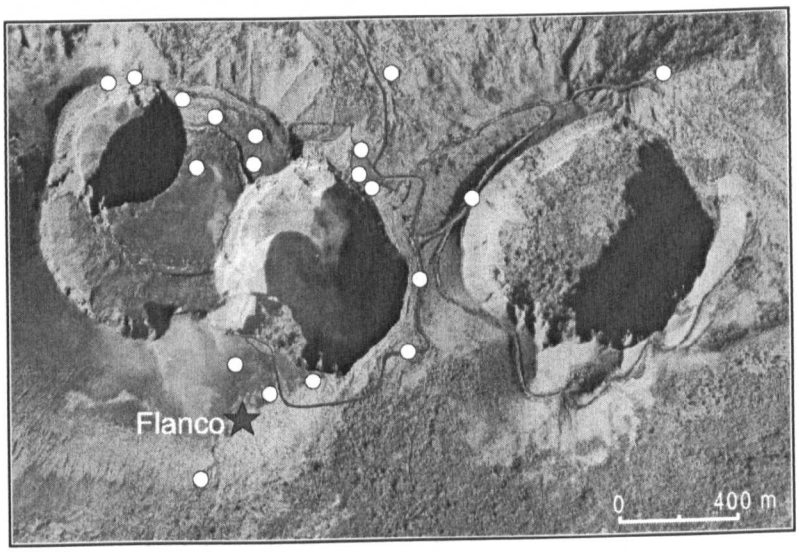

Location:

Elevation	Easting	Northing	Latitude	Longitude
492.31 m	590393.00 m	1324510.00 m	11°58'49.0"	86°10'11.0"

Description:

Down slope from the 2nd car park. Follow a path of loose scoria down straight from station A10. The station is a steel pin planted in a large outcrop of lava. Marked by a white arrow and circle.

Station: *LaClinica*

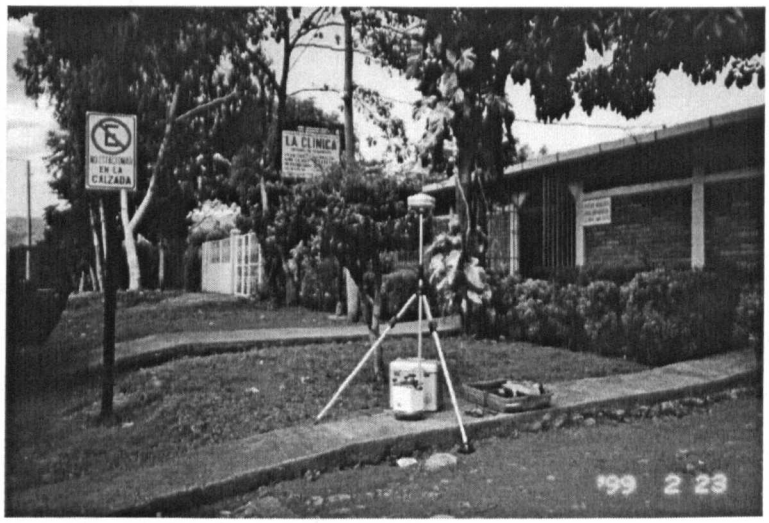

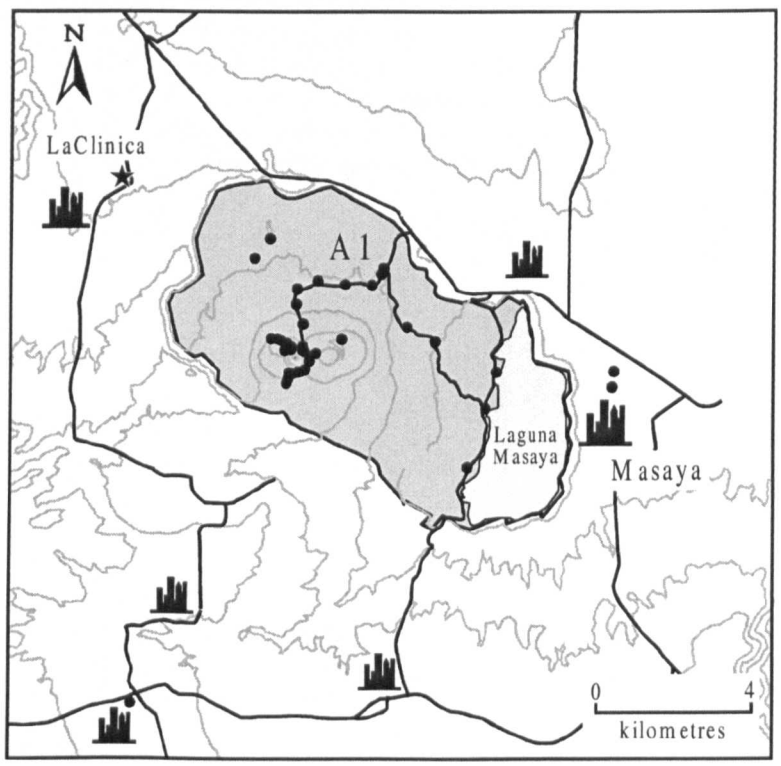

Location:

Elevation	Easting	Northing	Latitude	Longitude
284.80 m	586367.54 m	1329327.68 m	12º01'26.3"	86º12'23.6"

Description:

Located at a medical clinic in Ticuantepe at the intersection of the road from Masaya/Managua to Ticuantepe and the road to San Marcos. Near a "no parking" sign. The station is a steel pin set in the concrete walkway of the clinic.

Station: *Laguna1*

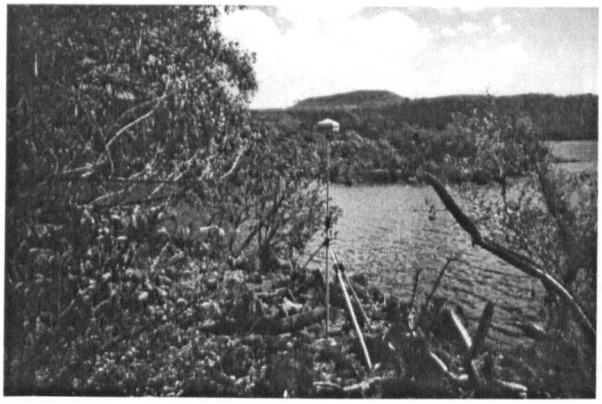

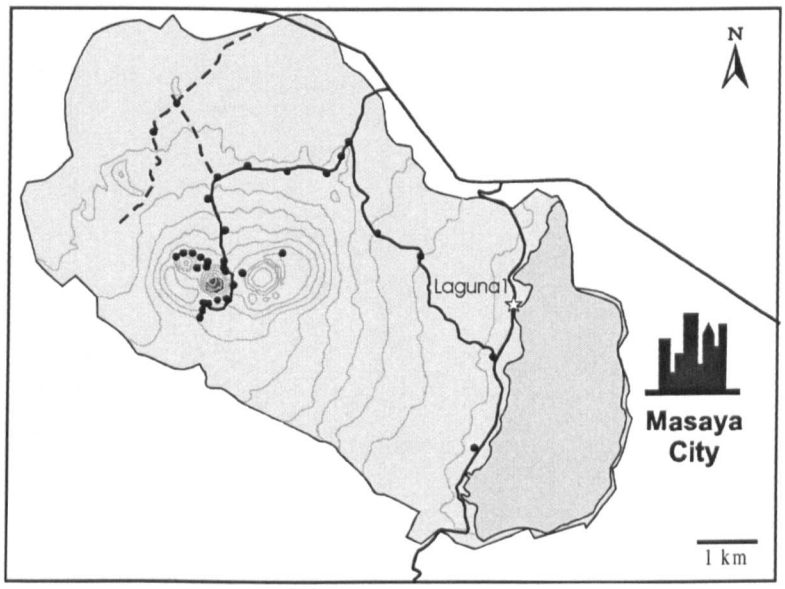

Location:

Elevation	Easting	Northing	Latitude	Longitude
118.53 m	595575.70 m	1324618.00 m	11°58'52.0"	86°07'19.6"

Description:

Located in a small bay near the Masaya lake. Down a small road off the main lake road. Approximately 900 m N of the Fence2 station and~3.4 km S of the main Masaya-Managua road. The station is a steel pin set in lava near the waters edge.

Station: *Laguna2*

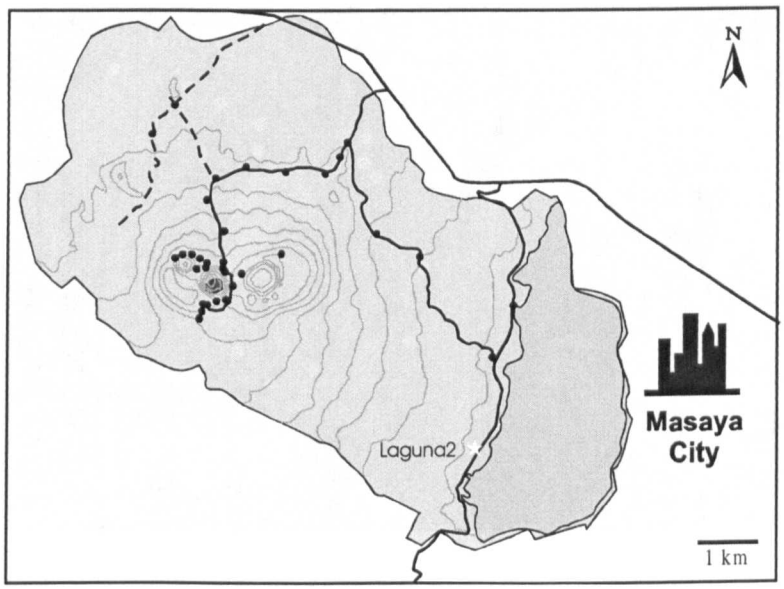

Location:

Elevation	Easting	Northing	Latitude	Longitude
130.32 m	594888.10 m	1322322.00 m	11°57'37.3"	86°07'42.6"

Description:

Located approximately 2.4 km from station Laguna1 in a open lava field to the right of the road along the Masaya lake. Approx. 5 km S of the main Masaya-Managua road. The station is a steel pin set in lava. A wall made of lava blocks is in the background.

Station: *Lengua*

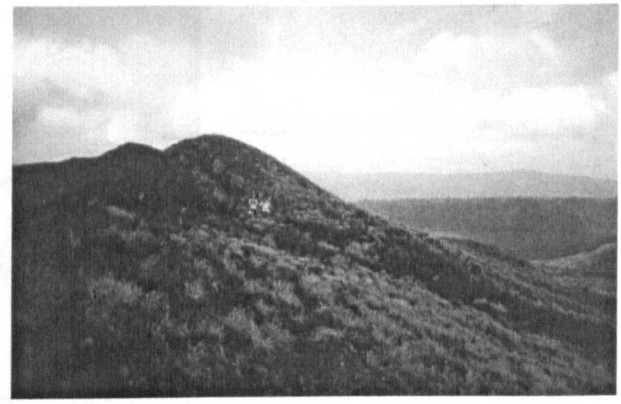

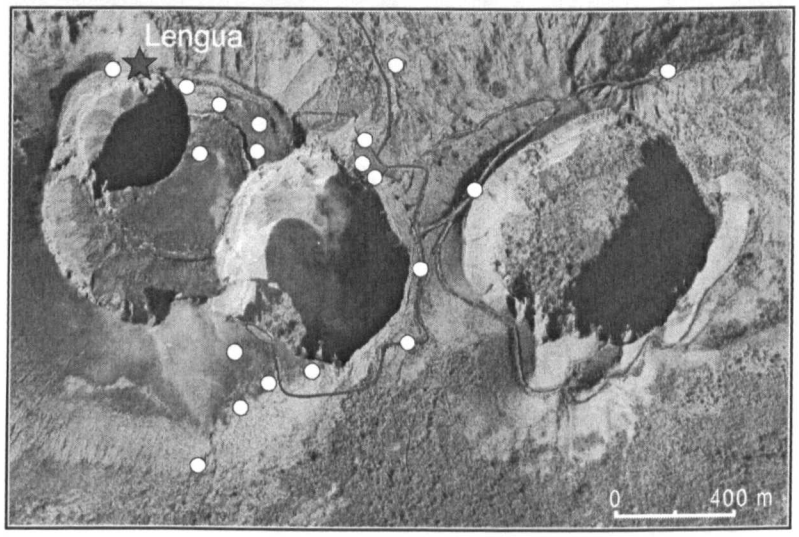

Location:

Elevation	Easting	Northing	Latitude	Longitude
540.00 m	590130 m	1325469 m	11°59'20.3"	86°10'19.6"

Description:

Located approximately 100 m at 160° on from station Pedro2 around the rim of San Pedro crater. The station is a steel pin set in a small tongue of lava that overflowed the rim. Station marked by a white circle.

Station: *Montoso*

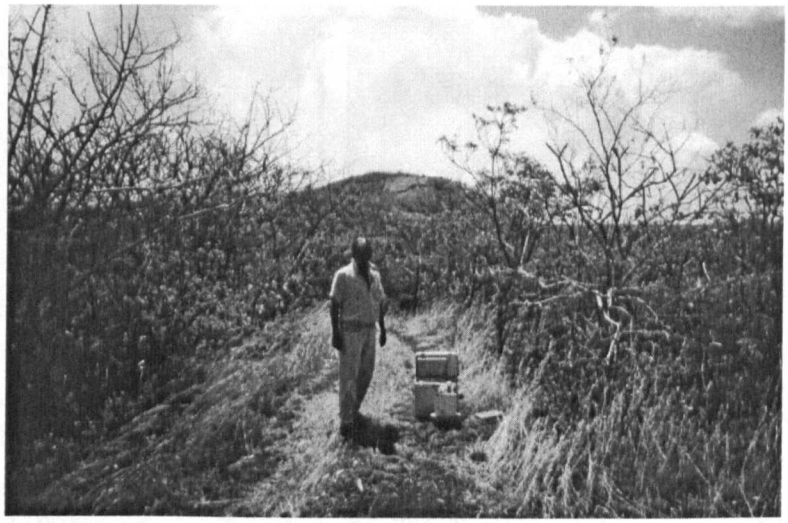

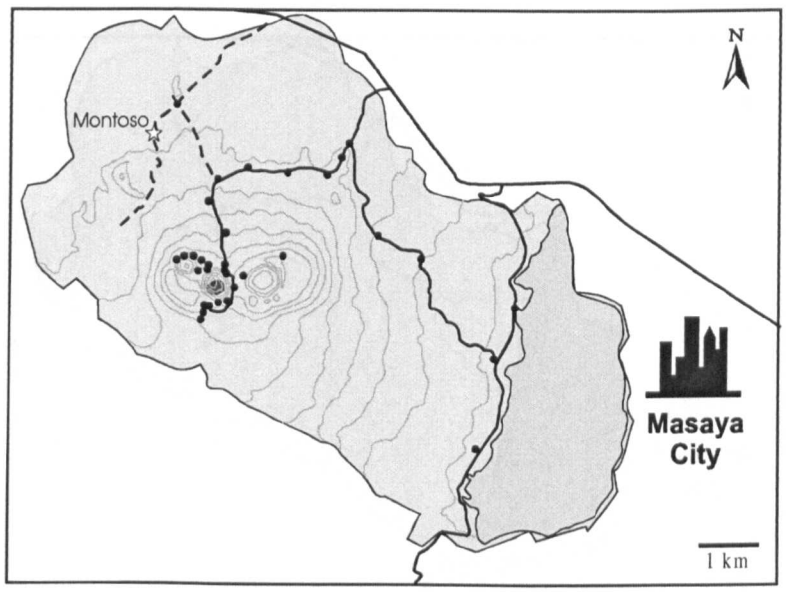

Location:

Elevation	Easting	Northing	Latitude	Longitude
287.65 m	589559.50 m	1327432.00 m	12º00'24.2"	86º10'38.3"

Description:

Approximately 700 m from station Arenal (turn left at the intersection with the dirt road intersecting the main road). Approx. 150 m further on is the Cerro Montoso cinder cone. The station is a steel pin planted in middle of the dirt road in an outcrop of lava. The spot in marked by a white circle.

Station: *Muertes*

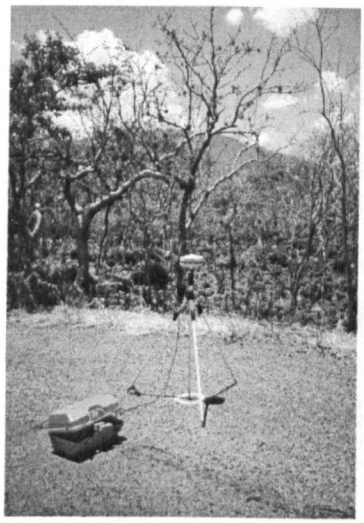

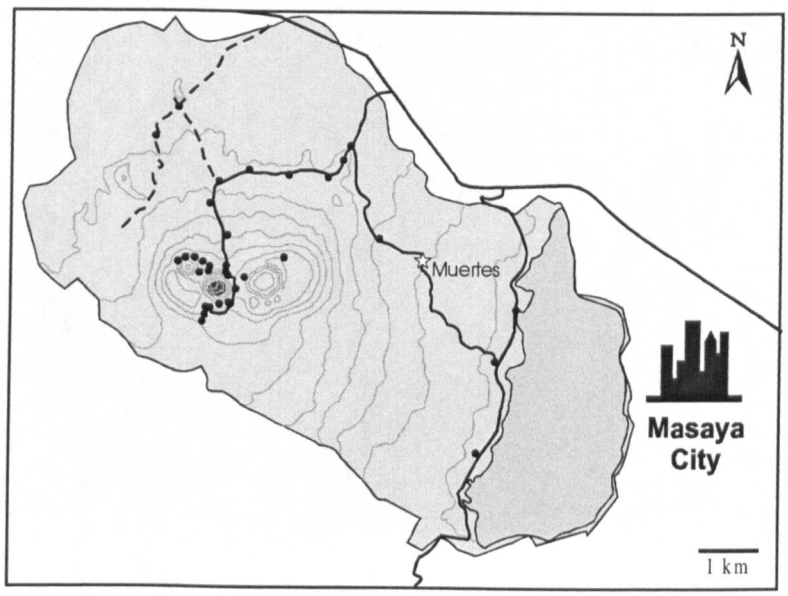

Location:

Elevation	Easting	Northing	Latitude	Longitude
199.02 m	593993.60 m	1325417.00 m	11°59'18.2"	86°08'11.8"

Description:

Approximately 2.7 km down the Los Coyotes road (intersecting the main road). The station was a steel pin (now stolen!) planted in middle of the road. The spot in marked by a white circle. Just before a sharp turn in the road, with open lava fields on both sides.

Station: *MuroDeLava*

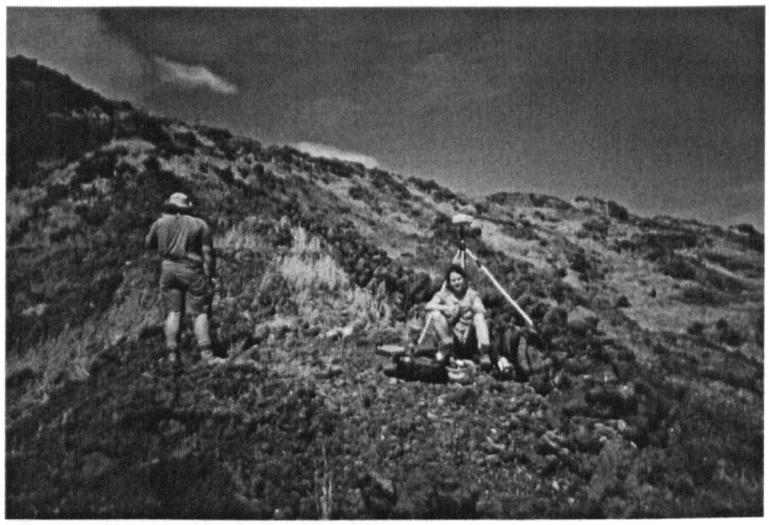

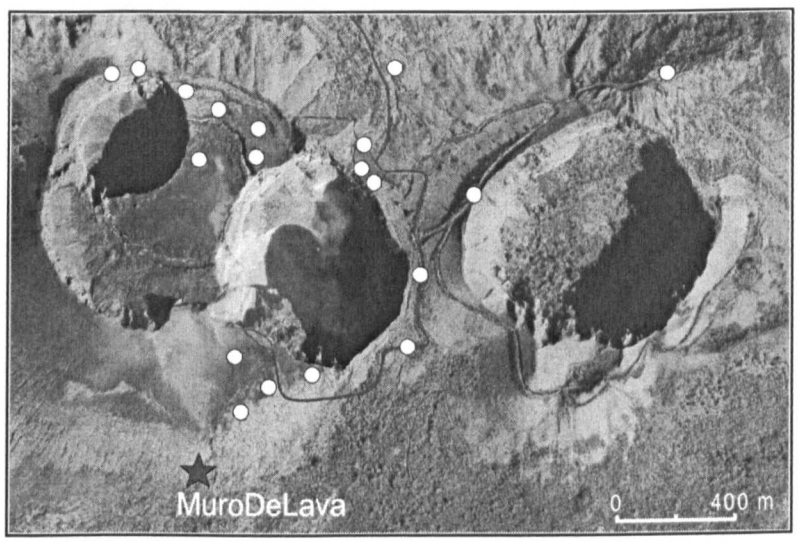

Location:

Elevation	Easting	Northing	Latitude	Longitude
454.74 m	590349.50 m	1324396.00 m	11°58'45.3"	86°10'12.4"

Description:

Near a wall made from lava blocks and down slope from the 2nd car park and the Flanco station. A small path runs down to the wall. The station is a steel pin planted in an outcrop of lava. The spot in marked by a white circle. About 100 m from the station (at 296°) stands a lone tree on the side of the San Pedro cone.

Station: *Museo*

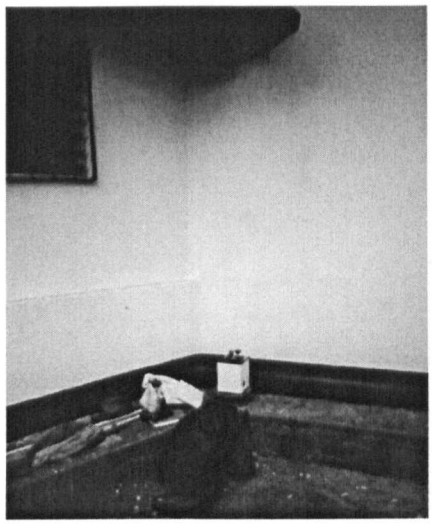

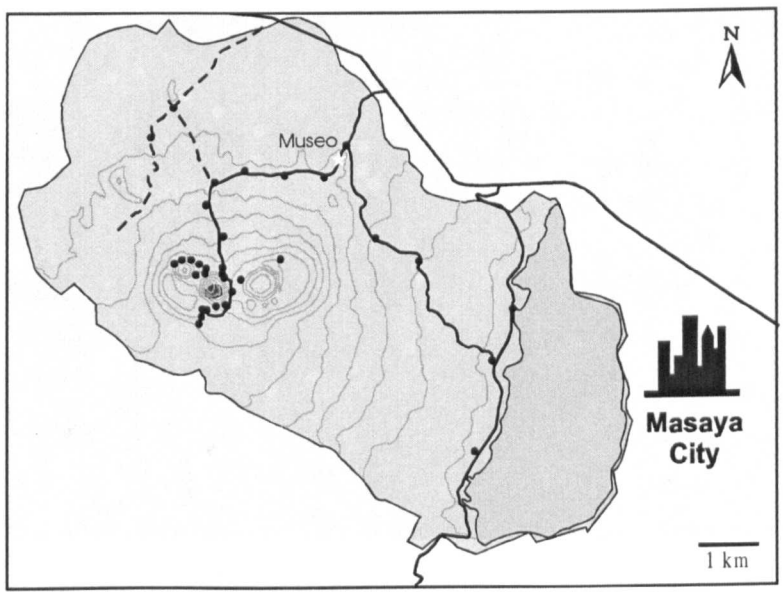

Location:

Elevation	Easting	Northing	Latitude	Longitude
310.10 m	592679.20 m	1327057.00 m	12°00'11.7"	86°08'55.1"

Description:

In the corner of the Museum/Visitor centre on the front wall, facing the parking lot and main road. The station is the square of concrete on the rim (bench?) of the Museum wall, closest into the corner.

Station: *Nindiri*

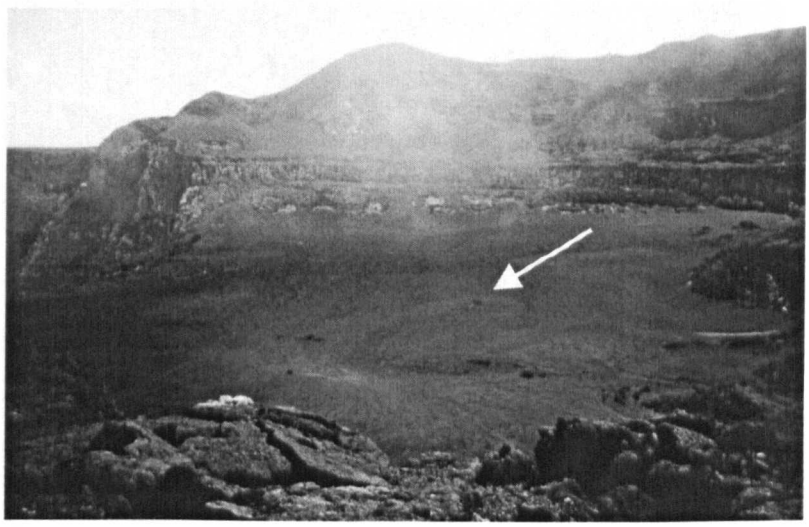

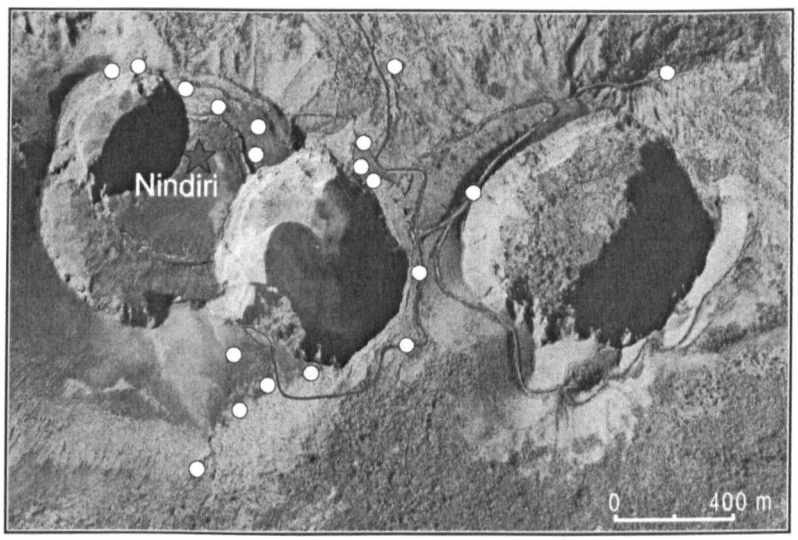

Location:

Elevation	Easting	Northing	Latitude	Longitude
485.32 m	590306.60 m	1325202.00 m	11°59'11.6"	86°10'13.8"

Description:

On the lava lake floor of the Nindiri crater, more or less in the middle between Santiago and San Pedro craters. Approximately 40 paces from the edge of San Pedro and 55 paces from the northern wall of Nindiri. The station is pin in some outcropping lava and marked by a small white circle. Also marked by a small cairn of stones.

Station: *ParqueSM*

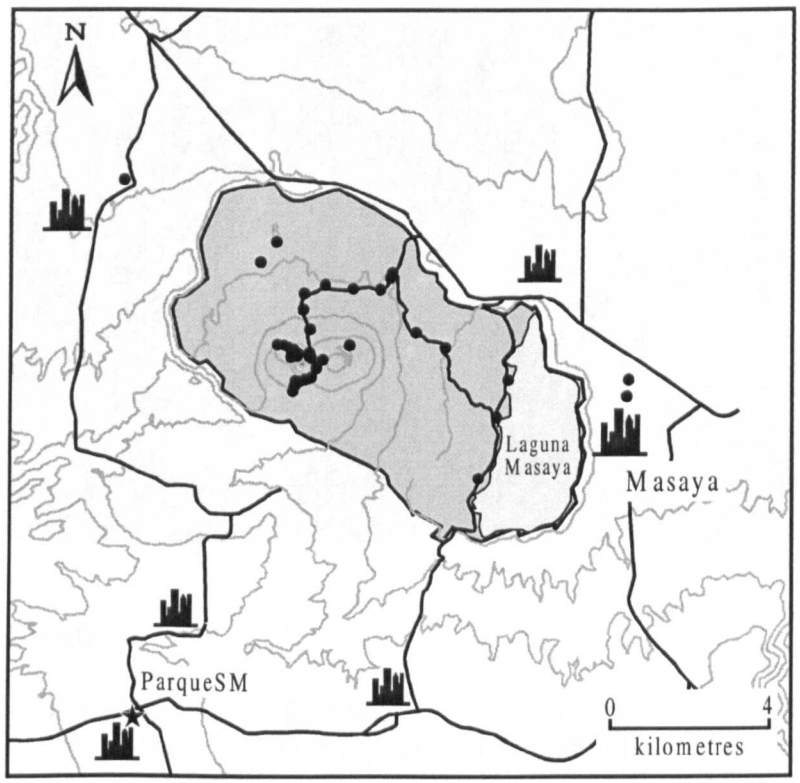

Location:

Elevation	Easting	Northing	Latitude	Longitude
652.78 m	586582.06 m	1316657.51 m	11°54'33.8"	86°12'17.7"

Description:

Located in the middle of the San Marcos Park. In a secondary circular area off the central Pagoda. Near the "El Rio Grande" shop and back from the kids slides. The station is a steel pin set in the concrete.

Station: *Pedro*

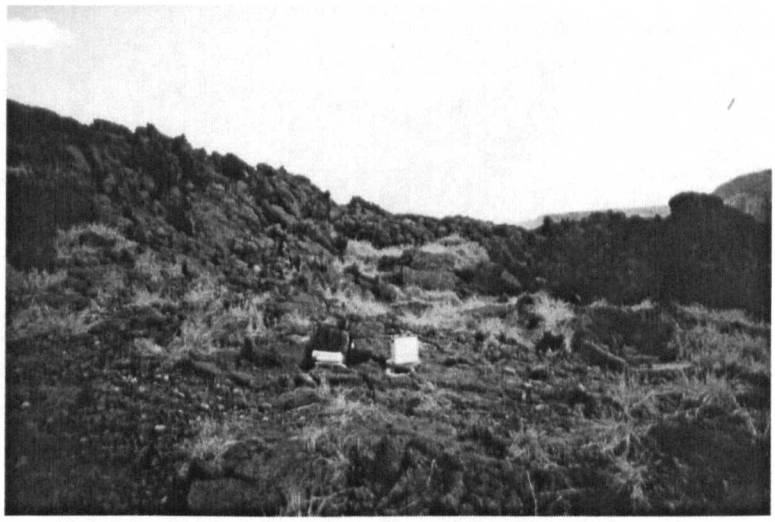

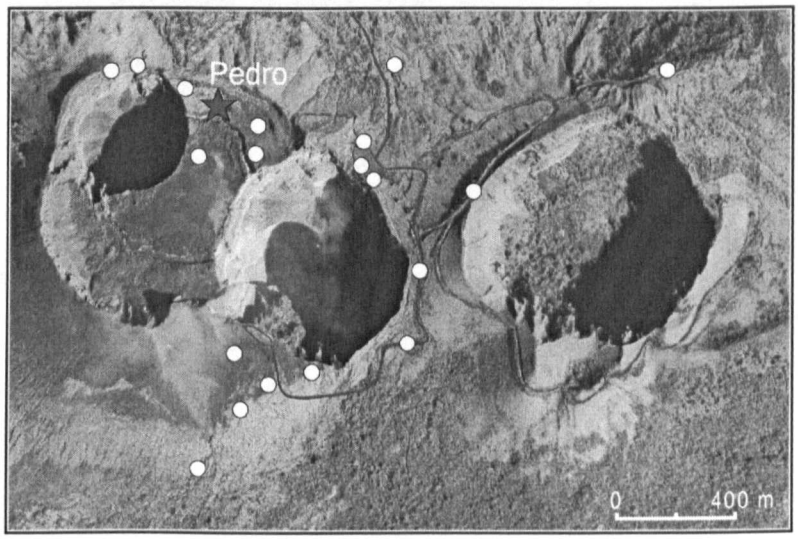

Location:

Elevation	Easting	Northing	Latitude	Longitude
517.11 m	590357.30 m	1325385.00 m	11°59'17.5"	86°10'12.1"

Description:

West, around behind the cross (on the ridge), from the 1st car park. On an old, subsided lava lake and above the subsided Nindiri crater. Approximately 16 paces from a Japanese box (or remnants of one!) overlooking San Pedro crater. Just past a butte of lava and 20 m east of the furthest Japanese box. The station is a steel pin planted in pahoehoe lava. Marked by a white circle (now yellow due to the gas!).

Station: *Pedro2*

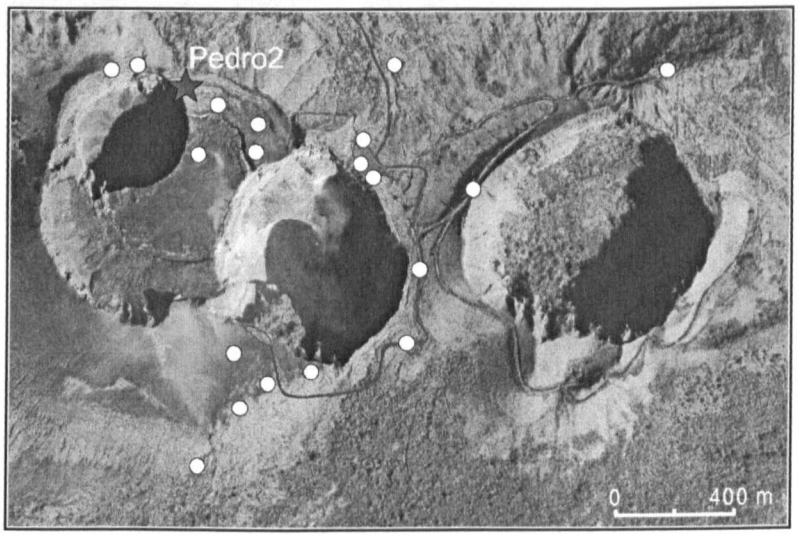

Location:

Elevation	Easting	Northing	Latitude	Longitude
520.15 m	590228.60 m	1325444.00 m	11°59'19.5"	86°10'16.3"

Description:

West, around behind the cross (on the ridge), from the 1st car park. On an old, subsided lava lake and above the subsided Nindiri crater. Directly overlooking San Pedro crater and at the furthest edge of the approximately flat area. Ends in a "wall" of lava. The station is a steel pin planted in pahoehoe lava. Marked by a white circle (now yellow due to the gas!).

Station: *Regis*

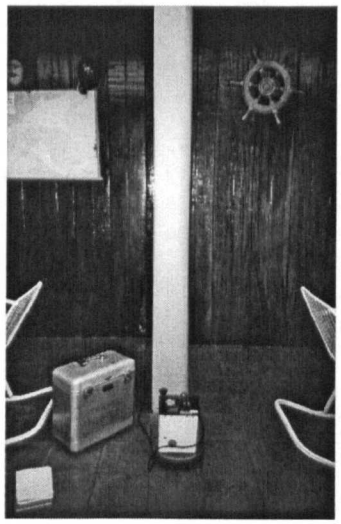

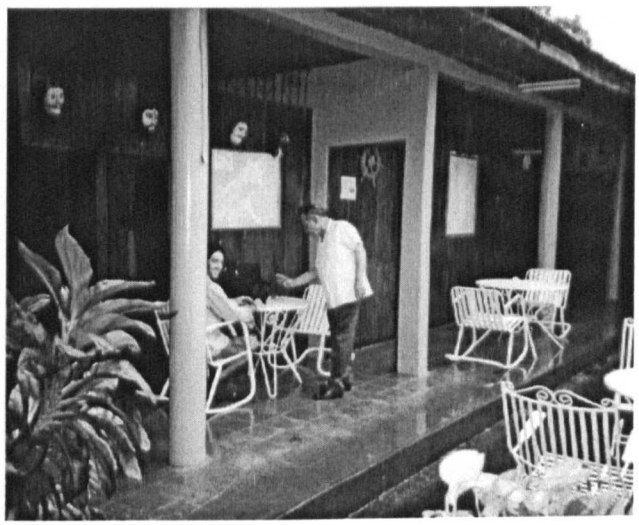

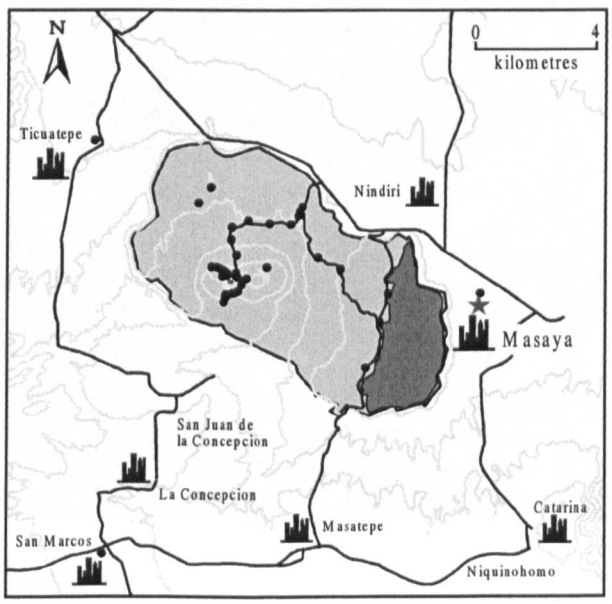

Location:

Elevation	Easting	Northing	Latitude	Longitude
285 m	598351 m	1324274 m	11°58'40.5"	86°05'47.9"

Description:

Located in the inner courtyard of the Hotel Regis in Masaya, #448-B Avenida Sergio Delgadillo. The station is on the middle tile (of 3 tiles) in front of the third column (from left to right). Map of Central America on the wall behind the column.

Station: *Sismo*

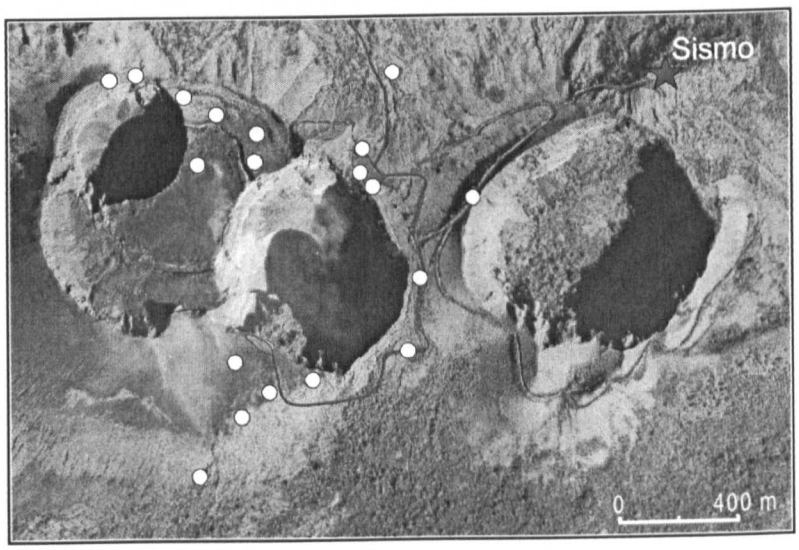

Location:

Elevation	Easting	Northing	Latitude	Longitude
589.58 m	591710.30 m	1325471.00 m	11°59'20.2"	86°09'27.3"

Description:

Located around the north side of the old Masaya cone looking out across the caldera. The station is a steel pin embedded in the middle of a slab of concrete next to the INETER seismic station.

Appendix B.

SO_2 flux measurement methodology

B.1. Introduction

Initially developed by Barringer Research (Canada) in the 1960s for pollution monitoring of N_2 and SO_2 from industrial stacks, the ultraviolet correlation spectrometer (COSPEC) was first applied to the study of volcanoes by Stoiber et al. (1983) in 1971. Since then, it has been used extensively for the study both active and passively degassing volcanoes (cf. Stoiber et al., 1983; Stoiber et al., 1986; Williams et al., 1990; Caltabiano et al., 1994; Williams-Jones et al., 2000).

The accumulation of long-term data on degassing rates of active volcanoes allows one to investigate deviations from background gas levels, which can be useful indicators of significant change in volcanic activity. The rate at which these measurements are made is greatly influenced by access to the equipment and by safety, budgetary, and time considerations. Ideally, measurements would be made all day, each day for 365 days a year. In reality this is rarely feasible, and thus one must determine the number of measurements during a day/week/month needed to characterise the degassing activity. During the recent crisis (1994-present) at Popocatépetl, Mexico, ground and airborne measurements were made on average 5-10 times a day, three days a week (H. Delgado, personal communication, 1997). At Masaya, where the plume degasses at a relatively

constant rate, 10 measurements per day, ~10-15 times per month (field time permitting) are deemed sufficient.

Volcanoes such as Galeras, Colombia, Mt. Etna, Italy, and Soufrière Hills, Montserrat, are currently measured quite frequently, at least several times a week, due to their continued activity and the availability of resources (Zapata et al., 1997; Young et al., 1998; Bruno et al., 1999), whereas volcanoes such as Masaya, are measured only sporadically (every six months since 1997). Villarica volcano, Chile, on the other hand, is measured very infrequently due to difficult access (P. Delmelle, personal communication, 1999). The type of activity also will affect decisions on the frequency of data collection. If the volcano is constantly emitting gas, fewer measurements may be necessary to characterise the plume than if the activity is intermittent. In the case of increased seismic activity and/or deformation, a large number of daily COSPEC measurements may prove useful in better understanding the state of the volcano.

Ideally, measurements should be made as close to the volcano as possible, in order to reduce dispersion and dilution of the plume. However, as one nears the volcano, the plume becomes more heterogeneous due to the initial turbulence and mixing. This increases the variability and if SO_2 concentrations are elevated, it may be necessary to increase the distance from the crater to allow for some dilution and stabilisation of the plume and a lower SO_2 concentration, albeit over a larger width. Thus it is important to choose a distance from the crater where the plume is relatively homogeneous without being so far removed that there is significant attenuation and dispersion of the gas. Masaya is an excellent case in point. During field campaigns in 1996 and 1997, low flux levels on the order or 300-600 t d^{-1} required that measurements be made proximally to the volcano (~ 5 km downwind of Santiago crater; Chapter 2). Between 1998 and 2000, however, the significantly increased flux levels (~ 1800 t d^{-1}) necessitated that measurements be made much further downwind (15-30 km) so as not to "saturate" the instrument (Figure B.1).

Segments

Llano Pacaya route

L-2: Blue water reservoir
L-1: Entering Diriamba
L0: Near village market/buses
L1: Las Esquinas
L1.5: El Brasilito sign - inter. with cobble entrance
L2: Bottom of hill before CocaCola sign
L3: Las Conchitas statue
L4: Exiting El Crucero
L4.5: Intersection
L5: Blue pole near turnoff
L6: Blue water reservoir
L7: Mini Super Mil-Cas (CocaCola)
L8: before Church San Francisco de la Comunion

Managua-Masaya route

M-3: Intersection
M-2: Bend before hill
M-1: Los Ranchitos
M1: Park entrance
M2: Esso station
M3: Intersection
M4:
M5: Intersection
M6: farmhouse on rise
M7: Intersection
M8:
M9: Entering Masatepe
M10: Entering San Marcos

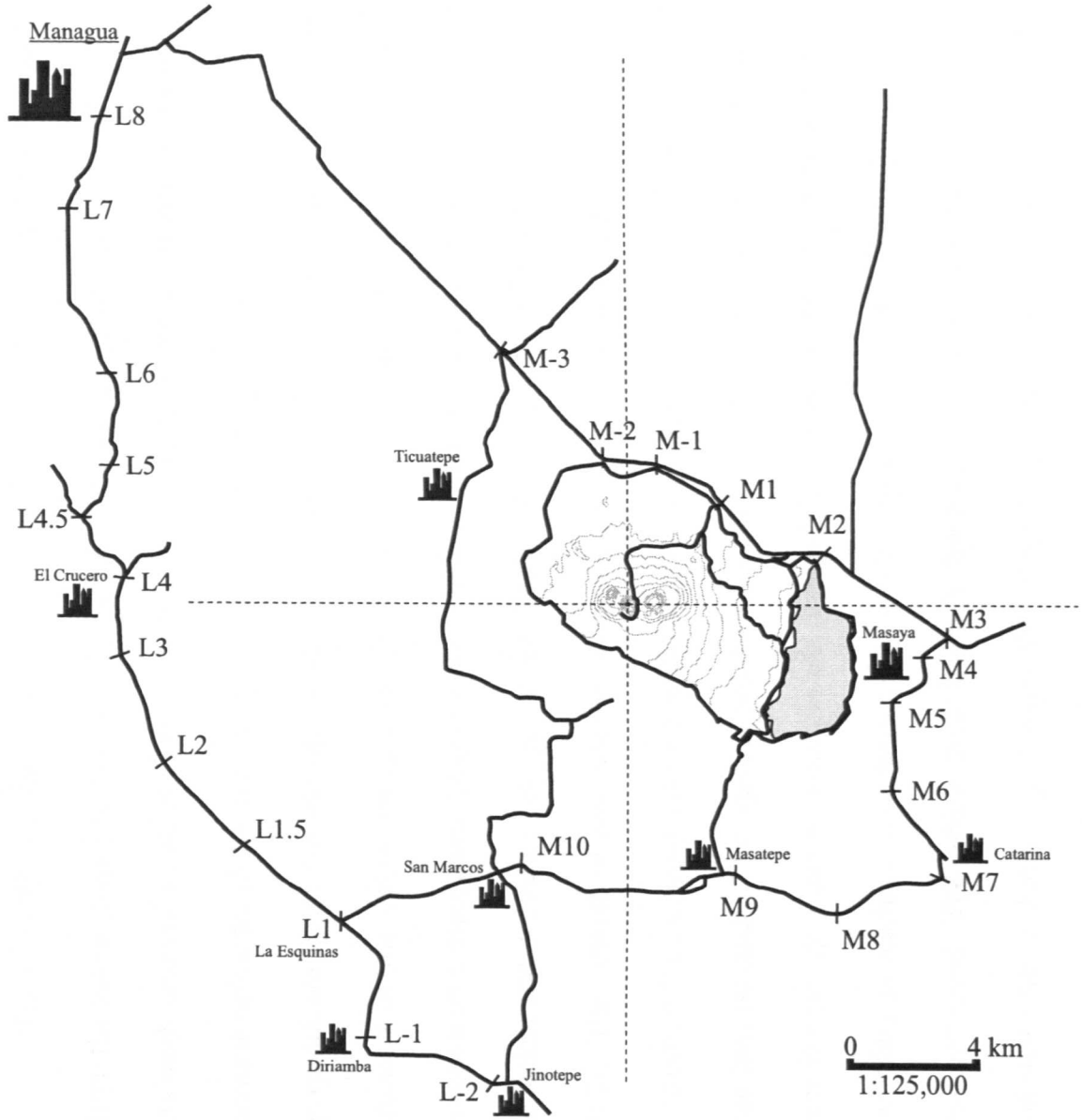

Figure B.1: Segments used for COSPEC gas flux measurements and calculations at Masaya.

B.2. Using the COSPEC

In the field, the COSPEC is connected to either a 12-volt DC car battery or other 12-volt power source. The instrument should be allowed to warm up for at least half an hour prior to use in order to stabilise. The COSPEC is also connected to a chart recorder (analogue) and/or a computer or datalogger (digital).

B.2.1. Making the measurements

The COSPEC traverses are made beneath the volcanic plume at a given distance from the active crater (see above) and as perpendicular to the plume direction as possible. As roads near volcanoes are rarely straight or perpendicular to the gas plume, an individual traverse below the plume is divided into segments in order to correct for the deviation from perpendicularity of the traverse segment with respect to the plume (Figure B.1). The azimuth of the plume (from geographic north) is determined by locating the ground position on a topographic map at which the maximum SO_2 peak on the chart record was detected, and drawing a line on the map from this point to the volcano's summit (Figure B.2). The azimuth of each segment must also be measured from a map so that a cosine correction (i.e., corrected such that the segment is perpendicular to the plume direction) can later be made. The segment positions are marked on the chart recorder with the event recorder (or by hand) or noted for the computer by recording the time when a segment boundary is reached. The instrument is driven below the column at an approximately constant speed. The vehicle speed is highly dependent upon the width of the plume. On a volcano such as Popocatépetl where the plume is typically very wide (20-50 km), the vehicle is driven at ~60-70 km hr^{-1}, whereas on volcanoes such as Arenal, Costa Rica, with narrow plumes (2-3 km), 10-20 km hr^{-1} is the typical vehicle speed. The quality of the roads where the measurements are made also will affect the optimum vehicle speed; one can drive much faster on a fully tarred road than on a gravel road full of potholes. Masaya

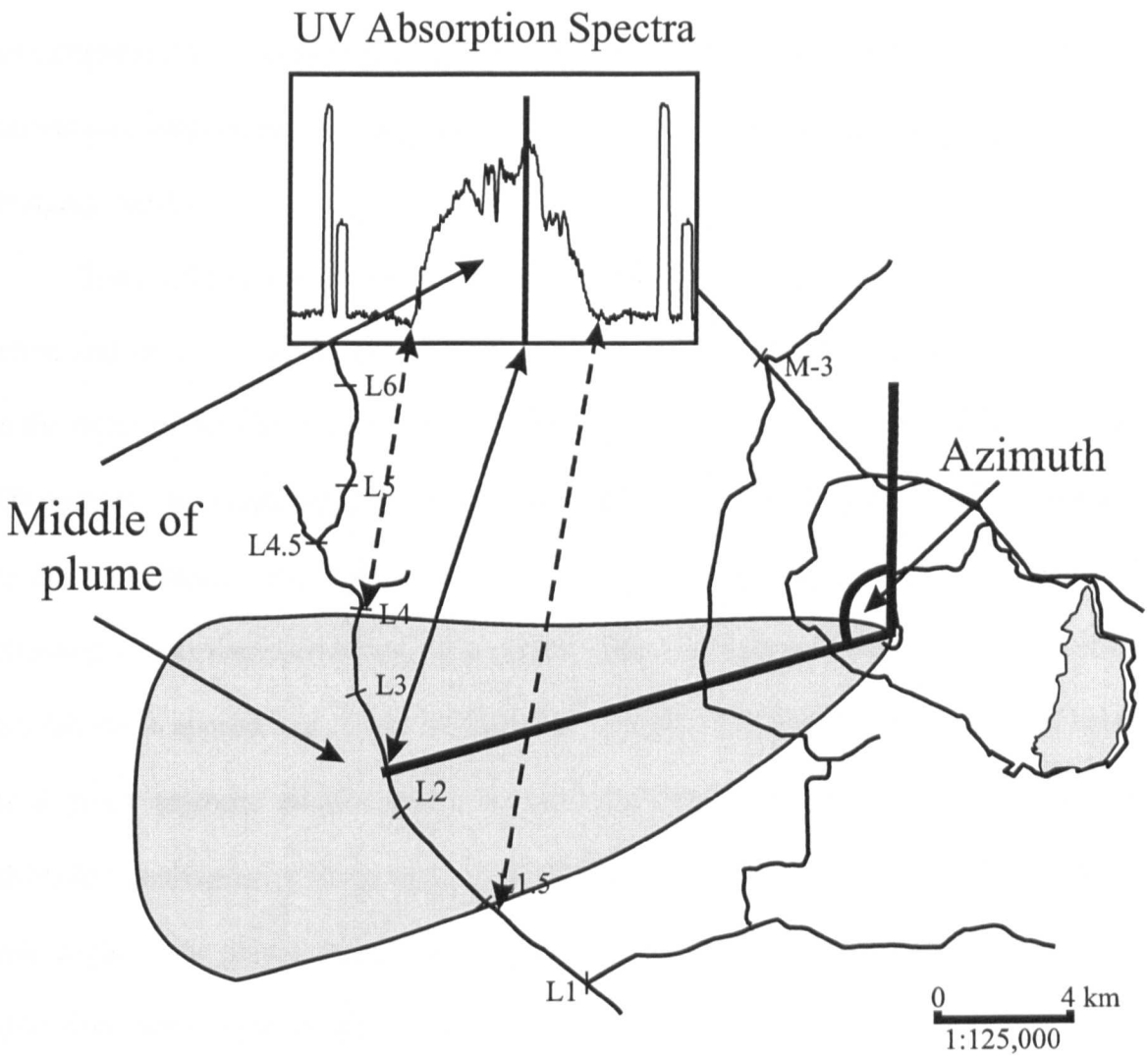

Figure B.2: An example of the method used to determine the plume azimuth taken from the maximum peak of the chart record (inset). Note that the inset UV absorption spectra also shows the calibration peaks made before and after any measurement.

has a very good road network as well as a fairly restricted plume (during the dry season) allowing for rapid measurements. The time constant of the COSPEC should be set to either 1 or 2 in order to reduce the effect of overhanging trees (see below). Gas-cell calibrations are made before and after each traverse in order to calculate the plume concentrations later. Both gas cells should be used. It is also wise to perform quick calibrations while in the gas column if conditions (e.g., ultraviolet light level, ash, etc.) are changing rapidly.

The COSPEC comes equipped with two SO_2 gas cells that are used for calibration before and after field measurements are made. The low concentration gas cell is typically on the order of 50-150 ppm-m while the high concentration gas cell varies between 300-500 ppm-m. Although only one of the calibration cells (low or high) is actually required for the flux calculations, both calibration cells should nevertheless be used prior to and following measurements through a gas plume. This allows one to determine which of the calibrations is appropriate for the calculations. Ideally, the maximum plume peak height for a given segment should always be less than the high calibration, with the high calibration consequently being used in the flux calculations. However, if the maximum peak height of the plume segment is less than that of the low calibration cell, then the low calibration should be used in calculations. If the plume concentrations substantially exceed the high concentration cell, measurements should be made farther from the volcano where the plume is more dispersed and dilute. Alternatively, a high concentration correlator assembly may be installed, allowing for the measurement of concentrations ranging from ~1000-10 000 ppm-m. However, changing a correlator assembly is difficult for the user to perform in the field (Figure B.3).

In the field, it is advisable to make a note of the typical segment heights and the peak height ratio of the two calibration peaks as they appear on the chart recorder paper for

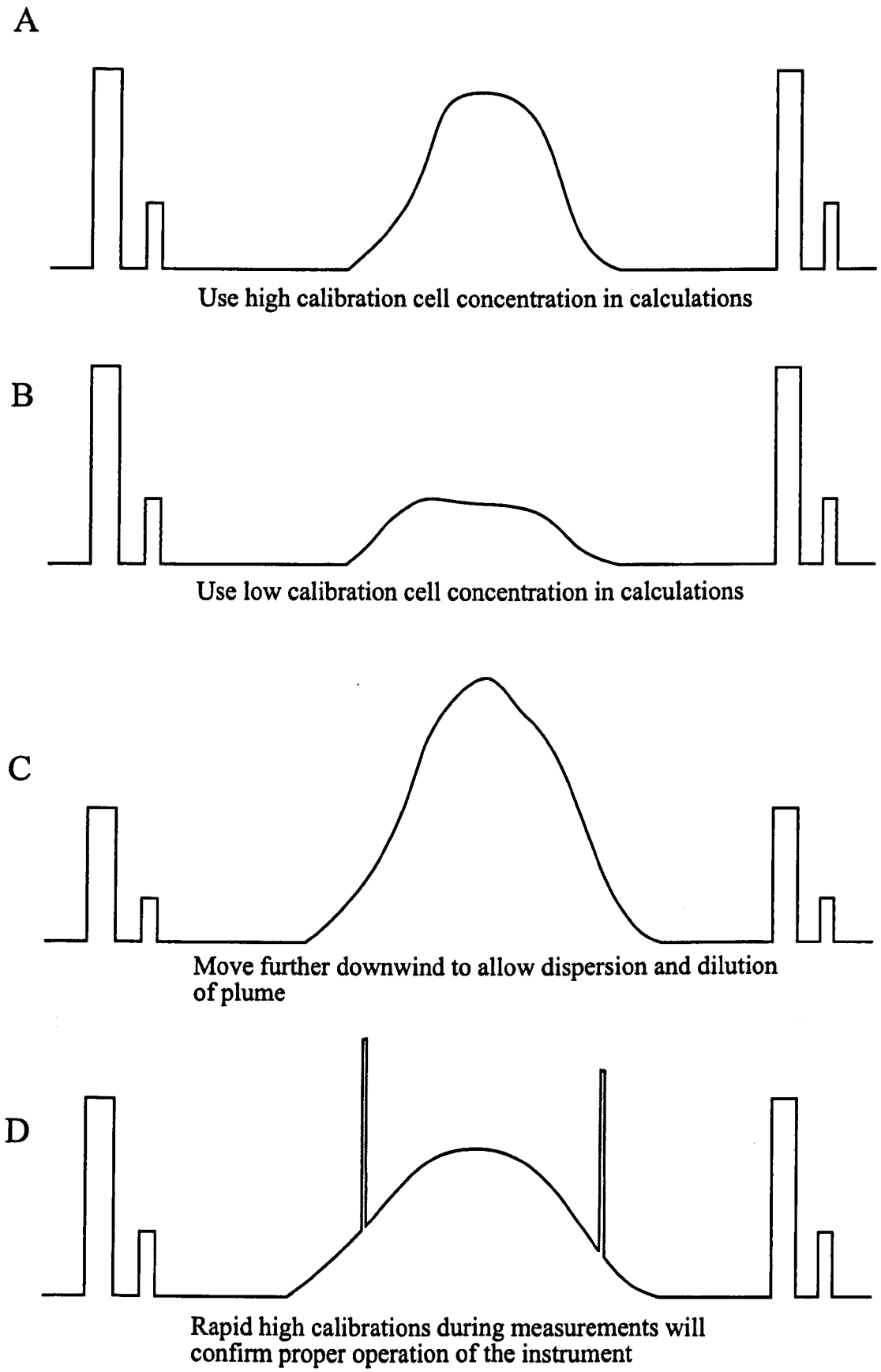

Figure B.3: a) the plume signal is of similar height to the high calibration; b) the plume signal is of similar height to the low calibration; c) the plume signal is significantly higher than the high calibration; d) rapid calibrations during the measurement will verify proper function of the COSPEC.

a given voltage (e.g., 0.5 V). If the ratio of the calibration peaks is different from that normally observed, this may indicate problems with the COSPEC.

In the case of ground-based mobile COSPEC measurements, the instrument is mounted in a vehicle (car, jeep, or van). In some cases where roads were unavailable, the COSPEC has been mounted on horseback or even onto a backpack frame (Stoiber et al., 1983). A minivan is an ideal vehicle as it allows for the easy installation of equipment through sliding side doors. The instrument is normally placed in the passenger seat on a box or crate (plastic Coke or beer crates work well and are easy to find in the field) and is secured to both the crate and seat with elastic cords or webbing (Figure B.4).

To minimise vibration of the instrument, foam padding should be placed between the COSPEC and the straps and the boxes. This brings the COSPEC to the level of the window and allows the right angle mirror of the Cassegrain telescope to protrude from the side window. The extension tube is attached to the right angle mirror so that the instrument is effectively "looking" vertically. There must be sufficient clearance between the doorframe and the Cassegrain telescope so that the telescope is never in danger of hitting the frame of the vehicle. Foam padding should be attached around the tube as a precaution. The right angle mirror should be oriented such that the extension tube is vertical (i.e., the COSPEC may be angled into the seat) to ensure that the field of view is as close to vertical as possible. A 12-volt battery or the vehicle's battery acts as the power supply for the COSPEC. The battery is connected by a power cable with alligator clips on one end, supplied with the instrument. The clips should be secured with duct tape ("gaffer tape") or electrical tape on the battery to prevent accidental slippage that can result in electrical short-circuits. The COSPEC is connected to a chart recorder, portable computer, and/or datalogger for data collection.

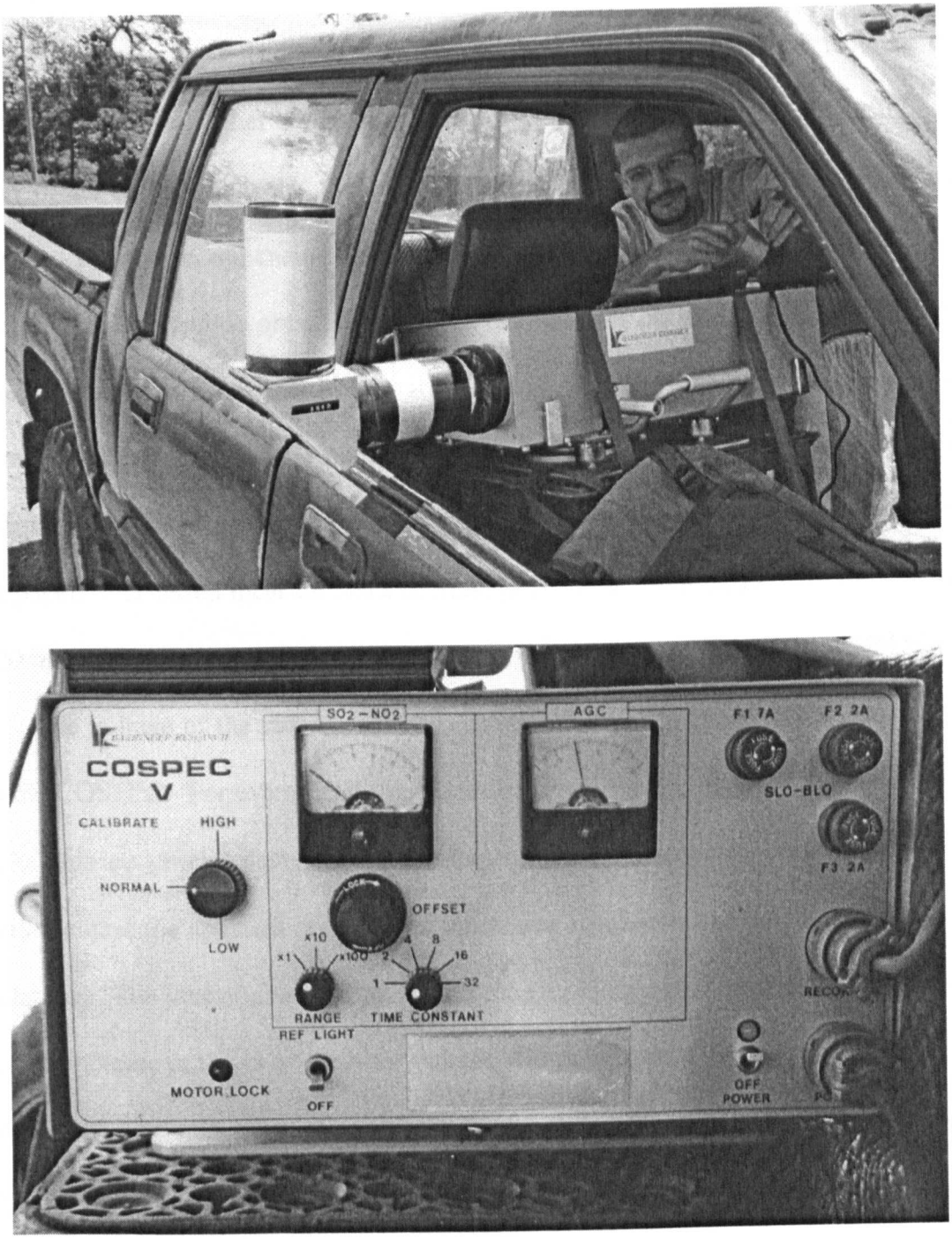

Figure B.4: Example of a COSPEC V installed in an INETER truck. Note that the telescope is vertical with respect to the roof of the truck.

B.3. Recording the Data

Data from the COSPEC is in analogue form, and thus a chart recorder is the usual form of data collection. The chart recorder is connected to the COSPEC recorder outlet and may be powered either by internal batteries or a 12-volt power source such as a car battery or gel-cell battery pack. Some recorders come with internal gel-cell rechargeable batteries. Prior to commencing measurements, the chart recorder should be set to an appropriate chart speed to obtain the required resolution is obtained. For example, over a medium duration measurement on the ground (e.g., 30 min.), the chart may be set to 20 mm min^{-1}, while for longer measurements (e.g., 1-2 hrs), the speed may be set to 160 or 180 mm/hr (2.7-3.0 mm min^{-1}) in order to maintain reasonable resolution, while preserving chart paper. Car-based measurements at Masaya between 1998-2000, with traverse times of ~20 minutes, had chart speeds of 20-30 mm min^{-1}.

The voltage of the recorder can be changed in order to enhance the signal coming from the COSPEC. For example, if the concentration in the plume is low and the resulting peak heights are small, a decrease in the voltage of the chart recorder (e.g., from 1 V to 0.5 V) will increase the apparent peak height, increasing resolution and facilitating subsequent calculations. The inverse is also true; should the incoming signal be too high for the chart paper, an increase in the chart recorder voltage will decrease the apparent peak height. As a rough guideline, one wants to maximise the height of the high calibration peak on the chart paper, assuming that the maximum peak height of the plume will be smaller.

When passing under obstacles or trees, the pens of the chart recorder can be lifted off the paper in order to reduce the interference (Figure B.5). Once the pen has returned to the previous level, it may be placed back on the paper. Should stretches of road have significant amounts of tree coverage, it is advisable to stop briefly in clear areas every so often in order to get at least some measurements for that section of the traverse. One also

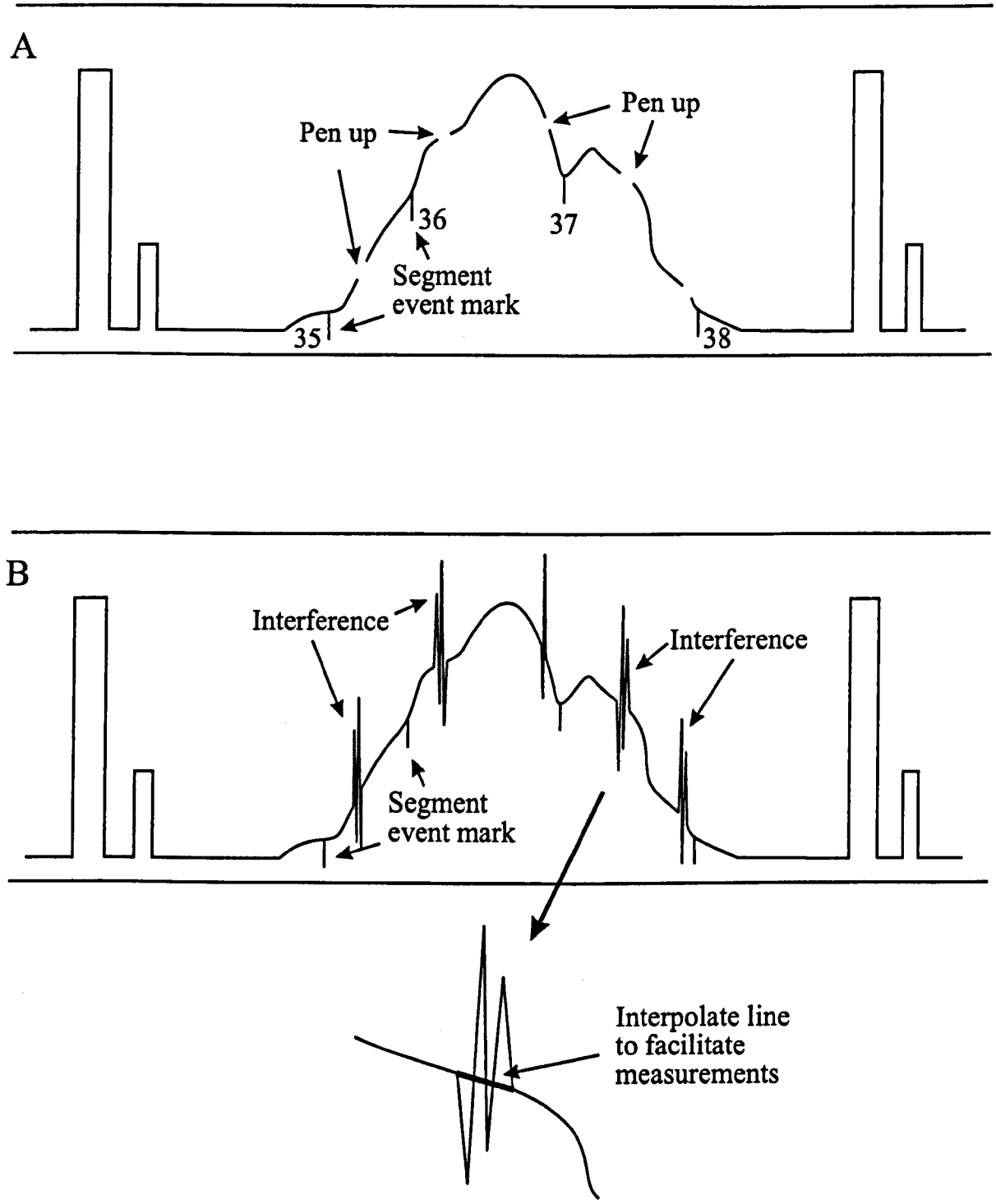

Figure B.5: a) an example of a signal when the pen is lifted up and then lowered to avoid interference. b) an example of a typical chart record showing interference from trees or radio frequencies. A line can also be drawn through the "noise" to facilitate subsequent planimeter measurements.

may leave the pen recording continuously, despite the interference, and attempt a best fit to the curve in order to aid in calculations. In this case, a time constant of 1 on the COSPEC is essential so that the recording pen will quickly return to its correct position once the trees have been passed.

B.3.1. Electrical fields

Electrical fields such as those generated by ground-based radio antennae (e.g., at Masaya on the Llano Pacaya ridge in El Crucero) and pilot transmission/communication (during airborne measurements) may affect COSPEC measurements by causing spikes or noise on the chart record. These are often difficult to avoid and must be eliminated from the chart record or digital record before doing the flux calculations. With a digital record (computer or datalogger), the spikes may be removed using commercial spreadsheet software. In the case of analogue chart recorders, these points may be ignored by simply plotting a line through the interference pattern (Figure B.5).

B.4. Reducing the Data

A traverse below the gas plume is divided into segments in order to correct for the deviation from perpendicularity of the traverse with respect to the column (Figure B.1, B.2). The SO_2 flux for each segment is calculated and summed to determine the total SO_2 flux for a given traverse. The SO_2 flux in metric tonnes per day (F) is calculated using the following equation:

$$F = \cos\theta \cdot d \cdot v \cdot 0.00023 \cdot [SO_2] \qquad (B.1)$$

where θ (°) is the deviation from perpendicularity of the segment of road with respect to the gas column; d is the width (m) of a particular segment determined from a topographic map; v is the average windspeed (m s^{-1}) at approximately column height; 0.00023 is a conversion factor from ppm-m^3 s^{-1} to metric tonnes per day (t d^{-1}); and $[SO_2]$ is the path-

length concentration of SO_2 (ppm-m) in the column. One ppm-m of SO_2 is one cubic centimetre of SO_2 gas uniformly mixed in one million cubic centimetres of air and viewed by the COSPEC over an optical path of one metre at a pressure of 101.325 kPa and a temperature of 20°C. Thus, the conversion factor (C_F) is derived as follows:

$$C_F = \rho_{SO2} \cdot Cf_{STP} \cdot 10^{-9} \cdot 86400 \qquad \text{(B.2)}$$

where ρ_{SO2} is the density of SO_2 gas at standard temperature and pressure STP (2.8579691 $kg \cdot m^{-3}$ at 0°C and 101.325 kPa), Cf_{STP} is a correction factor (273.15/293.15 = 0.9317755) to change the SO_2 gas density from 0°C to 20°C, 10^{-9} is the conversion from ppm to metric tonnes, and 86 400 is the number of seconds in one day. Thus, C_F is equal to 0.00023008194, with units of $t \cdot s \cdot m^{-3} \cdot d^{-1} \cdot ppm^{-1}$.

The concentration of SO_2 in the plume was calculated from:

$$[SO_2] = \left(\frac{P_{seg}}{P_{cal}} \right) \cdot C_{cal} \qquad \text{(B.3)}$$

where P_{cal} is the peak height of the calibration gas cell in arbitrary units; P_{seg} is the average peak height for the segment; and C_{cal} is the concentration of the calibration gas cell in ppm-m. As discussed above, the high calibration cell is normally used.

B.4.1. Chart recorder

The chart record first should be broken into segments (if necessary) so that individual calculations and corrections can be made. One then determines the baseline or background signal, which should be an approximately horizontal line, above which is the plume signal. This position is then set to zero and the data of the plume signal assigned values relative to this baseline. This average value thus represents the average concentration of the plume for that segment in arbitrary units (e.g., mm). The same is done with respect to the calibration peaks. The average segment height is then related to the calibration peak height so that the plume-segment concentration in ppm-m may be

determined. Normally one would choose the calibration peaks closest to the plume on the chart record for calculating the concentration of SO_2 of the segment. If the plume is relatively thin and both calibration peaks are close to the plume, the average of the two calibration peak heights can be used in the calculations if they are similar. If there is a significant difference in calibration peak heights, the calibration closest to the plume should be used (Figure B.6).

The chart data are analysed using a mechanical or digital planimeter to measure the area beneath the segment of the plume (Figure B.7). The "bull's-eye" or pointer of the planimeter is placed on the chart record and zeroed. Moving in a clockwise direction, one then uses the "bull's-eye" to trace the SO_2 curve for the segment in question. One must start and end at the same segment point, i.e., follow the curve to the end of the segment and return along the baseline to the starting position. One then reads the area (in mm^2 or cm^2) and divides this value by the width of the chart segment (in mm or cm) to obtain the average peak height for the segment. Typically, two to three planimeter measurements are made for each segment to check precision and accuracy. The average then is compared to the height (in mm or cm) of the calibration peak(s) to obtain the concentration of SO_2 for the segment.

B.4.2. Error calculations

Variations in measured SO_2 fluxes may be due, in part, to fluctuations in windspeed and direction, changes in cloud cover, and change in sun angle, resulting in variable amounts of solar ultraviolet radiation. The opacity of an eruptive plume also varies due to changes in ash content that will increase the absorption of ultraviolet radiation. Instrumental uncertainties include instrument calibration (± 2%), digital/analogue chart reading error (± 2%), varying vehicle/aircraft speed (± 5%), and windspeed measurement (± 0-60%) (Casadevall et al., 1981; Stoiber et al., 1983).

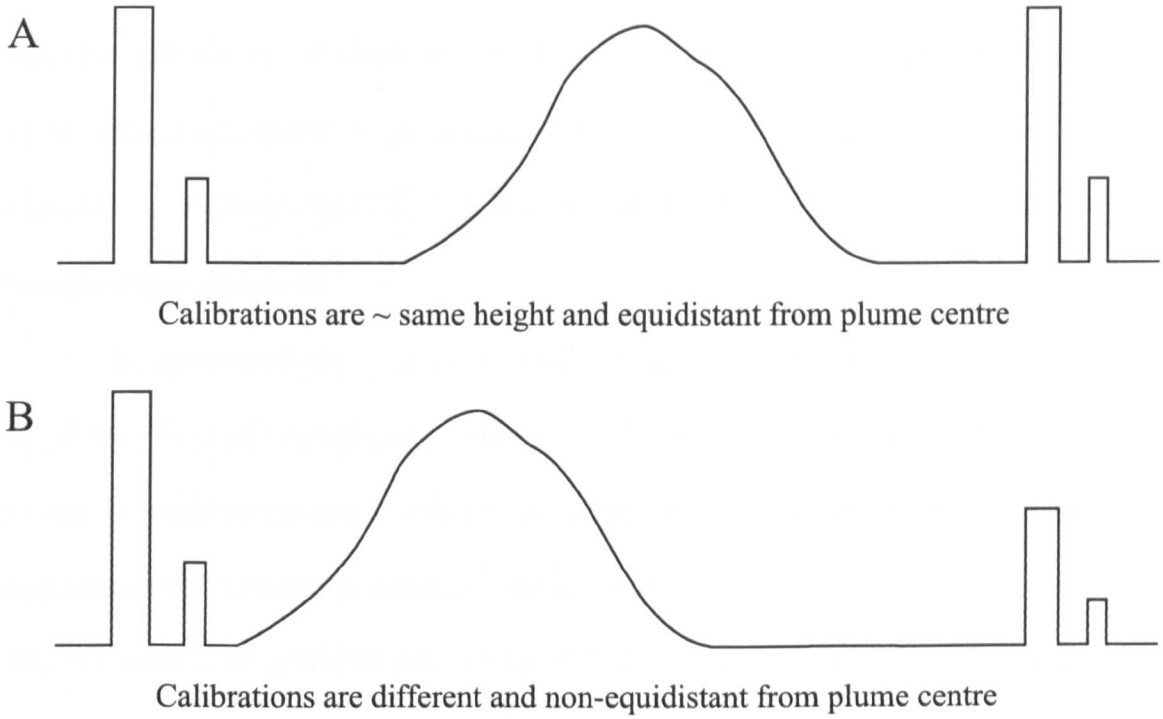

Figure B.6: a) When the calibrations are of similar height and equidistant from the centre, the average of the two heights should be used. b) When the calibrations are of different height and non-equidistant, the calibration closest to the plume centre should be used.

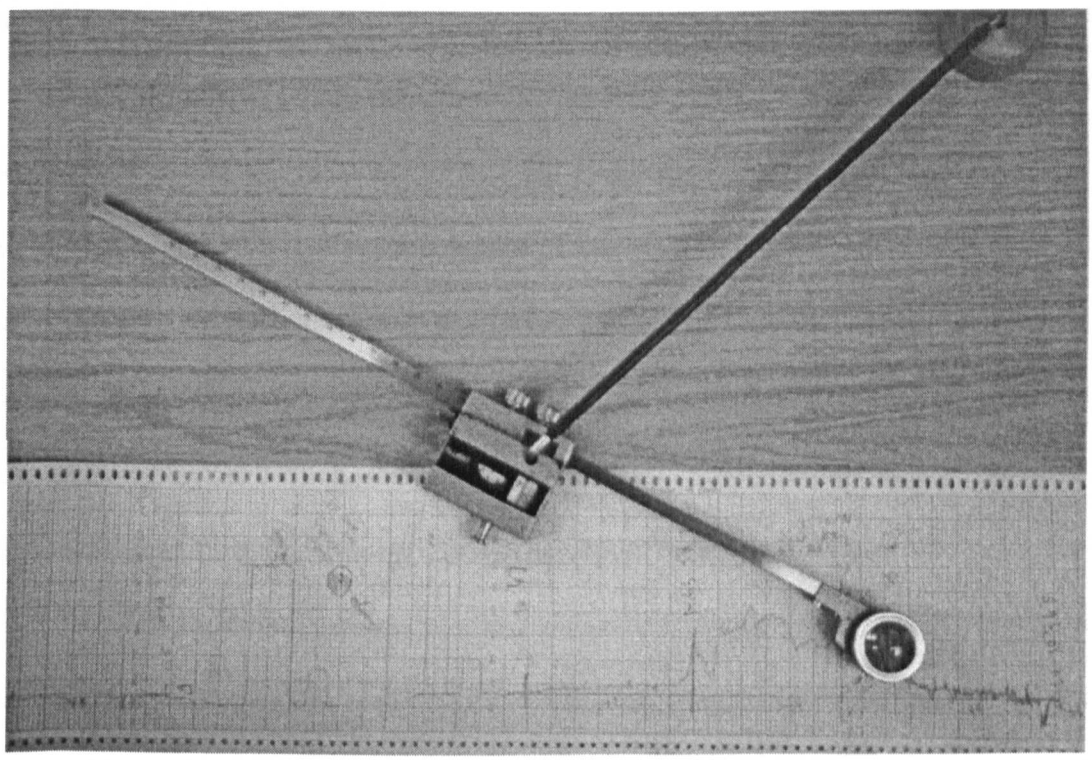

Figure B.7: A mechanical planimeter used to calculated the area beneath the plume signal, from which the average segment height can then be determined.

Uncertainties in plume azimuth have a comparatively minor impact on the final SO_2 flux calculation. A difference of one degree, for example, gives a deviation of only 0.3%, while a difference of ten degrees results in deviation of 4.6%. Even in an extreme case with a difference of twenty degrees between actual and measured plume direction, there is only a 12% error.

As mentioned above, a large long-term data set can provide useful information about the "normal" background degassing behaviour of the volcano. Thus, a potential source of uncertainty arises when one merges these data sets, which may have been acquired using different instruments and/or techniques. This is the case for the Masaya data set, where the pre-1996 data where collected by Stoiber et al. (1986) using a mix of stationary and mobile COSPEC techniques; all measurements from 1996 onwards have been made by myself and colleagues. Furthermore, the actual instruments used over the years have varied and unfortunately, there is very little cross calibration between instruments.

Many of these uncertainties could be overcome if there was a concerted international effort to calibrate COSPECs by simultaneously measurement of SO_2 flux from a known source (e.g., coal-fired power plant). While this was attempted at an NSF-funded workshop in Arizona, USA, none of the data was ever published. Ideally, there would also be detailed verification of the concentrations of the SO_2 calibration cells used by the COSPECs. However, this is now also problematic as Barringer Canada, the manufacturer of COSPECs, no longer builds or supports the instruments.

Nevertheless, these data sets can still prove to be extremely useful if one is aware of the limitations and uses the data properly. In other words, one should not look for very small fluctuations in gas flux, but rather large changes (on the order of magnitude) such as those seen at Masaya between 1997 and 1998.

B.5. Meteorological Conditions

B.5.1. Wind

SO_2 flux calculations are dependent upon knowledge of the plume direction and speed (i.e., velocity); however, direct measurement of these components is exceedingly difficult. We therefore measure windspeed and wind direction, which we assume to represent the plume velocity. Ideally, this information is obtained from instruments in the downwind plume of the volcano (e.g., using a radiosonde). In reality, this is often unfeasible, and thus other methods are required. Should the volcano be near an airport or large city, one can obtain the windspeed and wind direction by contacting the local meteorological stations, or, as is the case at Popocatépetl volcano, Mexico, getting the data directly from overflying aircraft. Windspeed measurements also may be made using a handheld or automated anemometer. At volcanoes where the plume is close to the ground such as Masaya, this technique is extremely useful. Some electronic anemometers will automatically average windspeeds (e.g., Kestral 1000 pocket anemometer) for a given interval, reducing the uncertainty due to wind gusts. Over a day of COSPEC measurements, at least three sets of windspeed measurements should be made at the beginning, middle, and end of the day, in order to characterise the fluctuations in windspeed. A more detailed study of windspeed variation can be made using a continuously recording automated anemometer. In March 1998, February 1999 and March-April 2000, continuous windspeed measurements were made downwind at an Instituto Nicaragüense de Estudio Territoriales (INETER) seismic station in El Crucero (Figure B.8). Located on the Llano Pacaya ridge (930 m a.s.l.), the station is at least 300 m above the active vent with the result that windspeed measurements are essentially made almost at the column height.

Care should be taken when deciding upon the placement of ground-based windspeed instruments. According to the World Meteorological Organisation (WMO),

"The standard exposure of wind instruments over level, open terrain is 33 feet (10 metres) above the ground" (WMO, 1971). If there are obstacles present, the anemometer should be located at a distance from the obstacle that is at least ten times the height of the obstacle (Figure B.9). If the instrument must be near a tall building, it should be placed upwind at a distance from the building equal to the building's height, to avoid turbulence caused by the building. This turbulence will clearly result in an inaccurate measure of the actual plume speed and therefore affect flux measurements. However, if one were to strictly apply this rule to volcanoes, the wind station would have to be quite far from the volcano to avoid the effects of turbulence; for example, one should be five to ten kilometres away from a 1000 m high volcano. Towers such as those used for TV, radio and cellular transmissions are ideal for siting an anemometer. In practice, however, the installation of such stations in proximity to volcanoes is not always possible, leaving handheld/automated anemometers or overflying aircraft as the most likely sources of windspeed data.

The direction of the wind and therefore the gas plume is also important for the calculation of SO_2 flux. The wind direction can be obtained from meteorological stations or overflying aircraft. However, the most accurate and reliable method entails determining the direction from the chart record. As discussed above, the plume azimuth is required to correct for the lack of perpendicularity of the traverse segments with respect to the plume direction. During the dry season (December to April), there is a relatively steady easterly trade wind that blows across Masaya caldera. In the rainy season, winds tend to be more variable in direction and speed but generally blow eastwards over the city of Masaya.

B.5.2. Humidity

Humidity in the atmosphere above the COSPEC also may have an effect on the SO_2 signal. Condensed water vapour in the plume may increase the path of ultraviolet rays in the plume, resulting in a scattering effect that will overestimate the observed SO_2 burden

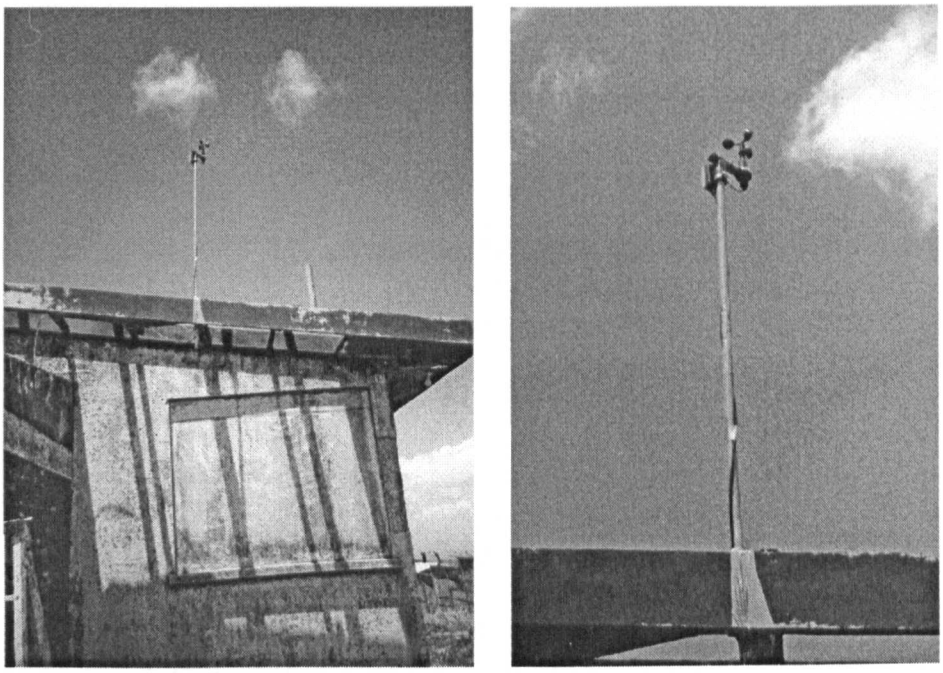

Figure B.8: Example of a continuously recording anemometer installed downwind of Masaya at the INETER seismic station in El Crucero, Nicaragua.

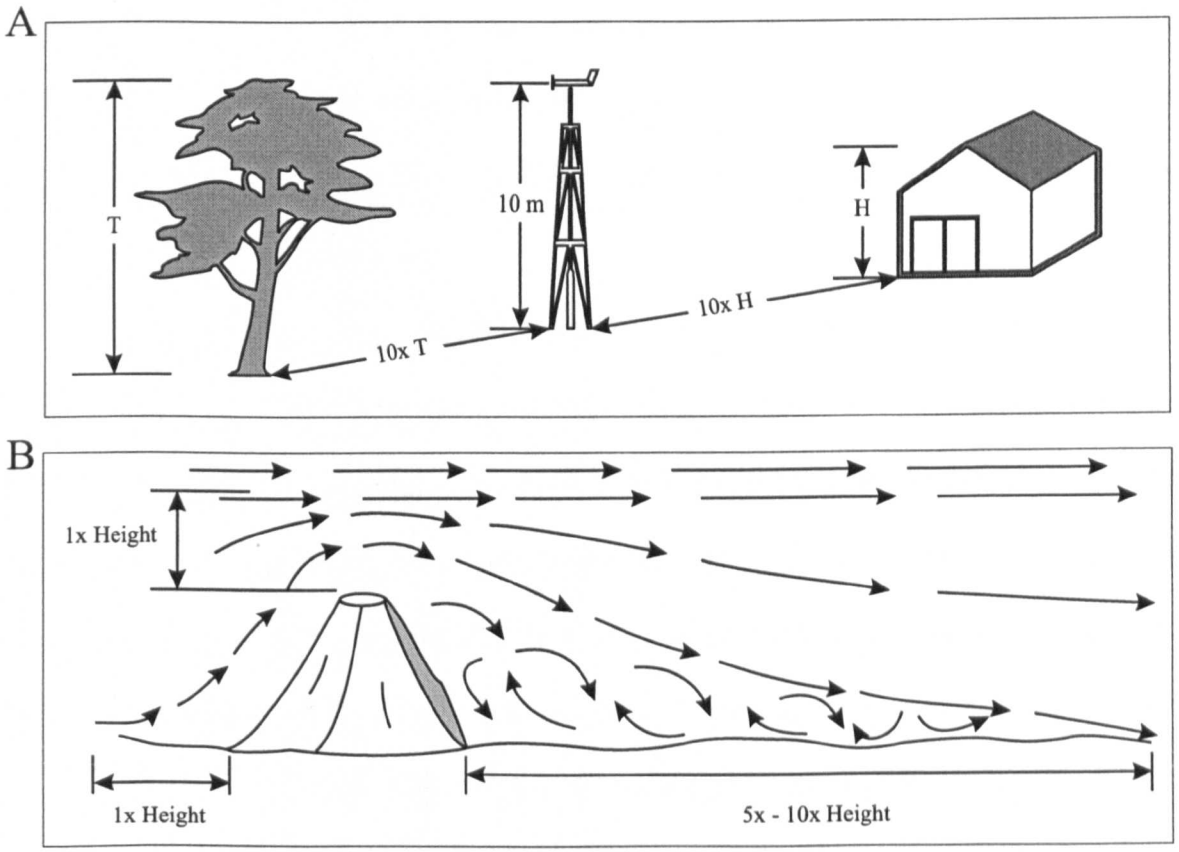

Figure B.9: a) Standard positioning for wind instrumentation recommended by the World Meteorological Organisation; b) Suggested siting of anemometer near ground level.

by as much as 10%. By contrast, clouds situated between the plume and the ground may act to block SO_2 absorption by absorbing part of the ultraviolet radiation before it reaches the COSPEC (Millán, 1980; Stoiber et al., 1983). As mentioned in Chapter 2, the significantly underestimated flux measurements during the wet season in September 1998 are likely, at least in part, to be the result of this absorption.

B.5.3. Background sky dynamics

Since the COSPEC is an ultraviolet spectrometer, it is affected by the amount of ultraviolet radiation entering the instrument. The ultraviolet radiation that reaches the instrument originates from the sun but is composed of two main components when it reaches the ground. One component has a direct path from the sun while the other is more diffuse, originating from the scattering of solar radiation by the atmosphere. This scattered component arises mainly in the upper troposphere in the primary scattered radiation, which itself originates from just below the ozone layer (Millán, 1985). This is important, as ozone will absorb a portion of the ultraviolet radiation, thus reducing the observed burden on SO_2 measured at ground level.

In the early morning and late afternoon, the lower sun angle results in reduced levels of ultraviolet radiation entering the telescope. This leads to higher background noise and reduced precision. Measurements should therefore be made during periods of high sun angle so that sufficient ultraviolet radiation enters the instrument. In general, measurements are made between 09:00 and 16:00 hrs local time in order to minimise this effect. However, during solar noon, i.e., when the sun is directly overhead, excessive amounts of ultraviolet radiation entering the COSPEC may cause spikes in the signal. This problem is reduced in the COSPEC V by baffles in the spectrometer and the Cassegrain telescope, which buffer some of the ultraviolet radiation entering the instrument. Earlier versions for the COSPEC have baffles only in the telescope and are thus more vulnerable

to the ultraviolet radiation of solar noon (R. Dick, Barringer Research, personal communication, 1997). Nevertheless, it is advisable to stop measurements and turn off the COSPEC for approximately half an hour while the sun passes its apex.

B.5.4. Plume dynamics

Plumes are rarely completely compositionally homogenous in width and length, although they can be more homogeneous with distance downwind. Nevertheless, heterogeneities in SO_2 concentrations in the plume may affect the observed burden. However, if mobile measurements are being made directly below the plume, the ultraviolet radiation will pass through the entire plume thickness and be absorbed by SO_2, minimising scattering effects and allowing for complete measurement of SO_2 in the vertical axis. Only at the thin edges of the plume will there be an increased scattering effect. Spatial heterogeneities in the plume then can be integrated into the measurement by completely transecting the plume during a traverse.

The opacity of the plume also may have an effect on the accuracy of the COSPEC measurements. If the plume is heavily laden with ash, ultraviolet radiation is partially blocked by the ash rather than being absorbed by the SO_2, reducing the measured SO_2 by raising the effective background levels. Aerosols between the plume and the ground also will scatter ultraviolet radiation, further reducing the measured SO_2 (Millán, 1980). However, laboratory experiments by Andres and Schmid (1997) indicate that the COSPEC reliably measures SO_2 burdens within a 10% accuracy for plumes that are up to 50% opaque. However at Masaya, the fact that the plume is essentially ash-free makes this effect negligible.

B.6. References

Andres, R. J. and Schmid, J. W., 1997. The effects of volcanic ash on COSPEC measurements (Abstract). Puerto Vallarta, Mexico, 27.

Bruno, N., Caltabiano, T. and Romano, R., 1999. SO_2 emissions at Mt. Etna with particular reference to the period 1993-1995. Bull. Volcanol., 60, 405-411.

Caltabiano, T., Romano, R. and Budetta, G., 1994. SO_2 flux measurements at Mount Etna (Sicily) . J. Geophys. Res., 99, 12809-12819.

Casadevall, T. J., Johnson, D. A., Harris, D. M., Rose, W. I., Malinconico, L. L., Stoiber, R. E., Bornhorst, T. J., Williams, S. N., Woodruff, L., and Thompson, J. M. 1981. SO_2 emission rates at Mount St. Helens from March 29 through December, 1980. In: Lipman, P. W. and Mullineaux, D. R. (Editors), The 1980 Eruptions of Mount St. Helens. 1250: 193-200

Millán, M. M., 1980. Remote sensing of air pollutants. A study of some atmospheric scattering effects. Atmos. Environ., 14, 1241-1253.

Millán, M. M., 1985. COSPEC observation of Mt. St. Helens volcanic SO_2 eruption cloud of 18 May 1980 over southern Ontario. Atmos. Environ., 19, 255-263.

Stoiber, R. E., Malinconico, L. L. and Williams, S. N., 1983. Use of the correlation spectrometer at volcanoes. In: H. Tazieff and J. C. Sabroux (Editors), Forecasting Volcanic Events, Elsevier, New York, pp. 424-444.

Stoiber, R. E., Williams, S. N. and Huebert, B. J., 1986. Sulfur and halogen gases at Masaya caldera complex, Nicaragua: Total flux and variations with time. J. Geophys. Res., 91, 12215-12231.

Williams-Jones, G., Stix, J., Heiligmann, M., Barquero, J., Fernandez, E. and Duarte-Gonzalez, E., 2000. A model of degassing and seismicity at Arenal volcano, Costa Rica. J. Volcanol. Geotherm. Res., In Press.

Williams, S. N., Sturchio, N. C., Calvache V., M. L., Mendez F., R., Londono C., A. and

Garcia P., N., 1990. Sulfur dioxide from Nevado del Ruiz Volcano, Colombia: Total flux and isotopic constraints on its origin. J. Volcanol. Geotherm. Res., 42, 53-68.

Young, S. R., Francis, P. W., Barclay, J., Casadevall, T. J., Gardner, C. A., Daroux, B., Davies, M. A., Delmelle, P., Norton, G. E., Maciejewski, A. J. H., Oppenheimer, C. M., Stix, J. and Watson, I. M., 1998. Monitoring SO_2 emission at the Soufrière Hills volcano: Implications for changes in eruptive conditions. Geophys. Res. Lett., 25, 3681-3684.

Zapata, J. A., Calvache V., M. L., Cortés J., G. P., Fischer, T. P., Garzon V., G., Gómez M., D., Narváez M., L., Ordoñez V., M., Ortega E., A., Stix, J., Torres C., R., and Williams, S. N. 1997. SO_2 fluxes from Galeras Volcano, Colombia, 1989-1995: Progressive degassing and conduit obstruction of a Decade Volcano. J. Volcanol. Geotherm. Res., 77, 195-208

Appendix C.

Thermal flux calculations

C.1. Thermal flux Equations

These equations are used for a first order estimate of thermal flux and cooling rate of a given volume of magma. All equations are from Harris et al., 1999 and developed from cited references (cf. Pieri et al., 1990; Oppenheimer, 1991; Holman, 1992; Salisbury and D'Aria, 1992; Harris and Stevenson, 1997).

Relevant parameters are found in Table C.1.

The thermal flux by **radiation** (Q_{rad} / W):

$$Q_{rad} = \sigma \varepsilon A_{lake} T_e^4 \qquad (1)$$

where σ is the Stefan-Boltzman constant, ε is emissivity and A_{lake} is the surface area of the lava lake (or glowing vent). The effective temperature, $T_e = (f_{crust} T_{crust}^4 + f_{cracks} T_{cracks}^4)^{0.25}$ with f_{crust} and f_{cracks} representing the fraction of lava lake surface area covered by crust and exposed molten material, respectively. Similarly, T_{crust} and T_{cracks} are the temperatures of the solidified crust and molten magma appearing through cracks in the lava crust. During instances when the "lake" is beneath the crater floor of Masaya, T_e is assumed to be equal to temperature of the gas measured at the vent opening by infrared thermometer (Chapter 2, Table 2.4).

The thermal flux by **convection** (Q_{conv} / W):

$$Q_{conv} = 0.14 A_{lake} \kappa_{air} (g \alpha_{air} \rho_{air} / \mu_{air} \beta_{air})^{1/3} (T_e - T_{air})^{4/3} \qquad (2)$$

where g is the acceleration due to gravity, κ_{air}, α_{air}, ρ_{air}, μ_{air}, and β_{air} are the thermal conductivity, cubic expansivity, density, viscosity and thermal diffusivity of air, set using standard thermal properties of air (Kays and Crawford, 1980) for an ambient air temperature (T_{air}) of 25 C.

The thermal flux by **conduction** (Q_{cond} / W):

$$Q_{cond} = 2\pi\kappa_{rock}Dr_v[(T_{gas}-T_{rock})/r_c] \quad (3)$$

where κ_{rock} is wall rock thermal conduction, D is the magma depth, r_v is the vent radius and r_c is the horizontal distance from the conduit wall to T_{rock}, the ambient wall rock temperature. $T_{gas} = T_{exit}-T_{magma}$ with T_{exit} being the temperature of the gas measured at the vent opening by infrared thermometer (Chapter 2, Table 2.4).

The thermal flux by **degassing** (Q_{gas} / W):

$$Q_{gas} = F_{gas}C_{gas}\Delta T_{gas}+F_{H2O}H_C \quad (4)$$

where F_{gas} and F_{H2O} the total gas and water flux for Masaya, estimated from COSPEC SO_2 flux measurements and gas species ratios obtained by FTIR. C_{gas} specific heat capacity of gas, ΔT_{gas} is the change in temperature of the gas from magmatic (T_{magma}) to ambient (T_{air}). H_C is latent heat of condensation.

The thermal flux from **ejecta** (Q_{ejecta} / W):

$$Q_{ejecta} = (C_{magma}\Delta T_{ejecta} + H_X)\, M_{ejecta} \quad (5)$$

where ΔT_{ejecta} is cooling of ejecta from magmatic (T_{magma}) to ambient (T_{air}) temperatures, C_{magma} is the specific heat capacity of the magma, H_X is the latent heat of crystallisation and M_{ejecta} is the mass flux of erupted material.

The **cooling rate** (h_c / °C yr^{-1}) of a volume of magma:

$$h_c = Q_{tot}/(M_{res}C_{magma})\ 3.15 \times 10^7 \qquad (6)$$

where M_{res} is the mass of cooling magma (kg) and 3.15×10^7 is the conversion from seconds to years. The time to cool from liquidus to just near solidus (ΔT ~150°C, Archambault and Tanguy, 1976) is thus $h_c / \Delta T$. This is a first-order cooling equation and does not include heat loss in the reservoir such as from forced convection.

Table C.1: Parameters for thermal flux calculations at Masaya volcano.

Parameter	Description	Value	Units
σ	Stefan-Boltzman constant	5.67×10^{-8}	$W\ m^{-2}\ K^{-4}$
ε	emissivity	0.9	
g	acceleration due to gravity	9.81	$m\ s^{-2}$
κ_{air}	thermal conductivity of air	2.61×10^{-2}	$W\ m^{-1}\ K^{-1}$
κ_{rock}	thermal conductivity of wall rock	1	$W\ m^{-1}\ K^{-1}$
α_{air}	cubic expansivity of air	3.0×10^{-3}	
ρ_{air}	density of air	1.18	$kg\ m^{-3}$
ρ_{magma}	density of magma	2600	$kg\ m^{-3}$
μ_{air}	viscosity of air	1.85×10^{-5}	Pa s
β_{air}	thermal diffusivity of air	2.37×10^{-5}	$m^2\ s^{-1}$
T_{air}	ambient air temperature	25	°C
T_e	effective radiation temperature of lava lake surface	625†	°C
T_{magma}	initial magma temperature	1100	°C
T_{crust}	lava lake crust temperature	337	°C
T_{cracks}	temperature of molten material from cracks in the lava crust	986	°C
T_{exit}	exit temperature of gas measured at vent opening by IR camera	300‡	°C
T_{amb}	ambient surface temperature	25	°C
A_{lake}	Area of lava lake	0.16	km^2
D	magma depth	100	m
r_V	vent radius	5	m
r_c	distance into conduit wall to reach T_{amb}	10	m
F_{gas}	total gas flux	432*	$kg\ s^{-1}$
F_{H2O}	water flux	372*	$kg\ s^{-1}$
C_{gas}	specific heat capacity of gas	1600	$J\ kg^{-1}\ K^{-1}$
C_{magma}	specific heat capacity of magma	1150	$J\ kg^{-1}\ K^{-1}$
H_X	latent heat of crystallisation	3×10^5	$J\ kg^{-1}$
H_C	latent heat of condensation	2.26×10^6	$J\ kg^{-1}$

† see Equation 1; ‡ see Chapter 2, Table 2.4; * based on an average SO_2 flux of 1700 t d^{-1}. Constants from the convection equation are set using an ambient air temperature of 25°C.

C.2. References

Archambault, C. and Tanguy, J. C., 1976. Comparative temperature measurements on Mount Etna lavas: problems and techniques. J. Volcanol. Geotherm. Res., 1, 113-125.

Harris, A. J. L., Flynn, L. P., Rothery, D. A., Oppenheimer, C. and Sherman, S. B., 1999. Mass flux measurements at active lava lakes: Implications for magma recycling. J. Geophys. Res., 104, 7117-7136.

Harris, A. J. L. and Stevenson, D. S., 1997. Magma budgets and steady-state activity of Vulcano and Stromboli. Geophys. Res. Lett., 24, 1043-1046.

Holman, J. P., 1992. Heat Transfer, McGraw-Hill, New York, pp. 713.

Kays, W. M. and Crawford, M. E., 1980. Convective Heat and Mass Transfer, McGraw-Hill, New York, pp. 420.

Oppenheimer, C., 1991. Lava flow cooling estimated from Landsat Thematic Mapper infrared data: The Lonquimay eruption (Chile, 1989). J. Geophys. Res., 96, 21865-21878.

Pieri, D. C., Glaze, L. S. and Abrams, M. J., 1990. Thermal radiance observations of an active lava flow during the June 1984 eruption of Mount Etna. Geology, 18, 1018-1022.

Salisbury, J. W. and D'Aria, 1992. Emissivity of terrestrial materials in the 8-14 μm atmospheric window. Remote Sens. Env., 42, 83-106

Appendix D.

Micro-gravity and deformation methodology

D.1. Introduction.

Subsurface mass and density changes within a volcano can be quantified and located using a combination of high-resolution ground deformation and micro-gravity monitoring techniques (cf., Rymer and Brown, 1986; Eggers, 1987; Yokoyama, 1989; Berrino, 1994; Rymer et al., 1998a). Micro-gravity monitoring involves the measurement of small gravity changes with time and space across a network of stations. The theory and field practice for volcano micro-gravity monitoring has been discussed fully in the literature (cf. Rymer, 1989; Rymer, 1996) and therefore will only be summarised briefly.

In a conventional (static) gravity survey, such as those performed by Connor and Williams (1990) and Métaxian (1994) at Masaya, observations are made at several field stations and at a reference station in order to generate a Bouguer anomaly map. The static survey is commonly used to investigate subsurface density structures such as caldera infill and magma feeder pipes (Rymer and Brown, 1986). Several corrections (latitude, free air gradient, density, terrain) must be applied to the data before they can be expressed as relative gravity differences with respect to a local base station or international gravity station. The spatial anomalies of a Bouguer survey are typically on the order of tens to hundreds of milligals in magnitude and often have a wavelength of several kilometres.

Dynamic micro-gravity surveys, on the other hand, are temporal in nature, i.e., one measures the change in gravity (relative to a base station) over time. Theses changes are typically much smaller than the anomalies measured during a static survey; on the order of tens to hundreds μGal per year (1 μGal = 10^{-9} Gal). For the purpose of this study, we concentrate on the methodology for dynamic micro-gravity measurements.

D.2. The Instrument

The instrument is essentially composed of a mass on the end of a beam fixed at one end by a horizontal supporting beam and balanced by a pair of wires and springs that act as a frictionless hinge for the beam (Figure D.1). The beam is supported by a metal alloy "zero length" spring, at an angle of ~45° from horizontal. When the torque on the mass (due to the force of gravity) is balanced by the restoring torque of the spring, the net torque on the mass becomes zero. Variations in gravity are compensated by changing the torque on the spring using the nulling dial; the amount of adjustment required is a measure of the change in gravity. The alloy, from which the spring is made, is extremely sensitive to temperature and pressure variations. The gravity meter is therefore insulated and controlled by a thermostat and pressure compensator (typically powered by a 12V DC gel-cell battery; Figure D.2).

D.3. Transporting the instrument

Although the LaCoste and Romberg instrument is quite robust, care must nevertheless be taken to minimise/eliminate any knocks or shocks which can result in a "tare", or sudden irreversible jump in the meter reading (Rymer, 1989). These can be minimised during transport by keeping the instrument in its padded metal carry case. Where this is not feasible (e.g., walking across rough terrain), the instrument should be placed securely in a properly padded backpack (e.g., use the pads from the carry case to

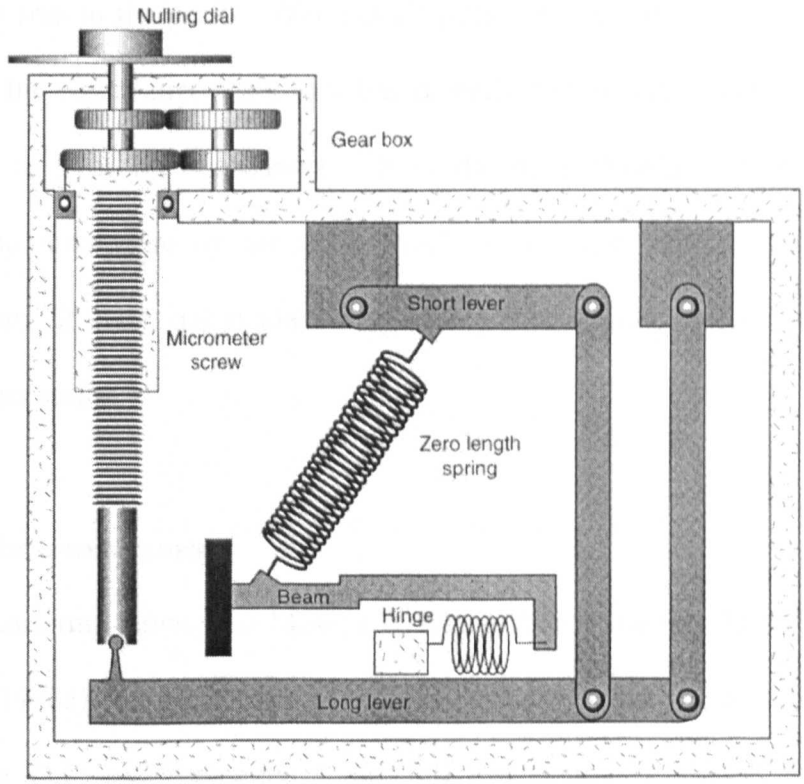

Figure D.1: Schematic of a LaCoste and Romberg gravity meter. Used with permission of M. Davies, 2000.

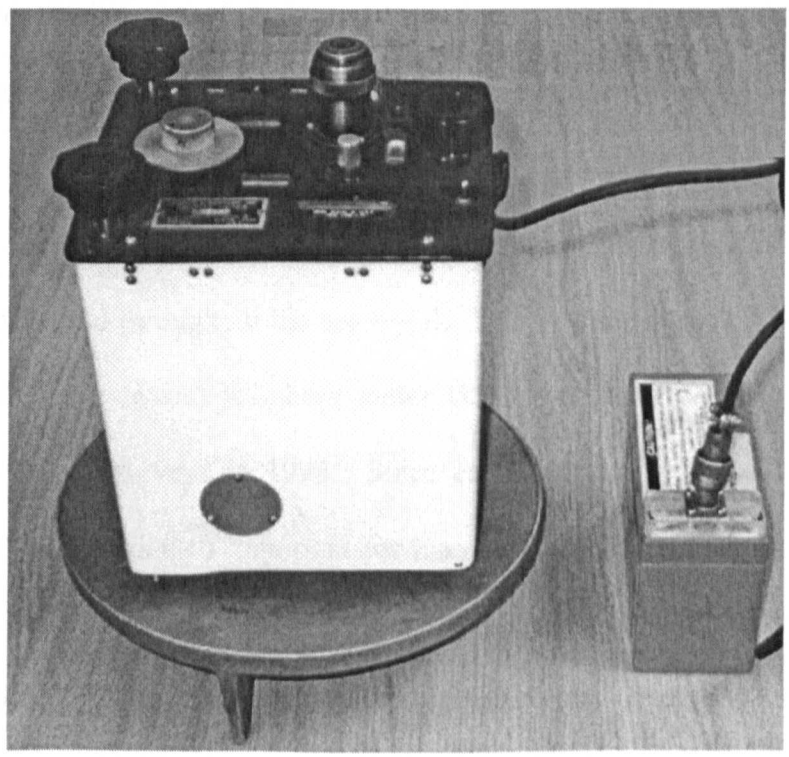

Figure D.2: LaCoste & Romberg G meter (G513) on a typical base plate and connected to a 12V gel-cell battery. The white outer case acts to protect and insulate the instrument, while the three black knobs on the top of the instrument are used for levelling.

form a padded area in the pack). When at all possible, the instrument should always be kept upright. Increased airport security has recently led to difficulties with the gel-cell batteries used to heat the instrument. It is therefore strongly advisable that when transporting the instrument by air (in a "hot" mode), that batteries have **"non-spill"** stamped on them. If this is not available, the battery manufacturer's documentation should be taken as a precaution.

D.4. Making the measurements

The monitoring network at Masaya was initially installed by Métaxian (1994) and Rymer et al. (1998a) and during this study has been increased to 38 stations across the caldera (Figure D.2; see Appendix A for full description of station locations). All measurements are made in relation to a base station A1 (Figure D.3). The assumption is made that the reference or field base station A1 is outside the area of gravity variation. In order to confirm this, a set of 4 secondary reference stations were installed (Regis, LaClinica, ParqueSM, EstacionT) outside the caldera, at distances of up to 15 km (Figure D.3).

In order for data to be comparable from one year to the next, it is crucial that the same instrument is used throughout the survey(s). This was the case at Masaya where the same instrument, LaCoste and Romberg meter G513, has been used since the start of dynamic micro-gravity surveys in 1993. Since each operator may read the meter in a slightly different way, it is also important for internal consistency that the same operator always read the same instrument during a given survey and make each reading in the same way (Rymer, 1989). Stations should be clearly marked and when possible, consist of a large purpose built concrete block with deep footings (tens of cm). This is not always feasible and therefore an existing rock outcrop may be used with the location marked by a

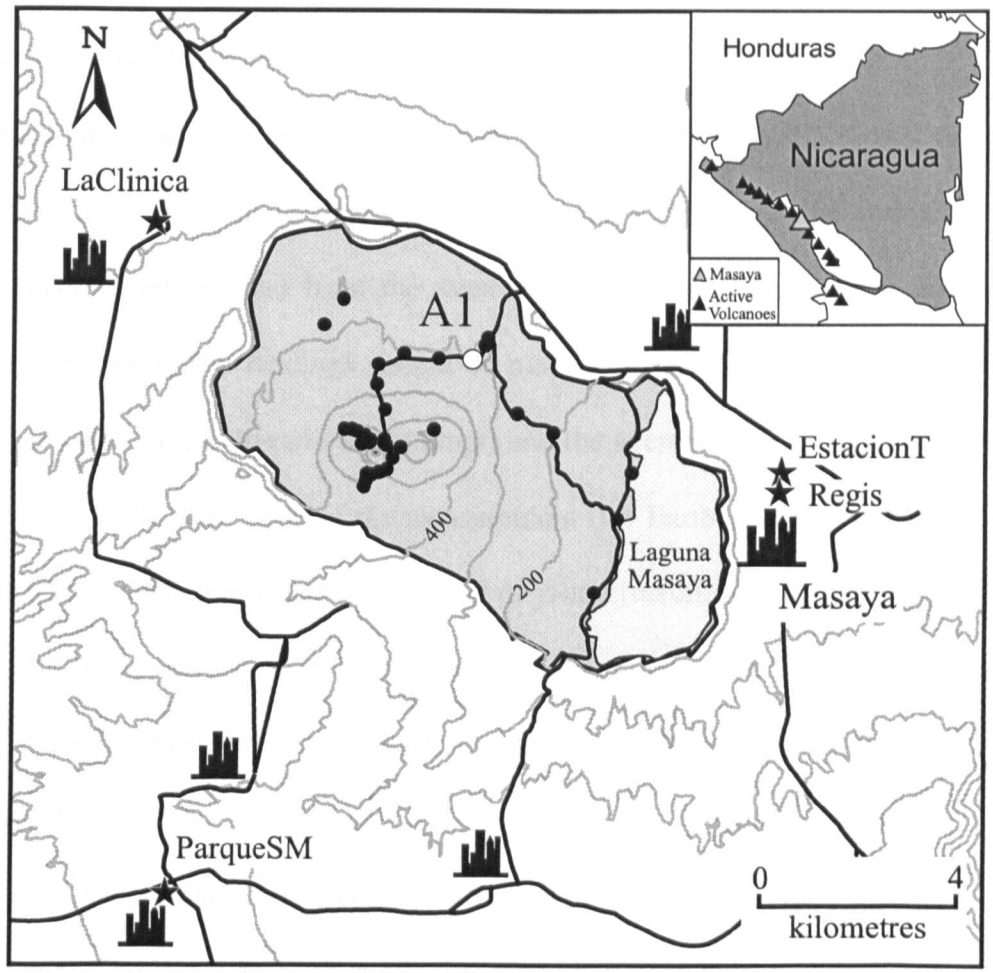

Figure D.3: Masaya caldera (shaded area) with the inter-caldera gravity/GPS stations (black dots) and extra-caldera reference stations (black stars). All gravity measurements are quoted relative to station A1 (white dot). Contours are 100 m. Inset map indicates Masaya (grey triangle) and the active volcanoes (black triangles) of the Central American Volcanic Front.

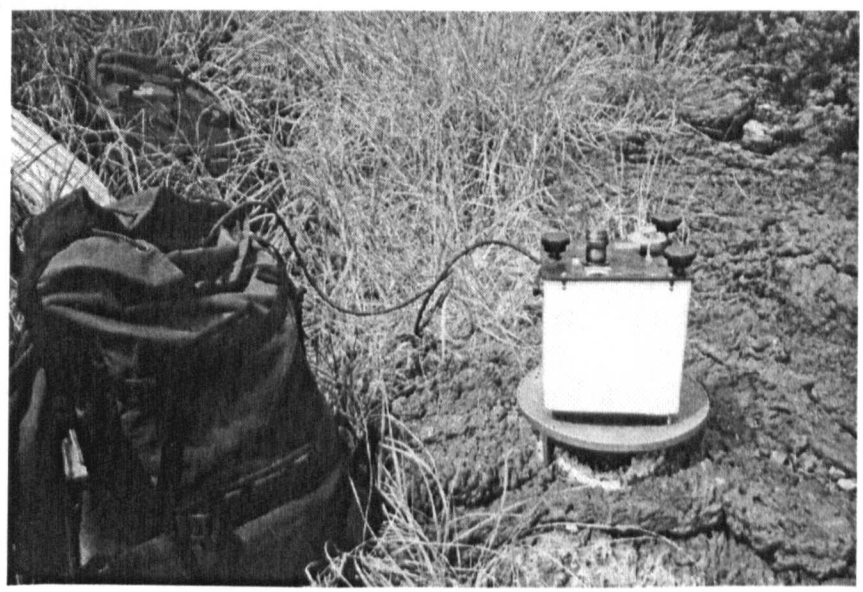

Figure D.4: Gravity meter (G513) placed on base plate above a metal levelling pin and marked by a white paint circle.

nail and/or paint spot (Figure D.4). To facilitate repeat measurements, the position of the base plate legs should also be marked.

Once the gravity meter has been levelled (following the manufacturer's guidelines), a reading is made. In order to avoid possible whiplash effects on the spring, a reading should always be approached from the same direction (e.g., always from downscale – clockwise). A few repeat readings should be made at each station (i.e., turn the reading dial off the reading line between each attempt) and the average of the readings taken. It is important to note the exact time of the measurement (for Earth tide correction; see below) and whether the instrument has been knocked or jolted (resulting in a potential "tare"). A tare may also be caused by vibration of the instrument due to seismic noise (Davies et al., 2000). If there is a tare, one should return to the last station and repeat the measurement (Rymer, 1989).

There is essentially no instrumental drift for G513, at least during a day of measurements. The entire network at Masaya now requires at least two days to completely reoccupy, however, as each measurement is taken relative to the base station, any effect of drift is negated. Measurements across the network are generally made using a multiple cross-looping method:

A1→A2→A3→A4→A5→**A1**→A6→A7→A8→**A1**→ etc.

where the first measurement is made at the base station (A1), followed by a number of measurements and then reoccupation of the base station to "close" the loop. In this way, any significant difference between the "looped" base station measurements will identify the presence of a tare, which can therefore be re-measured or corrected for.

D.5. Data Reduction

Once the measurement has been made (and time of measurement noted), the raw data must be corrected for the effects of the Solid Earth tide – the visco-elastic deformation

of the Earth due to the gravitational attraction of the Sun and Moon. This deformation, which can vary by up to 40 cm in the lower latitudes, results in a gravity change that can be easily determined using software developed by (Broucke et al., 1972). As the gravity meter spring does not behave in a perfectly linear manner across the range of gravitational forces seen at Masaya, the data must also be corrected using calibration factors supplied by the manufacturer. For example, at station Muertes, a gravity reading of 1791.431 mGal was made at 21:00 GMT with a tidal effect of 0.116 mGal (Figure D.5). The resulting gravity value (in mGal) is calculated using as follows:

$$(91.431 \times 1.02186) + 1736.09 + 0.116 = 1829.636$$

where 91.431 is the last part of the reading, 1.02186 is the correction factor for the 1700 mGal interval, 1736.09 is the cumulative value (both supplied by the manufacturer), and 0.116 is the tidal effect. The resulting gravity value (for each station) is then subtracted from the base station (A1 for Masaya) prior to temporal comparison.

D.6. Factors affecting measurements

Since a gravity meter (such as the one used in this study), functions essentially like a long-period seismometer, it is extremely sensitive to seismic noise. Due in large part to the continuous degassing-induced volcanic tremor at Masaya (Métaxian et al., 1997), the reading line of the instrument can vibrate quite seriously making gravity measurements difficult (Davies et al., 2000). Therefore, at Masaya, only changes greater than 20 μGal are considered significant.

Seasonal effects at Masaya are generally quite limited as the water table is at a depth of at least 300 m. One field campaign during the wet season (June 1999) showed no obvious seasonal effect (gravity continued to decrease at a similar rate to that of the previous and subsequent field seasons). Measurements were nevertheless generally made during the dry season because of greater facility of making measurements.

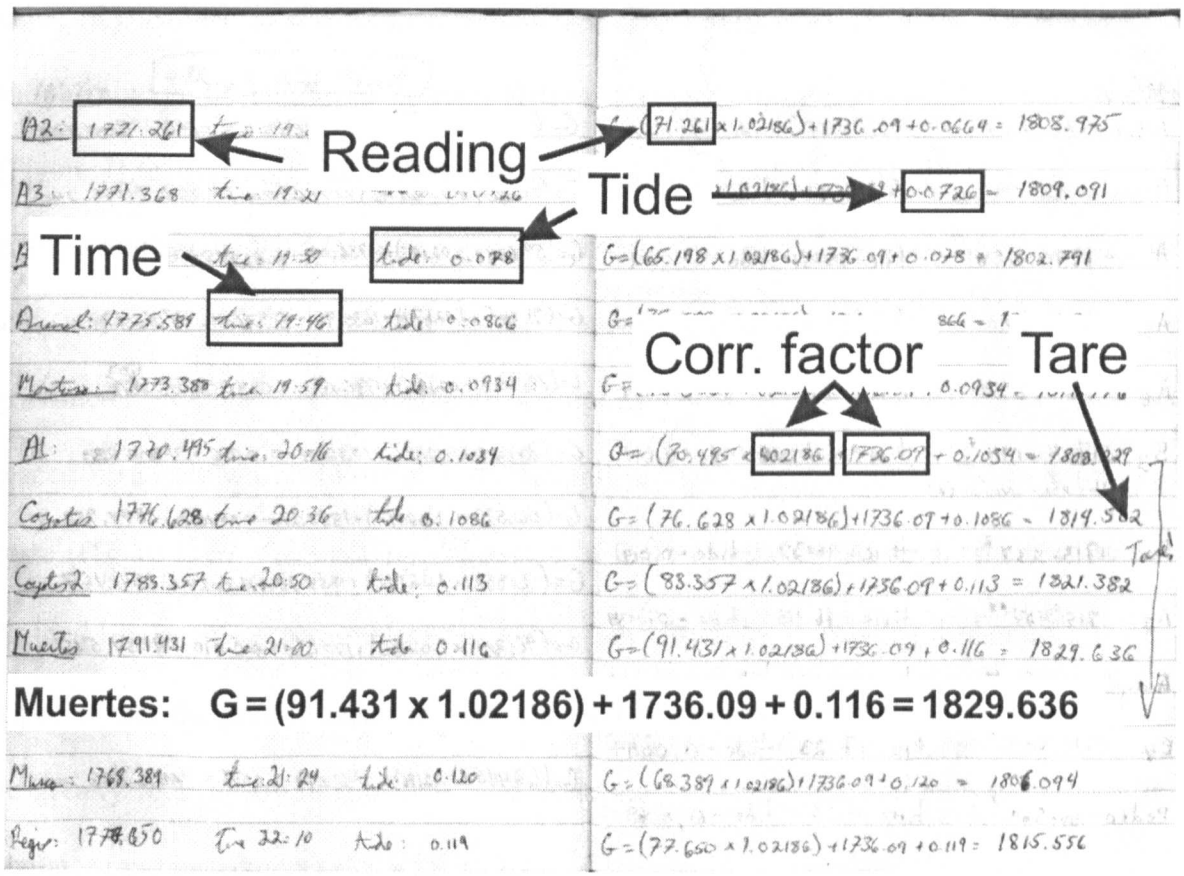

Figure D.5: Copy of a typical field notebook and calculation (for Muertes station)

D.7. Free Air Gradient measurements

The amount by which gravity varies with elevation is given by the free air gradient (FAG); a theoretical value of –308.6 μGal m^{-1} is typically used. However, terrain effects and Bouguer anomalies can cause this value to differ by up to 40% from the theoretical value (Rymer, 1994) and references therein). Therefore, when possible, the actual FAG should always be measured at each station during a micro-gravity/deformation survey (Figure D.6; Berrino et al., 1984; Yokoyama, 1989; Rymer, 1994; Chapter 3). This is easily accomplished at Masaya by making micro-gravity measurements first at the surface and then some distance off the ground (~1 m) using a levelling tripod adapted to hold a gravimeter base plate. Where adapters are not available, two base plates can be used: one placed upside down on the tripod, the second placed right side up on the inverted base plate (Figure D.6). The gravity difference of the two sets of measurements (Δg) is then divided by the difference in elevation (Δh). One difficulty in making measurements on a tripod is that the gravity meter is more exposed to wind-induced "noise". This effect can be greatly reduced by having two field assistants hold a large rigid suitcase around the operator (and instrument) as a wind shield.

D.8. Ground Deformation using GPS

Ground deformation over the entire network was measured at least once every field season using Leica GPS 200 dual-frequency differential receivers (Figure D.7); the instruments are essentially identical, except for more memory on the base station receiver. One receiver is used as a base station and installed, prior to start of the survey, behind the Museum (see Appendix A) and left to gather data throughout the day. The other instrument is used as a mobile receiver and placed over each station and allowed to collect data for approximately 15-20 minutes. The data from both receivers are then downloaded to a laptop computer at the end of the day and "run" through software supplied by Leica.

Figure D.6: FAG measurements made using a levelling tripod and two baseplates. The tripod should be placed directly above the station marker. San Pedro2 station.

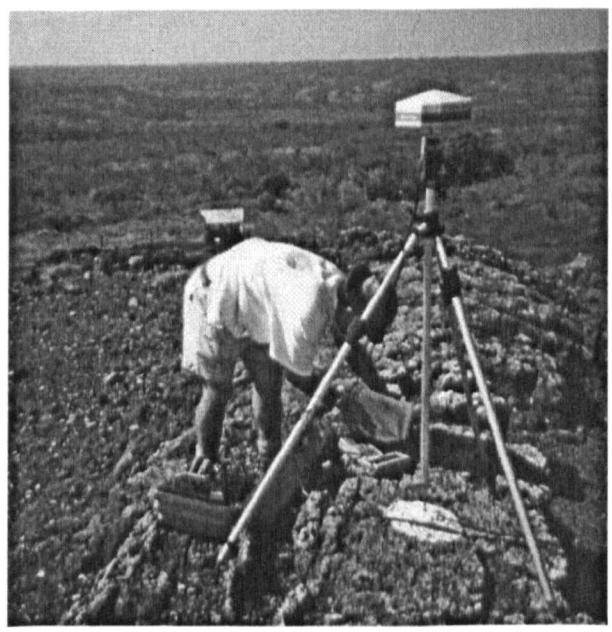

Figure D.7: GPS measurements at station E3, Masaya. Vertical precision is on the order of 1-2 cm.

The horizontal and vertical position of each station in then determined. To within ± 1 cm horizontally and ± 2 cm vertically, the change in position with respect to a chosen fixed reference (station A1) can be determined in this way.

D.9. References

Berrino, G., 1994. Gravity changes induced by height-mass variations at the Campi Flegrei caldera. J. Volcanol. Geotherm. Res., 61, 293-309.

Berrino, G., Corrado, G., Luongo, G. and Toro, B., 1984. Ground deformation and gravity changes accompanying the 1982 Pozzuoli uplift. Bull. Volcanol., 47, 187-200.

Broucke, R. A., Zürn, W. E. and Slichter, L. B., 1972. Lunar tidal acceleration on a rigid earth. Flow and Fracture of Rocks, American Geophysical Union, Geophysical Monograph, 16, pp. 319-324.

Connor, C. B. and Williams, S. N., 1990. Interpretation of gravity anomalies, Masaya caldera complex, Nicaragua. In: Larue, D. K. and Draper, G. Transactions of the 12th Caribbean Geological Conference, United States Virgin Islands,

Davies, M. A., Harrop, N. D. and Rymer, H., 2000. Experimental investigation of temporary tares induced by ground vibration in LaCoste and Romberg gravity meters. Geophys. Prospect., In press.

Eggers, A. A., 1987. Residual gravity changes and eruption magnitudes. J. Volcanol. Geotherm. Res., 33, 201-216.

Métaxian, J.-P., 1994. Étude Sismologique et Gravimétrique d'un Volcan Actif: Dynamisme Interne et Structure de la Caldera Masaya, Nicaragua, Ph.D. Thesis, Université de Savoie, France.

Métaxian, J.-P., Lesage, P. and Dorel, J., 1997. Permanent tremor of Masaya Volcano, Nicaragua: Wave field analysis and source location. J. Geophys. Res., 102, 22529-22545.

Rymer, H., 1989. A contribution to precision microgravity data analysis using LaCoste and Romberg gravity meters. Geophys. J., 97, 311-322.

Rymer, H., 1994. Microgravity change as a precursor to volcanic activity. J. Volcanol.

Geotherm. Res., 61, 311-328.

Rymer, H., 1996. Microgravity monitoring. In: R. Scarpa and R. I. Tilling (Editors), Monitoring and Mitigation of Volcano Hazards, Springer-Verlag, Berlin, pp. 169-198.

Rymer, H. and Brown, G. C., 1986. Gravity fields and the interpretation of volcanic structures: Geological discrimination and temporal evolution. J. Volcanol. Geotherm. Res., 27, 229-254.

Rymer, H., van Wyk de Vries, B., Stix, J. and Williams-Jones, G., 1998. Pit crater structure and processes governing persistent activity at Masaya Volcano, Nicaragua. Bull. Volcanol., 59, 345-355.

Yokoyama, I., 1989. Microgravity and height changes caused by volcanic activity: four Japanese examples. Bull. Volcanol., 51, 333-345.

Appendix E.

SO_2 flux Data

E.1. Individual COSPEC measurements, 1972-2000

Date	Time (local)	SO_2 Flux ($t\ d^{-1}$)	Windspeed ($m\ s^{-1}$)	Route	COSPEC Version
01/10/72		180			
08/12/76	11:45	450	5.4	Stationary	IV?
08/12/76	12:45	650	5.4	Stationary	IV?
08/12/76	15:45	880	5.4	Stationary	IV?
26/11/77	12:45	360	3.93	Stationary	IV?
26/11/77	13:00	400	3.93	Stationary	IV?
26/11/77	13:30	370	3.91	Stationary	IV?
26/11/77	14:00	470	3.93	Stationary	IV?
17/06/78	09:00	220	5.7	Stationary	IV?
17/06/78	09:15	200	5.7	Stationary	IV?
17/06/78	09:30	420	5.7	Stationary	IV?
17/06/78	09:45	550	5.7	Stationary	IV?
17/06/78	10:00	320	5.7	Stationary	IV?
17/06/78	10:15	310	5.7	Stationary	IV?
17/06/78	10:30	310	5.7	Stationary	IV?
17/06/78	10:45	300	5.7	Stationary	IV?
17/06/78	11:00	280	5.7	Stationary	IV?
17/06/78	11:15	350	5.7	Stationary	IV?
18/06/78	11:00	380	5	Stationary	IV?
18/06/78	11:15	230	5	Stationary	IV?
18/06/78	11:30	290	5	Stationary	IV?
18/06/78	11:45	240	5	Stationary	IV?
18/06/78	12:00	350	5	Stationary	IV?
18/06/78	12:15	350	5	Stationary	IV?
07/02/80	13:55	1757	11.5	LP	IV?
07/02/80	14:10	1194	11.5	LP	IV?
07/02/80	15:20	1719	11.5	LP	IV?
10/02/80		1221	6.4	LP	IV?
10/02/80		1483	8.3	LP	IV?
10/02/80		1053	8.3	LP	IV?
24/06/80		970		LP	IV?
24/06/80		820		LP	IV?
24/06/80		1073		LP	IV?
24/06/80		858		LP	IV?
28/06/80		614		Air	IV?
01/08/80		801		LP	IV?
01/08/80		1253		LP	IV?
01/08/80		851		LP	IV?
01/08/80		1552		LP	IV?
01/08/80		733		LP	IV?
02/08/80		1174	4.5	Air	IV?
05/08/80		160	2.7	LP	IV?
05/08/80		350	2.7	LP	IV?
06/08/80	11:04	1506	4.4	Air	IV?
06/08/80		1359	4.4	Air	IV?
15/08/80		1290		LP	IV?
15/08/80		1775		LP	IV?
17/11/80		734	3.4	LP	IV?
17/11/80		953	3.4	LP	IV?
17/11/80		600	3.4	LP	IV?
17/11/80		630	3.4	LP	IV?
20/01/81	11:05	1107	4.1	LP	IV?
20/01/81	11:29	1059	3.6	LP	IV?
20/01/81	11:52	1073	4	LP	IV?
20/01/81	12:28	877	3.5	LP	IV?
20/01/81	12:54	856	2.8	LP	IV?
20/01/81	14:50	759	2	LP	IV?
20/01/81	15:10	707	1.8	LP	IV?
20/01/81	15:30	588	1.9	LP	IV?
21/01/81	09:04	1502	5.2	LP	IV?
21/01/81	09:28	1104	5.2	LP	IV?
21/01/81	10:03	1153	5.2	LP	IV?
21/01/81	10:22	1737	5.3	LP	IV?
21/01/81	10:42	1507	5.3	LP	IV?
21/01/81	11:57	617	1.5	LP	IV?
21/01/81	13:01	813	1.5	LP	IV?
22/01/81	09:05	609	3.6	LP	IV?
22/01/81	09:49	614	4.6	LP	IV?
22/01/81	10:21	492	3.7	LP	IV?
22/01/81	11:52	2177	3.7	LP	IV?
23/01/81	13:55	1193	3.6	LP	IV?
23/01/81	14:06	1370	4.4	LP	IV?
23/01/81	14:35	1497	4.8	LP	IV?
24/01/81	12:20	3349	1.4	LP	IV?
24/01/81	12:54	4927	2.1	LP	IV?
25/01/81	09:26	849	4.1	LP	IV?
25/01/81	10:02	1011	4.1	LP	IV?
25/01/81	10:40	1082	4	LP	IV?
25/01/81	11:10	1262	3.7	LP	IV?
25/01/81	12:09	1429	3.5	LP	IV?
27/01/81	08:36	1318	3.8	LP	IV?
27/01/81	08:55	1214	3.9	LP	IV?
27/01/81	09:19	962	2.9	LP	IV?
27/01/81	09:42	754	2.4	LP	IV?
28/01/81	08:20	2765	4.6	LP	IV?
28/01/81	09:00	2616	4.7	LP	IV?
28/01/81	09:26	1933	4.6	LP	IV?
28/01/81	10:02	1157	4.2	LP	IV?
28/01/81	10:39	1028	3.6	LP	IV?
28/01/81	10:58	648	3.1	LP	IV?
28/01/81	11:20	818	2.5	LP	IV?
28/01/81	11:35	506	2.5	LP	IV?
28/01/81	14:35	1518	4	LP	IV?
28/01/81	15:00	1420	4	LP	IV?
28/01/81	15:30	980	3.3	LP	IV?
28/01/81	16:05	806	2.6	LP	IV?
29/01/81	09:10	894	4.5	LP	IV?
29/01/81	09:30	754	7.6	LP	IV?
29/01/81	10:32	1243	7.6	LP	IV?
29/01/81	12:10	1540	8.3	LP	IV?
29/01/81	12:38	1634	8.3	LP	IV?
29/01/81	12:57	1161	8.2	LP	IV?
29/01/81	14:50	631	4.4	LP	IV?
29/01/81	15:10	1273	6.8	LP	IV?
29/01/81	15:30	909	9.4	LP	IV?
30/01/81	07:21	780	5.8	LP	IV?
30/01/81	07:49	423	5.5	LP	IV?
30/01/81	08:11	575	5.3	LP	IV?
30/01/81	08:22	1001	5.5	LP	IV?
30/01/81	08:38	643	5.7	LP	IV?
30/01/81	09:02	609	5.9	LP	IV?
31/01/81	07:30	757	4.9	LP	IV?
31/01/81	07:44	786	5.9	LP	IV?
31/01/81	07:59	736	6.8	LP	IV?
31/01/81	08:14	1237	7.2	LP	IV?
31/01/81	08:30	1117	6.9	LP	IV?
31/01/81	08:42	992	5.8	LP	IV?
01/02/81	15:31	574	3	LP	IV?
01/02/81	15:43	550	3.7	LP	IV?
01/02/81	15:57	626	4.5	LP	IV?
03/02/81	09:25	702	5.6	LP	IV?
03/02/81	09:36	768	6.3	LP	IV?
03/02/81	09:58	1031	7.8	LP	IV?
03/02/81	10:08	854	9	LP	IV?
05/02/81	09:51	1133	9.6	LP	IV?
05/02/81	10:03	1116	9.6	LP	IV?
12/02/81	09:45	677	7.1	LP	IV?
12/02/81	09:52	475	8.5	LP	IV?

Date	Time (local)	SO_2 Flux (t d^{-1})	Windspeed (m s^{-1})	Route	COSPEC Version
12/02/81	10:05	1240	8.5	LP	IV?
12/02/81	10:15	505	9.9	LP	IV?
13/02/81	10:16	695	7.7	LP	IV?
13/02/81	10:26	1091	7.6	LP	IV?
13/02/81	10:35	671	7.7	LP	IV?
13/02/81	10:50	810	8	LP	IV?
17/02/81	13:25	497	4.3	LP	IV?
17/02/81	13:42	573	4.3	LP	IV?
01/03/81	14:24	1589	10.1	LP	IV?
01/03/81	14:46	1100	10.2	LP	IV?
01/03/81	14:55	1208	10.4	LP	IV?
01/03/81	15:32	1569	8.5	LP	IV?
01/03/81	16:00	927	6.7	LP	IV?
19/03/81	16:10	2198	4.9	LP	IV?
19/03/81	16:40	1831	4.9	LP	IV?
26/11/81		617	2.7	LP	IV?
26/11/81		586	4.6	LP	IV?
26/11/81		1088	6.6	LP	IV?
27/11/81		591	2.3	LP	IV?
27/11/81		493	2.8	LP	IV?
27/11/81		581	2.8	LP	IV?
27/11/81		504	2.9	LP	IV?
01/02/82		323	2	LP	IV?
01/02/82		332	2.3	LP	IV?
01/02/82		425	2.3	LP	IV?
01/02/82		829	4.9	LP	IV?
01/02/82		1074	5.9	LP	IV?
08/02/82		580	2.5	LP	IV?
08/02/82		474	2.5	LP	IV?
08/02/82		503	3	LP	IV?
08/02/82		1793	5.6	LP	IV?
26/04/92		10			IV?
16/03/96		462	3.92	MM	IV
16/03/96		362	3.92	MM	IV
16/03/96		501	3.92	MM	IV
16/03/96		918	3.92	MM	IV
16/03/96		540	3.92	MM	IV
16/03/96		237	3.92	MM	IV
16/03/96		1098	3.92	MM	IV
16/03/96		708	3.92	MM	IV
12/02/97		214	3.5	T	V
12/02/97		207	3.5	T	V
12/02/97		56	3.5	T	V
12/02/97		157	3.5	T	V
13/02/97		399	2.8	T	V
13/02/97		352	2.8	T	V
13/02/97		463	2.8	T	V
13/02/97		1140	2.8	T	V
13/02/97		635	2.8	T	V
13/02/97		169	1.4	T	V
13/02/97		157	1.4	T	V
14/02/97		280	3.9	T	V
14/02/97		409	3.9	T	V
14/02/97		269	3.9	T	V
14/02/97		290	3.9	T	V
07/03/97	10:30	368	8.7	T	V
07/03/97	11:09	484	8.7	T	V
07/03/97	11:37	372	8.7	T	V
07/03/97	12:30	436	8.7	LP	V
07/03/97	13:05	232	10.5	LP	V
07/03/97	13:50	380	10.5	LP	V
07/03/97	14:26	288	10.5	LP	V
07/03/97	14:55	403	10.5	T	V
12/03/97	09:23	568	8.2	T	V
12/03/97	10:08	323	8.2	LP	V
12/03/97	10:37	368	8.2	LP	V
12/03/97	11:04	317	8.2	LP	V
12/03/97	11:30	321	8.2	LP	V
12/03/97	11:51	312	8.2	LP	V
12/03/97	12:15	213	8.2	LP	V
12/03/97	12:35	398	8.5	LP	V
12/03/97	13:32	197	8.5	LP	V
12/03/97	13:55	267	7.8	LP	V
12/03/97	14:26	414	7.8	LP	V
12/03/97	14:45	445	7.8	LP	V
12/03/97	15:10	345	7.8	LP	V
12/03/97	15:46	305	6.8	T	V
25/03/97	12:04	501	5.3	T	V
25/03/97	13:42	331	5.3	LP	V
25/03/97	14:17	384	6.6	LP	V
25/03/97	14:38	333	6.6	LP	V
25/03/97	15:36	1053	6.6	T	V
27/03/97	12:43	993	5.6	T	V
27/03/97	13:24	424	5.1	LP	V
27/03/97	13:35	277	5.1	LP	V
27/03/97	14:10	285	5.4	T	V
27/03/97	15:59	323	4.1	T	V
27/03/97	16:19	315	4.1	T	V
28/03/97	10:19	561	7.4	T	V
28/03/97	10:39	444	7.4	LP	V
28/03/97	11:37	560	7.4	LP	V
28/03/97	12:23	630	7.4	LP	V
28/03/97	12:45	469	7.4	T	V
28/03/97	14:46	433	5.1	T	V
21/02/98		1610	10.4	LP	V
21/02/98		1440	10.9	LP	V
21/02/98		1560	10.9	LP	V
21/02/98		800	6.9	LP	V
21/02/98		1440	6.7	LP	V
21/02/98		2260	7.0	LP	V
22/02/98	11:00	948	5.8	LP	V
22/02/98	11:26	1224	5.1	LP	V
22/02/98	12:15	2768	6.9	LP	V
22/02/98	12:51	1836	5.9	LP	V
22/02/98	13:20	2527	6.1	LP	V
22/02/98	13:50	2125	7.1	LP	V
22/02/98	14:17	3016	7.7	LP	V
22/02/98	14:53	736	5.8	LP	V
23/02/98	13:05	3290	9.1	LP	V
23/02/98	14:00	3672	9.1	LP	V
23/02/98	14:35	3744	9.1	LP	V
23/02/98	15:05	3947	9.1	LP	V
24/02/98		2060	8.5	LP	V
24/02/98		2180	8.5	LP	V
24/02/98		960	8.5	LP	V
24/02/98		1850	8.5	LP	V
24/02/98		1460	8.5	LP	V
24/02/98		1030	9.7	LP	V
24/02/98		1820	9.7	LP	V
24/02/98		1650	9.7	LP	V
24/02/98		1430	9.7	LP	V
24/02/98		1270	9.7	LP	V
25/02/98	10:58	1305	7.4	LP	V
25/02/98	11:40	1042	7.4	LP	V
25/02/98	12:00	1174	8.5	LP	V
25/02/98	12:30	955	8.5	LP	V
25/02/98	13:03	1618	8.5	LP	V
25/02/98	13:25	1145	8.5	LP	V
25/02/98	13:48	1420	8.5	LP	V
25/02/98	14:11	1205	8.5	LP	V
25/02/98	14:36	1689	6.5	LP	V
25/02/98	14:58	1233	6.5	LP	V
01/03/98	09:44	6740	4.9	LP	V
01/03/98	10:23	6047	4.2	LP	V
01/03/98	11:15	7691	5.4	LP	V
01/03/98	12:40	3994	5.0	LP	V
02/03/98		2184	8.0	LP	V
02/03/98		1151	8.0	LP	V
02/03/98		2342	8.0	LP	V
02/03/98		2176	8.0	LP	V
03/03/98		523	4.7	LP	V
03/03/98		696	4.7	LP	V
03/03/98		807	4.7	LP	V
07/03/98		1004	5.8	LP	V
07/03/98		574	5.8	LP	V
07/03/98		823	5.8	LP	V
07/03/98		843	5.8	LP	V
07/03/98		873	5.8	LP	V
07/03/98		802	5.8	LP	V
07/03/98		1289	5.8	LP	V
07/03/98		1419	5.8	LP	V
08/03/98		3204	5.8	LP	V
08/03/98		2011	5.8	LP	V
08/03/98		3414	5.8	LP	V
10/03/98		598	5.1	LP	V
10/03/98		790	6.5	LP	V
10/03/98		1111	6.9	LP	V
10/03/98		510	6.9	LP	V
13/03/98		277	10.6	LP	V
13/03/98		824	10.6	LP	V
13/03/98		728	10.6	LP	V
13/03/98		771	10.6	LP	V

Date	Time (local)	SO_2 Flux ($t\ d^{-1}$)	Windspeed ($m\ s^{-1}$)	Route	COSPEC Version
13/03/98		645	10.6	LP	V
13/03/98		321	10.6	LP	V
13/03/98		633	10.6	LP	V
13/03/98		606	10.6	LP	V
13/03/98		1248	10.4	LP	V
13/03/98		618	10.4	LP	V
13/03/98		771	10.4	LP	V
13/03/98		950	10.4	LP	V
14/03/98	10:35	1666	16.2	LP	V
14/03/98	11:24	1586	16.2	LP	V
14/03/98	11:45	1223	15.9	LP	V
14/03/98	11:58	1811	15.5	LP	V
14/03/98	12:15	2356	17.0	LP	V
14/03/98	12:31	2161	16.3	LP	V
17/03/98		3060	10.6	LP	V
17/03/98		2259	10.6	LP	V
17/03/98		2872	10.9	LP	V
17/03/98		2136	10.9	LP	V
17/03/98		2681	12.5	LP	V
17/03/98		2244	9.7	LP	V
17/03/98		1736	8.6	LP	V
17/03/98		3228	10.4	LP	V
17/03/98		2618	10.6	T	IV
17/03/98		1929	10.6	T	IV
17/03/98		3045	10.6	T	IV
17/03/98		2083	10.6	T	IV
17/03/98		2340	10.6	T	IV
17/03/98		2396	10.6	T	IV
17/03/98		2821	10.6	T	IV
17/03/98		3276	10.6	T	IV
17/03/98		3023	10.6	T	IV
17/03/98		2405	10.6	T	IV
17/03/98		3220	10.9	T	IV
17/03/98		2609	10.9	T	IV
17/03/98		5672	12.5	T	IV
17/03/98		4306	12.5	T	IV
17/03/98		4880	9.7	T	IV
17/03/98		2630	9.7	T	IV
17/03/98		2347	8.6	T	IV
17/03/98		3803	10.4	T	IV
17/03/98		3017	10.4	T	IV
17/03/98		3857	10.4	T	IV
18/03/98		1732	8.7	LP	IV
18/03/98		2218	8.4	LP	IV
18/03/98		1689	8.4	LP	IV
18/03/98		1637	8.3	LP	IV
18/03/98		826	6.5	LP	IV
18/03/98		1565	8.1	LP	IV
18/03/98		1812	8.6	LP	IV
18/03/98		2154	8.2	LP	IV
18/03/98		1560	8.2	LP	IV
18/03/98		1079	7.3	LP	IV
21/03/98		3192	5.2	LP	V
21/03/98		1076	5.2	LP	V
21/03/98		1325	5.2	LP	V
21/03/98		1255	5.1	LP	V
21/03/98		1758	5.1	LP	V
21/03/98		1693	4.6	LP	V
21/03/98		2202	5.2	LP	V
21/03/98		1365	4.9	LP	V
21/03/98		1745	4.4	LP	V
21/03/98		825	3.1	LP	V
21/03/98		455	3.1	LP	V
25/03/98		939	8.4	LP	V
25/03/98		871	8.4	LP	V
25/03/98		1684	9.8	LP	V
25/03/98		1149	10.2	LP	V
25/03/98		1070	10.2	LP	V
25/03/98		1133	8.4	LP	V
25/03/98		1020	8.4	LP	V
25/03/98		681	8.4	LP	V
25/03/98		709	7.7	LP	V
25/03/98		1659	7.7	LP	V
11/04/98		4404	13.5	LP	V
11/04/98		2129	13.6	LP	V
11/04/98		1364	12.1	LP	V
11/04/98		1346	12.9	LP	V
11/04/98		2196	10.8	LP	V
11/04/98		2223	9.5	LP	V
11/04/98		1396	9.6	LP	V
11/04/98		1979	9.7	LP	V
11/04/98		2380	10.2	LP	V
11/04/98		1311	8.8	LP	V
11/04/98		1154	8.2	LP	V
17/04/98		3958	11.8	LP	V
17/04/98		2031	12.1	LP	V
17/04/98		2965	11.2	LP	V
17/04/98		2865	10.7	LP	V
17/04/98		3003	10.9	LP	V
17/04/98		2765	12.0	LP	V
17/04/98		3167	11.6	LP	V
17/04/98		2751	10.4	LP	V
17/04/98		3637	10.5	LP	V
18/04/98		2524	12.3	LP	V
18/04/98		2336	11.6	LP	V
18/04/98		2723	10.9	LP	V
18/04/98		2184	10.9	LP	V
18/04/98		2112	10.6	LP	V
18/04/98		2685	10.2	LP	V
18/04/98		2859	10.6	LP	V
20/04/98		3231	12.4	LP	V
20/04/98		1997	12.1	LP	V
20/04/98		2047	12.1	LP	V
20/04/98		2418	12.2	LP	V
20/04/98		2294	12.0	LP	V
20/04/98		2226	13.0	LP	V
23/04/98		1199	13.3	LP	V
23/04/98		1503	12.9	LP	V
23/04/98		2248	12.6	LP	V
23/04/98		1767	12.7	LP	V
23/04/98		897	12.8	LP	V
23/04/98		1854	12.3	LP	V
27/04/98		1523	12.8	LP	V
27/04/98		1203	12.8	LP	V
27/04/98		1382	12.8	LP	V
27/04/98		1101	12.8	LP	V
27/04/98		1318	12.8	LP	V
27/04/98		1792	12.8	LP	V
27/04/98		1395	12.8	LP	V
07/09/98	13:27	1217	2.4	MM	V
07/09/98	14:06	891	2.4	MM	V
08/09/98	11:00	1480	3.4	MM	V
08/09/98	12:44	1392	3.4	MM	V
08/09/98	14:19	1062	3.4	MM	V
08/09/98	15:01	1752	3.4	MM	V
09/09/98	10:01	525	1.2	MM	V
09/09/98	10:54	430	1.2	MM	V
09/09/98	11:53	243	1.2	MM	V
09/09/98	13:13	175	1.2	MM	V
09/09/98	13:42	344	1.2	MM	V
09/09/98	14:18	180	1.2	MM	V
10/09/98	11:56	1692	3.4	MM	V
10/09/98	13:44	1017	3.4	MM	V
10/09/98	14:35	576	3.4	MM	V
10/09/98	14:52	1010	3.4	MM	V
11/09/98	09:49	574	2.1	MM	V
11/09/98	10:45	664	2.1	MM	V
11/09/98	11:13	1480	2.1	MM	V
11/09/98	11:52	1902	2.1	MM	V
16/09/98	11:18	180	0.5	MM	V
16/09/98	12:44	266	0.5	MM	V
16/09/98	13:41	215	0.5	MM	V
16/09/98	14:02	247	0.5	MM	V
16/09/98	14:25	236	0.5	MM	V
16/09/98	14:49	223	0.5	MM	V
16/09/98	15:13	191	0.5	MM	V
16/09/98	15:48	291	0.5	MM	V
17/09/98	10:41	479	1.0	MM	V
17/09/98	11:12	508	1.0	MM	V
17/09/98	11:40	309	1.0	MM	V
17/09/98	13:49	413	1.0	MM	V
17/09/98	14:19	586	1.0	MM	V
17/09/98	14:48	357	1.0	MM	V
17/09/98	15:10	349	1.0	MM	V
18/02/99	11:23	5339	6.1	LP	V
18/02/99	11:58	3822	6.1	LP	V
18/02/99	12:24	4387	6.1	LP	V
18/02/99	12:55	4380	6.1	LP	V
18/02/99	13:25	3516	6.1	LP	V
18/02/99	13:45	3030	6.1	LP	V
18/02/99	14:16	5535	6.1	LP	V
18/02/99	14:43	4713	6.1	LP	V

Date	Time (local)	SO_2 Flux ($t\ d^{-1}$)	Windspeed ($m\ s^{-1}$)	Route	COSPEC Version
19/02/99	10:30	1607	3.4	LP	V
19/02/99	10:53	1392	3.6	LP	V
19/02/99	11:12	1635	3.4	LP	V
19/02/99	11:29	1592	3.4	LP	V
19/02/99	11:47	1910	3.6	LP	V
19/02/99	12:33	1224	3.2	LP	V
19/02/99	12:52	2479	3.6	LP	V
19/02/99	13:16	1916	3.3	LP	V
19/02/99	13:39	2890	2.8	LP	V
19/02/99	14:06	1963	1.1	LP	V
22/02/99	09:47	2469	11.2	LP	V
22/02/99	09:58	1523	11.3	LP	V
22/02/99	10:13	1704	10.5	LP	V
22/02/99	10:28	1447	9.1	LP	V
22/02/99	10:40	1223	9.0	LP	V
22/02/99	10:54	893	9.1	LP	V
22/02/99	11:06	2127	9.8	LP	V
22/02/99	11:18	885	9.4	LP	V
22/02/99	11:31	1199	10.3	LP	V
22/02/99	11:45	1134	9.4	LP	V
22/02/99	11:56	1455	10.0	LP	V
23/02/99	09:47	1601	7.8	LP	V
23/02/99	10:13	1042	7.7	LP	V
23/02/99	10:32	1748	8.4	LP	V
23/02/99	10:52	1708	7.7	LP	V
23/02/99	11:10	2141	9.8	LP	V
23/02/99	11:28	1564	10.5	LP	V
23/02/99	11:57	1998	10.1	LP	V
23/02/99	12:28	1855	10.1	LP	V
23/02/99	13:00	2103	9.6	LP	V
23/02/99	13:20	1238	9.9	LP	V
27/02/99	10:16	3502	10.0	LP	V
27/02/99	10:32	3463	10.0	LP	V
27/02/99	10:50	2436	10.2	LP	V
27/02/99	11:05	1884	9.7	LP	V
27/02/99	11:15	2944	10.1	LP	V
27/02/99	11:28	1460	10.7	LP	V
27/02/99	11:38	1632	10.6	LP	V
27/02/99	11:50	1244	9.9	LP	V
27/02/99	12:00	1882	11.0	LP	V
27/02/99	12:12	1392	10.1	LP	V
02/03/99	12:08	2323	6.7	LP	V
02/03/99	12:29	1493	5.7	LP	V
02/03/99	13:13	2021	5.6	LP	V
02/03/99	13:30	2069	5.8	LP	V
02/03/99	13:45	3260	5.2	LP	V
02/03/99	14:00	1415	5.3	LP	V
02/03/99	14:14	1226	5.6	LP	V
02/03/99	14:28	1276	5.7	LP	V
02/03/99	14:41	2088	5.9	LP	V
02/03/99	14:53	2214	5.9	LP	V
04/03/99	11:18	1726	11.9	LP	V
04/03/99	11:38	1371	11.9	LP	V
04/03/99	11:58	1044	11.7	LP	V
04/03/99	12:10	1314	11.3	LP	V
04/03/99	12:45	1476	10.9	LP	V
04/03/99	13:03	1681	11.3	LP	V
04/03/99	13:14	1246	11.1	LP	V
04/03/99	13:26	946	10.8	LP	V
04/03/99	13:42	789	10.9	LP	V
04/03/99	14:00	1588	10.2	LP	V
05/03/99	09:18	1565	11.7	LP	V
05/03/99	09:30	2055	11.9	LP	V
05/03/99	09:48	950	11.4	LP	V
05/03/99	10:01	1321	11.4	LP	V
05/03/99	10:14	1438	11.6	LP	V
05/03/99	10:27	1575	10.4	LP	V
05/03/99	10:45	1538	10.3	LP	V
05/03/99	11:26	1250	11.1	LP	V
05/03/99	11:38	1510	11.4	LP	V
05/03/99	11:51	725	11.5	LP	V
05/03/99	12:12	1148	11.0	LP	V
05/03/99	12:30	1622	11.0	LP	V
05/03/99	12:41	1153	10.1	LP	V
05/03/99	13:02	1202	9.5	LP	V
05/03/99	13:24	1199	9.7	LP	V
05/03/99	13:40	1114	10.0	LP	V
07/03/99	09:47	2513	13.4	LP	V
07/03/99	10:35	1416	12.5	LP	V
07/03/99	10:48	3234	12.5	LP	V
07/03/99	11:03	2082	12.4	LP	V
07/03/99	11:31	1359	11.7	LP	V
07/03/99	11:52	2077	11.5	LP	V
07/03/99	12:28	1578	11.4	LP	V
07/03/99	12:49	2002	10.6	LP	V
07/03/99	01:09	848	10.0	LP	V
07/03/99	01:27	2174	10.5	LP	V
10/03/99	10:10-10:26	1586	10.7	LP	V
10/03/99	10:26-10:39	1191	11.8	LP	V
10/03/99	10:39-10:56	1088	11.0	LP	V
10/03/99	10:56-11:09	946	11.8	LP	V
10/03/99	11:09-11:22	1231	11.3	LP	V
10/03/99	11:22-11:41	1315	10.7	LP	V
10/03/99	11:41:12:30	1361	10.2	LP	V
10/03/99	12:30-12:45	1558	9.6	LP	V
10/03/99	12:45-13:01	1288	10.1	LP	V
10/03/99	13:01-13:24	660	8.9	LP	V
10/03/99	13:24-13:48	1536	9.3	LP	V
11/03/99	10:21-10:33	1721	9.7	LP	V
11/03/99	10:37-10:51	1142	9.1	LP	V
11/03/99	11:15-11:28	1467	10.2	LP	V
11/03/99	11:30-11:40	1260	9.3	LP	V
11/03/99	11:43-11:52	1533	10.2	LP	V
11/03/99	11:55-12:05	1377	9.1	LP	V
11/03/99	12:08-12:19	1755	9.0	LP	V
11/03/99	12:21-12:33	1975	10.2	LP	V
11/03/99	12:34-12:47	1206	8.5	LP	V
11/03/99	12:50-13:03	1312	8.7	LP	V
13/03/99	10:28-11:01	1343	8.4	LP	V
13/03/99	11:01-11:27	2084	7.7	LP	V
13/03/99	11:29-11:46	2104	7.5	LP	V
13/03/99	11:49-12:08	1799	7.5	LP	V
13/03/99	12:10-12:26	2426	7.0	LP	V
13/03/99	12:29-12:47	2510	6.8	LP	V
13/03/99	12:50-13:08	2326	6.7	LP	V
17/03/00	10:22	1561	8.7	LP	V
17/03/00	11:52	1331	9.2	LP	V
17/03/00	12:18	751	8.9	LP	V
17/03/00	12:37	1035	9.1	LP	V
17/03/00	12:51	1348	8.3	LP	V
17/03/00	13:26	1438	7.9	LP	V
17/03/00	13:47	1936	8.5	LP	V
17/03/00	14:04	1830	8.5	LP	V
18/03/00	11:25	1666	9.1	LP	V
18/03/00	11:47	1268	9.5	LP	V
18/03/00	12:11	1020	8.4	LP	V
18/03/00	12:42	1220	8.3	LP	V
18/03/00	12:52	966	8.3	LP	V
18/03/00	13:14	1474	8.1	LP	V
18/03/00	13:31	1386	9.2	LP	V
18/03/00	13:53	1255	8.2	LP	V
22/03/00	10:10	1508	9	LP	V
22/03/00	10:32	1234	9.9	LP	V
22/03/00	10:50	1009	10.6	LP	V
22/03/00	11:12	1426	9.3	LP	V
22/03/00	11:31	1365	9.4	LP	V
22/03/00	11:46	1560	9.9	LP	V
22/03/00	15:33	1102	9.4	LP	V
22/03/00	15:47	1735	9.5	LP	V
24/03/00	09:39	1702	10	LP	V
24/03/00	10:02	2575	10	LP	V
24/03/00	10:18	1502	10	LP	V
24/03/00	10:35	2117	10	LP	V
24/03/00	10:55	2422	10	LP	V
24/03/00	11:17	1440	10	LP	V
24/03/00	11:31	1462	10	LP	V
24/03/00	11:57	1579	10	LP	V
31/03/00	10:41	819	8.3	LP	V
31/03/00	11:04	1506	8.3	LP	V
31/03/00	11:28	683	8.3	LP	V
31/03/00	11:53	1337	8.3	LP	V
31/03/00	13:02	1349	8.3	LP	V
31/03/00	13:53	1329	8.3	LP	V
01/04/00	12:23	1645	12.5	LP	V
01/04/00	13:03	1716	12.5	LP	V
01/04/00	13:30	1458	12.5	LP	V
01/04/00	13:55	1945	12.5	LP	V
01/04/00	15:33	1996	12.5	LP	V
01/04/00	15:52	2319	12.5	LP	V
02/04/00	09:50	964	10.7	LP	V
02/04/00	10:16	706	10.7	LP	V
02/04/00	11:10	1304	10.7	LP	V

Date	Time (local)	SO_2 Flux ($t\ d^{-1}$)	Windspeed ($m\ s^{-1}$)	Route	COSPEC Version
02/04/00	11:30	1152	10.4	LP	V
02/04/00	11:49	779	10.6	LP	V
02/04/00	12:06	995	10	LP	V
02/04/00	12:25	715	8.9	LP	V
02/04/00	12:48	1280	9.5	LP	V
04/04/00	09:34	476	5.8	LP	V
04/04/00	10:00	1023	5.8	LP	V
04/04/00	10:25	1021	6.4	LP	V
04/04/00	10:51	1409	6.6	LP	V
04/04/00	11:18	1456	6.9	LP	V
04/04/00	11:43	1562	7.4	LP	V
04/04/00	12:36	1077	8.0	LP	V
06/04/00	10:35	1106	12.0	LP	V
06/04/00	10:59	660	13.7	LP	V
06/04/00	11:15	977	12.2	LP	V
06/04/00	11:36	1128	12.6	LP	V
06/04/00	11:58	1159	11.5	LP	V
06/04/00	12:55	1525	11.1	LP	V
06/04/00	13:17	1078	10.6	LP	V
06/04/00	13:37	939	10.2	LP	V
06/04/00	14:00	1212	10.1	LP	V
06/04/00	14:22	1342	10.4	LP	V
07/04/00	10:40	926	10.9	LP	V
07/04/00	11:00	689	10.5	LP	V
07/04/00	11:16	1002	10.4	LP	V
07/04/00	13:11	1116	9.9	LP	V
07/04/00	13:57	1026	10.3	LP	V
07/04/00	14:41-15:00	2237	10.3	LP	V
10/04/00	12:59-13:15	886	11.5	LP	V
10/04/00	13:48-14:05	597	10.1	LP	V
11/04/00	15:00-15:24	1469	8.7	LP	V

Data from 1972 to 1982 from Stoiber et al. (1986) and used with permission. All data between 1996 and 2000 was measured by the author in conjunction with colleagues from Université de Montréal; Université de Louvain, and INETER.

Route: LP = Llano Pacaya; T = Ticuantepe; MM = Managua-Masaya, Air = airborne; see Figure B.1 for locations.

Dark grey shading denotes minimum values (e.g., due to rain, cloud cover, etc.).

Light grey shading denotes "blowback" values, caused by the column blowing back upon itself. These value are not considered representative. See Appendix B for further discussion.

E.2. Average daily COSPEC measurements, 1972-2000

Date	SO_2 Flux ($t\ d^{-1}$)	1 σ std. dev. ($t\ d^{-1}$)	Windspeed ($m\ s^{-1}$)	n
01/10/72	180			
08/12/76	660	215	5.4	3
26/11/77	400	50	3.9	4
17/06/78	326	100	5.7	10
18/06/78	307	63	5.0	6
07/02/80	1557	315	11.5	3
10/02/80	1252	217	7.7	3
24/06/80	930	115		4
28/06/80	614			1
01/08/80	1038	352		5
02/08/80	1174		4.5	1
05/08/80	255	134	2.7	2
06/08/80	1433	104	4.4	2
15/08/80	1533	343		2
17/11/80	729	160	3.4	4
20/01/81	878	189	3.0	8
21/01/81	1205	403	4.2	7
22/01/81	973	805	3.9	4
23/01/81	1353	153	4.3	3
24/01/81	4138	1116	1.8	2
25/01/81	1127	225	3.9	5
27/01/81	1062	254	3.3	4
28/01/81	1350	741	3.6	12
29/01/81	1115	344	7.2	9
30/01/81	672	198	5.6	6
31/01/81	938	210	6.3	6
01/02/81	583	39	3.7	3
03/02/81	839	142	7.2	4
05/02/81	1125	12	9.6	2
12/02/81	724	355	8.5	4
13/02/81	817	193	7.8	4
17/02/81	535	54	4.3	2
01/03/81	1279	292	9.2	5
19/03/81	2015	260	4.9	2
26/11/81	764	281	4.6	3
27/11/81	542	51	2.7	4
01/02/82	597	338	3.5	5
08/02/82	838	639	3.4	4
26/04/92	10			
16/03/96	603	288	3.9	8
12/02/97	159	73	3.5	4
13/02/97	474	338	2.4	7
14/02/97	312	65	3.9	4
07/03/97	370	80	9.6	8
12/03/97	342	95	8.0	14
25/03/97	520	306	6.1	5
27/03/97	436	278	4.9	6
28/03/97	516	79	7.0	6
21/02/98	1518	467	8.8	6
22/02/98	1897	859	6.3	8
23/02/98	3663	275	9.1	4
24/02/98	1517	400	9.2	9
25/02/98	1279	236	7.9	10
01/03/98	6118	1568	4.9	4
02/03/98	1963	547	8.0	4
03/03/98	675	143	4.7	3
07/03/98	953	276	5.8	8
08/03/98	2876	757	5.8	3
10/03/98	752	266	6.4	4
13/03/98	699	258	10.5	12
14/03/98	1800	409	16.2	6
17/03/98	2946	892	10.6	28
18/03/98	1627	425	8.1	10
21/03/98	1536	731	4.6	11
25/03/98	1092	345	8.8	10
11/04/98	1989	917	10.8	11
17/04/98	3016	551	11.2	9
18/04/98	2489	286	11.0	7
20/04/98	2369	450	12.3	6
23/04/98	1578	485	12.8	6
27/04/98	1388	225	12.8	7

Date	SO_2 Flux ($t\ d^{-1}$)	1 σ std. dev. ($t\ d^{-1}$)	Windspeed ($m\ s^{-1}$)	n
07/09/98	1054	231	2.4	2
08/09/98	1422	284	3.4	4
09/09/98	316	142	1.2	6
10/09/98	1074	461	3.4	4
11/09/98	1155	643	2.1	4
16/09/98	231	37	0.5	8
17/09/98	429	100	1.0	7
18/02/99	4287	919	6.1	0
19/02/99	1861	502	3.1	0
22/02/99	1460	491	9.9	11
23/02/99	1700	357	9.2	10
27/02/99	2184	852	10.2	0
02/03/99	1939	618	5.7	10
04/03/99	1318	316	11.2	0
05/03/99	1335	314	10.9	16
07/03/99	1928	670	11.6	10
10/03/99	1251	279	10.5	11
11/03/99	1475	270	9.4	10
13/03/99	2085	406	7.4	7
17/03/00	1404	389	8.6	8
18/03/00	1282	229	8.6	8
22/03/00	1367	243	9.6	8
24/03/00	1850	456	10.0	8
31/03/00	1170	334	8.3	6
01/04/00	1846	305	12.5	6
02/04/00	987	242	10.2	8
04/04/00	1146	370	10.2	8
06/04/00	1112	233	11.4	10
07/04/00	1166	544	10.4	6
10/04/00	742	204	10.8	2
11/04/00	1469		8.7	1

Appendix F.

Gravity and GPS Data

F.1. Example of relative microgravity data manipulation

Date	Raw A1	Raw Regis	(Raw - A1) Regis	Raw Museo	(Raw - A1) Museo	Raw A2	(Raw - A1) A2	Raw A3	(Raw - A1) A3
18/02/98	1774.874	1782.198	7.324	1772.710	-2.163	1775.580	0.707	1775.707	0.833
19/02/98	1774.890	1782.230	7.340	1772.750	-2.139				
27/02/98	1775.073			1772.908	-2.166	1775.810	0.736	1775.942	0.868
28/02/98	1775.085	1782.427	7.342	1772.955	-2.130				
11/03/98	1775.611	1782.935	7.324	1773.460	-2.151	1776.339	0.728	1776.468	0.857
14/03/98	1775.414	1782.743	7.329	1773.279	-2.135				
04/09/98	1773.989	1781.292	7.303	1771.821	-2.168	1774.719	0.730	1774.839	0.850
08/09/98	1774.256	1781.513	7.257	1772.085	-2.171	1774.975	0.719	1775.118	0.862
10/09/98	1774.390	1781.669	7.279	1772.218	-2.172				
12/09/98	1774.516	1781.812	7.296	1772.352	-2.164	1775.215	0.699		
13/09/98	1774.560	1781.860	7.300	1772.403	-2.157			1775.357	0.841

Corrected values for calibration jump of G513 in 1994, using correction factor of $8x10^{-4}$.

Date	(Raw - A1) Regis	Calibrated Regis	(Raw- A1) Museo	Calibrated Museo	(Raw - A1) A2	Calibrated A2	(Raw - A1) A3	Calibrated A3
18/02/98	7.324	7.318	-2.163	-2.161	0.707	0.706	0.833	0.833
19/02/98	7.340	7.334	-2.139	-2.138				
27/02/98			-2.166	-2.164	0.736	0.736	0.868	0.867
28/02/98	7.342	7.336	-2.130	-2.128				
11/03/98	7.324	7.318	-2.151	-2.150	0.728	0.728	0.857	0.857
14/03/98	7.329	7.323	-2.135	-2.134				
04/09/98	7.303	7.297	-2.168	-2.166	0.730	0.729	0.850	0.849
08/09/98	7.257	7.251	-2.171	-2.169	0.719	0.719	0.862	0.862
10/09/98	7.279	7.273	-2.172	-2.170				
12/09/98	7.296	7.290	-2.164	-2.162	0.699	0.699	0.841	0.841
13/09/98	7.300	7.294	-2.157	-2.155				

The tide-corrected raw data (mGal) for each station is first subtracted from the measurement for base station A1. Data are subsequently corrected for a calibration jump in the instrument (G513) that occurred in 1994 using a calibration factor [$\Delta g_{new} = \Delta g_{old} - (\Delta g_{old} \times 8.5 \times 10^{-4})$].

F.2. Micro-gravity changes (relative to A1 / mGal)

F.2.1. Changes between 1993 and 2000

Date	Δ A2	Δ A3	Δ A4	Δ A5	Δ A6	Δ A7	Δ A8	Δ A9	Δ A10	Δ E1	Δ E3	Δ E4
Feb-93	0.000	0.000	0.000	0.000	0.000	0.000	0.000	0.000	0.000	0.000	0.000	0.000
Apr-94	-0.012	0.018	0.001	-0.022	-0.004	-0.078	-0.071	-0.080	-0.080	0.025	-0.192	-0.070
Oct-94	-0.009	0.025	-0.012	0.022	0.021	-0.088						-0.058
Mar-96	-0.022	0.008	-0.022	-0.010	0.065	-0.051	-0.052	-0.113	-0.065	0.038	-0.154	-0.061
Mar-97		0.030		0.024		-0.054	-0.055	-0.064	-0.024	0.061	-0.138	-0.050
27/01/98		-0.009	-0.015			-0.070	-0.067		-0.047	-0.075	-0.165	-0.066
18/02/98	-0.031	-0.007	-0.024	-0.018		-0.090	-0.084		-0.080	0.018	-0.172	
19/02/98												-0.052
27/02/98	-0.001	0.027	0.006	0.039		-0.024						
28/02/98						-0.048	-0.051		-0.038	0.078	-0.149	-0.035
11/03/98	-0.009	0.017	-0.003	0.017		-0.038						
14/03/98				0.012		-0.065	-0.071	-0.066	-0.047	0.050	-0.194	-0.014
04/09/98	-0.008	0.009	-0.005	0.034		-0.061						
08/09/98	-0.018	0.022	-0.008									
10/09/98				-0.010		-0.085	-0.081	-0.084	-0.077	0.042	-0.168	-0.093
12/09/98	-0.038	0.001	-0.025	-0.011		-0.075	-0.085	-0.081	-0.066	0.042	-0.151	
13/09/98												-0.066
08/02/99	-0.010	0.008	-0.026	0.002		-0.089	-0.088	-0.070	-0.073		-0.170	-0.093
11/02/99	-0.013	0.015	-0.018	0.007	0.080	-0.063						-0.085
12/02/99												
13/02/99							-0.076	-0.100	-0.045	0.059	-0.158	
20/02/99	-0.015	0.011	-0.008	-0.026	0.055	-0.084						-0.089
21/02/99							-0.085	-0.084	-0.081	0.069	-0.177	
06/03/99	-0.007	0.025		-0.007		-0.091	-0.090	-0.111		0.043	-0.215	
07/03/99			-0.010		0.057				-0.096			-0.088
18/06/99	0.009	0.022	-0.017									
19/06/99				0.016	0.033	-0.128	-0.075	-0.125	-0.106	0.058	-0.227	-0.136
23/06/99										0.071	-0.247	-0.156
24/06/99	0.008	0.024	-0.020	0.051	0.058	-0.147	-0.102	-0.175	-0.143			
25/06/99						-0.143	-0.071		-0.145		-0.221	
21/03/00			-0.045			-0.153	-0.087		-0.120		-0.221	-0.149
23/03/00	-0.039	-0.027	-0.029	0.026	0.066							
24/03/00						-0.136				0.082		-0.155
25/03/00							-0.065	-0.131	-0.151		-0.227	
29/03/00						-0.135	-0.072	-0.131	-0.127		-0.217	-0.143
03/04/00						-0.130	-0.078	-0.138	-0.121		-0.233	-0.128
10/04/00						-0.122	-0.076	-0.146	-0.118		-0.232	-0.159

F.2.2. Changes between 1994 and 2000

Date	Δ A2	Δ A3	Δ A4	Δ A5	Δ A6	Δ A7	Δ A8	Δ A9	Δ A10	Δ E1	Δ E3	Δ E4	Δ B2	Δ Coyotes
Apr-94	0.000	0.000	0.000	0.000	0.000	0.000	0.000	0.000	0.000	0.000	0.000	0.000	0.000	0.000
Oct-94	0.003	0.007	-0.013	0.044	0.025	-0.010						0.012		0.008
Mar-96	-0.010	-0.010	-0.023	0.012	0.069	0.027	0.019	-0.033	0.015	0.013	0.038	0.009	0.029	0.020
Mar-97		0.012		0.046		0.024	0.016	0.016	0.056	0.036	0.054	0.020	-0.015	
27/01/98		-0.027	-0.016			0.008	0.004		0.033	-0.100	0.027	0.004	-0.022	
18/02/98	-0.019	-0.025	-0.025	0.004		-0.012	-0.013		0.000	-0.007	0.020		-0.037	
19/02/98												0.018		0.006
27/02/98	0.011	0.009	0.005	0.061		0.054							0.028	0.006
28/02/98						0.030	0.020		0.042	0.053	0.043	0.035		
11/03/98	0.003	-0.001	-0.004	0.039		0.040								-0.002
14/03/98				0.034		0.013	0.000	0.014	0.033	0.025	-0.002	0.056	-0.011	
04/09/98	0.004	-0.009	-0.006	0.056		0.017								
08/09/98	-0.006	0.004	-0.009											-0.014
10/09/98				0.012		-0.007	-0.010	-0.004	0.003	0.017	0.024	-0.023	-0.026	
12/09/98	-0.026	-0.017	-0.026	0.011		0.003	-0.014	-0.001	0.014	0.017	0.041		-0.042	
13/09/98												0.004		0.003
08/02/99	0.002	-0.010	-0.027	0.024		-0.011	-0.017	0.010	0.007		0.022	-0.023	-0.033	
11/02/99	-0.001	-0.003	-0.019	0.029	0.084	0.015						-0.015	-0.026	
12/02/99														0.006
13/02/99							-0.005	-0.020	0.035	0.034	0.034		-0.034	
20/02/99	-0.003	-0.007	-0.009	-0.004	0.059	-0.006						-0.019		
21/02/99							-0.014	-0.004	-0.001	0.044	0.015		-0.039	-0.018
06/03/99	0.005	0.007		0.015		-0.013	-0.019	-0.031		0.018	-0.023		-0.041	0.000
07/03/99			-0.011		0.061				-0.016			-0.018		
18/06/99	0.021	0.004	-0.018											0.020
19/06/99				0.038	0.037	-0.050	-0.004	-0.045	-0.026	0.033	-0.035	-0.066	-0.096	
23/06/99										0.046	-0.055	-0.086	-0.092	
24/06/99	0.020	0.006	-0.021	0.073	0.062	-0.069	-0.031	-0.095	-0.063					-0.026
25/06/99						-0.065	0.000		-0.065		-0.029			
21/03/00			-0.046			-0.075	-0.016		-0.040		-0.029	-0.079	-0.136	
23/03/00	-0.027	-0.045	-0.030	0.048	0.070									-0.025
24/03/00						-0.058				0.057		-0.085		
25/03/00							0.006	-0.051	-0.071		-0.035			
29/03/00						-0.057	-0.001	-0.051	-0.047		-0.025	-0.073	-0.083	
03/04/00						-0.052	-0.007	-0.058	-0.041		-0.041	-0.058	-0.085	
10/04/00						-0.044	-0.005	-0.066	-0.038			-0.040	-0.076	

F.2.3. Changes between 1997 and 2000

Date	Δ Museo	Δ A3	Δ A5	Δ A7	Δ A8	Δ A9	Δ A10	Δ A11	Δ E1	Δ E3	Δ E4	Δ B1a	Δ B2	Δ Edge	Δ Pedro
Mar-97	0.000	0.000	0.000	0.000	0.000	0.000	0.000	0.000	0.000	0.000	0.000	0.000	0.000	0.000	0.000
27/01/98	-0.024	-0.039		-0.016	-0.012		-0.023	0.078	-0.136	-0.027	-0.016	-0.005	-0.007	0.009	-0.034
18/02/98	-0.079	-0.037	-0.042	-0.036	-0.029		-0.056	-0.049	-0.043	-0.034		-0.018	-0.022		
19/02/98	-0.056								74.459		-0.002			-0.012	
27/02/98	-0.082	-0.003	0.015	0.030								0.027	0.043		
28/02/98	-0.046			0.006	0.004		-0.014	-0.027	0.017	-0.011	0.015			0.015	-0.006
11/03/98	-0.068	-0.013	-0.007	0.016											
14/03/98	-0.052		-0.012	-0.011	-0.016	-0.002	-0.023	-0.031	-0.011	-0.056	0.036	-0.011	0.004	0.010	0.005
04/09/98	-0.084	-0.021	0.010	-0.007											
08/09/98	-0.087	-0.008													
10/09/98	-0.088		-0.034	-0.031	-0.026	-0.020	-0.053	-0.054	-0.019	-0.030	-0.043	-0.050	-0.011	-0.048	-0.053
12/09/98	-0.080	-0.029	-0.035	-0.021	-0.030	-0.017	-0.042	-0.048	-0.019	-0.013		-0.029	-0.027		
13/09/98	-0.073										-0.016			-0.033	-0.046
08/02/99	-0.076	-0.022	-0.022	-0.035	-0.033	-0.006	-0.049	-0.058		-0.032	-0.043	0.055	-0.018	-0.070	-0.063
11/02/99	-0.067	-0.015	-0.017	-0.009							-0.035	0.077	-0.011	-0.050	-0.033
12/02/99	-0.078														
13/02/99	-0.074				-0.021	-0.036	-0.021	-0.035	-0.002	-0.020			-0.019		
20/02/99	-0.079	-0.019	-0.050	-0.030							-0.039			-0.057	-0.060
21/02/99	-0.079				-0.030	-0.020	-0.057	-0.068	0.008	-0.039		0.053	-0.024		
06/03/99	-0.073	-0.005	-0.031	-0.037	-0.035	-0.047		-0.092	-0.018	-0.077			-0.026		
07/03/99	-0.074						-0.072				-0.038			-0.048	-0.052
18/06/99	-0.071	-0.008													
19/06/99	-0.075		-0.008	-0.074	-0.020	-0.061	-0.082	-0.101	-0.003	-0.089	-0.086		-0.081	-0.157	-0.150
23/06/99	-0.052							-0.114	0.010	-0.109	-0.106		-0.077	-0.118	-0.124
24/06/99	-0.068	-0.006	0.027	-0.093	-0.047	-0.111	-0.119								
25/06/99	-0.049			-0.089	-0.016		-0.121	-0.099		-0.083				-0.084	-0.096
21/03/00	-0.095			-0.099	-0.032		-0.096			-0.083	-0.099			-0.114	
23/03/00	-0.057	-0.057	0.002												
24/03/00				-0.082					0.021		-0.105			-0.111	-0.116
25/03/00					-0.010	-0.067	-0.127	-0.110		-0.089					
29/03/00	-0.054			-0.081	-0.017	-0.067	-0.103	-0.094		-0.079	-0.093		-0.068	-0.126	-0.101
03/04/00	-0.075			-0.076	-0.023	-0.074	-0.097	-0.112		-0.095	-0.078		-0.070	-0.103	-0.120
10/04/00				-0.068	-0.021	-0.082	-0.094	-0.110		-0.094	-0.109		-0.054	-0.115	-0.106

F.2.4. Changes between 1999 and 2000

Date	Δ Regis	Δ Museo	Δ A2	Δ A3	Δ A4	Δ A5	Δ A6	Δ A7	Δ A8	Δ A9	Δ A10	Δ A11	Δ E1	Δ E3	Δ E4
08/02/99	0.000	0.000	0.000	0.000	0.000	0.000		0.000	0.000	0.000	0.000	0.000		0.000	0.000
11/02/99	-0.032	0.009	-0.003	0.007	0.008	0.005	0.000	0.026							0.008
12/02/99	0.000	-0.002							0.012	-0.030	0.028	0.023	0.000	0.012	
13/02/99	0.005	0.002													0.004
20/02/99	-0.003	-0.003	-0.005	0.003	0.018	-0.028	-0.025	0.005	0.003	-0.014	-0.008	-0.010	0.010	-0.007	
21/02/99	0.008	-0.003													
23/02/99	-0.001	0.003										-0.034	-0.016	-0.045	
06/03/99	0.014	0.003	0.003	0.017		-0.009		-0.002	-0.002	-0.041					0.005
07/03/99	0.013	0.002			0.016		-0.023				-0.023				
18/06/99	0.011	0.006	0.019	0.014	0.010										
19/06/99		0.001				0.014	-0.047	-0.039	0.013	-0.055	-0.033	-0.043	-0.001	-0.057	-0.043
23/06/99	0.034	0.024						-0.058	-0.014	-0.104	-0.070	-0.056		-0.076	-0.062
24/06/99	0.022	0.008	0.017	0.015	0.006	0.049	-0.022						0.011		
25/06/99	0.033	0.027						-0.054	0.017		-0.072	-0.041		-0.051	
26/06/99	0.011	-0.001													
21/03/00		-0.019			-0.019			-0.064	0.001		-0.047			-0.051	-0.056
23/03/00	0.048	0.019	-0.029	-0.035	-0.002	0.024	-0.013						0.022		-0.061
24/03/00	0.049							-0.046						-0.056	
25/03/00	0.043								0.023	-0.060	-0.078	-0.052		-0.047	-0.050
29/03/00	0.032	0.022						-0.046	0.016	-0.061	-0.054	-0.036		-0.063	-0.035
03/04/00	0.023	0.001						-0.040	0.010	-0.068	-0.048	-0.054		-0.061	-0.065
10/04/00	0.039	0.009						-0.032	0.011	-0.075	-0.045	-0.052			

Date	Δ B1a	Δ B2	Δ B3	Δ Sismo	Δ Coyotes	Δ Coyotes2	Δ Muertes	Δ Laguna1	Δ Laguna2	Δ Fence2	Δ Arenal	Δ Montoso	Δ Edge
08/02/99	0.000	0.000	0.000										0.000
11/02/99	0.022	0.007	0.006										0.020
12/02/99					0.000	0.000	0.000	0.000	0.000	0.000			
13/02/99		-0.001		0.000							0.000	0.000	0.013
20/02/99													
21/02/99	-0.002	-0.006	-0.029	0.003	-0.024	-0.001	-0.009	-0.013	-0.022	-0.017			
23/02/99													
06/03/99		-0.008	-0.014	-0.011	-0.006	0.002	-0.007	-0.009	-0.031	0.001			
07/03/99											0.025	0.016	0.022
18/06/99					0.015	-0.018	-0.073	-0.009	-0.049	-0.033	0.044	0.041	
19/06/99		-0.063	-0.058	0.005									-0.039
23/06/99		-0.059	-0.075										-0.048
24/06/99				0.025	-0.032	-0.035	-0.059	-0.034	-0.066	-0.050	0.024	0.042	
25/06/99			-0.046										-0.014
26/06/99													
21/03/00		-0.103											-0.044
23/03/00		-0.001			-0.030	-0.067	-0.072	-0.001	-0.052	-0.022	-0.069	0.014	
24/03/00				0.030									-0.041
25/03/00													
29/03/00		-0.050											-0.056
03/04/00		-0.052											-0.033
10/04/00		-0.043											-0.045

Date	Δ Pedro	Δ Pedro2	ΔLengua	ΔBuenaVista	Δ MuroDeLava	Δ Flanco	Δ Nindiri	ΔLa Clinica	ΔParqueSM	ΔEstacionT
08/02/99	0.000	0.000								
11/02/99	0.030	0.018					0.000			
12/02/99					0.000	0.000				
13/02/99							0.001			
20/02/99	0.003	0.012			-0.001	0.008				
21/02/99								0.000	0.000	0.000
23/02/99										
06/03/99					-0.019	-0.019	-0.012			
07/03/99	0.011	0.020						0.013	-0.023	0.008
18/06/99					-0.034	-0.039	-0.038			
19/06/99	-0.040	-0.030								
23/06/99	-0.061	-0.035	0.000	0.000	-0.034	-0.039				
24/06/99										
25/06/99	-0.033						-0.057	0.009	-0.019	-0.002
26/06/99			-0.011	0.007						
21/03/00										
23/03/00							-0.038			
24/03/00	-0.053	-0.045	0.002	-0.006				-0.003	0.011	0.017
25/03/00					-0.028	-0.036				
29/03/00	-0.038	-0.038					-0.019			
03/04/00	-0.057						-0.027			
10/04/00	-0.043	-0.039	-0.003		-0.017	-0.031	-0.008			

F.3. Elevations of GPS stations

Station	Oct-94 (m)	Mar-96 (m)	Mar-97 (m)	Jan-98 (m)	Feb-98 (m)	Mar-98 (m)	Feb-99 (m)	Mar-99 (m)	Mar-00 (m)	1 std. dev. (cm)
base				301.64	301.53	301.53	301.60	301.60	301.60	4.3
A1	302.11	302.11	302.11	302.11	302.11		302.11	302.11	302.11	0.0
A2	295.59	295.58			295.53		295.60		295.61	3.1
A3	297.78	297.77		297.83	297.75		297.82		297.80	2.9
A4	319.70	319.68			319.64		319.70		319.70	2.5
A5	365.73	365.85	365.81							6.0
A6	439.13						439.15		439.13	1.4
A7	520.73		520.75	520.83	520.71		520.79		520.81	4.4
A8	565.92	565.96	565.93	566.00	565.91		565.99		565.99	3.7
A9	511.88	511.92	511.89			511.87	511.96		511.95	3.9
A10	509.09	509.13		509.19	509.09		509.19			4.9
A11			503.21	503.27	503.16		503.26		503.24	3.8
Arenal					281.96			282.04	282.09	6.5
B1a		525.48	525.49	525.56	525.45					4.4
B2	524.79	524.78	524.78	524.83	524.75		524.81		524.85	3.3
B3							521.39			
B3a									521.22	
Coyotes	284.69				284.62		284.71		284.75	5.4
Coyotes2					236.66					
E1	587.72			587.77	587.68		587.78		587.77	4.4
E3	509.51		509.55	509.61	509.51		509.60		509.58	4.1
E4	517.36	517.37		517.43	517.33		517.40		517.42	3.8
Edge				519.82	519.70		519.76		519.77	4.7
Fence2							123.86		123.84	1.7
Flanco					492.28		492.34		492.35	3.5
Laguna					118.51		118.66		118.64	8.4
Laguna2					130.29		130.35		130.35	3.1
Montoso					287.63				287.63	0.5
Muertes					198.99		199.08			5.8
MuroDeLava					454.72		454.79		454.78	3.8
Museo				310.12			310.10	310.10		1.2
Nindiri						485.31	485.30		485.33	1.2
Pedro			517.08	517.13			517.10		517.08	2.0
Pedro2					520.13		520.18		520.20	3.9
Sismo					589.56		589.60		589.64	3.8

Station A1 was levelled precisely in 1993 by J.B. Murray and is used as a benchmark from which all other stations are referenced.
Note the lack of data for March 1998 and March 1999 due to technical difficulties.

Appendix G.

Volcanic eruption prediction: Magma chamber physics from gravity and deformation measurements

---

H. Rymer and G. Williams-Jones; Paper published in *Geophysical Research Letters*, 27 (16), 2389-2392, 2000.

G.1. Abstract

One of the greatest remaining problems in modern volcanology is the process by which volcanic eruptions are triggered. It is generally accepted that eruptions are preceded by magma intrusion (Sigurdsson and Sparks, 1978). The degree of interaction between previously ponded magma in a chamber and newly intruded magma determines the nature and rate of eruption and also the chemistry of erupted lavas and shallow dykes. Here, we investigate the physics of this interaction. Volcano monitoring at its most effective is a synergy between basic science and risk assessment, while hazard mitigation depends on reliable interpretation of eruption precursors. The simple and much used Mogi model relates ground deformation (Δh) to changes in magma chamber volume. Gravity changes (Δg) combined with ground deformation provide information on magma chamber mass changes. Our new models predict how the Δg/Δh gradient will evolve as a volcano develops from a state of dormancy through unrest into a state of explosive activity. Thus by simultaneous measurement of deformation and gravity at a few key stations, magma chamber processes can be identified prior to the onset of conventional eruption precursors.

G.2. Introduction

Conventional (high-precision) micro-gravity monitoring at active volcanoes is used to identify shallow processes within the feeder conduit using repeated Δg and Δh measurements at a network of stations in and around the active crater or caldera (Rymer,

1994; Rymer et al., 1998a,b). There are obvious risks associated with this practice and recent high profile cases of volcanologists being killed emphasise this point (Baxter and Gresham, 1997; Fujii and Nakada, 1999). Monitoring volcanoes from a safe distance can entail reduced signal strength in the data. Other eruption pre-cursors such as tremors, gas flux/chemistry and temperature fluctuations reflect relatively shallow processes which are a source of noise in $\Delta g/\Delta h$ data in the active vent region. Processes within the magma chamber, which occur months or years before conventional pre-cursors, are interpreted here from $\Delta g/\Delta h$ data which may be obtained at some distance from the active vent, where the signal to noise ratio is enhanced. Hazard mitigation is thus greatly facilitated by the additional time afforded.

G.3. Observations

Ground deformation measurements have long been used to monitor active volcanoes (Murray et al., 1995). The volume of surface deformation (the change in edifice volume ΔVe; Figure G.1) can be estimated from ground deformation measurements simply by integrating the observed height changes over the area of deformation. The Mogi (Mogi, 1958) model relates ΔVe to the change in sub-surface magma chamber volume (ΔVch) assuming the country rocks to behave elastically and the magma chamber to behave as though it is a spherical pressure source whose depth is large compared with its radius. Without any other information, ground deformation provides no indication of the processes taking place inside the magma chamber. Variations in the acceleration due to gravity can also be monitored on active volcanoes and by integrating over the area of variations, the change in sub-surface magma mass (ΔMm) can be quantified (Berrino et al., 1992). Simultaneous gravity and deformation measurements provide an estimate of ΔMm and ΔVch so changes in the average density of the magma chamber may be deduced, providing insights into the process of vesiculation (density decrease) or crystallisation (density increase).

Deviations from the free air gradient (FAG) are due to sub-surface mass changes (Figure G.2). When the density of the magma chamber is taken into account, the Bouguer corrected free air gradient (BCFAG) can be calculated. The value of the BCFAG depends on the model used - spherical source or slab (Berrino et al., 1992; Rymer et al., 1995). Data plotting above the BCFAG on a $\Delta g/\Delta h$ graph (Figure G.2) reflect density increases whereas data plotting below the BCFAG reflect density decreases.

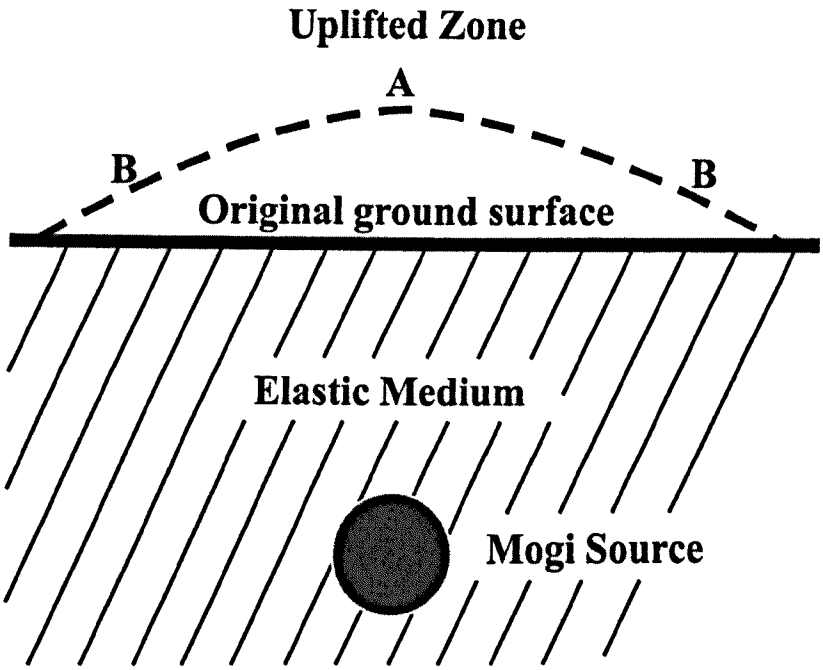

Figure G.1: To a first approximation, a magma reservoir can be modelled as a spherical body. If the depth is large compared with its radius, the gravitational effect is that of a point source. The essence of the Mogi model is that dilation of a point source in an elastic half space causes deformation at the surface, which will depend on the amount of dilation and the elastic properties of the medium. By inserting measured or estimated values for the elastic properties of the surrounding rock, the amount of ground deformation measured at the surface by techniques such as GPS, SAR interferometry, altimetry or levelling, can therefore be used to estimate the change in sub-surface magma reservoir volume (ΔVch). The largest ground deformation changes are observed in zone A, but measurable effects are also seen in distal zones such as B. Gravity measurements may also be made at these points and when combined with ground deformation measurements, this is an extremely powerful method for investigating sub-surface density changes. Quantifying the magnitude and rate of these changes provides a means to detect eruption pre-cursors within the magma chamber, before the magma begins it's journey through conduits to the surface, thus affording more time for hazard mitigation and evacuation.

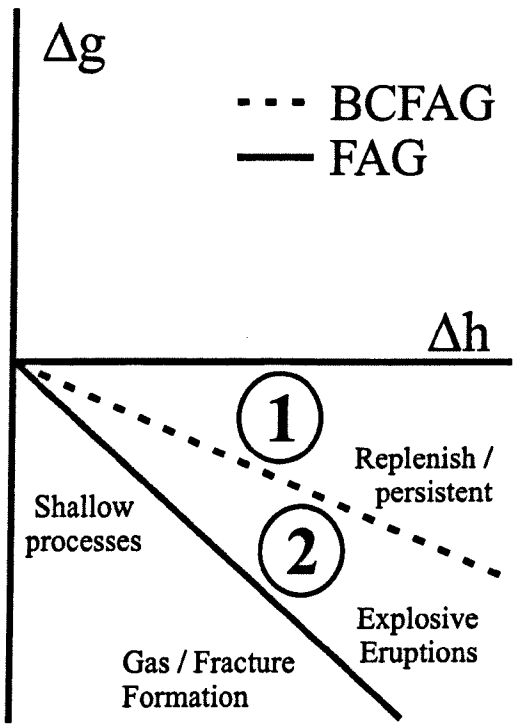

Figure G.2: During periods of inflation, increasing elevation (Δh) is accompanied by decreasing gravity (negative Δg), described by the BCFAG. For the Mogi model and for an infinite Bouguer slab, the relationship is linear. For other models (e.g., dyke, sill etc.), the relationship is not linear, but Δg/Δh data will fall between the BCFAG lines for these two end member models. The actual gradient of the BCFAG will depend on the density assumed for the surrounding rock. It ranges from -224 μGal m^{-1} to -252 μGal m^{-1} for a density of 2000 kg m^{-3} and 113 μGal m^{-1} to -233 μGal m^{-1} for a density of 2700 kg m^{-3} for the slab and sphere models respectively. The free air gradient (FAG) is typically 308.6 μGal m^{-1}, but may vary by about 10% depending on the local terrain and Bouguer anomaly (Rymer, 1994). Thus the BCFAG is model dependent and the FAG should always be measured. Region 1 represents anomalously large gravity increases accompanying inflation and could be interpreted in terms of magma intrusion increasing the average density of the magma chamber. Data falling into region 2 reflect density decrease and mass increase during inflation (and volume increase) which we interpret in terms of the build up of gas within the magma chamber the most likely trigger process for an eruption. Data falling close to the Δg line reflect shallow processes such as magma and gas fluctuations within the feeder conduit or may not even be of immediate volcanological interest (e.g., water table level excursions).

There is an interesting area between the FAG and the BCFAG where during inflation there are mass increases and density decreases and this is crucial to understanding the physics of magma chamber processes and the detection of eruption pre precursors.

G.4. Discussion

Micro-gravity and ground deformation surveys are frequently carried out in the region of maximum uplift, central to the volcanic region (zone A, Figure G.1), in order to investigate relatively shallow sub surface processes. However, sensitive instrumentation can detect the small off axis variations away from the active region (zone B, Figure G.1). The advantage of making observations off axis is that the signal to noise ratio in the data is considerably increased as shallow volcanic effects within the edifice (vesiculation cycles within the feeder conduit, fracturing etc.; (Rymer et al., 1998b) are reduced. Another potential source of uncertainty is the variation in groundwater levels. The effects of water table fluctuations can be minimised by measuring gravity at stations located on crystalline bedrock (Jachens and Roberts, 1985) while seasonal variations in groundwater can be reduced by making measurements at approximately the same time every year (Rymer et al., 1995; Arnet et al., 1997). It is therefore possible to detect subtle changes within a Mogi-type magma chamber of 10^{11} kg to 10^{12} kg at 2-5 km depth at up to 3.5 km and 10 km horizontal distance, respectively. Although, the Mogi model represents an oversimplified magma chamber, many published geophysical data are consistent with this type of source (Berrino et al., 1992; Arnet et al., 1997; Avallone et al., 1999). Here we present two end member models that illustrate how, by observing density changes within the magma chamber, the hazard potential of a volcanic system can be determined.

Intruding magma with a relatively low Reynolds number (low velocity, high viscosity), as illustrated in model 1 (Figure G.3), will interact very little with the chamber magma. There will be an overall mass increase in the system, which would be measurable at the surface as a gravity increase. The intrusion would produce some ground deformation and the Δg/Δh gradient would fall into region 1 or along the BCFAG (Figure G.2) indicating an overall increase in density (region 1) or no density change (BCFAG) within the magma chamber. Constant or increasing density within a magma chamber is indicative of a low potential hazard system, as magma is not able to rise. In a closed system, the chamber will eventually stagnate, but if magma pressure exceeds the local lithostatic pressure, dykes may form which can in some cases eventually feed lava eruptions.

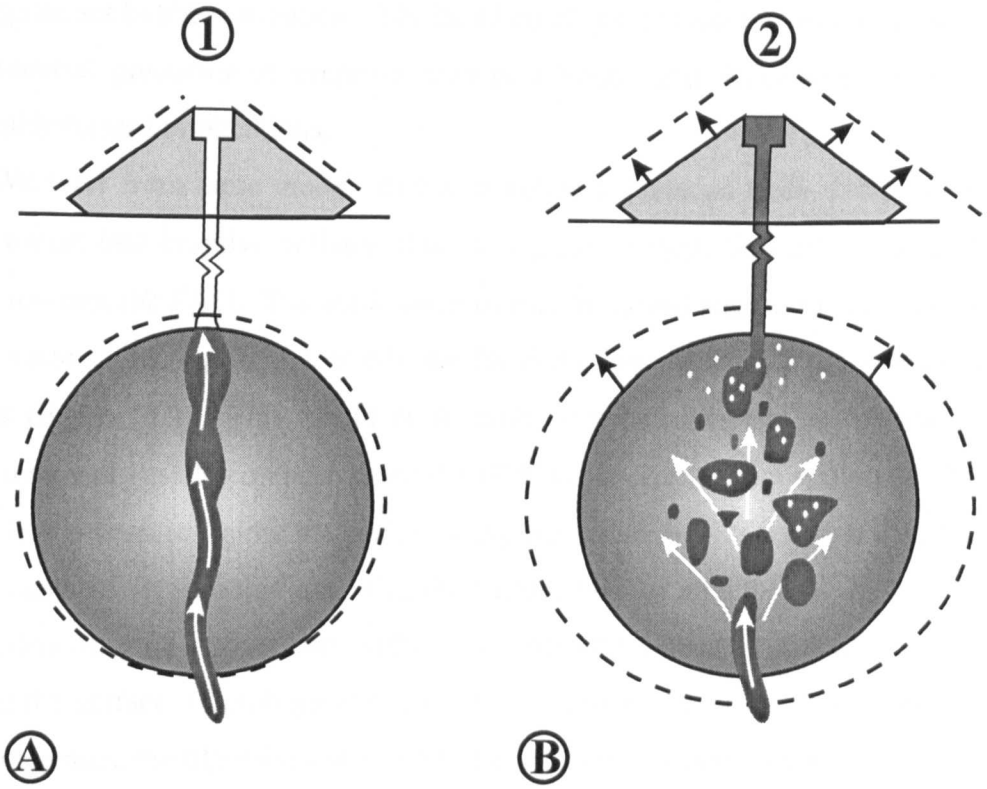

Figure G.3: a) Model 1 depicts a low Reynolds number magma (relatively low velocity and high viscosity) entering a magma chamber and not interacting significantly with the surrounding magma. b) Model 2 has the same magma mass influx as model 1, but the Reynolds number is higher. In this case, the magma interacts with the surrounding magma, heating it, and causing vesiculation and expansion of the chamber. In model 1 the $\Delta g/\Delta h$ gradient will fall into region 1 of Figure G.2; in model 2, the gradient will fall into region 2 of Figure G.2.

Model 2 assumes an intruding magma with a high Reynolds number which will interact with the chamber magma, heating it and inducing vesiculation (Figure G.3). This results in a net subsurface mass increase and density decrease observable at the surface as a Δg/Δh relationship falling into region 2, between the FAG and BCFAG (Figure G.2). In this case, the interaction (Sparks et al., 1980) between the intruding magma and the older magma is critically, more pervasive than in model 1. Magma mixing and mingling will cause significant bubble formation. The build up of gas pressure within a magma chamber is an essential precursor to eruptive activity (Woods and Koyaguchi, 1994) and has considerable hazard implications.

We infer from these models that as a volcano develops from a state of dormancy through unrest into eruptive activity, that the Δg/Δh gradient will evolve away from the BCFAG towards the FAG. The application of this to hazard warning is as follows. As the gradient varies from region 1 towards the BCFAG, the density of the magma chamber decreases (Figure G.2). This would be a result of reduced crystallisation and increased buoyant melt and vesicle content. Once the BCFAG is crossed, the density of the magma chamber has decreased below the previous average value of the chamber and the system becomes unstable. It is at this stage that the magma will be able to rise. If there is limited heating, then magma convection within the chamber (recently linked with pulses of activity at the surface; (Kazahaya et al., 1994) will follow, but with excess heating, as gas pressure increases, the likelihood of an eruption increases (Woods and Koyaguchi, 1994).

G.5. Conclusions

Target areas are calderas in a state of unrest and large composite volcanoes. An open magmatic system is one that displays persistent surface manifestations ranging from a stable lava lake to explosive eruptions and vigorous fumarolic activity. At these systems measurements made in region A (Figure G.1) will be dominated by shallow processes. In order to investigate processes within a Mogi-type source and to increase the signal to noise ratio from this source, measurements must be made in region B. A closed system on the other hand, has little or no surface activity and therefore Δg/Δh gradient measurements may be made safely in both regions A and B. A prime example of a closed system is the Campi Flegrei caldera (Naples, Italy) which was characterised by a bradyseismic crisis in the early 1980s. The average Δg/Δh gradient (-213 ± 6 μGal m^{-1}) during inflation, measured at stations in regions A and B, fell into region 1 (Figure 2). As our model predicts, there was no eruption. Indeed, as data in Berrino (Berrino, 1994) show, the

gradient actually evolved (February 1981 to March 1983) from the BCFAG towards the horizontal axis, well within region 1 (Figure G.2). This episode was interpreted in terms of intrusion into a magma chamber (Berrino et al., 1984) or mobilisation of the hydrothermal system (Bonafede, 1991). Our model predicts that if the $\Delta g/\Delta h$ gradient steepens beyond -220 $\mu Gal\ m^{-1}$ during inflation an eruption will follow (Table G.1). Given the considerable history of caldera unrest at Campi Flegrei and the increasing population of the region, there is a vital need to distinguish between magma chamber processes such as those presented here in models 1 and 2 (Figure G.3).

Data from Campi Flegrei, Rabaul and Long Valley all fall into region 1 of our model (Table G.1). This is consistent with the fact that no eruption occurred at these sites. The Krafla data on the other hand fall within region 2 and are consistent with the eruption that followed. The actual value of the BCFAG will depend on the FAG, the Bouguer anomaly and the density of the intrusion (Rymer, 1994). However even if the theoretical

Table G.1. *Summary of rigorously documented gravity-height changes observed during inflation and associated with caldera unrest.*

Volcano	Inflationary Period	$\Delta g/\Delta h$ (μGal)	FAG ($\mu Gal\ m^{-1}$)	BCFAG ($\mu Gal\ m^{-1}$)
Campi Flegrei *Italy*	Feb. 1981-Mar. 1983	-213 ± 6[a]	-290 ± 5[a]	-220[a]
Rabaul *PNG*	1973-1985	-216 ± 4[b]	-300[a]	-238[a]
Krafla *Iceland*	Jan.-June 1978	-250 ± 20[c]	-308*	-200[d]
Long Valley *USA*	1982-1998	-215 ± 11[e]	-308*	-233*

[a] Berrino et al. (1992); [b] McKee et al. (1989); [c] Johnson et al. (1980); [d] Rymer et al. (1998a); [e] Battaglia et al. (1999)
* Theoretical

values for the FAG (- 308 $\mu Gal\ m^{-1}$) and the BCFAG (-233 $\mu Gal\ m^{-1}$ for a density of 2700 $kg\ m^{-1}$) are used, the data from all the published examples still fall into the same regions.

Simultaneous measurements of deformation and gravity at a few key stations may therefore be used to identify magma chamber processes prior to the onset of conventional eruption precursors. The method is expected to find greatest application in regions where a

Mogi type chamber is located at 2-5 km depth, where the magma system is essentially closed and where early hazard warning is essential.

G.6. Acknowledgements

This research was supported by the Royal Society, The Open University Research Development Fund and NERC. We are grateful to C. A. Locke, J. Cassidy and J. B. Murray for helpful discussions. This work was greatly improved by the comments of G. Berrino and A.T. Linde.

G.7. References

Arnet, F., Kahle, H.-G., Klingelé, E., Smith, R. B., Meertens, C. M. and Dzurisin, D., 1997. Temporal gravity and height changes of the Yellowstone caldera, 1977 - 1994. Geophys. Res. Lett., 24, 2741-2744.

Avallone, A., Zollo, A., Briole, P., Delacourt, C. and Beauducel, F., 1999. Subsidence of Campei Flegrei (Italy) detected by SAR interferometry. Geophys. Res. Lett., 26, 2303-2306.

Baxter, P. J. and Gresham, A., 1997. Deaths and injuries in the eruption of Galeras Volcano, Colombia, 14 January 1993. J. Volcanol. Geotherm. Res., 77, 325-338.

Berrino, G., 1994. Gravity changes induced by height-mass variations at the Campi Flegrei caldera. J. Volcanol. Geotherm. Res., 61, 293-309.

Berrino, G., Corrado, G., Luongo, G. and Toro, B., 1984. Ground deformation and gravity changes accompanying the 1982 Pozzuoli uplift. Bull. Volcanol., 47, 187-200.

Berrino, G., Rymer, H., Brown, G. C. and Corrado, G., 1992. Gravity-height correlations for unrest at calderas. J. Volcanol. Geotherm. Res., 53, 11-26.

Bonafede, M., 1991. Hot fluid migration; an efficient source of ground deformation; application to the 1982-1985 crisis at Campi Flegrei-Italy. J. Volcanol. Geotherm. Res., 48, 187-198.

Fujii, T. and Nakada, S., 1999. The 15 September 1991 pyroclastic flows at Unzen Volcano (Japan): a flow model for associated ash-cloud surges. J. Volcanol. Geotherm. Res., 89, 159-172.

Jachens, R. C. and Roberts, C. W., 1985. Temporal and areal gravity investigations at Long Valley Caldera, California. J. Geophys. Res., 90, 11210-11218.

Kazahaya, K., Shinohara, H. and Saito, G., 1994. Excessive degassing of Izu-Oshima volcano: magma convection in a conduit. Bull. Volcanol., 56, 207-216.

Mogi, K., 1958. Relations between the eruptions of various volcanoes and the deformations of the ground surfaces around them. Bull. Earth. Res. Inst., 36.

Murray, J. B., Pullen, A. D. and Saunders, S., 1995. Ground deformation surveying of active volcanoes. In: B. McGuire, C. R. J. Kilburn and J. Murray (Editors), Monitoring Active Volcanoes, UCL Press, London, pp. 113-150.

Rymer, H., 1994. Microgravity change as a precursor to volcanic activity. J. Volcanol. Geotherm. Res., 61, 311-328.

Rymer, H., Cassidy, J., Locke, C. A. and Murray, J. B., 1995. Magma movements in Etna

volcano associated with the major 1991-1993 lava eruption: evidence from gravity and deformation. Bull. Volcanol., 57, 451-461.

Rymer, H., van Wyk de Vries, B., Stix, J. and Williams-Jones, G., 1998a. Pit crater structure and processes governing persistent activity at Masaya Volcano, Nicaragua. Bull. Volcanol., 59, 345-355.

Rymer, H., Cassidy, J., Locke, C. A. and Sigmundsson, F., 1998b. Post-eruptive gravity changes from 1990 to 1996 at Krafla volcano, Iceland. J. Volcanol. Geotherm. Res., 87, 141-149.

Sigurdsson, H. and Sparks, R. S. J., 1978. Rifting episode in North Iceland in 1874-1875 and the eruptions of Askja and Sveinagia. Bull. Volcanol., 41, 149-167.

Sparks, R. S. J., Meyer, P. and Sigurdsson, H., 1980. Density variation amongst Mid-Ocean Ridge basalts: Implications for magma mixing and the scarcity of primitive lavas. Earth Planet. Sci. Lett., 46, 419-430.

Woods, A. W. and Koyaguchi, T., 1994. Transitions between explosive and effusive eruptions of silicic magmas. Nature, 370, 641-644.